KU Leuven

Biomedical Sciences Group

Faculty of Medicine, Campus Kulak Kortrijk

Department of Development and Regeneration

KU LEUVEN

DOCTORAL SCHOOL
BIOMEDICAL SCIENCES

ANATOMICAL ADAPTATIONS TO VARYING FUNCTIONAL DEMANDS IN THE PRIMATE THUMB

An integrated anatomical and biomechanical study of bonobos, gibbons, and rhesus macaques

Timo van Leeuwen

Supervisor:

Prof. dr. Evie E. Vereecke

Co-supervisor:

Prof. dr. ir. G. Harry van Lenthe

Chair examining committee:

Prof. dr. Lieven Thorrez

Jury members:

Prof. dr. Ilse Degreef

Prof. dr. Jos Snoeks

Prof. dr. Tracy L. Kivell

Prof. dr. John A. Nyakatura

Dissertation presented in partial fulfilment of the requirements for the degree of

Doctor in Biomedical Sciences

June 2021

Anatomical adaptations to varying functional demands in the primate thumb

An integrated anatomical and biomechanical study of bonobos, gibbons, and rhesus macaques

Timo van Leeuwen

ISBN/EAN: 978-94-93255-06-7

Cover illustration: Timo van Leeuwen

Cover design: EZBook.nl, Blaricum, The Netherlands

Printed by: EZBook.nl, Blaricum, The Netherlands

Copyright © 2021 by Timo van Leeuwen. All rights reserved. No parts of this publication may be reproduced, stored in a retrieval system, or transmitted in any form or by any means electronic, mechanical, photocopying, recording, or otherwise without prior permission of the author.

Preamble: to all those who have supported me

Hier zijn we dan. De persoon die dit dankwoord zit te schrijven, in het zonnetje in een park aan de Schelde, is ver verwijderd van de persoon die begon aan dit wetenschappelijk avontuur. Naar het einde van mijn studie in Wageningen dacht ik degelijk voorbereid te zijn op de volgende stap in de academische mallemolen. Ik had mijn best gedaan om de juiste vakken, stages en projecten te kiezen om een PhD te doorlopen, met de overtuiging dat dit de middelen waren die ik nodig had om zo'n traject met succes te behalen. De eerste twee jaar van het project leek dit ook zo te zijn. Maar ergens halverwege mijn tijd aan de Kulak brak een periode aan waarin ik een aantal van mijn mede-doctoraatstudenten zag worstelen met motivatie en waarin ik sommigen zelfs zag stoppen. Dit was het punt waarop ik me meer ging bezig houden met de psychologische kant van doctoreren. Snel brak er ook voor mij een lastige periode aan waarin mijn motivatie werd getest en waarin ik mezelf beter heb leren kennen. Een van mijn belangrijkste ondervindingen was, kort gezegd, dat de personen die mij hebben ondersteund in mijn tijd aan de KU Leuven niet alleen medeverantwoordelijk zijn voor de inhoud van dit werk, maar boven al de reden zijn dat dit werk bestaat. Zonder jullie had ik het werkelijk niet gehaald. Ik ben jullie allen veel verschuldigd en ik weet hoe graag sommigen van jullie het dankwoord van een thesis lezen, dus laten we beginnen.

Allereerste wil ik mijn promotor, prof. dr. Evie Vereecke, bedanken voor haar steun die de afgelopen vier en een half jaar lang vrijwel onvoorwaardelijk leek te zijn. Je gaf me de ruimte om me te kunnen ontwikkelen als persoon, je gaf me de uitdagingen om te ontwikkelen als onderzoeker en je nam het voor me op tijdens confrontaties met het academische circus. Bedankt voor je inzicht, je geduld en je wijze woorden.

Ook wil ik mijn co-promotor, prof. dr. ir. Harry van Lenthe, bedanken voor de sobere en kritische blik op mijn werk. Laat het aan mij over om met wilde ideeën te komen voor een analytische aanpak of innovatieve visualisatie en laat het aan jou over om ervoor te zorgen dat ik niet te veel met mijn hoofd in de wolken loop. Je hield me met de voetjes aan de grond, je hield het realistisch en waarborgde daarbij zowel de haalbaarheid als de kwaliteit van het project.

I also owe much to the four members of my jury. Prof. dr. Ilse Degreef met haar oog voor structuur en leesbaarheid, prof. dr. Jos Snoeks voor zijn gedetailleerde en kritische blik, prof. dr. John Nyakatura for helping me think outside my own box, and Tracy Kivell for her ever thoughtful and extremely thorough reviews. Thanks to all of you for your extensive feedback, your critical comments, and your constructive suggestions. I am quite confident in saying that without your input, this thesis would be partially unreadable and mostly incomprehensible. Hierbij wil ik ook Lieven Thorrez bedanken voor het opnemen van het voorzitterschap van mijn verdediging en de betrokkenheid die hij daarbij toonde.

Uiteraard heb ik ook veel te danken aan mijn mede lab- en al dan niet bureaugenoten, zowel oud als nieuw. Allereerst Faes, die mij ontving met de woorden: "Je bent te cynisch

voor een eerstejaars", maar vervolgens geen poging deed om mij dit af te leren. Ik heb veel van je geleerd zowel binnen de wetenschap, als hoe te overleven op de campus en als Hollander in West-Vlaanderen. Dankzij jou kwam mijn project goed van de grond en veel van jouw 'wijze' woorden zijn me bijgebleven over de gehele periode van mijn doctoraat. Je wordt bedankt!

Elise, altijd behulpzaam, altijd goed voor sjouw- en zaagavonturen in de koel/diepvries ruimtes én mijn vooraanstaande kanaal van nieuws op de campus. Bedankt voor de leuke babbels en de sfeer aan het bureau. Zonder jou zou de boel ineenstorten.

Maarten, bedankt voor je inzicht. Gesprekken met jou gaven mij vaak de frisse blik die ik nodig had om mijn analyses netjes uit te werken. Natuurlijk ook veel dank voor alles wat je hebt gedaan rond KAS/JOKE, een enorme klus zowel in Matlab als Python waar ik ook veel gebruik van heb kunnen maken. Je sarcasme en net iets te duistere humor aan de lunchtafel werden zeer gewaardeerd.

Dan hebben we Marie, over de jaren mijn medestander tijdens lange, zomerse dissecties waarin de snijzaal de enige bescherming tegen de hitte leek te bieden. Of we nou samen in de weer waren met lunchritjes naar het AZ, het ronselen van primaten of het plannen van een educatief parcours in de naam van Osteologie, altijd was er ruimte voor een babbel en een lach. Medeplichtig aan de sfeer op het bureau; het feit dat ik vrijwel altijd met mijn hoofdtelefoon op zat, had (meestal) niet te maken met dat ik er niet van genoot. Naast jouw eigen drukke schema stond je altijd klaar om een helpende hand te bieden, ongeacht de uitdaging. In mijn ogen was er dan ook altijd veel meer gaande dan alleen maar handjes draaien. Bedankt voor de mooie tijden.

I would like to thank Benjamin for showing me around Kortrijk and the Kulak. You gave me the ins and outs when I first moved to Belgium and you gave me the option to join some of the international communities on campus. You also introduced me to the biomechanical analyses which got me off on the right foot. I enjoyed our technical discussions and talks about Vancouver. I hope you enjoy your Canadian citizenship!

Priscilla, although we never technically shared the office space, I enjoyed your visits to the lab when you were finishing up your PhD. You always brought positivity and plenty of heartfelt compliments for the entire team. Even after you finished, you came back to help me out with the ligament dissections, for which I am grateful to you.

Sandrine, bedankt voor de gesprekken en gezelligheid aan het bureau, de lunchtafel, in de gangen en tijdens de meetings. Ik heb je vanwege Covid al een tijd niet meer gezien, maar ik hoop dat alles goed gaat met jou en Morgane.

Dario, we mostly got to talk during the online lab meetings as the big C came in and sent us all (but mostly me) to work from home. I'm glad you took over after Maarten left and I hope you will be able to continue your work at the Kulak. Thank you for the good times.

Elaine, since you joined the lab you have shown immense involvement in not only my work, but also in my personal experience of being a finishing doctoral student. Thank you for your help in proofreading my work and for your tips and suggestions on new endeavors,

but most of all thank you for your uplifting words during the most intense times of my PhD. I owe you much and I hope that I will be able to return the favor in the future.

Natuurlijk ook bedankt aan mijn Kulak collega's voor de velen babbels in de wandelgangen en de gezellige discussies en gesprekken aan de lunchtafel en op de borrels. Vincent, Dacha, Joke, Charlotte, Elien, Tessa en Lisanne, met dank aan jullie voelde ik mij uiterst welkom als Hollander in West-Vlaanderen. Dank ook aan Ester, Celine, Melani, Petra en Hans voor de interessante gesprekken en prettige samenwerking. Bedankt ook aan Christèle, Kathy en Sigrid voor de ondersteuning.

A big thank you also to Konstantinos, Felipe, Fateme, Jasper, and Alireza, some of my fellow internationals (yes, I am technically an international at Kulak). Thank you for the interesting chats and discussions, I had fun hanging out with you at the various drinks and events.

Ook aan mijn Muscle and Movement collega's aan de campus Brugge; Henri, Ive, Saranda, Inti, Kurt, Elegast en Hans, dank voor de gezellige meetings met inspirerende feedback.

Hartelijk dank aan alle studenten aan de Kulak die betrokken waren bij mijn werk; Pieter, Jaron, Ismaël, Heline, Phillipe, Astrid, Robin en Lotte, voor de hulp in de snijzaal of achter de pc, maar ook de eerstejaars studenten Geneeskunde die prettig meewerkten tijdens de lessen Osteologie en die voor mij een aanleiding vormden tot didactische zelfreflectie.

Op AZ Groeninge, dank aan Olivier en met name aan Henk voor de hulp en het geduld tijdens de schijnbaar eindeloze reeks aan CT-scans waar we met een menagerie van primaten voorbijkwamen. En dat tijdens de lunch.

To my colleagues in Leuven; Karen, Steffi, Amelie, Alexandra, Haniyeh, Kimberly, Stefan, and everybody at BMe. Thank you for your support, your insights, and for taking me in as a (part-time) member of the department.

At the Auckland Bioengineering institute, Thor, Nynke, Ted, Mary, Ju, Mousa, Teo, and everybody at ABI, thank you for welcoming me with open arms. My stay in New Zealand was amazing and your enthusiasm made it even better. In particular, I want to thank Marco for being my temporary supervisor over there. Thank you for effort put into the FE project and for continuing to do so when I returned to Belgium. I have worked hard and learned a lot when I was at the ABI and it was mostly thanks to you that I was able to do so.

Aan Annechien, Anniek, Briek en Rosa in Gent, die mij ontvingen wanneer ik mij weer onder de levenden durfde te wagen, bedankt voor de gezelligheid en het medeleven.

Ook ontzettend bedankt aan de groep die, zeker tijdens de lockdown, een soort verdraaide, wekelijkse, online supportgroep wisten te vormen; Mark, Inge, Sander, Max, Elena, Ruben, en Bart. Bedankt voor de afleiding en het geouwehoer.

En uiteraard de harde kern hieruit. Liefkozend benoemd 'my associates'. Freek – onvrijwillig breingenoot en zelf uitgeroepen beste vriend. Tim – levensgenieter, wijze oude man en succesvol academisch ontsnappeling. Jens – kameraad, hype-persoon en bane of

my existence. En Bob, ex-pannenkoekenbakker, filosoof en Asian screen enthousiasteling. Heren, bedankt voor de steun, zowel uitgesproken als onuitgesproken. Bedankt voor het drijven van mijn motivatie door middel van jullie onuitstaanbare aanwezigheid. Maar bovenal, bedankt voor de mooie tijden die mij helpen te genieten van het leven.

Ik ben dankbaar aan mijn zussies; Sara en Margot, voor jullie steun en interesse in mijn werk, en aan oma Bep die altijd zeer geïnteresseerd naar de verhalen over mijn belevingen aan de universiteit in België luisterde, ook al beweerde ze zelf dat ze er niets van begreep.

Artur en Ingrid, jullie hebben met name de laatste en meest intense periode van mijn doctoraat van dichtbij mee gemaakt en wat jullie hierin voor mij hebben betekend kan en hoef ik hier niet uit te typen. Ik ben jullie ontzettend dankbaar voor deze periode en ik ben blij dat we ons nu op de toekomst kunnen richten.

Als allerlaatste, mijn ouders. Ik krijg vaak te horen hoe leuk en lief mijn ouders zijn en ik realiseer mij dat dit verre van vanzelfsprekend is. Jullie steun en interesse in zowel mijn werk als mijn mentale gesteldheid is daadwerkelijk oneindig en onvoorwaardelijk. Er was altijd ruimte voor ellenlange gesprekken en discussies over obscure wetenschappelijke concepten, psychologische wegversperringen of gewoon gemekker. Maar gelukkig was er vooral altijd ruimte voor positiviteit. Jullie hebben altijd in mij geloofd, vaak zelfs meer dan ik zelf deed. Ik ben net zo trots op jullie als dat ik weet dat jullie op mij zijn. Hartelijk bedankt voor alles, jullie zijn geweldig.

Dus hier zijn we dan, aan het einde van dit avontuur. Het is tijd voor mij om op te hoepelen van de KU Leuven, maar weet dat ik deze periode en de lessen die ik heb geleerd altijd bij me zal dragen. Bedankt allemaal!

Ik ga nog even van het zonnetje genieten.

Groetjes thuis.

Timo

Table of contents

Preamble **3**
Table of contents **7**
Summary **12**
Samenvatting **14**
List of abbreviations **16**
General Introduction **19**
Thesis motivation 20
General background 22
The primate taxa 22
The primate hand, thumb, and the trapeziometacarpal joint 27
Morphological adaptation 33
Project objectives 36
Main goal and broad hypotheses 36
Thesis outline 41
References 43
Part 1 ..... **53**
Chapter 1 ..... **55**
Abstract 56
Introduction 57
Materials and methods 58
Specimen selection 58
CT scanning and image segmentation 59
Dissection procedure 61
Data analysis 63
Results 64
Observations on bonobo hand musculature 64
Quantification of bonobo hand muscles 71
Discussion 74
High variability of bonobo hand musculature 74
Bonobo thumb musculature 76
Functional coupling 76
Critical considerations 77

Conclusions 78
Acknowledgements 78
Author contributions 78
Supplementary material 79
References 95
Part 2 99
Chapter 2. 101
Abstract 102
Introduction 103
Materials and methods 105
Specimen acquisition 105
CT scanning and image segmentation 106
Human volunteers 106
Kinematic analysis and 3D joint geometry 107
Dissection of the TMC joint ligaments 109
Results 109
Kinematics of the first metacarpal during thumb abduction and flexion 109
Curvature of the distal articular facet of the trapezium 111
Orientation and position of the trapezium relative to the radial styloid 112
Functional anatomy of the TMC joint ligaments 114
Discussion 116
Conclusions 120
Acknowledgements 121
Author contributions 121
References 122
Chapter 3. 127
Abstract 128
Objectives 128
Materials and methods 128
Results 128
Conclusion 128
Introduction 129
Methodology 132
Specimens 132
Imaging protocol 133

Kinematic analysis....133
Ligament anatomy....134
Results....135
Articular surface curvature....135
Kinematic analysis....137
Ligament anatomy....139
Discussion....141
Acknowledgements....146
Supplementary material....147
References....148
Part 3....153
Chapter 4....155
Abstract....156
Introduction....157
Materials & Methods....160
Specimens....160
Imaging protocol....161
Parametric meshing....161
FE model generation....164
Results....165
Discussion....167
Conclusions....172
Acknowledgements....173
References....174
Chapter 5....179
Abstract....180
Introduction....181
Methodology....183
Specimen information and scan protocol....183
FE model integration....184
Model generation....184
Results....188
Discussion....191
Conclusion....194
Acknowledgements....194

References 195
Chapter 6. 199
Abstract 200
Introduction 201
Methodology 204
Overview 204
Specimen information 204
Imaging protocols 206
FE model generation 207
μFE model generation 208
Results 210
Successful simulations 210
Stress distribution on the articular surface of the trapezium 210
Trapezial internal strain distribution 211
Discussion 215
Interpretation of stress distribution on the articular surface of the trapezium 217
Trapezial internal strain 217
Critical considerations 219
Conclusions 220
Acknowledgments 220
Supplementary material 221
References 221
General Discussion 227
Findings and conclusions per part 228
Findings and conclusions of Part 1 228
Findings and conclusions of Part 2 230
Findings and conclusions of Part 3 235
Main conclusions 241
Adaptations towards locomotion are clearly present 242
We encounter high amounts of intraspecific morphological variation 245
Medical imaging and imaging based modelling provide valuable tools 246
Holistic evolutionary research requires a broad and integrated approach 246
Methodological considerations and solutions for future work 247
Joint modelling 247
Material properties 249

Specimens 251
Interpretation 252
Future perspectives 253
What has been achieved, and what is next? 253
At the level of scientific communities 254
My part in this 254
References 256
Appendices 261
Appendix I: Curriculum vitae 261
Biography 261
Awards and funding 261
Research Experience 261
Peer reviewed publications 263
International conferences 264
Skills and qualifications 265
Appendix II: Author contributions 266
Appendix III: Author affiliations 268
Appendix IV: Scientific illustration 269

Summary

The hand has played a crucial role in the evolutionary development of primates. As one of the main anatomical structures to interact with the environment, the hands are a reflection of an organism's habitat. In contrast to modern humans, the non-human primate hand is involved in both locomotion and manipulative capabilities. Yet, despite their recruitment in locomotion, many non-human primates have highly dexterous hands, capable of precise gripping, powerful grasps, and even tool use. Such dexterity is largely by virtue of a well-developed and highly mobile thumb. This apparently contradicting functionality is facilitated by its basal joint; the trapeziometacarpal (TMC) joint. In humans, its unique saddle-shape is key to integrating both mobility and stability of the thumb. However, despite the broad functionality of the thumb and its role in primate evolution, our understanding of thumb anatomy, its biomechanics, and how these two interact is severely limited in non-human primates.

In this project, I focussed on the form and function of the thumb and TMC joint in three closely related primate taxa; bonobos (*Pan paniscus*), gibbons (fam. Hylobatidae), and rhesus macaques (*Macaca mulatta*). Each taxon has a different locomotor repertoire, and yet is capable of advanced manipulative tasks, leading to varying functional demands of the thumb. The overarching aim of this project was to investigate functional adaptation of the thumb by establishing form-function relationships in these primate taxa to provide pieces of the puzzle for interpretation in an evolutionary context. To achieve this goal, I set up a multidisciplinary study that converges in detail, from gross hand and thumb morphology, to TMC joint biomechanics, and concluding with finite-element analysis of the trapezium bone at the base of the thumb.

I performed detailed dissections of the forearm and hand musculature and TMC joint ligaments to document and quantify the soft-tissue morphology. The joint morphology and bone microstructure was studied using CT- and μCT-based methodologies. From the dissections we learn that although the overall soft-tissue blueprint of the thumb is highly similar between the studied taxa, morphological adaptations that may be related to the specific locomotor mode used are present. These adaptations are most notably represented in the relative dimensions of the functional muscle groups and their individual actors. Yet, while the general configuration of the muscle functional groups is similar between taxa, intraspecific variation is prevalent in each taxon.

To investigate the TMC joint function, I have modelled the capabilities of the TMC joint during the principal movements of the thumb. My colleagues and I have developed a CT scanning protocol and medical imaging-based kinematic analysis suite to determine the range of motion of the TMC joint in the different planes. The analysis demonstrated significant differences in TMC joint mobility between the different primate taxa, including humans. These range from markedly high mobility in the gibbon TMC joint, to a severely restricted joint in macaques.

Finally, I have integrated the information of form and function in the TMC joint by conducting advanced computational modelling. I have investigated how intra-articular stress is distributed within the trapezium during different grasp types, and how the resulting load patterns are further transmitted across the trapezium internal architecture. I have developed an integrated finite element – micro-finite element pipeline for the generation and processing of parametric models with the purpose of calculating stress and strain patterns in the TMC joint morphology. The results show that these taxa are capable of executing the varying grasps at the level of the bone microstructure, under the tested circumstances. Moreover, the pipeline is suitable for further testing within these taxa, but also for expansion to other taxa and joints.

This multi-levelled approach to investigating the morphology and biomechanics of the thumb yields valuable tools for the study of joint biomechanics. It gives detailed morphological insight in primate taxa that are underrepresented in the literature and sheds light on the mechanics of the TMC joint with respect to different hand functionalities, as well as on the functional adaptation of the primate thumb. The thesis presents a valuable addition to the scarce information on non-human primate thumb morphology and biomechanics, which may serve as a basis for the interpretation of primate hand evolution.

Samenvatting

De hand heeft een essentiële rol gespeeld in de evolutionaire ontwikkeling van de primaten. Het is één van de belangrijkste anatomische structuren voor interactie met de omgeving, en als gevolg hiervan geeft deze een weerspiegeling van de functionele capaciteit binnen een habitat. In tegenstelling tot de moderne mens, gebruiken andere primaten hun handen zowel voor voortbeweging als voor het manipuleren van objecten. Maar desondanks zijn niet-humane primaten toch in staat om behendige manuele activiteiten uit te voeren. Zo kunnen ze krachtig grijpen, precies manipuleren en sommigen kunnen zelfs gereedschap maken en gebruiken. Dit is grotendeels te danken aan de goed ontwikkelde en hoog mobiele duim en meer specifiek het gewricht dat aan de basis van de duim ligt; het trapeziometacarpaal (TMC) gewricht. In de mens is dit gewricht zadelvorming; een unieke vorm die essentieel is voor het combineren van zowel de stabiliteit als de mobiliteit van de duim. Ondanks het belang van de duim in de evolutie van zowel de mens als andere primaten is er nog weinig bekend over de anatomie en biomechanica van de duim en de interactie hiertussen bij niet-humane primaten.

In dit project focus ik op de vorm en functie van de duim en het bijbehorende TMC gewricht in drie primaten die dicht bij de mens staan in de evolutionaire stamboom; de bonobo (*Pan paniscus*), de gibbon (meerdere soorten uit de familie Hylobatidae) en de resusaap (*Macaca mulatta*). Elk van deze taxa gebruikt een andere manier van voortbewegen, maar is toch in staat om behendig objecten te manipuleren. Dit leidt tot een variatie in functionele eisen en belastingregimes. Het overkoepelende doel van dit project is om adaptatie van de duim te onderzoeken door de relatie tussen de vorm en functie van het duimgewricht bij deze primaten vast te leggen. Hiermee wil ik bijdragen aan de evolutionaire puzzel. Ik heb een studie opgezet die convergeert in niveau van detail; van de algemene anatomie van de hand en duim, via de biomechanica van het TMC gewricht, naar de analyse van het bot op microniveau.

Eerst heb ik de anatomie van de zachte weefsels van de onderarm, de hand en het TMC gewricht gedocumenteerd door het uitvoeren van gedetailleerde dissecties van de spieren en ligamenten. Daarnaast heb ik de benige anatomie gekwantificeerd via CT- en μCT-scan. De dissecties laten zien dat de spieren in deze taxa zich gelijkaardig in het lichaam bevinden. Toch zien we ook dat er verschillen zijn die mogelijk gerelateerd kunnen worden aan de verschillen in voortbeweging. Hierbij zien we vooral dat deze verschillen voornamelijk kwantitatief zijn en zich tussen zowel functionele groepen als individuele

spieren bevinden. In de kwalitatieve configuratie van de spieren zien we minder verschillen tussen de verschillende taxa, maar juist veel binnen de taxa zelf.

De functie van het TMC gewricht heb ik onderzocht door gebruik te maken van kinematische analyses gebaseerd op CT-scanbeelden. Samen met mijn collega's heb ik een computationele aanpak ontwikkeld die ons toelaat om het bewegingsbereik van het TMC gewricht in de verschillende vlakken nauwkeurig te kwantificeren. De resultaten van deze analyse tonen significante verschillen aan tussen de taxa in het bewegingsbereik van het TMC gewricht.

Tot slot heb ik geavanceerde modeleertechnieken ontwikkeld en toegepast om informatie over de vorm en functie van het TMC gewricht te integreren. Ik heb onderzocht hoe stress in het TMC gewricht wordt verdeeld bij verschillende grepen. Vervolgens heb ik geanalyseerd hoe deze stressverdelingen verder door de interne botstructuur van het trapezium worden verwerkt. Ik heb een nieuwe, geïntegreerde aanpak ontwikkeld voor het modelleren van bot-interacties in het TMC gewricht tijdens grijpen. Door 'finite element' en 'micro-finite element' methodes te combineren in één aanpak kon ik modellen genereren om de stressverdelingen in het gewricht en door het bot heen tussen de taxa te vergelijken. De resultaten tonen aan dat de botstructuur van deze taxa voldoende aangepast is om de verschillende grepen uit te voeren die we in dit onderzoek hebben bestudeerd. Daarnaast biedt deze geïntegreerde, modelmatige aanpak ook mogelijkheden om andere omstandigheden, zoals andere belastingen, te testen; ook in andere taxa en andere gewrichten.

Deze multidisciplinaire aanpak voor het bestuderen van de morfologie en biomechanica van de duim stelt ons in staat om inzicht te krijgen in de functionele adaptatie van de duim in primaten. Het project geeft gedetailleerde kennis over de anatomie van primaten die onder-gerepresenteerd zijn in de literatuur. Als laatste brengt het nieuwe inzichten in de biomechanica van het TMC gewricht met betrekking tot de functie, maar ook in de functionele adaptatie van de duim in primaten. Deze thesis levert hiermee een belangrijke bijdrage aan de missende anatomische en biomechanische informatie binnen de niet-menselijke primaten, wat vervolgens in toekomstig werk op verschillende niveaus kan worden gebruikt als basis voor evolutionaire interpretatie.

List of abbreviations

με	micro strain
μm	micrometre
μCT	micro computed tomography
μFE	micro finite element
ε_{yield}	yield strain
2D	two dimensional
3D	three dimensional
CSCS	Swiss National Supercomputing Centre
CT	computed tomography
DFOV	display field of view
FE	finite element
GPa	giga Pascal
ICP	iterative closest point
IP	interphalangeal
IUCN	International Union for Conservation of Nature
JOKE	joint kinematic analysis suite
MC	metacarpal
MCP	metacarpophalangeal
mm	millimetre
MPa	mega Pascal
MTU	muscle-tendon unit
PA	pennation angle
PCSA	physiological cross-sectional area
Power L	large diameter power grasp with the thumb abducted
Power LA	large diameter power grasp with the thumb adducted

Power LE	large diameter power grasp with the thumb extended
Power S	small diameter power grasp with the thumb abducted
Pp	*Pan paniscus*
Pt	*Pan troglodytes*
RBF	radial basis function
RMSE	root mean square error
STL	stereolithography
TMC	trapeziometacarpal

Ligaments

AOL	anterior oblique ligament
DCL	dorsal central ligament
DIML	deep intermetacarpal ligament
DRL	dorsoradial ligament
IML	intermetacarpal ligament
POL	posterior oblique ligament
UCL	ulnar colateral ligament

Muscles

m.	*musculus*
mm.	*musculi*
ADM	*m. abductor digiti minimi*
ADP	*m. adductor pollicis*
APB	*m. abductor pollicis brevis*
APL	*m. abductor pollicis longus*
BR	*m. brachioradialis*
ECRB	*m. extensor carpi radialis brevis*

ECRL	*m. extensor carpi radialis longus*
ECU	*m. extensor carpi ulnaris*
ED	*m. extensor digitorum*
EDM	*m. extensor digiti minimi*
EI	*m. extensor indices*
EPL	*m. extensor pollicis longus*
FBP	*m. flexor brevis profundi*
FCR	*m. flexor carpi radialis*
FCU	*m. flexor carpi ulnaris*
FDM	*m. flexor digiti minimi*
FDP	*m. flexor digitorum profundus*
FDS	*m. flexor digitorum superficialis*
FPB	*m. flexor pollicis brevis*
IM	*m. intermetacarpalis*
IOD	*m. interosseous dorsalis*
IOP	*m. interosseous palmaris*
LUMB	*m. lumbricalis*
ODM	*m. opponens digiti minimi*
OPP	*m. opponens pollicis*
PB	*m. palmaris brevis*
PL	*m. palmaris longus*
PT	*m. pronator teres*
PQ	*m. pronator quadratus*

General Introduction

Thesis motivation

The hand has played a crucial role in the evolutionary development of the primate taxonomic order. Its versatility as both a locomotor and a prehensile organ has allowed for many primate genera to thrive in a broad range of habitats, from terrestrial to arboreal, a combination of the two, or even fully urban lifestyles (Napier and Napier, 1967; Larson, 2018). The hands are one of the primary anatomical structures to interact with the environment (Napier *et al.*, 1993). Such frequent interactions require them to be optimally adapted to handle any challenge that they may face in their habitat. The modern human hand is a peculiar example of this. The absence of a primary locomotor function allowed the human hand to specialize towards the dextrous prehensility that facilitates the creation and use of tools (Lovejoy, 1988). This development, together with the increasing size of the brain, has had an immense impact on the evolutionary success of early hominins and by extension the modern humans, although the exact roles being played are still debated (Higuchi *et al.*, 2009; Stout and Chaminade, 2012; Biro, Haslam and Rutz, 2013; Teschke *et al.*, 2013). This also makes the primate hand such an interesting structure for the study of evolutionary adaptation; as primate species along a relatively small phylogenetic span display hands that appear adapted to their own specific environmental requirements in a variety of ways (Kivell *et al.*, 2016). There are numerous primates that, similarly to humans, are capable of complex manual tasks, even when they also use their hands in varying modes of locomotion (Christel, 1993; Marzke, 1997; Pouydebat *et al.*, 2008). Some of these species are the modern human's closest living relatives, i.e. non-human apes such as bonobos, chimpanzees, gorillas, orangutans, and gibbons, but also other Old World Monkeys like macaques and baboons (van Horn, 1972; Jordan, 1982; Toth *et al.*, 1993; Colell, Segarra and Pi, 1995; Marzke, 1997; Marzke and Marzke, 2000; Macfarlane and Graziano, 2009; Pouydebat *et al.*, 2009; Neufuss, Humle, *et al.*, 2017).

A key element in the versatility of the primate hand is the thumb, especially for its defining role in prehensility (Napier, 1956). The thumb, in most primates, is fully or at least partly opposable, allowing interaction with the other digits to form various grasps, from forceful power grasps to careful precision grips (Christel, 1993). It is a perplexing structure given that specific morphological adaptations to its broad functional repertoire appear to conflict with one another; the thumb needs to be mobile to facilitate dextrous movements required for precise manipulation, while it also needs to be stable enough to withstand heavy loading during strong grasps. In humans, most of this interplay of form and function takes place in the thumb's basal articulation (Napier, 1955; Cooney *et al.*,

1981). Here, the bone of the mid-hand, the first metacarpal (MC1), articulates with the trapezium, one of the wrist or carpal bones. The human trapeziometacarpal (TMC) joint has a unique saddle-shaped morphology that allows considerable movement in two planes, but also offers some restriction as the reciprocal concave-convex surfaces interlock (Cooney and Chao, 1977). In combination with its surrounding muscle and ligaments, the human TMC joint allows a large mobility of the thumb while also providing stabilization. An in depth understanding of the functioning of the TMC joint in other primates remains, however, largely lacking (Rafferty, 1990; Rose, 1992).

The human thumb plays an important role in daily activities. Due to the thumb's impact on daily life, the functional anatomy and biomechanics of the human thumb have been studied extensively (Ladd *et al.*, 2014; Crisco *et al.*, 2015; Halilaj *et al.*, 2015; Schneider *et al.*, 2015; Dourthe *et al.*, 2016; D'Agostino *et al.*, 2017; Kerkhof *et al.*, 2018). Much of the literature is from a medical perspective, investigating the form and function of the thumb to improve prevention, diagnosis, and treatment of thumb pathologies. But evolutionary questions have also shaped analyses; there are many anthropological and paleo-anthropological studies have investigated the hand and thumb and how their morphology relates to behaviour in not only modern humans, but also in our hominin relatives (e.g. Rafferty, 1990; Rose, 1992; Marzke, 1997; Feix et al., 2015; Skinner et al., 2015; Marchi et al., 2017). By expanding our research to living primate taxa, we can study hand and thumb morphology and function in a much broader context and establish form-function relationships that can be used to infer function in extinct species. Fossil remains can be analysed to infer function, behaviour, and how the hand and thumb may have changed into the structures we see in humans today.

Since anthropological research is humanly-centred, much of our knowledge on our closest family members is severely limited. Moving on from studying mostly one species to a whole phylogenetic tree of primates exponentially expands the amount of knowledge to be gained. Furthermore, some of these species are critically endangered and declining, possibly denying us the chance to study them in this broad context ever again (Fruth *et al.*, 2016; IUCN, 2020a, 2020b). For this project, my colleagues and I were able to acquire cadaveric specimens from three nonhuman primate taxa (**Fig. 1**); bonobos (*Pan paniscus,* which belongs to the great apes (Fam. Hominidae), like chimpanzees, gorillas, orangutans, and humans), gibbons (Fam. Hylobatidae or lesser apes), and rhesus macaques (*Macaca mulatta,* Fam. Cercopithecidae). Despite their close relationship to humans, and to each other (parvorder Catarrhini) (**Fig. 2**), all three inhabit different habitats and employ different modes of locomotion. Bonobos are semi-arboreal knuckle walkers, gibbons are

highly arboreal brachiators, and rhesus macaques are semi-terrestrial palmi- and digitigrade quadrupeds. These differences in locomotor repertoire come with differences in morphology, which also affects hand use. This allows us to study a variety of hand morphologies and functions across a relatively small phylogenetic gap, while remaining relevant for adaptation in modern humans. The hypothesis is that the integration of manipulation and locomotion has had different adaptive consequences for the TMC joint in each of these taxa. In this project, I aim to identify what the morphological and functional differences are between the TMC joint of bonobo, gibbons, and macaques, and how these relate to the functional repertoires in these primates.

General background

The primate taxa

The bonobo

The bonobo (*Pan paniscus*) and the chimpanzee (*Pan troglodytes*) are the two species of African great apes that form the genus *Pan*. Both are considered to be modern human's closest living relatives, as their common ancestor split from the modern human line 5 to 7 million years ago and they share a largely similar genome (Prüfer *et al.*, 2012). The bonobo is considered by some researchers to be a better model for evolutionary comparison with modern humans due to its adaptative stasis in contrast to the chimpanzee (Diogo, Molnar and Wood, 2017), although it could be argued that there is no such thing as a model species among extant non-human primates. Bonobos are only found south of the Congo river in the Democratic Republic of Congo. Presumably, the common chimpanzee/bonobo ancestor was separated about 2 million years ago by the river, leading to speciation (Fischer *et al.*, 2011). Despite their similarities, bonobos clearly deviate morphologically when compared to the four subspecies of chimpanzee (Gonder *et al.*, 2011). The bonobo is more gracile and childlike, with smaller and rounder crania (Zihlman and Cramer, 1978; Coolidge and Shea, 1982), and longer and more muscular legs (Zihlman, 1984, 1996) than chimpanzees. Skeletal distinctions have been reported in both the proportions of the pectoral and pelvic girdle, supporting the more narrow appearance of the bonobo (Zihlman and Cramer, 1978). The bonobo's social behaviour is also strikingly different. Whereas chimpanzees are male-dominated and relatively aggressive, bonobo males are far less competitive and largely subordinate to females (Manson, Perry and Parish, 1997; Hare, Wobber and Wrangham, 2012; Gruber and Clay, 2016). The global bonobo population is relatively small and remote

from human access, and their IUCN red-list status is currently endangered (Fruth *et al.*, 2016). The captive population of bonobos is likewise restricted. Due to the small wild and captive populations, far less is known about their behaviour and morphology when compared to the chimpanzee. While there are multiple studies on the anatomy of the chimpanzee (Tuttle, 1969; Marzke, 1997; Thorpe *et al.*, 1999; Myatt *et al.*, 2012; Almécija, Smaers and Jungers, 2015; Lesnik, Sanz and Morgan, 2015), only a few dissections documenting the musculoskeletal anatomy of the bonobo have been performed (Miller, 1952; Vereecke et al., 2005; Payne et al., 2006a; Payne et al., 2006b; Myatt et al., 2012; Diogo et al., 2017), and biomechanical studies on the bonobo hand were scarce up until the start of this thesis (Samuel *et al.*, 2018; Synek, Lu, *et al.*, 2019; Synek *et al.*, 2020).

The bonobo's natural habitat is a non-homogenous, tropical rainforest (Hashimoto *et al.*, 1998), where they combine various arboreal locomotor modes such as suspensory locomotion, vertical climbing and quadrumanous scrambling (Doran, 1993), with terrestrial knuckle-walking and occasional bipedalism (D'Aout *et al.*, 2004). During chimpanzee knuckle-walking, substrate interaction only occurs through the knuckles of digits 2 to 4, and the short thumb remains unloaded (Tuttle, 1967; Wunderlich and Jungers, 2009; Thompson, 2020). There are no studies documenting loading of the digits in knuckle walking bonobos, but the similar hand and finger proportions in bonobos and chimpanzees leads us to assume no difference between both species. The bonobo thumb is thus only engaged during grasping, in arboreal locomotion, or in manipulation. Neufuss and colleagues showed that other knuckle-walkers, i.e. chimpanzees and gorillas, use their thumb in vertical locomotion (Neufuss, Robbins, *et al.*, 2017). Samuel et al (2018) tested three types of grasping used by bonobos; all relatively large diameter grasps with the thumb adducted, extended, and mostly abducted. The results showed that the thumb was involved in all tested cases of vertical and suspensory locomotion, however, thumb pressure levels were relatively low. This suggests that locomotor-related loading on the thumb is likely low in bonobos, and presumably not a strong selective pressure on thumb morphology. Although bonobos have a relatively short and gracile thumb, they are dexterous and capable of complex manual tasks (Jordan, 1982; Toth *et al.*, 1993; Colell, Segarra and Pi, 1995; Takeshita and Walraven, 1996; Ingmanson, 1998; Neufuss, Humle, *et al.*, 2017). Despite there being no reported cases of tool use in the wild, tool creation and use has been reported in semi-wild populations (Neufuss, Humle, *et al.*, 2017). Studies on captive bonobos have shown that they use a thumb-tip to side-index position (intermediate phalanx) during precise manipulation (Christel, 1993; Christel, Kitzel and Niemitz, 1998).

For this project, I was able to study a unique sample of nine bonobo specimens from captive populations. These specimens were obtained in collaboration with the Royal Zoological Society of Antwerp, Belgium, Frankfurt Zoo, Germany, La Vallée des Singes, Le Gureau, France, and Wilhelmina Zoo, Stuttgart, Germany. The animals died of natural causes and were collected opportunistically.

The gibbon

Gibbons and siamangs (Hylobatidae, hereafter referred to as gibbons) are highly arboreal apes, which diverged from the common hominoid ancestor about 16-22 million years ago (Perelman *et al.*, 2011; Carbone *et al.*, 2014). The taxonomy of the Hylobatidae is quite complex and has changed several times in the last decades. Currently, four genera are identified including about 20 species, Roos (2016) reported 19 species, but since then *Hooloch tianxing* was added (Fan *et al.*, 2017). The 2020 IUCN red list marks all 20 gibbon species as either endangered or critically endangered and the populations are rapidly decreasing (IUCN, 2020a). Although there has been some academic interest into gibbon anatomy and biomechanics (Schultz, 1933, 1937; Tuttle, 1967, 1969; Fleagle, 1976; Zihlman, Mootnick and Underwood, 2011), detailed studies remained limited in number. In the past 15 years, Vereecke and colleagues have published a series of publications on gibbon fore- and hindlimb anatomy (e.g. Vereecke et al. 2005, Channon et al., 2009; Michilsens et al. 2009), and on the biomechanics of brachiation, bipedalism, and leaping (e.g., Channon et al. 2010; Michilsens et al. 2012), but without a detailed appreciation of the form and function of the gibbon hand.



Figure 1: The taxa studied in this thesis; the bonobo, the gibbon, and the macaque. Photography by courtesy of Marie Vanhoof and Kristiaan D'Août.

Members of the family Hylobatidae inhabit the rainforests in South and South-East Asia (Matsudaira and Ishida, 2010). Their main form of locomotion is brachiation or arm-swinging through the forest canopy (Napier and Napier, 1967; Rumbaugh, 1976; Michilsens *et al.*, 2009). They spent almost all their time in the trees and are adapted to an arboreal lifestyle with long forelimbs and a relatively low body weight (Grabowski and Jungers, 2017). Their hands and fingers are elongated and their thumb is clefted deeper into the carpal complex making it function as a shorter thumb, to avoid interference during brachiation (Straus, 1942). While the thumb is not used in the hook-grip that is adopted in brachiation or arm-hanging, it is used in vertical climbing and manipulation (Carpenter, 1941; van Horn, 1972; Christel, 1993). Wide power grasps (with a heavily abducted thumb) are used during climbing, and in precision grasping the gibbon's thumb tip connects with the radial aspect of the index digit's proximal interphalangeal joint (Christel, 1993).

For this project, we were able to study eight gibbon specimens, including five different species from three genera (*Hylobates lar*, *Hylobates pileatus*, *Nomascus concolor*, *Nomascus leucogenys*, and *Symphalangus syndactylus*). These specimens were obtained in collaboration with the National Museum of Scotland, Edinburgh, Ghent University, Merelbeke, Belgium, the Zoological and Botanical Park of Mulhouse, France, and the Olmense Zoo, Olmen, Belgium. The animals died of natural causes and were collected opportunistically.

The macaque

When we chronologically move further back beyond Hylobatidae along the phylogenetic tree, the first family outside the apes (Superfamily Hominoidae) is its sister group of the Old World Monkeys (Fam. Cercopithecidae) (**Fig. 2**). The last common ancestor of cercopithecids and humans lived around 25 million years ago (Kumar and Hedges, 1998). The Old World Monkeys consist of 24 genera, split in two subfamilies (Cercopithecinae and Colobinae), comprising 156 extant species (Fleagle and Seiffert, 2017). They are all quadrupedal species that inhabit terrestrial, arboreal and urban habitats in Africa and Asia (Napier and Napier, 1970; Davies, 1994), although most Cercopithecinae are found in Africa. The exceptions are the approximatively 23 Cercopithecinae species that form the genus *Macaca,* which are found widely in Asia and south Europe (Gibraltar) in addition to North Africa (Lewis and Prongay, 2015; Roos and Zinner, 2015). The current IUCN status for macaques covers a wide spectrum; some species are endangered or critically endangered and decreasing, while a few other species are of least concern and stable

(IUCN, 2020b). The rhesus macaque (*Macaca mulatta*) is part of these least concern species and one of the most important non-human primates for biomedical studies (Daza-Vamenta, 2004; Gibbs *et al.*, 2007; Lin *et al.*, 2009; Lewis and Prongay, 2015). Due to this large scientific interest from the medical field, rhesus macaque research specimens are relatively easy to obtain but surprisingly little is known (or published) on the anatomy and biomechanics of the macaque musculoskeletal system.

Rhesus macaque populations cover a large geographical range in South Asia where they inhabit incredibly diverse environments, including urban areas (Lewis and Prongay, 2015; Roos and Zinner, 2015). They are a primarily palmigrade and digitigrade terrestrial quadruped species, meaning they walk on the flat of the hands or on hyperextended fingers respectively (Thompson, 2020). The thumb is mainly in contact with the substrate during palmigrade locomotion, where the thenar pad and the underlying TMC joint are also loaded (Patel and Wunderlich, 2010; Thompson *et al.*, 2018). Vertical climbing and arboreal behaviour are observed, but even in arboreal environments they often employ their digitigrade terrestrial mode by walking on top of the branches (Dunbar, 1989; Rawlins, 1993; Hayama, Chatani and Nakatsukasa, 1994). During vertical climbing, a small repertoire of relatively simple hand wraps and hooks, in which the thumb is mostly adducted, is used (Macfarlane and Graziano, 2009). Like in bonobos, the locomotor-related loading on the macaque thumb seems moderate, with likely higher functional demands compared to gibbons. Macaques are also capable of many complex types of grasps; during object manipulation a large variety of both simple and complex grasps are employed, including multiple power grasps and advanced precision grips (Macfarlane and Graziano, 2009).

For this study, we were able to use seven rhesus macaque specimens obtained in collaboration with Ghent University, Merelbeke, Belgium, and KU Leuven, Belgium, originating from medical laboratories. No animals were sacrificed for the purposes of this study, the specimens were obtained opportunistically.

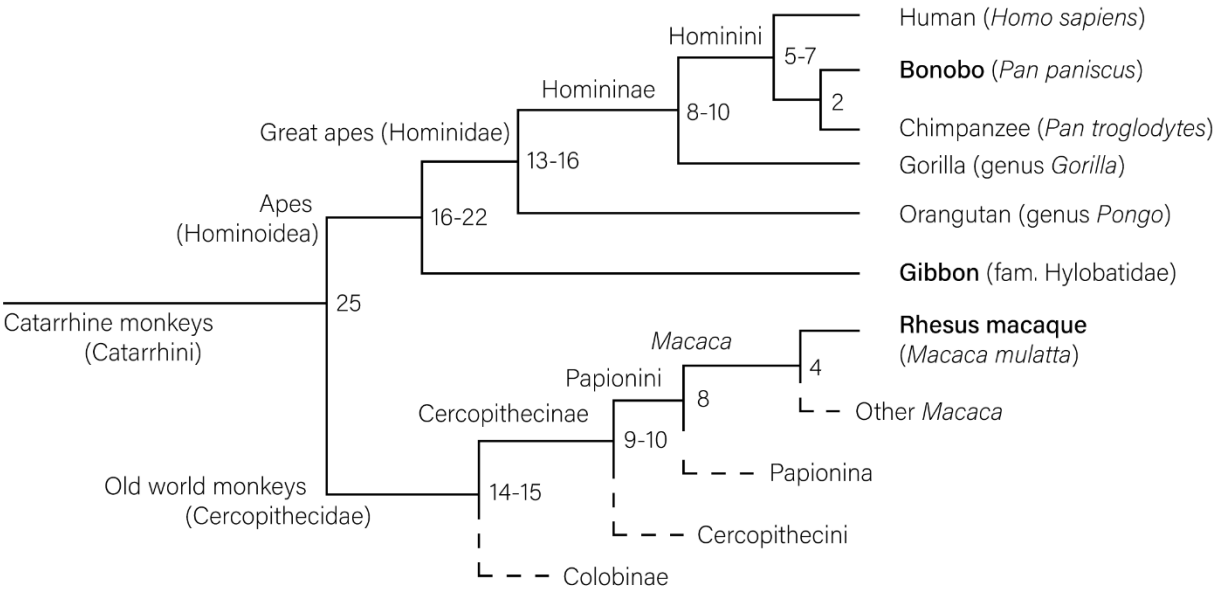

Figure 2: Catarrhine phylogeny. Main primate taxa used for this thesis are indicated in bold. Numbers indicate approximate time of split in million years ago. Figure generated from numbers reported in literature (Sibley and Ahlquist, 1984; Kumar and Hedges, 1998; Page, Chiu and Goodman, 1999; Fischer *et al.*, 2011; Perelman *et al.*, 2011; Prüfer *et al.*, 2012; Carbone *et al.*, 2014).

The primate hand, thumb, and the trapeziometacarpal joint

The hand

The hand has been recognized as a key organ, both in modern humans' daily activities as well as for any non-human primate. John Napier, who published many studies on primate hands, made a significant contribution to this field (Napier, 1952, 1955, 1956, 1960; Napier and Napier, 1967; Napier *et al.*, 1993). He recognised the importance of the thumb in grasping in modern humans and in other primates (Napier, 1952, 1955). Most later evolutionary studies on hand adaptation are based on his work and even clinical papers cite his publications. Since then, the primate hand has been the subject of many evolutionary studies, ranging from comparative morphology to biomechanical studies inferring behaviour from fossil remains (e.g. Susman, 1988; Rafferty, 1990; Marzke and Marzke, 2000; Tocheri et al., 2008; Orr et al., 2010; Kivell, 2016).

The active component of the functioning of the primate hand comes from the muscle and bone interaction of the musculoskeletal system in the forelimb. The blueprint for both hard- and soft tissue morphology is highly similar in primates, but the variations that do occur, be they qualitative or quantitative, reflect or are an adaptation to their specific niches in their respective habitats. As the vast majority of the available literature on the hand concerns the modern human, I will use the human condition to describe the general

morphology of the primate hand. As such it will serve as a reference for the bonobo, gibbon, and macaque. Note, however, that morphological variation occurs within species as well, and so for both the human description as well as other primates, there is no fixed blueprint for musculoskeletal morphology.

The hard tissue morphology are the bones that occupy the forelimb (**Fig. 3**). Starting from the elbow, we first encounter the two long bones that are the framework of the forearm, the *radius* and *ulna*. Proximally these bones connect to the *humerus* to form the hinge joint that is the elbow. The three articulations between them (proximal, distal, and via the *interosseus membrane*) allow the *radius* to rotate around the *ulna*, causing pronation and supination of the hand. As such, only the *radius* articulates distally with the *carpal complex* of the wrist to allow it to rotate separately from the *ulna* and the rest of the upper arm. The *carpal complex* forms the base of the hand. In humans, it consists of eight small bones situated in two rows of four. The proximal row from *radial* (thumb side) to *ulnar* (little finger side) consists of the *scaphoid, lunate, triquetrum,* and *pisiform*. While the distal row in the same order comprises the *trapezium, trapezoid, capitate,* and *hamate*. Some variations on the configuration of the carpals exist both within humans and in other primates (e.g. the non-fusion of the *scaphoid* and *os centrale* in gibbons and macaques, among other species (Kivell and Begun, 2007; Daver, Berillon and Grimaud-Hervé, 2012)). The distal carpal row articulates with five rays of *metacarpal* (MC) long bones that correspond with the five digits of the hand. Together with the surrounding soft tissue they form the palm of the hand. Each metacarpal articulates with a series of three tiny long bones, the *proximal, intermediate,* and *distal phalanges*. The only exception to this is the thumb, the first digit, which only has a *proximal* and *distal phalanx*.

As most of the prehensile abilities originate from within the hand, the relative dimensions of the MC's and phalanges is one of the key factors associated with prehensile capabilities. Having a relatively long thumb in comparison to other digits is related to grasping (Napier *et al.*, 1993; Lovejoy *et al.*, 2009; Almécija, Smaers and Jungers, 2015), and particularly the ratio between the first and the second digit plays a central role in the precision grasping (Christel, 1993). The human hand has relatively short fingers when compared to other primate species, but with a relatively long thumb at approximately 75% of index finger length (Almécija, Smaers and Jungers, 2015). In comparison, the thumb to index finger length is much smaller at approximately 42%, 47%, and 56% in bonobos, gibbons, and macaques respectively, and similarly so for other closely related primates (Napier and Napier, 1967; Marzke, 1971; Rafferty, 1990; Almécija, Smaers and Jungers, 2015).

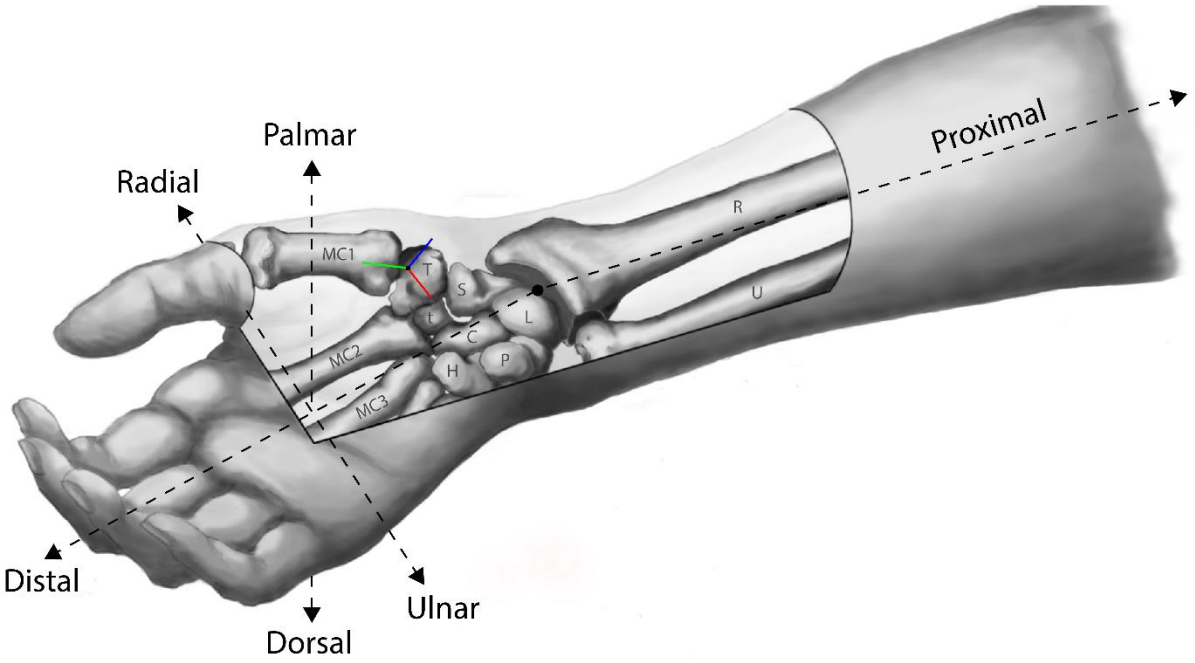

Figure 3: Illustration of a palmar view of a partly transparent human forelimb and the underlying internal skeletal structure. The image illustrates the anatomical planes used to describe the hand (Radial – Ulnar, or radioulnar; Dorsal – Palmar, or dorsopalmar; and Proximal – Distal, or proximodistal). The skeletal structure is represented here by the long bones of the forearm; the *radius* (**R**) and *ulna* (**U**); the eight carpal bones of the wrist: the *scaphoid* (**S**), *lunate* (**L**), *triquetrum* (behind the pisiform), *pisiform* (**P**), *hamate* (**H**), *capitate* (**C**), *trapezoid* (**t**), and *trapezium* (**T**). The **RGB** lines represent the coordinate system used for the TMC joint. Due to the unique position of the thumb within the hand, a separate coordinate system is used to define thumb motion, this coordinate system is described in detail in **Fig. 4**. Figure adapted from Kerkhof et al., (2018), illustration by Timo van Leeuwen.

The soft tissue that operates the bone of the hand is classified into functional groups. These functional muscle groups in the primate forearm and hand consist of flexors, extensors, deviators, and rotators. The general configuration of functional groups is similar across primates, but substantial variation occurs in relative size. Even within a species, variation in muscle configuration (qualitative) and dimensions (quantitative) can be substantial. Most muscles are classified and named after a specific function, but often muscles have a multitude of functions due to the antagonistic nature of the musculoskeletal system. Co-contraction or the absence of co-contraction of certain muscles can lead to more complex movements. For example, when both the superficial wrist flexors, the *musculus (m.) flexor carpi radialis* and *m. flexor carpi ulnaris,* are activated simultaneously, this causes wrist flexion, but activation of either of these muscles individually results in either radial or ulnar deviation of the wrist.

The functional groups are subdivided depending on region. Within the forearm we find the superficial wrist flexors (*m. flexor carpi radialis* and *m. flexor carpi ulnaris*), and extensors (*m. extensor carpi radialis* and *m. extensor capri ulnaris*), and the arm rotators (*m.*

brachioradialis, *m. pronator teres*, *m. pronator quadratus*, and *m. supinator*) that act upon the forearm. Here we also find the *extrinsic* muscles of the hand. The contractive bellies of the muscles are situated in the forearm, while the inserting tendons run over the carpal complex of the wrist to insert on the digits (or the palmar aponeurosis in the case of the *m. palmaris longus*, for those that have it (Thompson, Mockford and Cran, 2001)). The extrinsic muscles of the hand comprise the digital flexors (*m. flexor digitorum superficialis*, *m. flexor digitorum profundus*, and *m. flexor pollicis longus*) and the digital extensors (*m. extensor digitorum, m. extensor pollicis longus and brevis, m. extensor indicis, and m. extensor digiti minimi*). They also include the *m. abductor pollicis longus*, a separately classified muscle due to the unique position of the thumb.

The extrinsic and intrinsic muscles of the hand are the main muscles involved in grasping and manipulation. The large motions of the digits are controlled by the extrinsic digital flexors and extensors, while smaller digital excursions as well as joint stabilisation is mostly related to the intrinsic muscles which are fully situated within the hand. These are categorized into three groups; the thenar that operates the thumb (or first digit), the hypothenar that operates the little finger (fifth digit), and the intermediate or deep hand muscles for the mid-hand and second to fourth digits. The thenar includes the *m. flexor pollicis brevis*, *m. abductor pollicis brevis*, *m. adductor pollicis,* and *m. opponens pollicis*. The hypothenar comprises the *m. flexor digiti minimi, m. opponens digiti minimi, m. abductor digiti minimi,* as well the *m. palmaris brevis*. The intermediate hand muscles are three sets of muscles for each digit. A set a dorsal and palmar interosseus muscles (*m. interossei dorsalis* and *m. interosseus palmaris*), located between the metacarpals of the hand, and a lumbrical muscle (*m. lumbricalis*) that originates from the tendons of the *m. flexor digitorum profundus* and inserts onto the dorsal aponeurosis of each digit.

The thumb

The mobility of the primate thumb and the degree to which it can serve as a prehensile organ is determined by a set of morphological parameters: the position of the trapezium in the carpal complex (which determines the orientation of the distal trapezial joint facet and thus the orientation of the thumb relative to the fingers), the length of the thumb (relative to finger length), the thumb musculature, the trapeziometacarpal joint ligaments, and the 3D geometry of the metacarpophalangeal (MCP), interphalangeal (IP) and, in particular, the trapeziometacarpal (TMC) joint (Napier, 1952, 1955, 1960). The morphology of the TMC or basal thumb joint has been associated with the range of motion of the thumb and, as a result, with grip capability in different primate species (Rose, 1992).

In humans, the thumb is largely operated by nine muscles. The *m. flexor pollicis longus* and the *extensor pollicis longus,* which insert on the distal phalanx, affect the interphalangeal joint. The *m. extensor pollicis brevis* and *m. abductor pollicis longus* insert at the base of the first metacarpal (MC1), controlling motion at the base of the thumb at the TMC joint. Up to six additional tendon slips of the *m. abductor pollicis longus* that insert on the trapezium and other surrounding structures have been reported (van Oudenaarde, 1991). The thenar muscles and the first dorsal interosseus (*m. interosseus dorsalis I*) insert on the MC1, proximal phalanx base, and/or articular capsule of MCP joint. They control small excursions of the phalanges at the MCP joint, and larger motions at the TMC joint. Muscles and tendons that cross a joint are a large component of joint stabilisation (van Oudenaarde, 1991). The thenar originates from the flexor retinaculum, which is the connective tissue that forms the palmar aspect of the carpal tunnel of the wrist. The thenar muscles cover the base and shaft of the MC1 in a layered manner, with the *m. opponens pollicis* situated directly onto the MC1. Because the thenar muscles and the *m. abductor pollicis longus* tendon cover the TMC joint, muscle activation can not only cause motion, but provide joint stability as well.

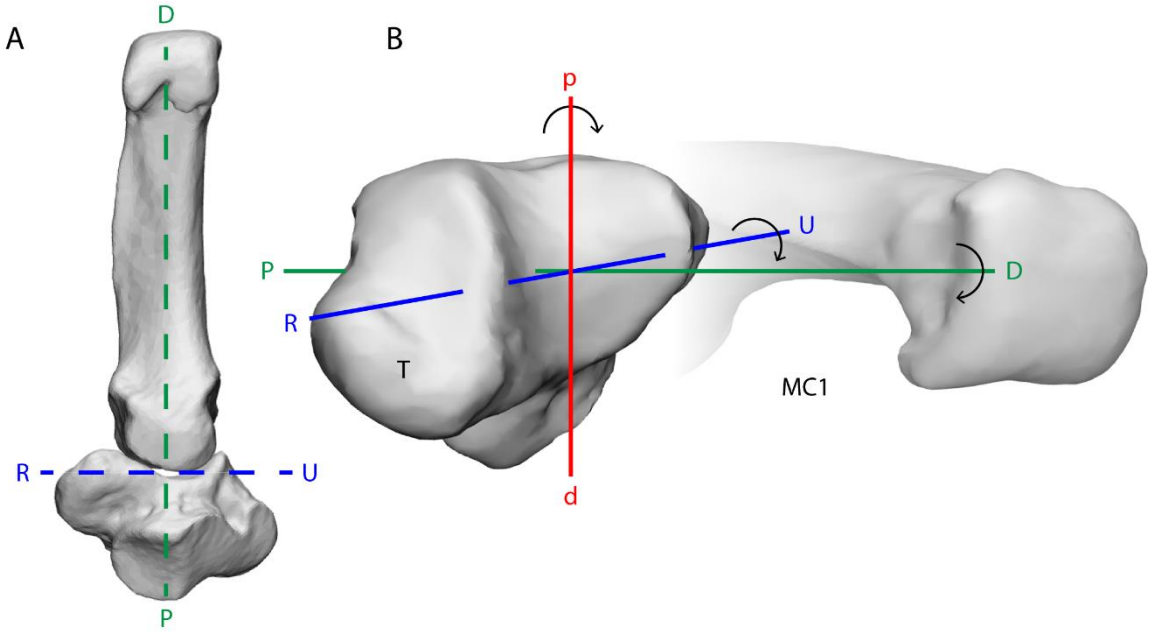

Figure 4: The bonobo left-hand TMC joint from palmar view (**A**), and from a radiodistal view (**B**). The coloured lines indicate the TMC joint principal axes of movement. **Red**: The dorsopalmar (**d-p**) axis, rotation along this axis results in palmar abduction and adduction of the thumb. **Blue**: The radioulnar (**R-U**) (thumb-to-little finger side) axis, rotation results in flexion and extension of the thumb. **Green**: the proximodistal (**P-D**) axis, rotation along this axis causes the thumb to rotate around its longitudinal axis (axial rotation).

The trapeziometacarpal joint

Although the hand and thumb have been of interest from an evolutionary perspective, biomechanical and anatomical studies have been mostly limited to analyses of fossils (Rafferty, 1990; Rose, 1992; Marzke, 1997; Marzke *et al.*, 2010; Feix *et al.*, 2015; Skinner *et al.*, 2015; Marchi *et al.*, 2017). But the importance of soft-tissue context has been more frequently stressed in evolutionary works published after the start of this project (Synek *et al.*, 2020; Karakostis *et al.*, 2021). In the clinical field, biomechanical studies on the TMC joint are much more common, but the main focus is on healthy function of the joint and pathologies. Due to the high impact of thumb pathologies, such as thumb osteoarthritis, on daily life, a large amount of clinical and biomechanical studies exist that form an excellent basis for understanding the non-modern human TMC joint (Ladd *et al.*, 2013, 2014; Crisco *et al.*, 2015; Halilaj *et al.*, 2015; Schneider *et al.*, 2015; Dourthe *et al.*, 2016; D'Agostino *et al.*, 2017; Kerkhof *et al.*, 2018; Ayhan and Ayhan, 2020).

The TMC joint in modern humans is the physiological equivalent of a universal joint (Cooney and Chao, 1977). This is a type of joint where the two opposing articular facets are reciprocal saddle-shaped facets. A perfect universal joint, when both surfaces are fully congruent, allows for only two degrees of freedom. Axial rotation (rotation about P-D in **Fig. 4**) is restricted while rotation in the other two planes is permitted. In practice, however, the human TMC joint is not perfectly congruent and some axial rotation is possible (Napier, 1955; Marzke, 1997). Motion at the TMC joint is operated by the extrinsic and intrinsic muscles of the thumb, the MC1 rotates about the free axes of the joint when the relevant muscles are activated while the trapezium is set within the carpal complex. Rotation about the dorsopalmar axis (**Fig. 4**: D-P) causes sideways movement of the MC1, and by extension the thumb; that is palmar abduction (away from the hand) or palmar adduction (towards the hand) in anatomical terms. Rotation about the radioulnar axis (**Fig. 4**: R-U) causes thumb extension or flexion. Furthermore, as the joint is not perfectly congruent, MC1 translation with respect to the trapezium is also possible. This technically means that the TMC joint has six degrees if freedom, but in practice the three degrees of translation are restricted by either passive or active stabilisation of the joint, unless the situation is pathological.

Stabilisation of the TMC joint comes in part from its congruent saddle-shaped morphology, which can be further increased actively with muscle activation (Napier, 1955). But is also passively reinforced by a configuration of ligament tissue. In modern humans, these are situated dorsally, palmarly, and ulnarly, while the radial aspect is restricted by the *m.*

abductor pollicis longus. The dorsal ligament complex (comprising the *dorsal radial ligament, dorsal central ligament,* and *posterior oblique ligament*) which resist dorsal subluxing forces that arise during power grips and pinches. Two volar ligaments (the *anterior oblique ligament* and *ulnar collateral ligament*) stabilize the thumb during extension to prevent palmar subluxation. On the ulnar side of the TMC joint, situated between the first and second metacarpal, are two ligaments (the *intermetacarpal ligament* and *deep intermetacarpal ligament*) that resist MC1 axial rotation as well as radial translation (Bettinger *et al.*, 1999).

The typical saddle-shaped TMC joint seen in modern humans is also found in bonobos and rhesus macaques. In comparison to humans and bonobos, however, the concavo-convex curvature of the macaque joint is more shallow (Rafferty, 1990). Gibbons are the only apes that deviate from the saddle-shaped pattern. Instead, the gibbon TMC joint is a ball-and-socket joint (Marzke, 1971), similar to the shoulder or hip joint. The ball-and-socket morphology allows for three degrees of freedom, and thus offers high mobility. However, it also comes with low intrinsic stability, therefore requiring more external structures for joint stabilisation to prevent dislocation (Rafferty, 1990).

Morphological adaptation

Use it or lose it

An important concept in morphological adaptation in organisms is a phenomenon that perhaps can be best described as the idea of "use it or lose it" (for a recent review on this subject, see Wisdom et al. (2015)). Living organisms are in a constant dynamic state of allocating resources to areas of the body that require them. But because these resources are finite, systems need to be prioritized. This occurs all over the body, but a clear example can be found in the muscular system. Humans that frequently use certain muscles, e.g. in sports or physical labour, will experience that these muscles will likely increase in size and become stronger (D'Antona *et al.*, 2006). The body is investing in them as they are perceived to be required for daily function. This increase in resource allocation is regulated in response to mechanical stimuli (Ferraro *et al.*, 2014). As soon as a person stops training the input of stimuli will cease, and these muscles will no longer be maintained at the same levels as before. This type of plastic adaptation occurs throughout the entire body.

Bone functional adaptation

In skeletal tissue this concept is known as functional bone adaptation (Kivell, 2016). On the tissue level, bone consists of two types of bone; cortical or compact bone, and cancellous, trabecular, or spongy bone (Currey, 2012) (**Fig. 4**). The external surface of any bone consists almost always entirely of cortical bone. This relatively dense tissue has a high stiffness that maintains the integrity of the structure. Bone, however, never fully consists of solid cortical bone. The internal structure is either hollow with the internal space occupied by bone marrow, as is usually the case with the diaphysis of long bones which has a medullar cavity, or an internal architecture of trabecular bone is present, like in the epiphyses of long bones, within flat bones, and within short bones such as the trapezium (Currey, 2012; Oftadeh *et al.*, 2015). In trabecular bone, only the lumina contain the bone marrow. The trabeculae within these bones serve as bony struts that reinforce the internal structure to withstand external loads. A trabecular system like this, as opposed to solid bone, increases bone stiffness over a hollow interior, while reducing the amount of resources to be allocated and minimizing weight. The effective stiffness of trabecular bone relies on the way the architecture is structured with respect to how external loads are applied (Currey, 2012). The trabecular struts are most effective when parallel to the load. These external loads, however, are not static. They are an amalgamation of various loading regimes. So similar to muscle tissue, bone can respond to mechanical stimuli via the resorption and/or deposition of bone to remodel the architecture (Huiskes *et al.*, 2000; Cowin, 2003; Ruff, Holt and Trinkaus, 2006; Eriksen, 2010; Currey, 2012). But bone adaptation is a slow process, and adaptation occurs mostly in response to prolonged or consistent stimuli. In this category, we find habitual loading, such as during daily tasks like locomotion or powerful grasping. While bone remodelling also occurs in cortical bone, it is most apparent in the internal trabecular architecture. The internal trabecular structure of bone therefore correlates with loading regimes and can be used to infer behaviour from skeletal tissue (Tsegai *et al.*, 2013; Stephens *et al.*, 2018; Dunmore *et al.*, 2019; Synek, Dunmore, *et al.*, 2019; Steiner, Synek and Pahr, 2020).

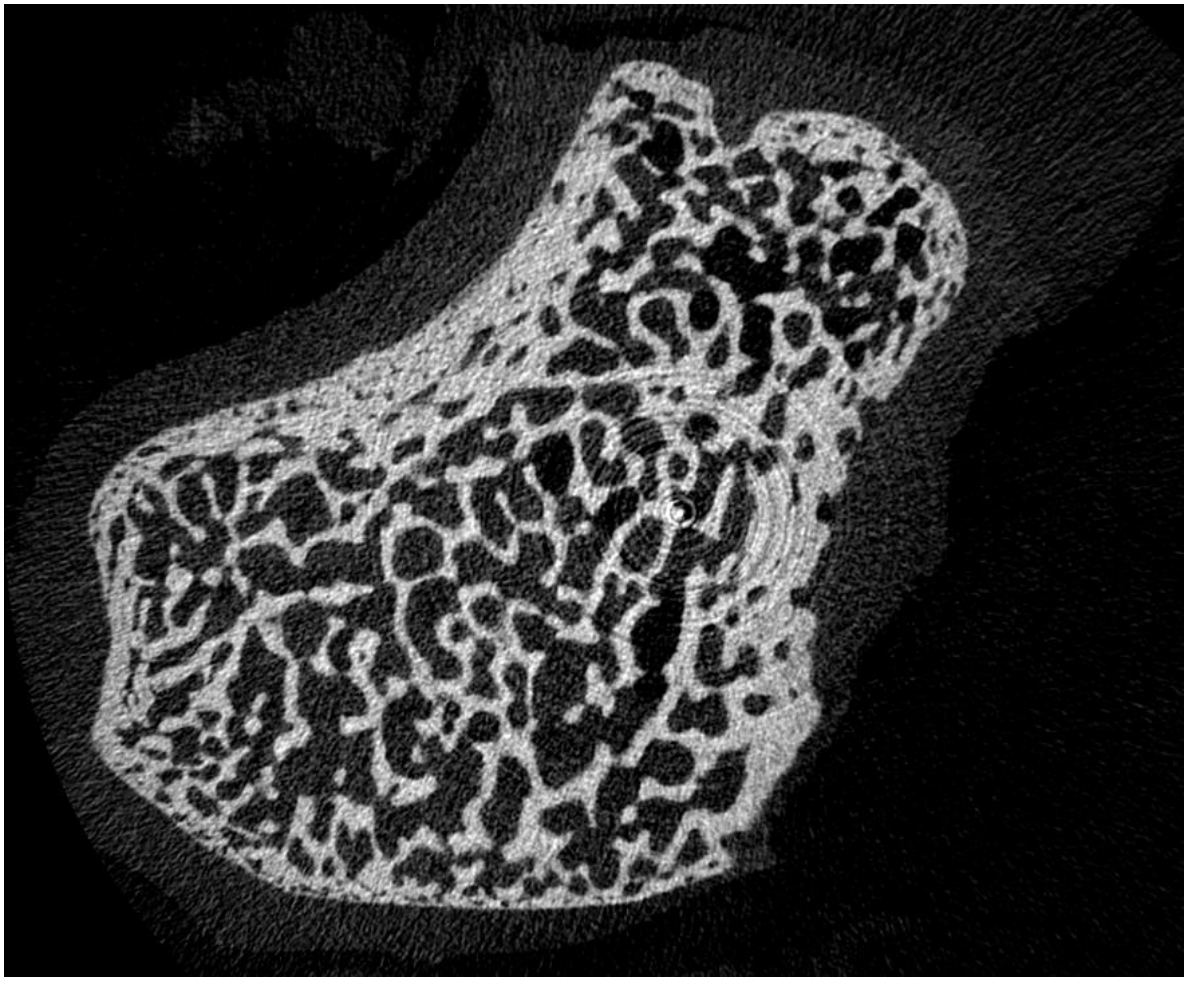

Figure 5: A slice through a bonobo trapezium visualizing the varying thickness of the outside layer of cortical or compact bone, and the internal architecture of trabecular, cancellous, or spongy bone.

Project objectives

Main goal and broad hypotheses

In the present thesis, my goal is to investigate the form and function of the primate thumb to study thumb adaptation in three distinct primate taxa. In doing so I aim to provide pieces of the puzzle for interpretation in an evolutionary context. To that end, I study the morphology and biomechanics of the TMC joint on multiple levels in the bonobo, the gibbon, and the macaque, three taxa with different functional repertoires. The main hypothesis is that the TMC joint in each of these taxa is morphologically adapted toward integrating the functional demands imposed by their specific locomotor mode and manipulation abilities. The goal is to characterize these morphological adaptations and how they influence function. The same specimens are used throughout the entire project, providing a large, multi-level data set for each specimen and allowing for better cross-study interpretation in the general discussion of this thesis.

Over the entire study I expect to find form and function adaptation related to each study taxon's locomotor type. For the gibbon this means adaptations to a highly arboreal lifestyle and relatively little thumb use in locomotion. I therefore expect the gibbon TMC joint to be highly mobile, with the capability of large ranges of motion, less restricting bone morphology due to the ball-and-socket morphology, and yet more restricting soft-tissue to compensate for this in joint stabilisation. The macaque is expected to be on the opposite of this spectrum. Due to their thumb use in palmigrade terrestrial locomotion I do expect adaptations to habitual loading. I expect more restricted ranges of motion, well developed stabilizing soft-tissue such as ligaments and thenar muscles, and resilient bone morphology. Finally, I expect the bonobo TMC joint to be intermediate on the mobility-stability spectrum, but leaning toward the restrictive side due to the involvement of the hand and thumb in vertical locomotion, as well as their relatively large body mass. I expect bonobos to have a mobile joint capable of large ranges of motion but with well-developed ligaments and musculature to reinforce this joint. The bone morphology is likely to be well equipped to withstand the higher loads due to their body mass, i.e. with a higher amount and density of trabeculae. To address the overall goal and test our hypotheses, six research objectives are determined.

Objective 1: To document the forelimb soft and hard tissue morphology through detailed dissections and medical imaging in order to provide a detailed anatomical dataset for bonobos, gibbons, and macaques.

Relatively little non-human primate anatomy has been documented in sufficient detail to facilitate a multi-level study of form and function. Muscle dissections usually focus on broad, full body documentation and lack the detail required for a focussed study of the hand and thumb. Hard tissue documentation in the form of medical imaging is more common, thanks to samples being available for scanning in museum collections. However, this means that the samples are often isolated skeletal elements, lacking the context of soft-tissue anatomy. Furthermore, available image data often lacks the resolution required for some of the detailed analyses intended in this project.

To address this lack of detailed morphological knowledge, my colleagues and I performed medical imaging and detailed dissections of the forelimb and hand in each of the three primate groups. In this way, we obtained a full quantitative dataset of forelimb musculature (although not fully included in this thesis), a detailed description of the TMC joint ligaments, and 3D geometry of the forelimb bones as well as highly detailed micro-CT scans of the individual elements of the TMC joint, the trapezium and MC1.

Objective 2: To compare morphological differences related to thumb function between the primate taxa.

The research focus of this second objective is based on the comparative anatomy between the three primate groups. The goal is to identify both quantitative and qualitative differences in anatomy that can be related to differences in function. The main difference between the primate groups is their locomotor repertoire, and how they combine that with manipulation. At this objective, the project starts to narrow in focus; I take a subsection of the total muscle data, and target only on the data relevant for thumb function. To allow for broader interpretation, comparisons are also made with the chimpanzee, and the modern human. Most of this information is based on the literature, but both one chimpanzee and one human specimen have also been included in this study, for comparison.

I hypothesize that the morphology of the thumb in all three primate groups is relatively well developed for manipulation purposes. This means well developed musculature to provide the required force-generating capacity, as well as a sufficiently mobile joint to allow for an opposable thumb. However, I also expect differences in morphology relating

to the differences in locomotor behaviour and habitual loading regimes on the thumb. For gibbons we know the ball-and-socket joint is highly mobile, and therefore I expect the soft-tissue that is involved in stabilizing the TMC joint, like ligaments, thenar muscles and the *m. abductor pollicis longus,* to be well developed. In bonobos I expect to find a saddle-shaped TMC joint similar to humans, that allows for a large range of motion, but with a strong development of thenar and thumb muscles to stabilize the joint. In macaques, I expect to find a saddle-shaped but shallow TMC joint, one that is relatively congruent, and surrounded by strong ligaments and well developed soft-tissue. These differences between taxa can be qualitative differences, such as the number and configuration of individual muscles or ligaments, or quantitative differences, such as differences in parameters like muscle volume or force generating capacity.

Objective 3: To investigate and compare the functional capabilities of the TMC joint in bonobos, gibbons and macaques.

We have a general idea of what the thumb is capable of in these three primate groups based on behavioural studies, observations in the wild, and joint morphology. An exact documentation of TMC joint capabilities in these primates, however, is lacking. All complex motions that the thumb is capable of are a combination of movements in the three principal directions of motion. To build a general understanding of the TMC joint function, we must understand what type of mobility the joint is capable of when isolated in these planes.

The focus of this objective is on joint mobility, and what restricts this mobility. My colleagues and I use CT-based, kinematic analysis on isolated movements to investigate the ranges of motion the thumb is capable of in each plane. I compare the joint capabilities both intra- and interspecifically. As in the previous objective, I include data from chimpanzee and human TMC joints in these biomechanical studies for a broader interpretation. Large ranges of motion are an indication of a relatively mobile TMC joint, while small ranges of motion are an indication of that the joint is restricted. Data from the morphology chapter is used to interpret the levels of mobility found. I hypothesize that, although the thumb is used for manipulation in each of the studied primates, relative recruitment of the thumb in daily locomotor modes (or habitual loading regime) will define how mobile the thumb is. I expect the gibbon to have a highly mobile thumb. Due to the ball-and-socket TMC joint morphology, the excursion range may exceed that of modern humans. In bonobos, I expect to find large ranges of motion due to the similar TMC joint

morphology of humans, however, with the stability required for vertical climbing, it is likely that the mobility of the bonobo thumb is lower than that of humans. The macaque TMC joint is expected to be highly restricted and so I expect small ranges of motion here.

Objective 4: To design and develop an integrated workflow to study trapezium internal stress distribution from simulated grasping positions.

Objective 4, 5, and *6* are based around form-function relationships and the concept of bone functional adaptation. Bone is a dynamic tissue that remodels itself in response to external stimuli. The trabeculae are assumed to be organized to withstand habitual loading patterns. To calculate the stress distribution in the trapezium bone (*Objective 6*), we can use micro finite element models (μFE). But before such a μFE model can be created, the loading regime associated with the different functional positions of the thumb must be calculated. This is done by creating five finite element models (FE) of the TMC joint, corresponding to five grasping positions, for each of the three primate groups (*Objective 5*).

In order to create these FE models for three primate groups in five positions, and to further integrate the resulting load distributions into μFE models, designing an efficient workflow is required. *Objective 4* is the design and development of an integrated workflow that builds the finite element models that yield TMC joint stress distribution which can subsequently be applied as boundary conditions for the micro finite element models that are used to evaluate internal stress distribution.

Objective 5: To determine how forces are distributed within the TMC joint during grasping, and how morphology influences the resulting stress patterns.

The articular surface of a joint is covered by hyaline cartilage and its 3D geometry facilitates smooth movement between skeletal elements. That does not mean, however, that the entire surface is fully in contact with the opposing articular surface at all times. Different positions of the thumb cause the MC1 to interact with different parts of the articular surface of the trapezium. How the two bones that form the joint interact is dependent on the position of the thumb, but also the curvature and congruency of the two joint surfaces.

In *Objective 5*, I investigate the TMC joint contact behaviour during five different grasping positions of the hand. I use parametric finite element models to simulate and compare each of these positions. From the resulting stress patterns, we derive how individual joint

morphology affects the function of the joint. I formulate hypotheses on the exact location of stress distribution per grasp and compare if these expected patterns are met in each taxa. I hypothesize that the stress distribution on the trapezial articular surface will be largely similar across grasp types and across the three primate groups. However, I also expect the stress patterns to reflect differences in joint morphology, both between primate groups and between individuals. In particular, I expect more disparate stress pattens based on the mobility of the joint. In gibbons, high joint mobility will allow for larger excursion of the thumb in each of the tested grasps, and therefore I expect larger differences in stress distribution between each grasp. The macaque TMC joint on the other hand, is expected to be more restricted and we expect to see smaller differences in stress distribution that correspond with each grasp type. For the bonobo, I expect to find stress patterns that fall in between those observed in gibbons and macaques.

In addition providing information on form-function interaction in the TMC joint, these stress distribution patterns will serve as force input for the μFE approach for *Objective 6*.

Objective 6: To investigate and compare the effect of different grasping types on the strain distributions in the trapezium

The focus of *Objective 6* the focus is on bone adaptation. My colleagues and I use micro CT (μCT) scans of the primate specimens' trapezia to create highly detailed volumetric finite element models. Each model is solved five times, each with a different applied load, determined for *Objective 5*, resulting in five different grasping positions of the hand. The goal is to evaluate the resulting stress patterns for bone regions subjected to high stress peaks. A well-adapted internal bone architecture distributes forces sufficiently to avoid high stress peaks that cause high amounts of strain and bone failure. As all tested grasps are theoretically part of the bonobo, gibbon, and macaque functional repertoire, my first hypothesis here is that the applied loads will not induce large enough strain levels to approach bone failure in any specimen and grasp combination. Furthermore, I am interested in how bone strain is distributed across the internal architecture between different grasps. I test the hypothesis that the loading regimes originating from different grasp types induce different strain distribution patterns within the internal architecture. But as the internal structure is expected to be similarly adapted to all grasps, similar overall strain magnitudes are expected between grasps.

Thesis outline

The thesis consists of eight chapters; a **General Introduction**, six research chapters (**Chapters 1 - 6**) organised into three parts, and a **General Discussion**. In the three research parts, I investigate form and function of the thumb and TMC joint in three primate taxa with increasing level of detail, from gross anatomy to joint level form and function, and converging at the trapezium bone microstructure.

Part 1 addresses **musculature of the forearm, hand, and thumb** through both quantitative and qualitative documentation of the gross anatomy in the upper limb. This part gives insight into the soft-tissue anatomy that is involved in the functioning of the hand and thumb, as well as the surrounding anatomy which up until this project either had not been investigated or had only scarcely been studied. This part addresses *Objectives 1* and *2*, and includes three published papers on the anatomy of the bonobo, gibbon, and macaque. All three papers were published under shared first authorship between myself and Marie Vanhoof (PhD student KU Leuven, 2017-2023), but as the gibbon and macaque papers have an interpretative narrative that focusses on the wrist instead of the thumb these publications are not included in this thesis. Discussion of the anatomical dataset, however, is part of this thesis and is included in the **General Discussion** with references to Vanhoof et al. (Vanhoof *et al.*, 2020; Vanhoof, van Leeuwen and Vereecke, 2020). The publication on the bonobo morphology has been included in this thesis as **Chapter 1**.

Part 2 focuses on the **form and function of the TMC joint**; how is the articulation shaped and what are the functional capabilities of the TMC joint in its principal planes of motion? The aim of this part is to investigate what the TMC joint is capable of in terms of maximal range of motion in each of the three taxa. In addition, we get a notion on which morphological elements, either hard or soft tissue, facilitate or restrict these capabilities. This part addresses *Objectives 1, 2,* and *3* and the includes in it are **Chapters 2** and **3** on the capabilities of the TMC joint in the bonobo, gibbon and macaque thumb.

Part 3 addresses the **trapezial morphology and load distribution** during different grasps. This part integrates form-function relationships which drive evolutionary adaptation. I investigated how the TMC joint distributes loads that are encountered during various types of grasping, and how the trapezium is morphologically adapted to process these forces. This part addresses *objectives 1, 4*, *5*, and *6* and includes **Chapters 4**, **5**, and **6** on stress distributions in the bonobo TMC joint, stress distributions in the bonobo trapezial bone architecture, and TMC joint force distribution and trapezium bone adaptation in gibbons and macaques.

Each part consists of multiple publications and/or manuscripts. **Chapter 1** was published in the *Journal of Anatomy* (van Leeuwen *et al.*, 2018). The gibbon and macaque anatomy was also published in the *Journal of Anatomy* as a comparative study, but in two parts; a quantitative and a qualitative paper (Vanhoof *et al.*, 2020; Vanhoof, van Leeuwen and Vereecke, 2020). **Chapter 2** was published in *The Biological Journal of the Linnean Society* (van Leeuwen *et al.*, 2019) as an invited publication based on a conference symposium, and **Chapter 3** is currently under revision at the *American Journal of Physical Anthropology*. **Chapter 4** was submitted to *PeerJ* and is also currently under revision. **Chapter 5** was submitted to *Journal of Biomechanics*. **Chapter 6** is the only chapter of the thesis that was not submitted for publication due to its explorative nature.

The methodology for each chapter was designed and completed for the first species, in this case the bonobo, before moving on to the next. This means that the methodology was always first designed and published for the bonobo, before it was applied to the gibbon, and after that the macaque. As a result, each chapter consists of a methodology focussed paper that discusses the bonobo only, while the second manuscript applies that same method but to the gibbon and macaque. The second manuscript, also references the previously published bonobo data, to allow for comparison and interpretation in an evolutionary context. The three parts are integrated and discussed in the context of adaption in the **General Discussion**.

References

Almécija, S., Smaers, J. B. and Jungers, W. L. (2015) 'The evolution of human and ape hand proportions', *Nature Communications*, 6(1), p. 7717. doi: 10.1038/ncomms8717.

Ayhan, Ç. and Ayhan, E. (2020) 'Kinesiology of the wrist and the hand', in *Comparative Kinesiology of the Human Body*. Elsevier, pp. 211–282. doi: 10.1016/B978-0-12-812162-7.00013-8.

Bettinger, P. C. *et al.* (1999) 'An Anatomic Study of the Stabilizing Ligaments of the Trapezium and Trapeziometacarpal Joint', *The Journal of Hand Surgery*, 24(4), pp. 786–798. doi: 10.1053/jhsu.1999.0786.

Biro, D., Haslam, M. and Rutz, C. (2013) 'Tool use as adaptation', *Philosophical Transactions of the Royal Society B: Biological Sciences*, 368(1630), p. 20120408. doi: 10.1098/rstb.2012.0408.

Carbone, L. *et al.* (2014) 'Gibbon genome and the fast karyotype evolution of small apes', *Nature*, 513(7517), pp. 195–201. doi: 10.1038/nature13679.

Carpenter, C. R. (1941) *A field study in Siam of the behavior and social relations of the gibbon (Hylobates lar)*. Baltimore, Md.: The Johns Hopkins Press.

Christel, M. (1993) 'Grasping techniques and hand preferences in Hominoidea', in Preuschoft, H. and Chivers, D. J. (eds) *Hands of Primates*. Vienna: Springer Vienna, pp. 91–108. doi: 10.1007/978-3-7091-6914-8_7.

Christel, M. I., Kitzel, S. and Niemitz, C. (1998) 'How precisely do bonobos (Pan paniscus) grasp small objects?', *International Journal of Primatology*, 19(1), pp. 165–193. doi: 10.1023/A:1020319313219.

Colell, M., Segarra, M. D. and Pi, J. S. (1995) 'Hand preferences in chimpanzees (Pan troglodytes), bonobos (Pan paniscus), and orangutans (Pongo pygmaeus) in food-reaching and other daily activities', *International Journal of Primatology*, 16(3), pp. 413–434. doi: 10.1007/BF02735795.

Coolidge, H. J. and Shea, B. T. (1982) 'External body dimensions of Pan paniscus and Pan troglodytes chimpanzees', *Primates*, 23(2), pp. 245–251. doi: 10.1007/BF02381164.

Cooney, W. P. *et al.* (1981) 'The kinesiology of the thumb trapeziometacarpal joint.', *The Journal of Bone & Joint Surgery*, 63(9), pp. 1371–1381. doi: 10.2106/00004623-198163090-00002.

Cooney, W. P. and Chao, E. Y. (1977) 'Biomechanical analysis of static forces in the thumb during hand function.', *The Journal of bone and joint surgery. American volume*, 59(1), pp. 27–36.

Cowin, S. C. (2003) 'Adaptive Elasticity: A Review and Critique of a Bone Tissue Adaptation Model', *Engineering Transactions*, Vol. 51, i, pp. 113–193.

Crisco, J. J. *et al.* (2015) 'In vivo kinematics of the trapeziometacarpal joint during thumb extension-flexion and abduction-adduction', *Journal of Hand Surgery*. Elsevier Inc, 40(2), pp. 289–296. doi: 10.1016/j.jhsa.2014.10.062.

Currey, J. D. (2012) 'The structure and mechanics of bone', *Journal of Materials Science*, 47(1), pp. 41–54. doi: 10.1007/s10853-011-5914-9.

D'Agostino, P. *et al.* (2017) 'In vivo biomechanical behavior of the trapeziometacarpal joint in healthy and osteoarthritic subjects', *Clinical Biomechanics*, 49, pp. 119–127. doi: 10.1016/j.clinbiomech.2017.09.006.

D'Antona, G. *et al.* (2006) 'Skeletal muscle hypertrophy and structure and function of skeletal muscle fibres in male body builders', *The Journal of Physiology*, 570(3), pp. 611–627. doi: 10.1113/jphysiol.2005.101642.

D'Aout, K. *et al.* (2004) 'Locomotion in bonobos (Pan paniscus): differences and similarities between bipedal and quadrupedal terrestrial walking, and a comparison with other locomotor modes', *Journal of Anatomy*, 204(5), pp. 353–361. doi: 10.1111/j.0021-8782.2004.00292.x.

Daver, G., Berillon, G. and Grimaud-Hervé, D. (2012) 'Carpal kinematics in quadrupedal monkeys: towards a better understanding of wrist morphology and function', *Journal of Anatomy*, 220(1), pp. 42–56. doi: 10.1111/j.1469-7580.2011.01448.x.

Davies, G. E. (1994) *Colobine monkeys: their ecology, behaviour and evolution*. Cambridge University Press.

Daza-Vamenta, R. (2004) 'Genetic Divergence of the Rhesus Macaque Major Histocompatibility Complex', *Genome Research*, 14(8), pp. 1501–1515. doi: 10.1101/gr.2134504.

Diogo, R. *et al.* (2017) *Photographic and Descriptive Musculoskeletal Atlas of Bonobos*. 1st edn. Springer International Publishing. doi: 10.1007/978-3-319-54106-8.

Diogo, R., Molnar, J. L. and Wood, B. (2017) 'Bonobo anatomy reveals stasis and mosaicism in chimpanzee evolution, and supports bonobos as the most appropriate extant model for the common ancestor of chimpanzees and humans', *Scientific Reports*. Springer US, 7(1), pp. 1–8. doi: 10.1038/s41598-017-00548-3.

Doran, D. M. (1993) 'Comparative locomotor behavior of chimpanzees and bonobos: The influence of morphology on locomotion', *American Journal of Physical Anthropology*, 91(1), pp. 83–98. doi: 10.1002/ajpa.1330910106.

Dourthe, B. *et al.* (2016) 'In vivo contact biomechanics in the trapeziometacarpal joint using finite deformation biphasic theory and mathematical modelling', *Medical Engineering & Physics*, 38(2), pp. 108–114. doi: 10.1016/j.medengphy.2015.11.003.

Dunbar, D. C. (1989) 'Locomotor behavior of rhesus macaques (Macaca mulatta) on Cayo Santiago.', *Puerto Rico health sciences journal*, 8(1), pp. 79–85.

Dunmore, C. J. *et al.* (2019) 'Metacarpal trabecular bone varies with distinct hand-positions used in hominid locomotion', *Journal of Anatomy*, p. Epub. doi: 10.1111/joa.12966.

Eriksen, E. F. (2010) 'Cellular mechanisms of bone remodeling', *Reviews in Endocrine and Metabolic Disorders*, 11(4), pp. 219–227. doi: 10.1007/s11154-010-9153-1.

Fan, P.-F. *et al.* (2017) 'Description of a new species of Hoolock gibbon (Primates: Hylobatidae) based on integrative taxonomy', *American Journal of Primatology*, 79(5), p. e22631. doi: 10.1002/ajp.22631.

Feix, T. *et al.* (2015) 'Estimating thumb-index finger precision grip and manipulation potential in extant and fossil primates', *Journal of The Royal Society Interface*, 12(106),

pp. 20150176–20150176. doi: 10.1098/rsif.2015.0176.

Ferraro, E. *et al.* (2014) 'Exercise-Induced Skeletal Muscle Remodeling and Metabolic Adaptation: Redox Signaling and Role of Autophagy', *Antioxidants & Redox Signaling*, 21(1), pp. 154–176. doi: 10.1089/ars.2013.5773.

Fischer, A. *et al.* (2011) 'Bonobos Fall within the Genomic Variation of Chimpanzees', *PLoS ONE*. Edited by E. Joly, 6(6), p. Epub. doi: 10.1371/journal.pone.0021605.

Fleagle, J. G. (1976) 'Locomotion and Posture of the Malayan Siamang and Implications for Hominoid Evolution', *Folia Primatologica*, 26(4), pp. 245–269. doi: 10.1159/000155756.

Fleagle, J. G. and Seiffert, E. R. (2017) 'The Phylogeny of Primates', in *Evolution of Nervous Systems*. Elsevier, pp. 1–34. doi: 10.1016/B978-0-12-804042-3.00061-0.

Fruth, B. *et al.* (2016) 'Pan paniscus', *The IUCN Red List of Threatened Species 2016*. doi: 10.2305.

Gibbs, R. A. *et al.* (2007) 'Evolutionary and Biomedical Insights from the Rhesus Macaque Genome', *Science*, 316(5822), pp. 222–234. doi: 10.1126/science.1139247.

Gonder, M. K. *et al.* (2011) 'Evidence from Cameroon reveals differences in the genetic structure and histories of chimpanzee populations', *Proceedings of the National Academy of Sciences*, 108(12), pp. 4766–4771. doi: 10.1073/pnas.1015422108.

Grabowski, M. and Jungers, W. L. (2017) 'Evidence of a chimpanzee-sized ancestor of humans but a gibbon-sized ancestor of apes', *Nature Communications*, 8(1), p. 880. doi: 10.1038/s41467-017-00997-4.

Gruber, T. and Clay, Z. (2016) 'A Comparison Between Bonobos and Chimpanzees: A Review and Update', *Evolutionary Anthropology: Issues, News, and Reviews*, 25(5), pp. 239–252. doi: 10.1002/evan.21501.

Halilaj, E. *et al.* (2015) 'Older asymptomatic women exhibit patterns of thumb carpometacarpal joint space narrowing that precede changes associated with early osteoarthritis', *Journal of Biomechanics*, 48(13), pp. 3634–3640. doi: 10.1016/j.jbiomech.2015.08.010.

Hare, B., Wobber, V. and Wrangham, R. (2012) 'The self-domestication hypothesis: evolution of bonobo psychology is due to selection against aggression', *Animal Behaviour*, 83(3), pp. 573–585. doi: 10.1016/j.anbehav.2011.12.007.

Hashimoto, C. *et al.* (1998) 'Habitat Use and Ranging of Wild Bonobos (Pan paniscus) at Wamba', *International Journal of Primatology*, 19(6), pp. 1045–1060. doi: 10.1023/A:1020378320913.

Hayama, S., Chatani, K. and Nakatsukasa, M. (1994) 'The Digitigrade Hand and Terrestrial Adaptation in Japanese Macaques', *Anthropological Science*, 102(Supplement), pp. 115–125. doi: 10.1537/ase.102.Supplement_115.

Higuchi, S. *et al.* (2009) 'Shared neural correlates for language and tool use in Broca's area', *NeuroReport*, 20(15), pp. 1376–1381. doi: 10.1097/WNR.0b013e3283315570.

van Horn, R. N. (1972) 'Structural Adaptations to Climbing in the Gibbon Hand', *American Anthropologist*, 74(3), pp. 326–334. doi: 10.1525/aa.1972.74.3.02a00050.

Huiskes, R. *et al.* (2000) 'Effects of mechanical forces on maintenance and adaptation of form in trabecular bone', *Nature*, 405(6787), pp. 704–706. doi: 10.1038/35015116.

Ingmanson, E. J. (1998) 'Tool-using behaviour in wild Pan paniscus: Social and ecological considerations', in Russon, A. E., Bard, K. A., and Parker, S. T. (eds) *Reaching Into Thought: The Minds of the Great Apes*. Cambridge University Press, p. 464.

IUCN (2020a) *Fam. Hylobatidae*, *The IUCN Red List of Threatened Species. Version 2020-3*.

IUCN (2020b) *Gen. Macaca*, *The IUCN Red List of Threatened Species. Version 2020-3*.

Jordan, C. (1982) 'Object manipulation and tool-use in captive pygmy chimpanzees (Pan paniscus)', *Journal of Human Evolution*, 11(1), pp. 35–39. doi: 10.1016/S0047-2484(82)80029-8.

Karakostis, F. A. *et al.* (2021) 'Biomechanics of the human thumb and the evolution of dexterity', *Current Biology*. doi: 10.1016/j.cub.2020.12.041.

Kerkhof, F. D. *et al.* (2018) 'Trapeziometacarpal stabilization through dorsoradial ligament reconstruction: An early post-surgery in vivo biomechanical analyses', *Journal of Orthopaedic Research®*, Manuscript. doi: 10.1002/jor.24103.

Kivell, T. L. (2016) 'A review of trabecular bone functional adaptation: what have we learned from trabecular analyses in extant hominoids and what can we apply to fossils?', *Journal of Anatomy*, 228(4), pp. 569–594. doi: 10.1111/joa.12446.

Kivell, T. L. *et al.* (2016) *The Evolution of the Primate Hand*. Edited by T. L. Kivell et al. New York, NY: Springer New York (Developments in Primatology: Progress and Prospects). doi: 10.1007/978-1-4939-3646-5.

Kivell, T. L. and Begun, D. R. (2007) 'Frequency and timing of scaphoid-centrale fusion in hominoids', *Journal of Human Evolution*, 52(3), pp. 321–340. doi: 10.1016/j.jhevol.2006.10.002.

Kumar, S. and Hedges, S. B. (1998) 'A molecular timescale for vertebrate evolution', *Nature*, 392(6679), pp. 917–920. doi: 10.1038/31927.

Ladd, A. L. *et al.* (2013) 'The thumb carpometacarpal joint: anatomy, hormones, and biomechanics.', *Instructional course lectures*, 62, pp. 165–79.

Ladd, A. L. *et al.* (2014) 'The 2014 ABJS Nicolas Andry Award: The Puzzle of the Thumb: Mobility, Stability, and Demands in Opposition', *Clinical Orthopaedics and Related Research®*, 472(12), pp. 3605–3622. doi: 10.1007/s11999-014-3901-6.

Larson, S. G. (2018) 'Nonhuman Primate Locomotion', *American Journal of Physical Anthropology*, 165(4), pp. 705–725. doi: 10.1002/ajpa.23368.

van Leeuwen, T. *et al.* (2018) 'Insights into the musculature of the bonobo hand', *Journal of Anatomy*, 233(3), pp. 328–340. doi: 10.1111/joa.12841.

van Leeuwen, T. *et al.* (2019) 'Mobility and structural constraints of the bonobo trapeziometacarpal joint', *Biological Journal of the Linnean Society*, 127(3), pp. 681–693. doi: 10.1093/biolinnean/bly162.

Lesnik, J. J., Sanz, C. M. and Morgan, D. B. (2015) 'The interdigital brace and other grips

for termite nest perforation by chimpanzees of the Goualougo Triangle, Republic of Congo', *American Journal of Physical Anthropology*, 157(2), pp. 252–259. doi: 10.1002/ajpa.22706.

Lewis, A. D. and Prongay, K. (2015) 'Basic Physiology of Macaca mulatta', in *The Nonhuman Primate in Nonclinical Drug Development and Safety Assessment*. Elsevier, pp. 87–113. doi: 10.1016/B978-0-12-417144-2.00006-8.

Lin, J. *et al.* (2009) 'A New Genetic Vaccine Platform Based on an Adeno-Associated Virus Isolated from a Rhesus Macaque', *Journal of Virology*, 83(24), pp. 12738–12750. doi: 10.1128/JVI.01441-09.

Lovejoy, C. O. (1988) 'Evolution of Human Walking', *Scientific American*. Scientific American, a division of Nature America, Inc., 259(5), pp. 118–125.

Lovejoy, C. O. *et al.* (2009) 'Careful Climbing in the Miocene: The Forelimbs of Ardipithecus ramidus and Humans Are Primitive', *Science*, 326(5949), pp. 70–70, 70e1-70e8. doi: 10.1126/science.1175827.

Macfarlane, N. B. W. and Graziano, M. S. A. (2009) 'Diversity of grip in Macaca mulatta', *Experimental Brain Research*, 197(3), pp. 255–268. doi: 10.1007/s00221-009-1909-z.

Manson, J. H., Perry, S. and Parish, A. R. (1997) 'Nonconceptive Sexual Behavior in Bonobos and Capuchins', *International Journal of Primatology*, 18(5), pp. 767–786. doi: 10.1023/A:1026395829818.

Marchi, D. *et al.* (2017) 'Morphological correlates of the first metacarpal proximal articular surface with manipulative capabilities in apes, humans and South African early hominins', *Comptes Rendus Palevol*, 16(5–6), pp. 645–654. doi: 10.1016/j.crpv.2016.09.002.

Marzke, M. W. (1971) 'Origin of the human hand', *American Journal of Physical Anthropology*, 34(1), pp. 61–84. doi: 10.1002/ajpa.1330340106.

Marzke, M. W. (1997) 'Precision grips, hand morphology, and tools', *American Journal of Physical Anthropology*, 102(1), pp. 91–110. doi: 10.1002/(SICI)1096-8644(199701)102:1<91::AID-AJPA8>3.0.CO;2-G.

Marzke, M. W. *et al.* (2010) 'Comparative 3D quantitative analyses of trapeziometacarpal joint surface curvatures among living catarrhines and fossil hominins.', *American journal of physical anthropology*. United States, 141(1), pp. 38–51. doi: 10.1002/ajpa.21112.

Marzke, M. W. and Marzke, R. F. (2000) 'Evolution of the human hand: Approaches to acquiring, analysing and interpreting the anatomical evidence.', *Journal of Anatomy*, 197, pp. 121–140. doi: 10.1046/j.1469-7580.2000.19710121.x.

Matsudaira, K. and Ishida, T. (2010) 'Phylogenetic relationships and divergence dates of the whole mitochondrial genome sequences among three gibbon genera', *Molecular Phylogenetics and Evolution*, 55(2), pp. 454–459. doi: 10.1016/j.ympev.2010.01.032.

Michilsens, F. *et al.* (2009) 'Functional anatomy of the gibbon forelimb: Adaptations to a brachiating lifestyle', *Journal of Anatomy*, 215(3), pp. 335–354. doi: 10.1111/j.1469-7580.2009.01109.x.

Miller, R. A. (1952) 'The musculature of pan paniscus', *American Journal of Anatomy*, 91(2), pp. 183–232. doi: 10.1002/aja.1000910202.

Myatt, J. P. *et al.* (2012) 'Functional adaptations in the forelimb muscles of non-human

great apes', *Journal of Anatomy*, 220(1), pp. 13–28. doi: 10.1111/j.1469-7580.2011.01443.x.

Napier, J. *et al.* (1993) *Hands*. Princeton University Press (Natural science).

Napier, J. R. (1952) 'The attachments and function of the abductor pollicis brevis.', *Journal of anatomy*, 86(4), pp. 335–41.

Napier, J. R. (1955) 'The form and function of the carpo-metacarpal joint of the thumb.', *Journal of anatomy*, 89(3), pp. 362–9.

Napier, J. R. (1956) 'The Prehensile Movements of the Human Hand', *The Journal of Bone and Joint Surgery. British volume*, 38-B(4), pp. 902–913. doi: 10.1302/0301-620X.38B4.902.

Napier, J. R. (1960) 'Studies of the hands of living primates', *Proceedings of the Zoological Society of London*, 134, pp. 647–657.

Napier, J. R. and Napier, P. H. (1967) *A Handbook of Living Primates: Morphology, Ecology and Behaviour of Nonhuman Primates*. Academic P.

Napier, J. R. and Napier, P. H. (1970) *Old world monkeys: evolution, systematics, and behavior: proceedings*. Academic Press.

Neufuss, J., Robbins, M. M., *et al.* (2017) 'Comparison of hand use and forelimb posture during vertical climbing in mountain gorillas (Gorilla beringei beringei) and chimpanzees (Pan troglodytes)', *American Journal of Physical Anthropology*, 164(4), pp. 651–664. doi: 10.1002/ajpa.23303.

Neufuss, J., Humle, T., *et al.* (2017) 'Nut-cracking behaviour in wild-born, rehabilitated bonobos (Pan paniscus): a comprehensive study of hand-preference, hand grips and efficiency', *American Journal of Primatology*, 79(2), pp. 1–16. doi: 10.1002/ajp.22589.

Oftadeh, R. *et al.* (2015) 'Biomechanics and Mechanobiology of Trabecular Bone: A Review', *Journal of Biomechanical Engineering*, 137(1). doi: 10.1115/1.4029176.

Orr, C. M. *et al.* (2010) 'Studying Primate Carpal Kinematics in Three Dimensions Using a Computed-Tomography-Based Markerless Registration Method', *The Anatomical Record: Advances in Integrative Anatomy and Evolutionary Biology*, 293(4), pp. 692–709. doi: 10.1002/ar.21137.

van Oudenaarde, E. (1991) 'Structure and function of the abductor pollicis longus muscle.', *Journal of Anatomy*, 174, pp. 221–227.

Page, S. L., Chiu, C. and Goodman, M. (1999) 'Molecular Phylogeny of Old World Monkeys (Cercopithecidae) as Inferred from γ-Globin DNA Sequences', *Molecular Phylogenetics and Evolution*, 13(2), pp. 348–359. doi: 10.1006/mpev.1999.0653.

Patel, B. A. and Wunderlich, R. E. (2010) 'Dynamic Pressure Patterns in the Hands of Olive Baboons (Papio anubis) During Terrestrial Locomotion: Implications for Cercopithecoid Primate Hand Morphology', *The Anatomical Record: Advances in Integrative Anatomy and Evolutionary Biology*, 293(4), pp. 710–718. doi: 10.1002/ar.21128.

Payne, R. C., Crompton, R. H., Isler, K., Savage, R., Vereecke, E. E., Günther, M. M., *et al.* (2006) 'Morphological analysis of the hindlimb in apes and humans. I. Muscle architecture', *Journal of Anatomy*, 208(6), pp. 709–724. doi: 10.1111/j.1469-7580.2005.00433.x-i1.

Payne, R. C., Crompton, R. H., Isler, K., Savage, R., Vereecke, E. E., G??nther, M. M., *et al.* (2006) 'Morphological analysis of the hindlimb in apes and humans. II. Moment arms', *Journal of Anatomy*, 208(6), pp. 725–742. doi: 10.1111/j.1469-7580.2006.00564.x.

Perelman, P. *et al.* (2011) 'A Molecular Phylogeny of Living Primates', *PLoS Genetics*. Edited by J. Brosius, 7(3), p. e1001342. doi: 10.1371/journal.pgen.1001342.

Pouydebat, E. *et al.* (2008) 'Evolution of grasping among anthropoids', *Journal of Evolutionary Biology*, 21(6), pp. 1732–1743. doi: 10.1111/j.1420-9101.2008.01582.x.

Pouydebat, E. *et al.* (2009) 'Biomechanical study of grasping according to the volume of the object: Human versus non-human primates', *Journal of Biomechanics*, 42(3), pp. 266–272. doi: 10.1016/j.jbiomech.2008.10.026.

Prüfer, K. *et al.* (2012) 'The bonobo genome compared with the chimpanzee and human genomes', *Nature*, 486(7404), pp. 527–531. doi: 10.1038/nature11128.

Rafferty, K. L. (1990) *The Functional and Phylogenetic Significance of the Carpometacarpal Joint of the Thumb in Anthropoid Primates*. New York University.

Rawlins, R. G. (1993) 'Locomotive and manipulative use of the hand in the Cayo Santiago macaques (Macaca mulatta)', in *Hands of Primates*. Vienna: Springer Vienna, pp. 21–30. doi: 10.1007/978-3-7091-6914-8_3.

Roos, C. (2016) 'Phylogeny and Classification of Gibbons (Hylobatidae)', in, pp. 151–165. doi: 10.1007/978-1-4939-5614-2_7.

Roos, C. and Zinner, D. (2015) 'Diversity and Evolutionary History of Macaques with Special Focus on Macaca mulatta and Macaca fascicularis', in *The Nonhuman Primate in Nonclinical Drug Development and Safety Assessment*. Elsevier, pp. 3–16. doi: 10.1016/B978-0-12-417144-2.00001-9.

Rose, M. D. (1992) 'Kinematics of the trapezium-1st metacarpal joint in extant anthropoids and Miocene hominoids', *Journal of Human Evolution*, 22(4–5), pp. 255–266. doi: 10.1016/0047-2484(92)90058-H.

Ruff, C., Holt, B. and Trinkaus, E. (2006) 'Who's afraid of the big bad Wolff?: "Wolff's law" and bone functional adaptation', *American Journal of Physical Anthropology*, 129(4), pp. 484–498. doi: 10.1002/ajpa.20371.

Rumbaugh, D. M. (1976) 'Suspensory behavior, locomotion, and other behaviors of captive gibbons, Gibbon and Siamang, a series of volumes on Lesser apes, vol. 4'. Karger, Basel, 316p.

Samuel, D. S. *et al.* (2018) 'Hand pressures during arboreal locomotion in captive bonobos (Pan paniscus)', *The Journal of Experimental Biology*, 221(8), p. jeb170910. doi: 10.1242/jeb.170910.

Schneider, M. T. Y. *et al.* (2015) 'Men and women have similarly shaped carpometacarpal joint bones', *Journal of Biomechanics*, 48(12), pp. 3420–3426. doi: 10.1016/j.jbiomech.2015.05.031.

Schultz, A. H. (1933) 'Observations on the Growth, Classification and Evolutionary Specialization of Gibbons and Siamangs (Concluded)', *Human Biology*. Johns Hopkins Press, 5(3), p. 385.

Schultz, A. H. (1937) 'Proportions, variability and asymmetries of the long bones of the limbs and the clavicles in man and apes', *Human Biology*. JSTOR, 9(3), pp. 281–328.

Sibley, C. G. and Ahlquist, J. E. (1984) 'The phylogeny of the hominoid primates, as indicated by DNA-DNA hybridization', *Journal of Molecular Evolution*, 20(1), pp. 2–15. doi: 10.1007/BF02101980.

Skinner, M. M. *et al.* (2015) 'Human evolution. Human-like hand use in Australopithecus africanus.', *Science (New York, N.Y.)*, 347(6220), pp. 395–9. doi: 10.1126/science.1261735.

Steiner, L., Synek, A. and Pahr, D. H. (2020) 'Comparison of different microCT-based morphology assessment tools using human trabecular bone', *Bone Reports*, 12, p. 100261. doi: 10.1016/j.bonr.2020.100261.

Stephens, N. B. *et al.* (2018) 'Trabecular bone patterning across the human hand', *Journal of Human Evolution*, 123, pp. 1–23. doi: 10.1016/j.jhevol.2018.05.004.

Stout, D. and Chaminade, T. (2012) 'Stone tools, language and the brain in human evolution', *Philosophical Transactions of the Royal Society B: Biological Sciences*, 367(1585), pp. 75–87. doi: 10.1098/rstb.2011.0099.

Straus, W. L. (1942) 'Rudimentary Digits in Primates', *The Quarterly Review of Biology*. University of Chicago Press, 17(3), pp. 228–243.

Susman, R. L. (1988) 'Hand function and tool behavior in early hominids', *Academic Press Journal of Human Evolution*, 35, pp. 23–36. doi: 10.1006/jhev.1998.0220.

Synek, A., Dunmore, C. J., *et al.* (2019) 'Inverse remodelling algorithm identifies habitual manual activities of primates based on metacarpal bone architecture', *Biomechanics and Modeling in Mechanobiology*, 18(2), pp. 399–410. doi: 10.1007/s10237-018-1091-y.

Synek, A., Lu, S.-C., *et al.* (2019) 'Musculoskeletal models of a human and bonobo finger: parameter identification and comparison to in vitro experiments', *PeerJ*, 7, p. e7470. doi: 10.7717/peerj.7470.

Synek, A. *et al.* (2020) 'Metacarpophalangeal joint loads during bonobo locomotion: model predictions versus proxies', *Journal of The Royal Society Interface*, 17(164), p. 20200032. doi: 10.1098/rsif.2020.0032.

Takeshita, H. and Walraven, V. (1996) 'A comparative study of the variety and complexity of object manipulation in captive chimpanzees (Pan troglodytes) and bonobos (Pan paniscus)', *Primates*, 37(4), pp. 423–441. doi: 10.1007/BF02381377.

Teschke, I. *et al.* (2013) 'Did tool-use evolve with enhanced physical cognitive abilities?', *Philosophical Transactions of the Royal Society B: Biological Sciences*, 368(1630), p. 20120418. doi: 10.1098/rstb.2012.0418.

Thompson, N. E. *et al.* (2018) 'Unexpected terrestrial hand posture diversity in wild mountain gorillas', *American Journal of Physical Anthropology*, 166(1), pp. 84–94. doi: 10.1002/ajpa.23404.

Thompson, N. E. (2020) 'The biomechanics of knuckle-walking: 3-D kinematics of the chimpanzee and macaque wrist, hand and fingers', *The Journal of Experimental Biology*, 223(14), p. jeb224360. doi: 10.1242/jeb.224360.

Thompson, N. W., Mockford, B. J. and Cran, G. W. (2001) 'Absence of the palmaris longus

muscle: a population study.', *The Ulster medical journal*, 70(1), pp. 22–4.

Thorpe, S. K. S. *et al.* (1999) 'Dimensions and moment arms of the hind- and forelimb muscles of common chimpanzees (Pan troglodytes)', *American Journal of Physical Anthropology*, 110(2), pp. 179–199. doi: 10.1002/(SICI)1096-8644(199910)110:2<179::AID-AJPA5>3.0.CO;2-Z.

Tocheri, M. W. *et al.* (2008) 'The evolutionary history of the hominin hand since the last common ancestor of Pan and Homo', *Journal of Anatomy*, 212(4), pp. 544–562. doi: 10.1111/j.1469-7580.2008.00865.x.

Toth, N. *et al.* (1993) 'Pan the Tool-Maker: Investigations into the Stone Tool-Making and Tool-Using Capabilities of a Bonobo (Pan paniscus)', *Journal of Archaeological Science*, 20(1), pp. 81–91. doi: 10.1006/jasc.1993.1006.

Tsegai, Z. J. *et al.* (2013) 'Trabecular bone structure correlates with hand posture and use in hominoids', *PLoS ONE*, 8(11). doi: 10.1371/journal.pone.0078781.

Tuttle, R. H. (1967) 'Knuckle-walking and the evolution of hominoid hands', *American Journal of Physical Anthropology*, 26(2), pp. 171–206. doi: 10.1002/ajpa.1330260207.

Tuttle, R. H. (1969) 'Quantitative and functional studies on the hands of the anthropoidea. I. The Hominoidea', *Journal of Morphology*, 128(3), pp. 309–363. doi: 10.1002/jmor.1051280304.

Vanhoof, M. J. M. *et al.* (2020) 'The forearm and hand musculature of semi-terrestrial rhesus macaques (Macaca mulatta) and arboreal gibbons (fam . Hylobatidae). Part II. Quantitative analysis', *Journal of Anatomy*, p. joa.13314. doi: 10.1111/joa.13314.

Vanhoof, M. J. M., van Leeuwen, T. and Vereecke, E. E. (2020) 'The forearm and hand musculature of semi-terrestrial rhesus macaques (Macaca mulatta) and arboreal gibbons (Fam. Hylobatidae). Part I. Description and comparison of the muscle configuration', *Journal of Anatomy*. John Wiley & Sons, Ltd, n/a(n/a). doi: 10.1111/joa.13222.

Vereecke, E. E. *et al.* (2005) 'Functional analysis of the foot and ankle myology of gibbons and bonobos.', *Journal of anatomy*, 206(5), pp. 453–76. doi: 10.1111/j.1469-7580.2005.00412.x.

Wisdom, K. M., Delp, S. L. and Kuhl, E. (2015) 'Use it or lose it: multiscale skeletal muscle adaptation to mechanical stimuli', *Biomechanics and Modeling in Mechanobiology*, 14(2), pp. 195–215. doi: 10.1007/s10237-014-0607-3.

Wunderlich, R. E. and Jungers, W. L. (2009) 'Manual digital pressures during knuckle-walking in chimpanzees (Pan troglodytes)', *American Journal of Physical Anthropology*, 139(3), pp. 394–403. doi: 10.1002/ajpa.20994.

Zihlman, A. (1996) 'Reconstructions reconsidered: chimpanzee models and human evolution', in *Great Ape Societies*. Cambridge University Press, pp. 293–304. doi: 10.1017/CBO9780511752414.023.

Zihlman, A. L. (1984) 'Body Build and Tissue Composition in Pan paniscus and Pan troglodytes, with Comparisons to Other Hominoids', in *The Pygmy Chimpanzee*. Boston, MA: Springer US, pp. 179–200. doi: 10.1007/978-1-4757-0082-4_8.

Zihlman, A. L. and Cramer, D. L. (1978) 'Skeletal Differences between Pygmy (Pan paniscus) and Common Chimpanzees (Pan troglodytes)', *Folia Primatologica*, 29(2), pp.

86–94. doi: 10.1159/000155830.

Zihlman, A. L., Mootnick, A. R. and Underwood, C. E. (2011) 'Anatomical Contributions to Hylobatid Taxonomy and Adaptation', *International Journal of Primatology*, 32(4), pp. 865–877. doi: 10.1007/s10764-011-9506-y.

Part 1.

Musculature of the forearm, hand, and thumb

In this part I address the soft tissue of the bonobo hand at the level of gross anatomy. Both the qualitative and quantitative documentation of the bonobo upper limb is provided in the following **Chapter 1**. Similarly, the musculature of the gibbon and macaque have also been documented for this project, but as they have been published under shared first authorship with Marie Vanhoof, these studies are not included as chapters in this thesis and are published as separate papers in *Journal of Anatomy*. The collected dataset, however, is part of the interpretation and will be referred to throughout the rest of the thesis and in the **General Discussion** as *Vanhoof et al. 2020,* and *Vanhoof, van Leeuwen, and Vereecke, 2020*. This chapter addresses *objective 1* and *objective 2* of the thesis.

Objective 1: To document the forelimb soft and hard tissue morphology through detailed dissections and medical imaging in order to provide a detailed anatomical dataset for bonobos, gibbons, and macaques.

Objective 2: To compare morphological differences related to thumb function between the primate taxa.

Chapter 1.

Insights into the musculature of the bonobo hand

Timo van Leeuwen*[1], Marie J.M. Vanhoof*[1], Faes D. Kerkhof[1], Jeroen M.G. Stevens[2,3], Evie E. Vereecke[1]

[1]Department of Development and Regeneration, KU Leuven, Belgium

[2]Centre for Research and Conservation, Royal Zoological Society Antwerp, Belgium

[3]Behavioural Ecology and Ecophysiology Group, University of Antwerp, Belgium

*joint first author

Published as:

van Leeuwen, T., Vanhoof, M. J. M., Kerkhof, F. D., Stevens, J. M. G., Vereecke, E. E. 2018, *Insights into the musculature of the bonobo hand*. Journal of Anatomy. 233, 3, pp. 328-340.

Abstract

The human hand is well known for its unique dexterity, largely facilitated by a highly mobile, long and powerful thumb that enables both tool manufacturing and use, a key component of human evolution. The bonobo (*Pan paniscus*), the closest extant relative to modern humans together with the chimpanzee (*Pan troglodytes*), also possesses good manipulative capabilities but with lower dexterity than modern humans. Despite the close phylogenetic relationship between bonobos and humans, detailed quantitative data of the bonobo forelimb musculature remains largely lacking. To understand how morphology may influence dexterity, we investigated the functional anatomy of the bonobo hand using a unique sample of eight bonobo cadavers, along with one chimpanzee and one human (*Homo sapiens*) cadaver. We performed detailed dissections of unembalmed specimens to collect quantitative datasets of the extrinsic and intrinsic hand musculature, in addition to qualitative descriptions of the forelimb muscle configurations, allowing estimation of force-generating capacities for each functional group. Furthermore, we used medical imaging to quantify the articular surface of the trapeziometacarpal joint to estimate the intra-articular pressure.

Our results show that the force-generating capacity for most functional groups of the extrinsic and intrinsic hand muscles in bonobos is largely similar to that of humans, with differences in relative importance of the extensors and rotators. The bonobo thumb musculature has a lower force-generating capacity than observed in the human specimen, while the estimated maximal intra-articular pressure is higher in bonobos. Most importantly, bonobos show a higher degree of functional coupling between the muscles of the thumb, index and lateral fingers than observed in humans. It is conceivable that differentiation and individualisation of the hand muscles rather than relative muscle development explain the higher dexterity of humans compared to bonobos.

Introduction

The thumb plays a key role in the functioning of the primate hand, known for its unprecedented dexterity. The modern human (*Homo sapiens*) hand is the prime example of such dexterity with a thumb fully devoted to manipulation. Despite the fact that non-human primates use their hand in locomotion and manipulation, many non-human primates also show advanced manipulative abilities, used in grooming and for processing food (e.g. capuchins (Spinozzi, Truppa and Laganà, 2004), orangutans, chimpanzees, and bonobos (Colell, Segarra and Pi, 1995; Furuichi and Thompson, 2008)) or for making and using tools (e.g. capuchins (Fragaszy *et al.*, 2004; Visalberghi *et al.*, 2009), gorilla (Breuer, Ndoundou-Hockemba and Fishlock, 2005), macaques (Gumert, Hoong and Malaivijitnond, 2011), chimpanzees and bonobos (Jordan, 1982; Toth *et al.*, 1993; Takeshita and Walraven, 1996; Boesch, Head and Robbins, 2009)). As the primate hand displays large varieties of phenotypes where form and function of the thumb are closely correlated, understanding these phenotypes in closely-related primate species may facilitate the interpretation of function in an evolutionary context. Despite the high importance of the thumb in human evolution, being key to the unique human dexterity, a complete understanding of the adaptive signals and form-function relationship in the primate thumb is lacking.

Within the extant primates, the bonobo (*Pan paniscus*) is one of the modern human's closest relatives, sharing approximately 98.7 percent of their genetic blueprint with modern humans (Prüfer *et al.*, 2012). The common *Homo-Pan* ancestor lived 7 to 13 million years ago (Young *et al.*, 2015), while the split in the genus *Pan* has to be situated between 2 and 1 million years (Myr) ago (Prado-Martinez, 2013; Kuhlwilm *et al.*, 2016). Both bonobos and chimpanzees possess a very diverse locomotor repertoire, but the thumb is predominantly used during arboreal locomotion (e.g. vertical climbing and quadrumanous scrambling) as their thumb is relatively short compared to the other fingers so that it is not involved during knuckle-walking. During manipulation and locomotion, they are capable of using both fine precision grips, in-hand manipulation, and forceful power grips, similar to humans (Christel, Kitzel and Niemitz, 1998; Crast *et al.*, 2009; Feix *et al.*, 2015; Bardo *et al.*, 2016). Additionally, they are capable of thumb opposition which seems to be facilitated by the saddle-shaped surfaces of the trapeziometacarpal (TMC) joint, as seen in modern humans (Marzke, 1997). Bonobos and chimpanzees favour precision grips in picking up small objects in which the thumb tip makes contact with the radial aspect of the index finger, from the distal to the proximal phalanx (Butterworth and Itakura, 1998; Christel, Kitzel and Niemitz, 1998). However, for grasping small objects, they do not always use their thumb whereas modern humans always use their thumb in precision gripping (Pouydebat *et al.*, 2009). For grasping large objects, bonobos and chimpanzees mostly use a power grip (Pouydebat *et al.*, 2009), but it does not provide the same accurate control as the power grip in modern humans (Marzke, Wullstein and Viegas, 1992). In

addition, both bonobos and chimpanzees are capable of using tools; a feature that has been observed both in captivity (Jordan, 1982; Toth *et al.*, 1993; Takeshita and Walraven, 1996) and in their natural environment (Ingmanson, 1998; Neufuss *et al.*, 2017).

While the anatomy of the chimpanzee hand has been studied in detail, based on dissections of approximately 50 arm specimens (e.g. (Tuttle 1969; Thorpe et al. 1999; Almécija et al. 2015; Lesnik et al. 2015; Myatt et al. 2012; Carlson & Lowe 2006; Oishi et al. 2009; Marzke 1997)), information about the bonobo hand musculature is limited (Miller 1952; Diogo et al. 2017a; Diogo et al. 2017b). Most previous studies focus only on hand proportions and external morphology of the hand and finger bones (Inouye, 1992; Alba, Moya-Sola and Kohler, 2003; Tocheri *et al.*, 2008; Almécija, Smaers and Jungers, 2015), while detailed quantitative data on the surrounding soft-tissue are largely missing in the literature.

In this study, we describe and quantify the extrinsic and intrinsic hand musculature of bonobos. We hypothesize that the bonobo hand, and specifically the thumb, musculature is relatively well developed, in terms of volume and force-generating capacity, possibly comparable to humans. Furthermore we expect morphological deviations from the human configuration that account for differences in the manipulative capabilities of the hand. Here we investigate if such deviations are present, and if they concern (a) quantitative differences in muscle volume and force-generating capacity, and/or (b) qualitative differences, such as muscle paths and other changes in muscle configuration, that have functional implications.

Materials and methods

Specimen selection

The hand and/or forearm of nine (sub)adult bonobos were obtained from different European zoos. All animals died of natural causes and were sampled opportunistically. The sample details are provided in **Table 1**. All specimens were stored at -18°C shortly after death and kept frozen until they were CT-scanned and dissected. Medical imaging (CT scanning) was obtained for all nine specimens while muscle data was obtained for eight of the nine animals; specimen Pp4 (Lomela; MIG12-29745517) was fixed in formaldehyde prior to freezing and it was impossible to dissect this specimen due to tissue dryness. in total, ten samples were dissected (forearm and hand (8/10) or only hand (2/10)) of which two samples of two specimens were dissected as part of the Bonobo Morphology Initiative which took place at the University of Antwerp in January 2016. As specimen Pp2 had been disarticulated at the elbow joint, not all of the extrinsic muscles could be quantified. The specimen has been included in the qualitative study for the muscles

present, but it has been excluded from the quantitative analysis as total muscle mass could not be determined.

Some cadaver hands showed musculoskeletal injuries (4/10), which is also indicated in **Table 1**. In two specimens, several distal phalanges were missing, either entirely (Pp7R: DP3) or partially (Pp7R: DP2 and 4; Pp8R: DP2 and 4). Soft-tissue at level of the fingers had already healed pre-mortem, but the extent of the scar tissue indicates repeated damage to the digits. In two other specimens, there was evidence of a dislocation at the metacarpophalangeal joint (Pp2L: MCP1) or trapeziometacarpal joint (Pp1R: TMC).

For comparison, anatomical data from a fresh-frozen chimpanzee (*Pan troglodytes*; Pt1) and a human cadaver (*Homo sapiens*, Hs1) are included. The chimpanzee specimen was obtained from Burger's Zoo, Arnhem (The Netherlands) and the human specimen was obtained via the Human Body Donation Program of the university. Both specimens were also dissected and CT-scanned.

CT scanning and image segmentation

Prior to dissection, the entire hand of each specimen (either the left or the right hand) was CT-scanned at the local hospital (AZ Groeninge, Kortrijk, Belgium) using a 64 slice Discovery HD 750 CT scanner (GE Healthcare, Little Chalfont, UK; Display Field of View [DFOV]: 250 mm, slice thickness: 0.625 mm, voxel size: 0.150 mm^3, 100 kV, 180 mA, 512x512).

The CT images were segmented manually using Mimics software (Mimics for Research 18.0, Materialise, Leuven) and 3D surface models of the trapezium and first metacarpal (MC1) were reconstructed to be able to measure the articular area of the trapeziometacarpal (TMC) joint. The articular area of the trapezium and MC1 was determined by manually delineating the border of the articular facet on each 3D bone model using 3-matic software (Materialise, Leuven). Articular area of the trapezium and MC1 were obtained from five bonobo specimens (Pp5, Pp6, Pp7, Pp8 and Pp9), from the chimpanzee (Pt1) and human (Hs1) and were used to estimate TMC joint pressure (see below).

Table 1: Specimen details

Code	Subject identifier	Sex	Age	Injury	Sample	Origin
Pp1	Dzeeta* 11957872	F	adult 31yr	TMC	R hand	Royal Zoological Society Antwerp, Belgium
Pp2	Zorba* 8365526	M	adult 35yr	MCP1	L forearm and hand	Wilhelma Zoo, Stuttgart, Germany
Pp3	X	?	adult	-	L hand	Royal Zoological Society Antwerp, Belgium
Pp4	Lomela MIG12-29745517	F	adult 17yr	-	no dissection, only CT	Royal Zoological Society Antwerp, Belgium
Pp5	Jasiri 15295295	F	sub-adult 8yr	-	L+R forearm and hand	Royal Zoological Society Antwerp, Belgium
Pp6	Kidogo MIG12-27564614	M	adult 25yr	-	L+R forearm and hand	Royal Zoological Society Antwerp, Belgium
Pp7	Ludwig MIG12-29882197	M	adult 32yr	DP2-3-4	R forearm and hand	Zoo Frankfurt, Germany
Pp8	Kirembo SB:177	M	adult 24yr	DP2 and 4	R forearm and hand	La Vallée des Singes, Le Gureau,
Pp9	Hermien* 27641621	F	adult 39yr	-	L forearm and hand	Wilhelma Zoo, Stuttgart, Germany
Pt1	Marlene 2082100004	F	adult 42yr	-	R forearm and hand	Burger's Zoo, Arnhem, The Netherlands
Hs1	692	M	adult 60yr	-	L forearm and hand	University of Leuven, Kortrijk, Belgium

*wild born, F: female, M: male, TMC: trapeziometacarpal joint, MCP: metacarpophalangeal joint, DP: distal phalanx.

Dissection procedure

The specimens were stored in freezers (-18°C) and were thawed at room temperature 24h-48h prior to the dissections. All muscles were isolated one by one and their origin and insertion were determined, using the same protocol as in previous anatomical studies (Vereecke *et al.*, 2005; Channon *et al.*, 2009). A complete dissection of the left and/or right forearm and hand was performed for five bonobo specimens (Pp5-9), but only one side per animal was included in the quantitative analysis. In addition, the left or right hand of three bonobo specimens (Pp1-3) were also carefully dissected. As such, the extrinsic hand musculature in five specimens and the intrinsic hand musculature in eight specimens could be quantified. Incidences for presence/absence of muscles could be obtained for all dissected arms (10 arms/hands from 8 bonobos).

For each muscle, the following parameters were measured: (1) muscle volume (V); (2) fascicle length (FL), which is the approximate length of the muscle fibres; and (3) pennation angle (PA), the average angle of the muscle fibres relative to the force-generating axis. Length measurements were taken to the nearest 0.1 mm with a digital calliper (Mitutoyo, UK, accurate to 0.01 mm) and muscle volume was determined to the nearest 0.1 ml by submersion in physiological saline solution (0.9% NaCl). Muscles were cut lengthwise along the tendon to determine muscle fascicle length and pennation angle. Digital photographs were taken of the muscles and pennation angle and fascicle length were measured using Fiji software (Schindelin *et al.*, 2012). The data provided for fascicle length and pennation angle are average values of at least three independent measurements taken on different places along the muscle belly.

Table 2: Functional muscle groups. *the PCSA of the muscles that are consistently crossing the TMC joint were included in the estimation of TMC joint pressure.

Muscle group	**Muscle**	**Abbreviation**	**Crossing TMC joint***
Extrinsic hand muscles			
wrist flexors	*m. flexor digitorum superficialis*	FDS	
	m. flexor digitorum profundus	FDP	only FDP1
	m. flexor carpi radialis	FCR	variable
	m. flexor carpi ulnaris	FCU	
	m. palmaris longus	PL	
	m. brachioradialis	BR	
Muscle group	**Muscle**	**Abbreviation**	**Crossing TMC joint***
wrist extensors	*m. extensor digitorum*	ED	
	m. extensor carpi radialis longus	ECRL	variable
	m. extensor carpi radialis brevis	ECRB	
	m. extensor digiti minimi	EDM	
	m. extensor carpi ulnaris	ECU	
	m. extensor indicis	EI	
arm rotators	*m. pronator teres*	PT	
	m. pronator quadratus	PQ	
	m. supinator	SUP	
thumb	*m. abductor pollicis longus*	APL	only APL I
	m. extensor pollicis longus	EPL	X
Intrinsic hand muscles			

thenar	*m. flexor pollicis brevis*	FPB	X
	m. abductor pollicis brevis	APB	X
	m. adductor pollicis	ADP	X
	m. opponens pollicis	OPP	X
intermediate	*m. intermetacarpalis I, II, III, IV*	IM	
	m. flexor brevis profundi III, IV, V, VI, VII, IIX, IX	FBP	
	m. interosseous dorsalis I, II, III	IOD	
	m. lumbricalis II, III, IV, V	LUMB	
hypothenar	*m. palmaris brevis*	PB	
	m. abductor digiti minimi	ADM	
	m. flexor digiti minimi	FDM	
	m. opponens digiti minimi	ODM	

Data analysis

Muscles were categorized into functional groups to facilitate comparison (**Table 2**). Physiological cross-sectional area (PCSA) of a muscle was calculated using equation 1.

$$PCSA = \frac{muscle\ volume \times \cos(pennation\ angle)}{muscle\ fascicle\ length} \quad [1]$$

However, we chose to omit pennation angle from the PCSA equation as (1) we observed that pennation angle is difficult to measure accurately during dissections, (2) the *in vitro* measurements are not fully representative of the pennation angles *in vivo* given that pennation angles changes during muscle contraction, and (3) the pennation angle of most muscles ranges between 0 and 30 degrees, the cosine of which ranges between 1 and 0.87, having only a minor influence on PCSA calculation. Therefore, equation 2 was used in our final analysis.

$$PCSA = \frac{muscle\ volume}{muscle\ fascicle\ length} \quad [2]$$

To obtain an estimate of the force generating capacity of a muscle (Fmax), PCSA was multiplied by 0.3 MPa, i.e. the maximal isometric stress of vertebrate muscle (Wells, 1965; Medler, 2002). The force generating capacity was calculated for the extrinsic thumb muscles and thenar muscles (for a definition see **Table 2**). To obtain an estimate of the maximal compressive force occurring in the bonobo TMC joint compared to the chimpanzee and human TMC joint, we calculated the total force-generating capacity of the muscles that cross the TMC joint (sum of PCSA values multiplied by 30 N/m^2). By dividing the total force-generating capacity by articular area of the trapezium (i.e. surface of the distal facet), we estimate the pressure occurring at the joint. These values were acquired for each specimen individually (n=5; only for the specimens for which both extrinsic and intrinsic hand muscles could be quantified). Average and standard deviation were calculated for the bonobo (based on the five pressure estimates) to allow comparison with the chimpanzee and human data.

Results

Observations on bonobo hand musculature

Extrinsic hand musculature

The origin, insertion and function of all extrinsic hand muscles are listed in the Supplementary material (**S1**). Differences regarding the origin and insertion between the specimens (n=8) are indicated in the **S1** table, but the most conspicuous differences are discussed below.

The *m. flexor carpi radialis* (FCR) originates from the medial epicondyle of the humerus (8/8). The FCR inserts either on the base of MC1 (3/8) or MC2 (5/8), and in case of the latter it may also extend towards MC3 with an additional tendon (1/8) or tendon slip (1/8) from MC2.

The *m. palmaris longus* (PL) originates from the medial epicondyle of the humerus, it inserts radially on the radial palmar aponeurosis and connects to the fascia of the *m. abductor pollicis brevis* (APB) (8/8). Occasional fusion with the FCR (3/8) is observed.

The *m. flexor digitorum superficialis* (FDS), in bonobos, usually consists of three muscle bellies, one for digit 2 (FDS II: 7/8), one for digits 3 and 4 (FDS III-IV: 8/8) and one for digit 5 (FDS V: 6/8). However, occasionally FDS II (1/8) and FDS V (2/8) might also be fused with the FDS III-IV belly. In most specimens, the FDS II shows a distinctive double muscle-tendon unit (MTU) configuration (5/8) (**Fig. 1**). FDS II originates from the medial

epicondyle of the humerus (8/8) and from the proximal ulna (1/8) and inserts on the intermediate phalanx of digit 2 (8/8) with an occasional cross-over tendon to the FDS III tendon (3/8). FDS III-IV originates from both the medial epicondyle (8/8) and proximal radius (7/8). In one specimen, FDS III-IV originates from the ulna instead of the radius. Its individual tendons insert on the intermediate phalanges of the digits 3 and 4 (8/8). FDS V originates from the medial epicondyle of the humerus (8/8) or from the radius (1/8) and inserts on the intermediate phalanx of digit 5 (7/8). In one specimen, FDS V inserts on the distal phalanx.

The *m. flexor digitorum profundus* (FDP) is separated into two muscle bellies. One head (FDP I-II) originates from the shaft of the radius – between the *m. supinator* (SUP) and *m. pronator quadratus* (PQ) – and inserts onto the distal phalanx of digit 1 and 2 (**Fig. 2**). The other head (FDP III-IV-V) originates from the interosseous membrane and the shaft of the ulna and inserts on the distal phalanx of digit 3, 4 and 5. In one specimen, FDP I and V are absent, subsequently the *m. lumbricalis* to the fifth digit (LUMB IV) is absent as well. Additionally, there is an extra tendon from FDP III-IV to the base of the lumbrical inserting on digit 2 (LUMB I).



Figure. 1: Photo of the *m. flexor digitorum superficialis* to digit 2 (FDS II), showing serial MTU organization. The black square indicates 10 mm.

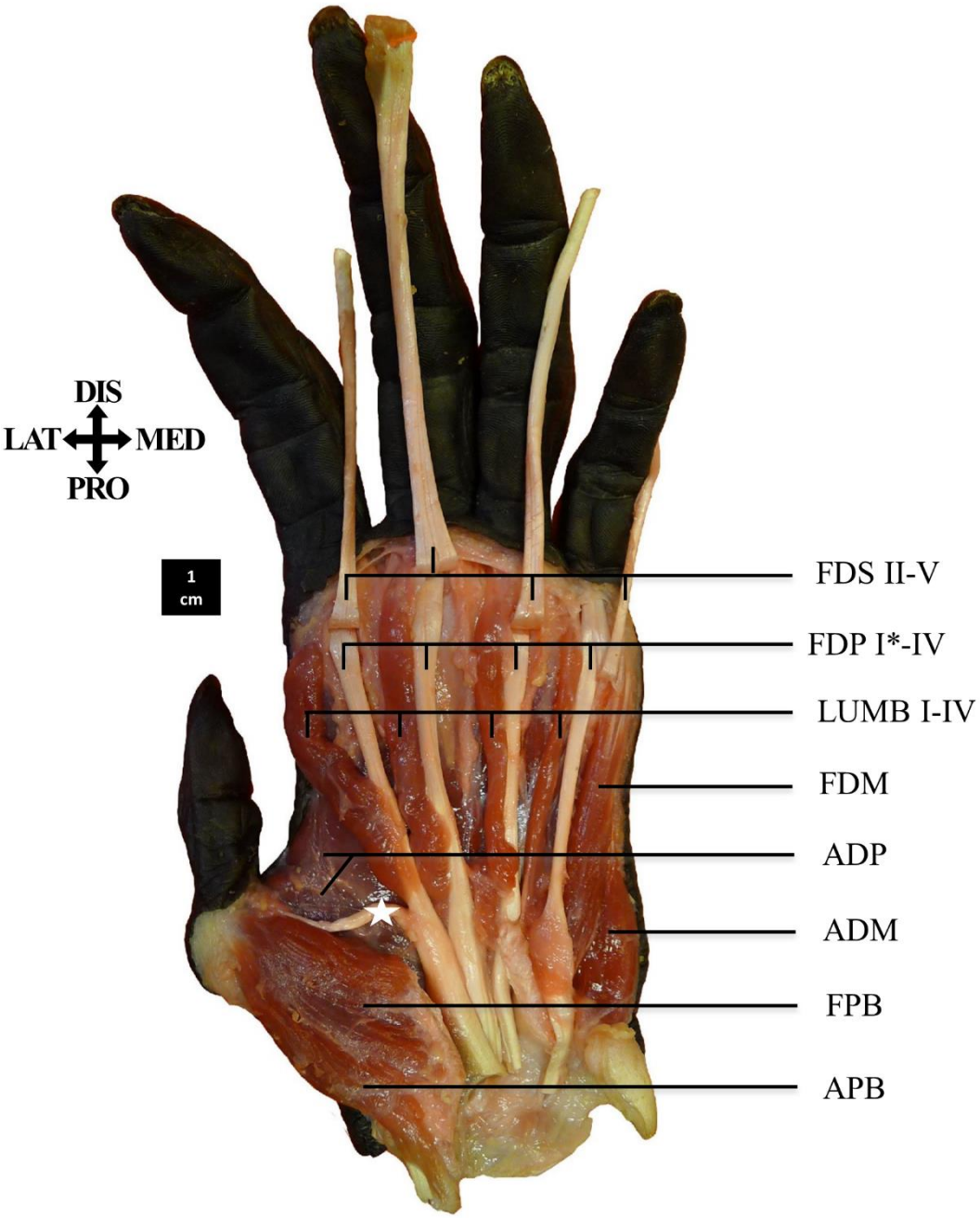

Figure 2: Palmar view of the superficial flexor muscles of the fingers. The *m. opponens pollicis* (OPP) and *m. opponens digiti minimi* (ODM) are not visible here. The *m. flexor digitorum profundus* has a mutual tendon going to the distal phalanx of the thumb (*; FDP I) and a tendon to digit 2 (FDP II).

The *m. flexor pollicis longus* (FPL) is not present as a separate muscle in bonobos. Instead, a tendon, here described as the FDP I tendon, splits from the FDP II tendon and inserts onto the distal phalanx of the thumb (7/8) (**Fig. 2**).

The *m. abductor pollicis longus* (APL) consists of two proximally fused muscle bellies, each its own insertion (8/8). Both originate from the interosseous membrane and the posterior side of the shaft of the radius and ulna, and are sometimes proximally fused with the *m. supinator* (3/8). One tendon (APL I) always inserts on the base of the MC1 (8/8), however, the second insertion (APL II) is variable. Most frequently it inserts on the trapezium (7/8), occasionally with an additional insertion on the pre-pollex (1/8), the dorsal ligament of the thumb (1/8) or the MC1 base (1/8) (**Fig. 3**). The APL II tendon can also insert solely on the pre-pollex (1/8), a sesamoid bone present in 7/8 of the specimens, located at the base of the thumb, generally articulating with the scaphoid and trapezium.

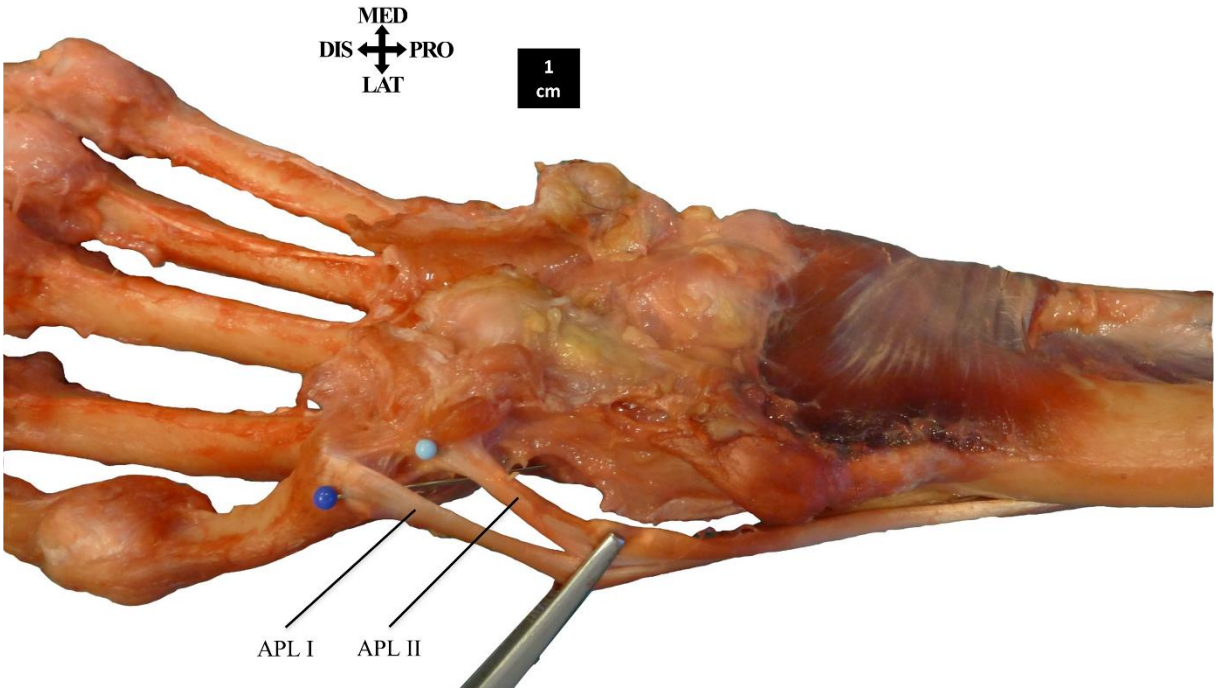

Figure 3: The insertion of *m. abductor pollicis longus* (APL). The tendon of APL I always inserts on the base of the MC1. The tendon of APL II inserts on the trapezium.

The *m. brachioradialis* (BR) invariably originates from the supracondylar ridge of the humerus and inserts onto the styloid process of the radius. The tendon either inserts directly onto the styloid process (5/8) or onto the shaft of the radius proximal to the styloid, continuing to the styloid process (2/8). In one specimen, the tendon is split in two distally, with one slip inserting on the styloid process and the other slip inserting adjacent to the groove of the APL.

The *m. extensor carpi radialis longus* (ECRL) and *m. extensor carpi radialis brevis* (ECRB) are clearly separated in the bonobo specimens. The ECRL usually inserts onto the base of MC2 (5/8) but can in addition insert onto MC1 as well (3/8). The ECRB inserts onto the dorsal side of the MC3 base (8/8) and can also be connected to the *mm. intermetacarpales* (IM) I and II (3/8).

The *m. extensor digitorum* (ED) originates from the lateral epicondyle of the humerus and is fused proximally with the *m. extensor carpi ulnaris* (ECU) (8/8). Its four differentiated muscle bellies are fused proximally to a varying degree. In most cases, each individual tendon inserts on its respective distal phalanx, after forming the extensor mechanism with the *m. lumbricalis* and *mm. interossei* (see intrinsic musculature) (7/8). Additionally, some tendons may interconnect between the digits (5/8). The ED IV and ED V muscle bellies may be completely fused, here a single tendon splits into two distally to insert onto digit 4 and 5 (1/8). On occasion, the ED V and EDM tendons also be fused, together inserting on the extensor mechanism of digit 5 (1/8) (**Fig. 4**).

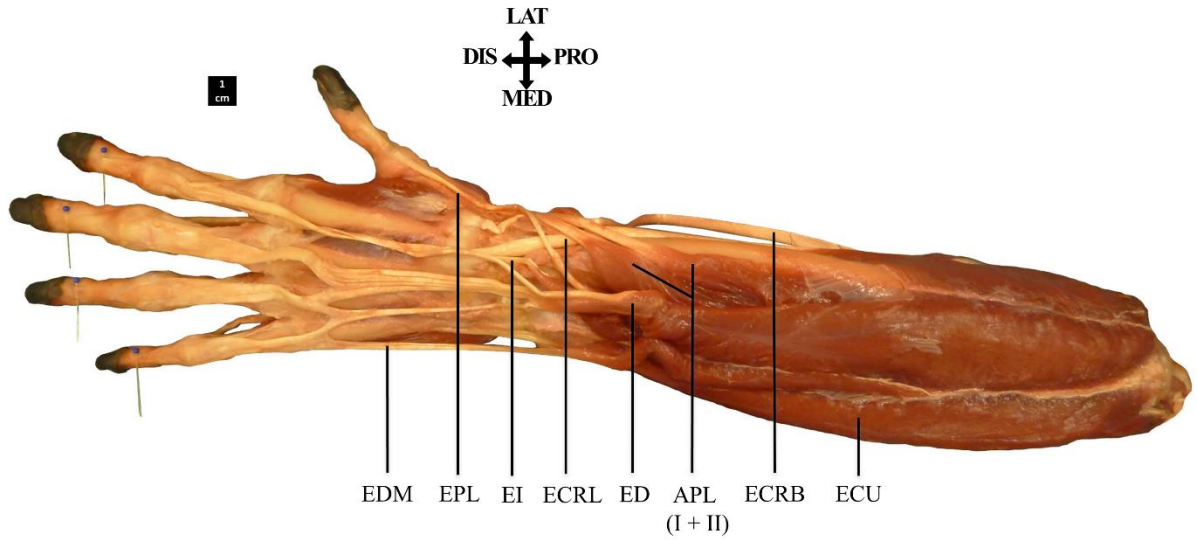

Figure 4: Dorsal view of the extrinsic extensor muscles. The muscle bellies of the *m. extensor digitorum* (ED) and *m. extensor digiti minimi* (EDM) are fused proximally. The tendon of ED V is fused with the EDM tendon, together inserting on the extensor mechanism of digit 5.

The *m. extensor indicis* (EI) inserts distally to the *m. extensor pollicis longus* (EPL) on the ulnar shaft and both muscles may be fused proximally (2/8). The EI has an underdeveloped tendon relative to other forearm muscles and its insertion is variable. It may insert dorsally on the proximal phalanx of the index finger (5/8) or dorsally on the MC2 base (1/8). On occasion, the EI tendon splits in two distally, with one slip inserting on the MCP2 and the other on the MCP3 joint (1/8). Furthermore, the EI may have two distinct tendons, one inserting on the proximal phalanx of digit 2, the other to that of digit 4 (1/8). The *m. extensor pollicis brevis* (EPB) as found in humans is not present in bonobos (8/8).

The *m. extensor digiti minimi* (EDM) originates from the lateral epicondyle of the humerus accompanied by the ECU (7/8) and is sometimes fused with the *m. extensor digitorum* (ED) proximally (2/8). The EDM tendon inserts either on the extensor mechanism of digit 5 together with the tendon of ED V (3/8), or on the proximal phalanx of digit 5 (4/8). In one specimen, in addition to its insertion onto digit 5, two short tendons inserting on the extensor retinaculum were observed. The EDM may also be absent in its entirety (1/8).

Intrinsic hand musculature

The origin, insertion and function of all intrinsic hand muscles are listed in the Supplementary material (**S2**). Differences regarding the origin and insertion between the specimens (n=10) are indicated in the **S2** table, but the most important differences are discussed below (see also **Fig. 2**).

In the majority of our specimens, each *m. intermetacarpalis* (IM I-IV) is fused with the *m. flexor brevis profundi* (FBP) of the respective digit (FBP III, V, VI and VIII) to form the *mm. interossei dorsales* (IOD I-IV), common to the human configuration (7/10) (**Fig. 5**). A minority displayed the ancestral non-human primate configuration of separated IM and FBP muscles (1/10) or an intermediate configuration where only one or two IOD are present while the other muscles are separated (2/10). These bonobo specimens thus show a continuum between the non-human primate configuration and the configuration associated with modern humans. A detailed visualisation of individual specimen's hand muscle configurations (i.e. IM and FPB, or IOD) is reported in the Supplementary material (**S3)**.

The *m. abductor pollicis brevis* (APB) originates from the flexor retinaculum in all specimens. However, additional origins from the shaft of MC3 (5/10) or pre-pollex (2/10) as well as fusions with the *m. opponens pollicis* (OPP) (3/10) and/or *m. flexor pollicis brevis* (FPB) (2/10) are present among the specimens. The APB inserts onto the radial sesamoid bone of the MCP1 joint but variations such as insertion on MC1 base (1/10) may occur.

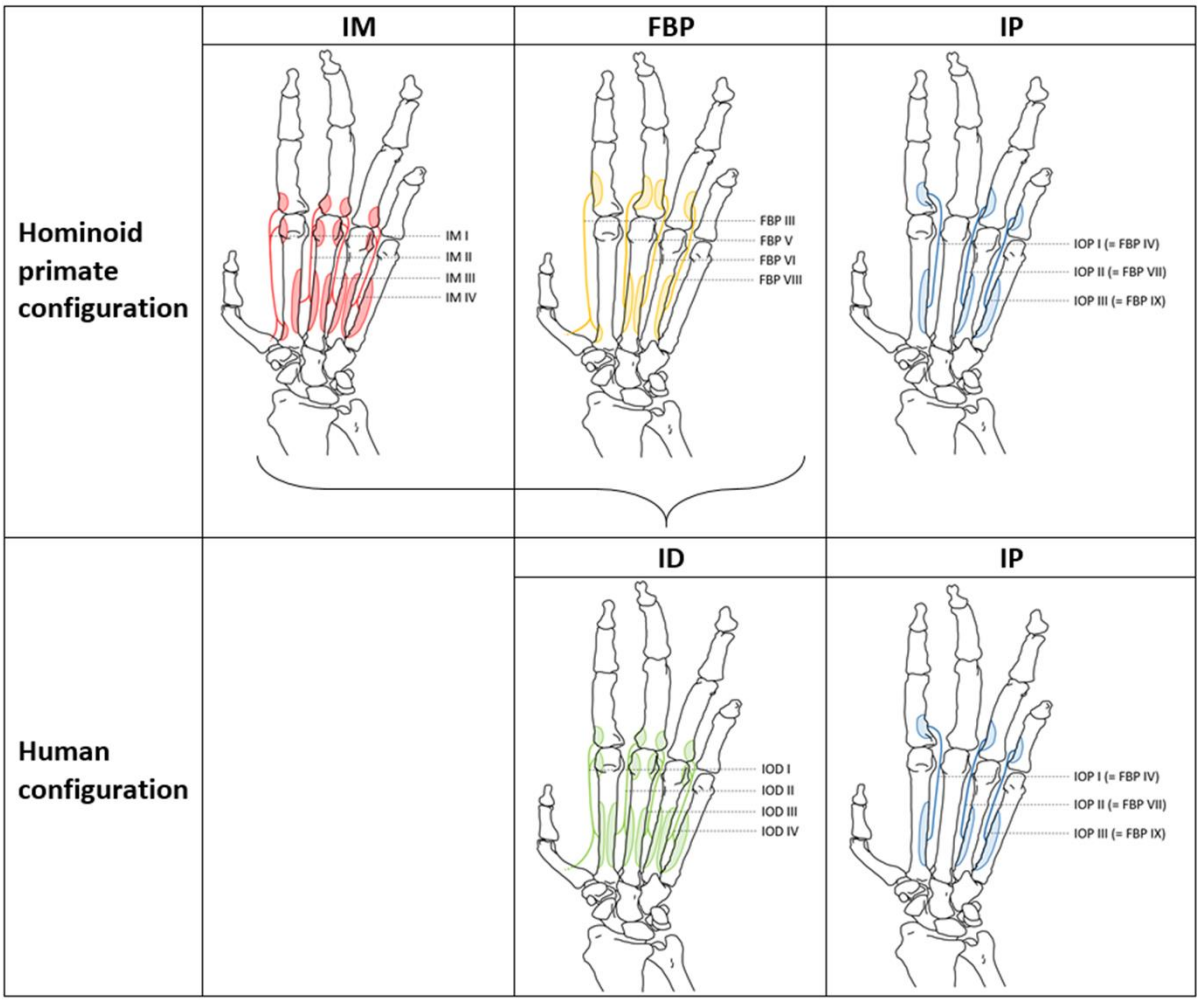

Figure 5: Human vs. hominoid primate configuration of the *mm. intermetacarpales* (IM), *mm. flexores breves profundi* (FBP), *mm. interossei dorsales* (IOD) and *mm. interossei palmares* (IOP). In modern humans, the IM and FBP are fused to form the IOD.

The *m. flexor pollicis brevis* (FPB) consists of a single MTU (10/10), in contrast to humans where a deep (*FPB profundum*) and a superficial (*FPB superficiale*) head can be distinguished. Additionally, the FPB may be fused proximally with the APB and OPP (2/10). The FPB originates from the flexor retinaculum and inserts onto the APB tendon, which in turn inserts onto the radial sesamoid bone of the MCP1 joint (10/10).

The *m. opponens pollicis* (OPP) originates from the flexor retinaculum similar to the origin of the APB and FPB and inserts onto to the radial side of the MC1 shaft (10/10), occasionally continuing onto the APB tendon (2/10) or onto the radial sesamoid of MC1 directly (1/10). Sometimes, it also can be fused with either APB (1/10), or both APB and FPB (2/10).

The *m. adductor pollicis* (ADP) consists of an oblique and transverse head, which both insert onto the ulnar sesamoid bone of the MCP1 joint. The oblique head most commonly originates from the palmar base of MC3 (7/10) or from the base of MC2 + MC3 (3/10). The transverse head often originates from the palmar side of the entire MC3 (6/10), with additional attachments on the head of MC2 (1/10) or MC4 (1/10). However, several variations on the site of origin of the transverse head were observed, originating from the *contrahens raphe* of MC3 + MC4 (2/10) or with an origin from the entire MC4 (1/10). In two specimens, a *m. adductor pollicis accessorius* (APA) was observed, consisting of a small bundle of muscle fibres originating distally from the *contrahens raphe* near the head of MC2 and inserting on the ulnar side of the MC1.

The hypothenar muscles (*m. palmaris brevis* (PB), *m. abductor digiti minimi* (ADM), *m. flexor digiti minimi* (FDM), *m. opponens digiti minimi* (ODM)) have a rather constant configuration similar to that seen in humans. However, a strong fusion between ADM, FDM and ODM was observed in one specimen.

Quantification of bonobo hand muscles

A detailed documentation of the quantitative muscle parameters discussed below is provided in the Supplementary material (**S4**). Additionally, an overview of both muscle fascicle length and pennation angle of the bonobo hand muscles can be found in the Supplementary material (**S5 and S6**).

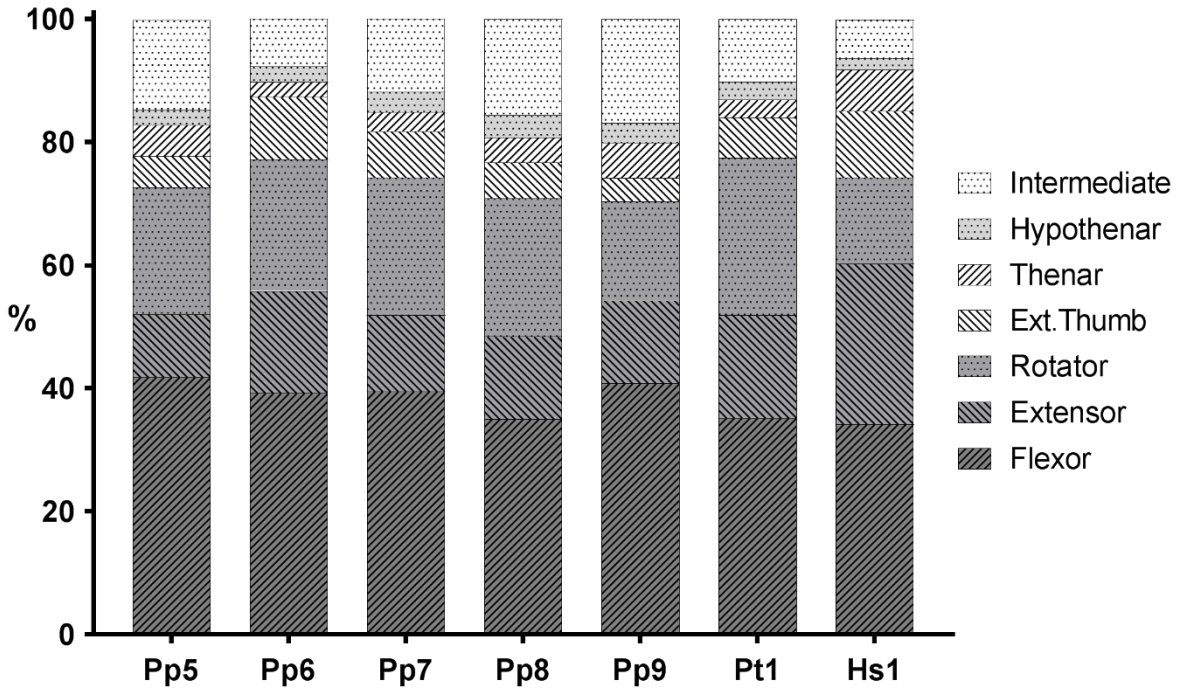

Figure 6: Functional muscle group PCSA as a percentage of total forelimb PCSA in bonobos (Pp), chimpanzee (Pt) and human (Hs).

Functional muscle groups

The PCSA of the functional muscle groups as a percentage of total forelimb muscle PCSA is depicted in **Figure 6** for each of the dissected specimens (5 bonobos, 1 chimpanzee and 1 human). Bonobos have an average flexor/extensor ratio of 3:1 with the PCSA of the forearm flexors making up on average 39.3% (s.d.: 2.6%) of the total forearm muscle PCSA, while the extensors on average only make up 13.2% (s.d.: 2.3%). The chimpanzee has a flexor/extensor ratio of about 2.1:1 with the flexors' PCSA amounting to 35.2% and the extensors PCSA to 16.7% of the total forearm muscle PCSA. The human specimen has a flexor/extensor ratio of 1.3:1 with 35.4% of the forearm muscle PCSA comprising flexors and 27.0% extensors. The rotators take up a greater proportion of the total forearm muscle PCSA in bonobos and chimpanzee (20.6% and 25.6% respectively) compared to the human specimen (14.0%).

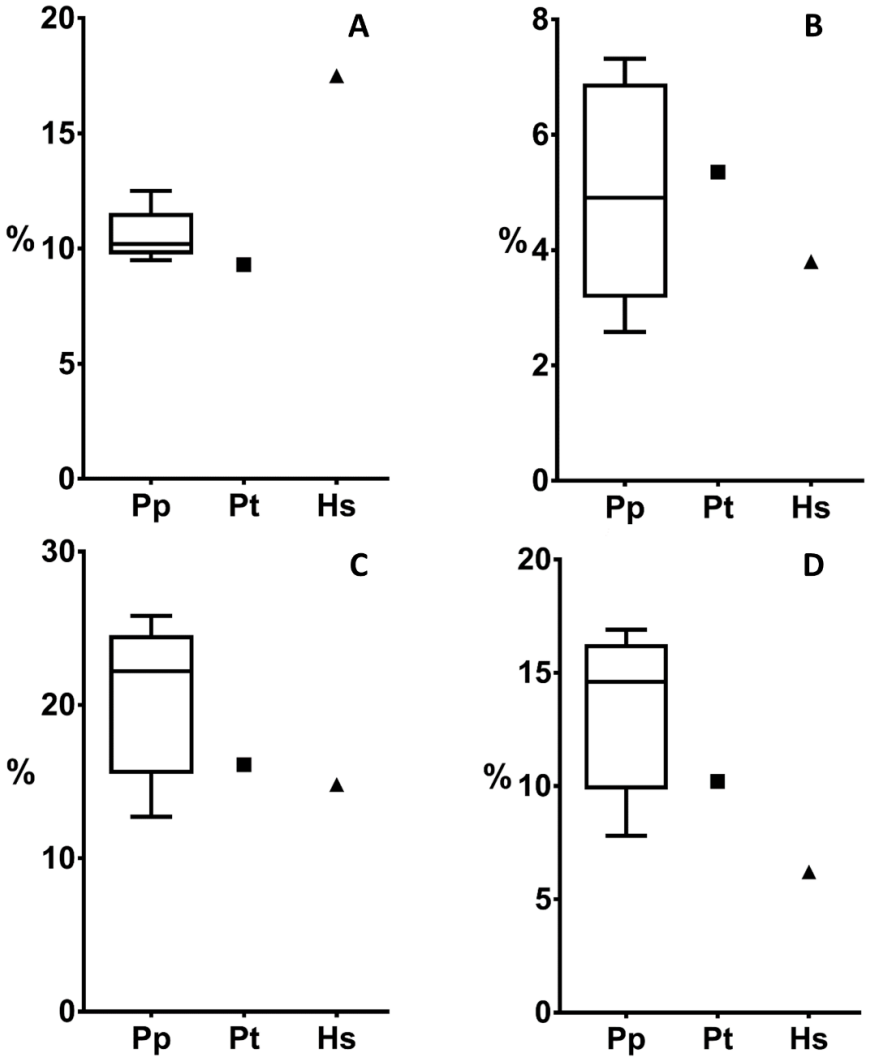

Figure 7: A comparison of the PCSA of (**A**) thumb muscles, (**B**) *m. abductor pollicis longus* (APL), (**C**) intrinsic hand muscles and (**D**) intermediate hand muscles, as a percentage of total PCSA in bonobos (Pp), chimpanzee (Pt) and human (Hs).

If we look at the intrinsic hand muscles as a percentage of total forearm muscle PCSA, we observe that these amount to, on average, 20.5% in bonobos, 16.1% in the chimpanzee and 14.8% in the human specimen (**Fig. 7C**). The configuration of the intrinsic hand muscles differs markedly between *Pan* and *Homo*, with a dominant development (%PCSA) of the intermediate hand muscles in *Pan* (~60%) and a similar development of the thenar and intermediate hand muscles in *Homo* (~42%).

Thumb muscles

The muscles that move and stabilize the thumb are composed of the extrinsic thumb muscles (APL, EPB, EPL, FPL), the thenar muscles (OPP, APB, FPB, ADP), and the first dorsal interosseous muscle (IOD I). The proportion of the thumb muscle PCSA as a percentage of total forearm muscle PCSA amounts to, on average, 10.6% in bonobos and 9.3% and 17.5% in respectively the chimpanzee and human specimen (**Fig. 7A**). Furthermore, the percentage of thenar musculature in proportion to the intrinsic hand muscles amounts to 25.1% on average in bonobos, 19.3% in the chimpanzee, and 45.8% in the human. The APL, in bonobos, takes up 5% of the total forearm muscle PCSA, similar to that found in the chimpanzee (5.3%). The relative contribution of the APL is lower in the human specimen (3.8%), even when including the EPB (4%), but falls within the large range observed for the bonobo specimens. However, in *Pan*, the APL appears to be the most important muscle within the thumb musculature, accounting for on average 47% of thumb muscle PCSA in bonobos and 58% in the chimpanzee, while the contribution in *Homo* is much lower (21%) (**Fig. 7B**).

Table 3. Estimated trapeziometacarpal joint pressure

TMC pressure	**Pp5**	**Pp6**	**Pp7**	**Pp8**	**Pp9**	**Bonobo average**	**Chimp Pt1**	**Human Hs1**
Surface area (mm^2)	100.7	106.4	145.0	130.0	138.1	**124.0**	**132.7**	**178.9**
PCSA (mm^2)	899.1	1827.2	1635.1	930.8	750.7	**1208.6**	**1401.8**	**1563.5**
Force (N)	269.7	548.2	490.5	279.3	225.2	**362.6**	**420.5**	**469.1**
Pressure (MPa)	2.7	5.2	3.4	2.2	1.6	**3.0**	**3.2**	**2.6**

Finally, by dividing the maximal force-generating capacity of the muscles crossing the TMC joint by the trapezial articular area, an estimate of the maximal pressure at the TMC joint was obtained. The pressure estimate amounts on average to 3.0 MPa for the bonobos, 3.2 MPa for the chimpanzee and 2.6 MPa in the human (**Table 3**).

Discussion

This study identifies important features of the hand musculature in bonobos, in comparison to the chimpanzee and human configuration, based on the detailed dissection of a unique sample of bonobo specimens. The three major findings are (1) the high variability in bonobo hand musculature, (2) the well-developed thumb musculature, and (3) the presence of functional coupling between muscles.

High variability of bonobo hand musculature

Both the qualitative and quantitative analysis of the bonobo hand musculature indicate a high variation among individuals. From the qualitative analysis, we report incidences of all observed configurations for all dissected specimens, also including left and right hands from the same animal. We find a particularly high degree of variability for the configuration of the intermediate hand muscles as well as many, often small, variations on site of insertion of the extrinsic hand muscles, most notable the long flexors (FDS, FDP) and EI muscle. Similarly, the quantitative analysis, which only includes unilateral sampling and a lower sample size (n=5), yields marked intra-specific variations in muscle volume and PCSA. We focus on muscle PCSA as this is the most functionally relevant parameter, being strongly correlated with force-generating capacity of a muscle (Marzke and Marzke, 2000; Vereecke *et al.*, 2005). However, analyses on muscle mass show similar results. We speculate that this high inter-individual variation in the soft-tissue configuration of the bonobo hand might be an indication that this region is under only mild selective pressure, and/or that the functional implications of these variations are limited. In contrast, variability in the bonobo thenar and extrinsic thumb muscles is relatively low. Such consistency may suggest that this region is more strictly regulated by selective pressure.

Despite the variability observed in the bonobo hand muscles, we are able to identify some diverging general trends for the muscle configuration between *Pan* and *Homo*. For example, when we look at the relative proportion of the different functional muscle groups, we observe a similar organization in the bonobo and chimpanzee specimens which deviates from the human configuration. Most importantly, the proportion of wrist extensors is increased in *Homo* relative to *Pan*, a trait potentially linked to tool use due to the

importance of wrist extension during tool-making (Williams, Gordon and Richmond, 2010), while *Pan* has a stronger development of the forearm rotators. The large amount of rotators has also been shown in previous anatomical studies on great apes (e.g. (Thorpe *et al.*, 1999; Myatt *et al.*, 2012)) and can be explained by the importance of pro-supination movements during arboreal locomotion of bonobos and chimpanzees. Wrist flexors show a similar relative development in *Pan* and *Homo*, in agreement with previous studies (Tuttle, 1969; Thorpe *et al.*, 1999). Other functional group ratios (e.g. wrist flexor to extensor ratio, thenar to intrinsic hand musculature) were found to be in agreement with Tuttle's results as well, despite the dissimilarity in methods used, *Gorilla gorilla* being included in *Pan*, and without inclusion of bonobos (Tuttle, 1969). The large amount of (wrist and finger) flexors in *Pan* is most likely due to their involvement in arboreal locomotion. Consequently, the emphasis on flexors may restrict extension of the wrist, favouring knuckle-walking over palmigrade quadrupedalism during terrestrial locomotion. Additionally, the recruitment of wrist flexors as shock absorbers during knuckle-walking (Simpson, Latimer and Lovejoy, 2018) may further reinforce the prominence of flexor muscles in the forearm of knuckle-walkers. Another example that may reflect differences in locomotion is found in the proportion of intrinsic hand muscle PCSA. Bonobos, on average, possess a somewhat larger proportion of intrinsic hand muscles compared to humans, although humans fall within the large range of bonobos (**Fig. 7C**). The difference between bonobos and humans is, however, most pronounced for the relative development of the intermediate hand muscles, which account for on average 13.6% of the total PCSA in bonobos and merely 6.4% in humans (**Fig. 7**). This too may be explained in the context of locomotion, either arboreal in the form of grasping which is of major importance for vertical climbing and clambering, or in the context of terrestrial knuckle walking, where the intermediates might play an important role (Susman and Stern, 1980), although, these two are not mutually exclusive.

Differences in forelimb musculature between bonobo and chimpanzee are limited. This was already indicated in a recent publication by Diogo and colleagues that points to an evolutionary stasis in the *Pan* clade using soft-tissue characters to underline the low divergence between chimpanzees and bonobos (Diogo et al. 2017b). One of the three divergent characters in the forelimb musculature described is the different configuration of the intermediate hand muscles in chimpanzees and bonobos. Our dissections indicate that, contrary to the statements of Diogo et al. (2017b), bonobos can have distinct intermetacarpales common to the configuration found in chimpanzees. Rather than invariably presenting the human configuration with four dorsal interossei (fusion of FBP III, V, VI, VIII with the intermetacarpales I-IV) and three palmar interossei (FBP IV, VII, IX), bonobos display all kinds of variations, and these variations can also occur between the left and right hand of one individual. The high variability seen in the organization of

the intermediate hand muscles of bonobos suggests that the functional implications are limited and that this trait cannot be used as divergent character of bonobos.

Bonobo thumb musculature

This study shows that bonobos possess a well-developed thumb musculature, on par with that of humans. While the relative PCSA of the thumb muscles in humans is higher, the estimate of intra-articular pressure to which the TMC is subjected is higher in bonobos (and chimpanzee). Moreover, this estimate is likely an underestimation of the actual maximal pressure in the bonobo as (i) the contribution of the FDP I is not accounted for in bonobos while FPL is included in the human pressure estimate, and (ii) in some bonobo specimens, the FCR and/or ECRL also cross the TMC joint and can therefore also generate compressive forces at this joint. Despite the strong thumb musculature of bonobos, they do have a lower dexterity compared to that of modern humans (Kivell, 2015; Bardo *et al.*, 2016; Neufuss *et al.*, 2017). A simple correlation between the force-generating capacity of the thumb muscles and dexterity does not apply; in addition to size, muscle configuration (and motor control) plays an important role.

One of the more explicit examples of differences in muscle configuration between humans, bonobos and chimpanzees can be found in the diverging morphology of the extrinsic thumb flexor. In chimpanzees, this flexor is present in the form of a vestigial tendon coming from the FDP II tendon that inserts onto the distal phalanx of the thumb, as observed both in our chimpanzee specimen and as reported in the literature (see figure 19 in Tuttle (1969)), but it can also be absent (Susman, 1998). In bonobos, however, we see that the tendon of the FDP to digit 1 is well developed, with similar dimensions as the tendons acting on other digits (**Fig. 2**) and as the human *m. flexor pollicis longus* (FPL). In humans, the FDP I has differentiated into a separate muscle, the FPL, and its presence has been linked to the unique dexterity of modern humans (Marzke, 1997; Wolfe *et al.*, 2006; Skinner *et al.*, 2015). The muscle is important for precision control and manipulation, and appears to be particularly active during power squeeze grips, rather than during precision grips (Hamrick, 1998; Marzke *et al.*, 1998). Although gibbons also have a distinct FPL (Susman, 1998), it has been posited that the presence of the FPL in modern humans fulfils the specific functional requirements of the thumb to be able to perform a variety of complex functions (Tocheri *et al.*, 2008; Skinner *et al.*, 2015). We believe that the configuration found in bonobos, with a stout tendon to the thumb and a shared muscle belly for FDP I and II, has important functional consequences regarding individual finger control and dexterity.

Functional coupling

Functional coupling between muscles results in a concerted action. The association between thumb and index finger flexion, enables bonobos to move digit 1 and 2

independently from digits 3, 4 and 5, which might contribute to differences in grasping capability, particularly in precision gripping in which the thumb and index finger play a very important role (Christel, Kitzel and Niemitz, 1998). A similar fusion was also observed between EPL and EI in two bonobo specimens, which points to a developmental relationship between these neighbouring muscles. A fusion between EPL and EI is also found in some New World monkeys, such as *Alouatta fusca* and *Saguinus geoffroyi*, forming a structure referred to as "*extensor pollicis et indicis longus*" (Aversi-Ferreira *et al.*, 2010). Such configuration might lead to joined extension of thumb and index finger. On the one hand, such functional coupling may be crucial to executing certain coordinated hand movements, on the other hand, it also complicates individual digit mobility and thus dexterity. In modern humans, as well as in common chimpanzees and our other bonobo specimens, the EPL goes exclusively to digit I and is not fused to the EI, resulting in a functional dissociation between the extension of the thumb and the index finger. This individualization is found more often in the more dextrous primates, with humans as a prime example. With the distinct FPL, EPL and EI configuration, we see this in the human thumb especially. It is therefore very likely that the increased amount of functional coupling found in bonobos compared to humans, rather than a difference in muscle development, plays a major role in the difference in dexterity.

Critical considerations

Our findings are based on a detailed dissection of eight bonobo specimens which were obtained from different European zoos. Although this is the largest series of bonobos that has been dissected so far, it remains a relatively small and heterogeneous sample (age, sex, body size). It is not possible to evaluate the effect of age and sex in the current dataset, but no apparent differences were observed for the subadult specimen (female of 8 years, unfused growth plates) or between the male and female specimens. This is to be expected for a species with a low sexual dimorphism (Coolidge and Shea, 1982; Zihlman and Bolter, 2015). To allow for comparison between specimens of different size (total forelimb muscle mass ranges from 500g to 1100g), we used total forelimb PCSA as a normalizing factor. Additionally, as our specimens originate from various zoos, the effect of captivity on muscle development should not go unremarked. Furthermore, for interspecific comparison we have made use of only one chimpanzee, and one human specimen. These were included as a representative for their species, an indication of how the bonobo relates to its close relatives. Therefore, no significant conclusions on interspecific variations between these species can be made. This has to be kept in mind while interpreting these data. Despite these limitations, we were able to fully document the bonobo forelimb musculature, both qualitatively and quantitatively, using a consistent protocol on a unique series of unembalmed bonobo cadavers. Not only is this research important to generate a general view of the bonobo anatomy, but in combination with in vivo research and behavioural

studies, it can be translated to complete form-function relationships of the thumb. This will provide important insights into the form-function relationship of the thumb in modern humans and aid accurate interpretation of hominin fossil remains.

Conclusions

This study shows that the bonobo forelimb musculature displays a relatively high variability and although the muscles of the hand and thumb are well developed, they show an increased amount of functional coupling compared to humans. It is likely that the strong differentiation and individualisation of the hand muscles in humans, rather than relative muscle development, explains the higher dexterity compared to bonobos.

Acknowledgements

The authors thank the *Bonobo Morphology Initiative* organized by dr. Nauwelaerts and dr. Pereboom from the Centre for Research and Conservation (Royal Zoological Society Antwerp, Belgium) in January 2016 that enabled access to a large part of the bonobo specimens and allowed dissection of these specimens by an international team of anatomists. We are also grateful to the different zoos which provided additional primate specimens: Jean-Pascal Guéry (La Vallée des Singes, Romagne, France), Christina Geiger (Zoo Frankfurt, Germany), Martina Balz (Wilhelma Zoo, Stuttgart, Germany) and Constanze Mager (Burgers' Zoo, Arnhem, The Netherlands). Furthermore, we thank dr. Olivier Vanovermeire and Henk Lacaeyse from the Medical Imaging Department, AZ Groeninge (Kortrijk, Belgium) for the CT-scanning of the specimens. Funding for this project was obtained from KU Leuven (project number: C14/16/082).

Author contributions

EEV conceived the study; EEV, TvL and MJMV further designed the study; JS provided the specimens and assisted in data collection; TvL, MJMV, FDK, and EEV performed the dissections; TvL, MJMV and EEV analysed the data and wrote the manuscript; all authors reviewed and approved the article. TvL and MJMV are joint first author on this publication.

Supplementary material

S1: The origin, insertion and function of all extrinsic hand muscles

Legend: 1: Pp6 L; 2: Pp6 R, 3: Pp5 R, 4: Pp5 L, 5: Pp7 R, 6: Pp8 R, 7: Pp2 L, 8: Pp9 L

Muscles	**Origin**	**Insertion**	**Primary function**
PT		halfway the radius,	pronation of the forearm
▪ caput humerale	medial epicondyle of humerus[1-8]	with 2 separate tendons[1] or with 1 tendon[2-8]	
▪ caput ulnare	medial side of proximal ulna[1-3,5-6,8] + fused with FDS[2,3] + articular capsule elbow[6] + insertion tendon of brachialis muscle and medial side of proximal ulna[8]		
FDS			flexion of PIP joints of digits 2 to 5; flexion of MCP joints and wrist
for[1,3-6,8]:			
FDS II	medial epicondyle of humerus	tendon to middle phalanx of digit 2 + additional tendon to tendon FDS III[1,3]	
FDS III-IV	medial epicondyle + radius	tendon to middle phalanx of digit 3 + 4	
FDS V	medial epicondyle[1,3-6,8] + fused with FCU[3,5]	tendon to middle phalanx of digit 5[1,4-6,8] tendon to distal phalanx of digit 5[3]	
for[2]:			
strong fusion between all muscle bellies	medial epicondyle of humerus + proximal ulna	tendons to middle phalanx of digits 2, 3, 4 + 5; extra small tendon of FDS II to FDS III	
for[7]:			
FDS II	medial epicondyle of humerus	tendon to middle phalanx of digit 2	
FDS III-IV-V	medial epicondyle + radius	tendon to middle phalanx of digits 3 + 4 + 5	
FCR	medial epicondyle of humerus[1-8] + fused with FDS[2] + fused with PT[5] + attached to radius with tendon sheet[6] + shares tendon sheet with PT, FDS and FCU[7]	tendon to palmar side of MC1 base[1-3] tendon to palmar side of MC2 base[4-8] + tendon fibres continue to radial base of MC3[6,7]	flexion and radial deviation of wrist

PL	medial epicondyle of humerus[1-8] + fused with proximal FCR[2,3,7]	fuses radially with palmar aponeurosis[1-8]	flexion of wrist
FCU ▪ caput humerale ▪ caput ulnare	 tendon sheet with FDS and FDP, medial epicondyle of humerus[1-8] oleocranon of ulna[1-6,8]	 tendon onto pisiform bone[1-8]	flexion and ulnar deviation of wrist
PQ	distal 5cm of ulna[1-8]	distal interosseus membrane + distal 5cm of radius[1,2,4-8] distal interosseus membrane + distal 2cm of radius[3]	forearm pronation
FDP for[1,3-8]: FDP I-II FDP III-IV-V for[2]: FDP II FDP III-IV *FDP I and FDP V*	 shaft radius (between SUP and PQ) interosseus membrane + shaft ulna (from oleocranon to PQ) shaft radius interosseus membrane and ulna *absent*	 distal phalanx of digits 1 + 2 distal phalanx of digits 3 + 4 + 5 distal phalanx of digit 2 distal phalanx of digits 3 + 4 → extra tendon to base of LUMB I	flexion of PIP and DIP joints of fingers 1 to 5, flexion of MCP joints and wrist
BR	supracondylar ridge of humerus[1-8]	tendon to styloid process (radius)[1-5] tendon attaches proximal and onto styloid process[6-8] + tendon splits in two; largest part inserts on styloid process and smallest part next to APL sulcus[8]	elbow flexion
ECRL	lateral supracondylar ridge of humerus[1-8] (distal from BR)	tendon to dorsoradial side MC2 base[1,2,4,5,7] + additional slip towards trapezium and TMC, inserting on volar beak MC1[5] tendon to dorsal side of MC2 base + dorsal-ulnar side of MC1 base[3,6,8]	extension and radial deviation of wrist
ECRB	lateral epicondyle of humerus + fused with ED[1-8]	tendon to dorsal base of MC3[1-8] + intermetacarpales (IM) II + III [1-3]	extension and radial deviation of wrist

ED II-III-IV-V	lateral epicondyle of humerus[1-8] + muscle bellies ED IV-V are fused[5] common tendon sheet (and variable degree of fusion) with ECU[2], EDM[2,7] and ECRB[1-8]	tendon to distal phalanges of digits 2-3-4-5[1-4,6-8] + connection between tendon 4 and 5 near CMC joint[1-3,5] + extra tendon from ED V to ED IV[2,7,8] + ED V tendon is fused with EDM tendon[6] + ED III-IV share a tendon which splits into several tendons inserting on extensor mechanism of digits 3 and 4[7]	extension of phalanges, wrist and elbow
EDM	muscle belly ECU (proximal)[1-4,5,7,8] + fused with ED[2,7] + fused with EI[3] *absent*[6]	tendon to dorsal side of proximal phalanx of digit 5[1-4] tendon connects with ED V tendon and inserts on extensor mechanism of digit 5[5,7] tendon fuses with ED V on extensor mechanism to digit 5 + 2 extra tendons that insert onto the extensor retinaculum[8]	extension of digit 5 (PIP and MCP), extension of wrist
ECU	dorsal side of proximal 3/4 of ulna[1,3-8] + lateral epicondyle of humerus[5,6] + shares tendon sheet with EI, EPL and APL towards lateral epicondyle[8] dorsal side of proximal 3/4 of ulna + fused with ED and APL[2]	tendon to ulnar side of MC5 base[1-6,8] tendon splits distally; main tendon inserts on MC5 shaft and second tendon inserts on MC5 base[7]	extension and ulnar deviation of wrist
SUP	proximal 1/3 of ulna[1-8] + lateral epicondyle of humerus[2,3]	proximal 1/3 of radius[1-8]	supination of forearm

S2: The origin, insertion and function of all intrinsic hand muscles

1: Pp6 L, 2: Pp6 R, 3: Pp5 R, 4: Pp5 L, 5: Pp7 R, 6: Pp8 R, 7: Pp2 L, 8: Pp9 L, 9: Pp3 L, 10: Pp1 R

Muscles	**Origin**	**Insertion**	**Primary function**
(a) Thenar muscles			
APB	flexor retinaculum[1-10] + fused with OPP[4,5,8] + fused with FPB[5,8] + pre-pollex[6,7]	tendon to radial sesamoid bone of MCP1 joint[1-3,5,6,8-10] muscle fibres insert along FPB tendon[4] radial base of MC1[7]	abduction of thumb
FPB	flexor retinaculum[1,2,4-10] + fused with OPP and APB[5,8] *absent*[3]	tendon of APB tendon to radial sesamoid bone of MCP1 joint[1,2,4-6,8-10] tendon joins ulnar side of APB tendon + inserts on distal ulnar side of MC1 shaft[7]	flexion of thumb at MCP1 joint
ADP ▪ caput transversum	palmar base and shaft of MC3[3,4,6-10] + MC4 head[7,10] + MC2 head[3] contrahens raphe of MC3 + MC4[1,2] base and shaft of MC4[5]	tendon to ulnar sesamoid bone of MC1 joint[1-10]	adduction of the thumb
▪ caput obliquum	palmar base of MC3[1-10] + palmar base of MC2[3,8,9] caput obliquum is composed of 2 distinct muscle bellies[1-3]	tendon to ulnar sesamoid bone of MC1 joint[1,2,4-10] tendon to ulnar side of MC1 (below head)[3]	
Adductor pollicis accessorius (APA)	contrahens raphe of near MC2 head[4,5]	ulnar side midshaft of MC1[4,5]	unclear
OPP	flexor retinaculum[1-10] + fused with FPB[5,8] + fused with APB[4,5,8] + MC1 base (at APL insertion)[7]	radial side of MC1 shaft (no contact with sesamoid bones of MC1)[1-3,7-10] total length of APB tendon[4,5] radial sesamoid of MCP1 joint[6]	opposition of thumb; assists in adduction of thumb

(b) Hypothenar muscles			
PB	flexor retinaculum[2-6,8] underneath flexor retinaculum[5] *absent[1,9,10]* *strongly reduced[7]*	palmar aponeurosis[2-6,8]	
ADM	pisiform bone[1-10] + flexor retinaculum and pisohamate ligament[3-9] + fused with FDM[5]	tendon to ulnar side of MCP5 joint[1-9] small tendon joins tendon of FDM[10]	abduction of digit 5
FDM	flexor retinaculum and hamulus ossis hamati[2-10] + fused with ADM[5] *absent[1]*	tendon to ulnar base of proximal phalanx of digit 5[3-6,9,10] + some muscle tissue to MCP5 joint[3] MCP5 joint[2,7,8] + ADM tendon[8]	flexion of digit 5 at MCP5 joint
ODM	flexor retinaculum and hamulus ossis hamati[1-10]	ulnar side of MC5[1-10] + base of proximal phalanx of digit 5[10]	opposition of digit 5
(c) Intermediate hand muscles			
LUMB	tendons of FDP	tendon to radial side of extensor sheath at proximal phalanx of:	flexion of the MCP joints; extension of the IP joints
▪ LUMB II	tendon of FDP II[1-10]	digit 2[1-10]	
▪ LUMB III	tendon of FDP III[4,5,10] tendon of FDP II[1-3,6-9] + tendon FDP III[3,6-9]	digit 3[1-10] digit 2[2]	
▪ LUMB IV	tendon of FDP IV[1-10] + tendon of FDP III[3,6-9]	digit 4[1-10]	
▪ LUMB V	tendon of FDP V[5,9] tendon of FDP IV[1,3,4,6-8,10] + tendon of FDP V[6-8,10] + muscle fibres to LUMB IV[3] *absent[2]*	digit 5[1,3-10]	

IM ▪ IM Ia ▪ IM Ib ▪ IM II ▪ IM III ▪ IM IV	ulnar side of base MC1[1] radial side of base MC2[1] ulnar shaft of MC2 + radial shaft of MC3[1,9,10] ulnar shaft of MC3 + radial shaft of MC4[1,9,10] ulnar shaft of MC4 + radial shaft of MC5[1,10] *absent*[9]	tendon to radial side MCP2 joint (deep to tendon of the Flexor 3)[1] tendon to radial side of MCP3 joint[1,9,10] tendon to ulnar side of MCP3 joint[1,9,10] tendon to ulnar side of MCP4 joint[1,10]	abduction of the digits; assist lumbricals: flexion at MCP joints and extension at PIP joints
FBP ▪ FBP III ▪ FBP IV (= IOP I) ▪ FBP V ▪ FBP VI ▪ FBP VII (= IOP II) ▪ FBP VIII ▪ FBP IX (= IOP III)	MC1 shaft and MC2 base + fused with IM I (dorsal)[1] *FBP III is fused with IM Ia-b to form IOD I*[2-10] shaft of MC2[1-10] + fused with IM II (middle)[1,5] shaft of MC3[1,9,10] *FBP V is fused with IM II to form IOD II*[2-8] shaft of MC3[1,9,10] *FBP VI is fused with IM III to form IOD III*[2-8] shaft of MC4[1-10] shaft of M4[1,10] + fused with IM IV[1] *FBP VIII is completely fused with IM IV to form IOD IV*[2-9] shaft of MC5[1-10]	tendon to radial side of proximal phalanx of digit 2[1] tendon to ulnar side of proximal phalanx of digit 2[1-10] + MCP2 joint[5,6,10] tendon to radial side of proximal phalanx of digit 3[1,9,10] tendon to ulnar side of proximal phalanx of digit 3[1,9,10] tendon to radial side of proximal phalanx of digit 4[1-6,8-10] tendon to MC4 head[7] tendon to ulnar side of proximal phalanx of digit 4[1,10] tendon to radial side of proximal phalanx of digit 5[1-10]	adduction of the digits; assist lumbricales: flexion at MCP joints and extension at PIP joints

IOD ▪ IOD I (cf. IM I)	ulnar side of MC1 and shaft of MC2[2-5,8-10] + trapezium[5] base of MC1[6,7]	tendon to radial side of MCP2 joint[2-4,7-10] + proximal phalanx of digit 2[5]	abduction of the digits; assist lumbricals: flexion at MCP joints and extension at PIP joints
▪ IOD II (cf. IM II)	shaft of MC2 + MC3[2-8] entire fusion of F5 and IM II[2-5,7,8] partial fusion of F5 and IM II[3,6]	tendon to radial side of MCP3 joint, joining extensor mechanism of digit 3[2-5,7,8] two distinct tendons; 1 inserting on MCP3 joint and 1 inserting on proximal phalanx[3,6]	
▪ IOD III (cf. IM III)	shaft of MC3 + MC4[2-8] entire fusion of F6 and IM III[2,4-8] partial fusion of F6 and IM III[3]	tendon to ulnar side of MCP3 joint, joining extensor mechanism of digit 3[2,4-8] two tendons; 1 inserting on MCP3 joint and 1 inserting on proximal phalanx[3]	
▪ IOD IV (cf. IM IV)	shaft of MC4 + MC5[2-7,9,10] shaft of MC5[8] entire fusion of F8 and IM IVI[2,4-8] partial fusion of F8 and IM IV[3]	tendon to ulnar side of MCP4 joint, joining extensor mechanism of digit 4[2,4-7,9,10] tendon to proximal phalanx of digit 4[8] two tendons; 1 inserting on MCP4 joint and 1 inserting on proximal phalanx[3]	

S3: A detailed visualisation of individual specimen's intermediate intrinsic hand muscle configurations

	IM	**FBP**	**IOP**	**IOD**
Pp1 R	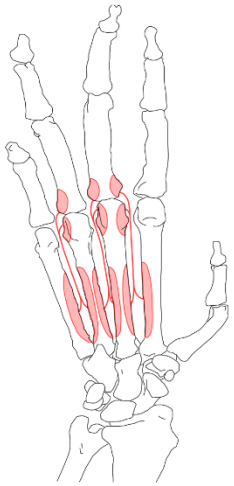	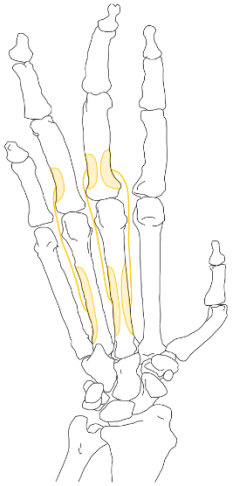	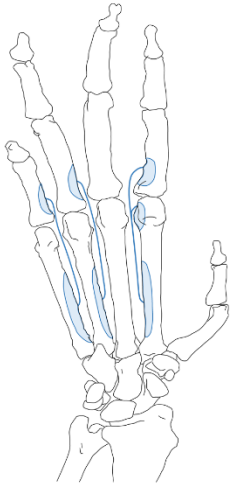	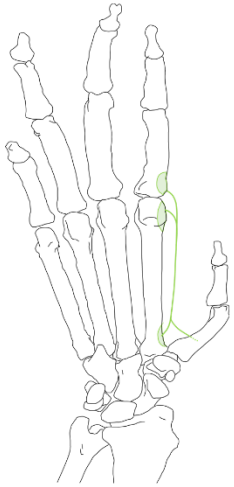
Pp2 L			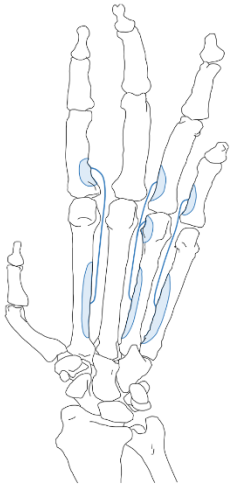	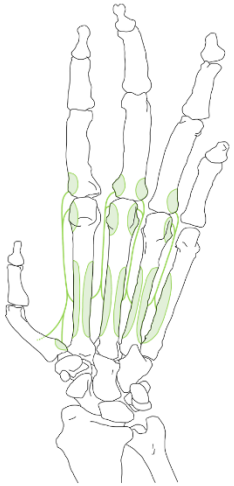

	IM	FBP	IOP	IOD
Pp3 L	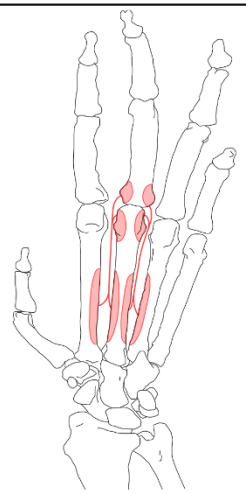	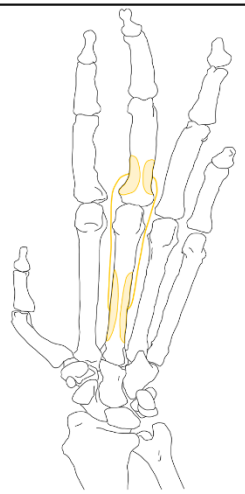	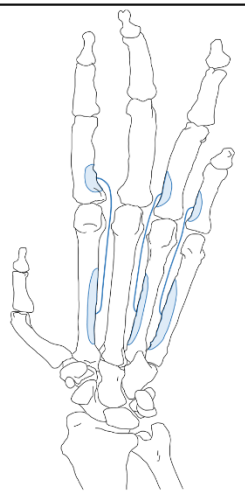	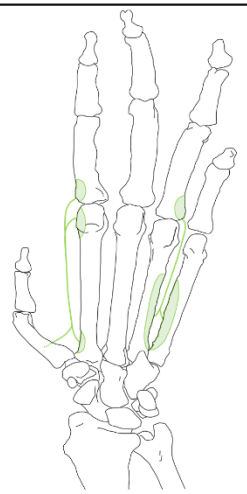
Pp5 L			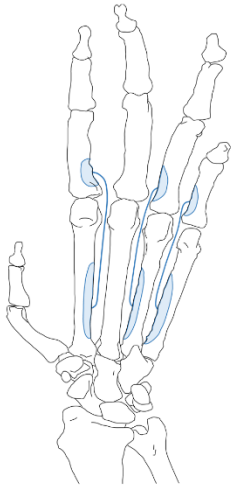	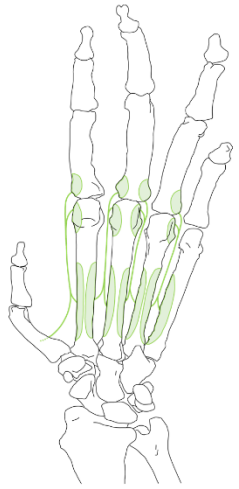

	IM	FBP	IOP	IOD
Pp5 R			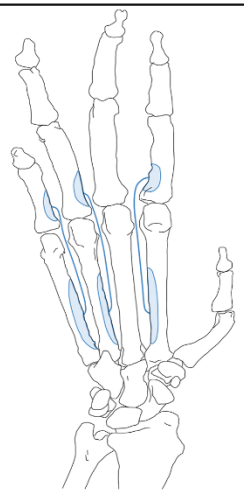	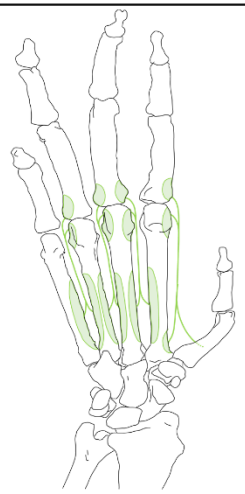
Pp6 L	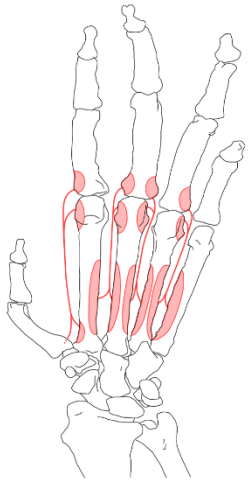	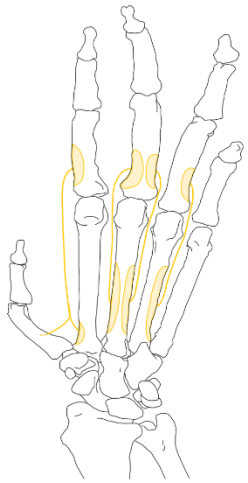	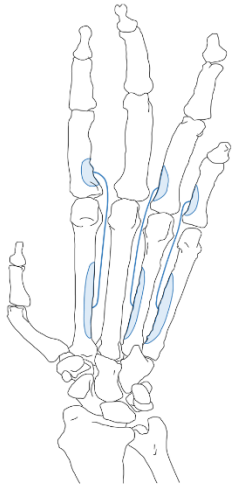	

	IM	FBP	IOP	IOD
Pp6 R			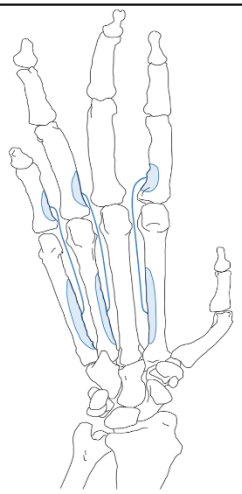	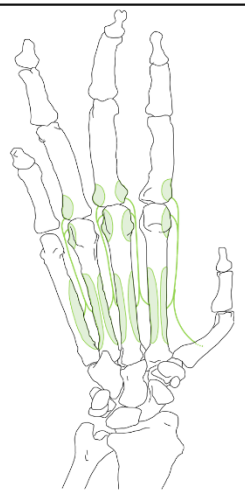
Pp7 R			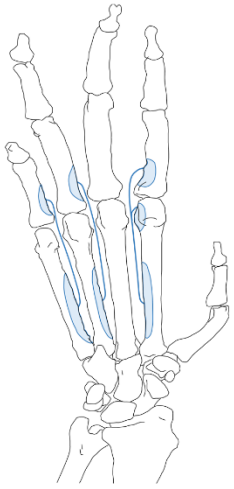	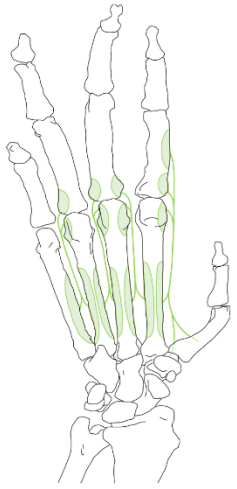

	IM	FBP	IOP	IOD
Pp8 R			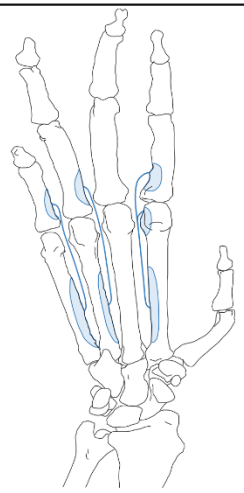	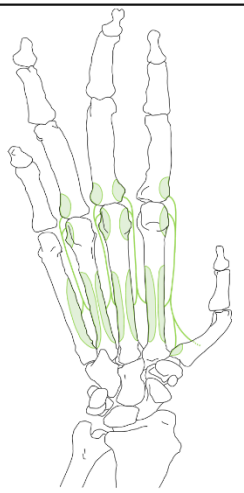
Pp9 L			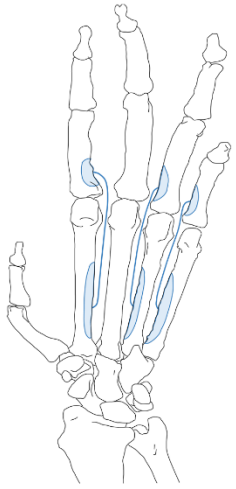	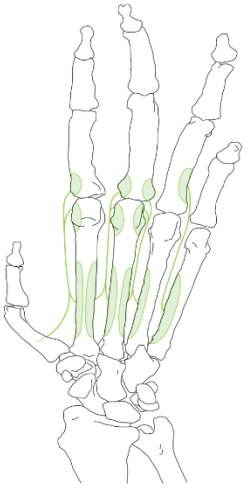

S4: A detailed documentation of the quantitative muscle parameters. Part 1

Muscle group	Muscle	Pp1	V (mm3)	FL (mm)	PCSA (mm2)	Pp2	V (mm3)	FL (mm)	PCSA (mm2)
Thenar	APB		4,5	27,1	130,9		5,5	32,5	146,7
	FPB		1,5	39,5	38,0		4,0	33,0	109,8
	ADP		11,0	88,4	120,6		11,0	41,5	246,5
	OPP		2,0	34,2	56,1		3,5	16,3	181,3
Hypothenar	ADM		7,0	30,5	201,8		7,5	37,4	189,6
	FDM		6,0	26,0	201,4		5,0	47,4	100,2
	ODM		3,0	12,9	219,2		2,5	33,3	72,3
Intermediate	LUMB		6,0	97,1	57,8		9,0	106,7	82,2
	IOD		29,0	17,3	1291,6		26,0	27,3	912,5
	IOP		14,0	23,4	506,3		13,5	29,5	444,8
Flexor	FDS								
	FCR								
	PL								
	FCU								
	FDP								
Extensor	ECRL								
	ECRB								
	ED								
	EDM								
	ECU								
	EI								
Rotator	BR								
	PT								
	SUP								
	PQ								
Ext. Thumb	FPL								
	EPL								
	EPB								
	APL								

Muscle group	Muscle	Pp7	V (mm3)	FL (mm)	PCSA (mm2)	Pp8	V (mm3)	FL (mm)	PCSA (mm2)
Thenar	APB		4,0	31,7	123,6		3,0	31,9	91,1
	FPB		3,0	32,7	89,5		4,0	37,0	108,0
	ADP		6,0	40,7	145,6		6,0	47,9	124,3
	OPP		4,0	33,9	115,1		2,0	35,2	56,9
Hypothenar	ADM		14,5	34,3	398,1		4,0	28,6	136,0
	FDM		Fused with ADM				3,0	35,0	85,0
	ODM		3,0	33,9	85,0		3,0	26,9	111,4
Intermediate	LUMB		7,5	107,9	69,5		3,5	107,1	32,7
	IOD		24,0	30,3	735,7		16,0	24,5	609,0
	IOP		15,5	26,8	562,3		9,0	22,7	368,3
Flexor	FDS		129,0	84,5	1406,9		83,0	106,9	721,6
	FCR		92,0	85,8	1026,3		53,0	64,9	779,8
	PL		5,5	50,4	106,8		4,5	48,4	89,8
	FCU		74,0	49,3	1275,1		32,0	55,4	547,6
	FDP		189,0	100,8	1727,3		110,0	108,7	966,7
Extensor	ECRL		42,0	140,3	265,5		30,0	111,4	259,7
	ECRB		40,0	60,4	600,6		21,0	75,2	272,8
	ED		47,0	103,5	434,5		36,0	129,3	273,8
	EDM		7,0	191,8	36,5		Fused with ED		
	ECU		31,0	71,6	381,2		19,0	50,1	360,9
	EI		2,5	88,9	26,2		3,0	64,1	46,5
Rotator	BR		112,0	242,9	419,1		92,0	212,7	421,6
	PT		41,0	32,5	1112,3		32,0	51,3	613,9
	SUP		57,0	37,2	1398,9		35,0	38,0	827,2
	PQ		12,0	61,4	195,4		6,0	49,4	121,4
Ext. Thumb	FPL		Absent				Absent		
	EPL		7,5	48,0	148,8		6,0	68,5	85,4
	EPB		Absent				Absent		
	APL		45,0	45,2	805,7		22,0	47,9	424,6

Pp3	V (mm3)	FL (mm)	PCSA (mm2)	Pp5	V (mm3)	FL (mm)	PCSA (mm2)	Pp6	V (mm3)	FL (mm)	PCSA (mm2)
	4,5	28,3	139,8		2,0	27,8	64,7		4,0	29,1	127,4
	2,0	36,8	54,4		4,0	22,8	175,6		1,0	30,1	27,3
	11,0	46,3	227,7		7,0	39,7	175,3		3,5	29,0	111,8
	4,0	23,9	167,4		1,0	32,8	30,5		2,0	28,2	70,8
	5,0	35,0	109,5		2,0	26,5	71,1		4,0	27,8	128,2
	4,0	30,4	120,3		2,5	33,1	72,5		2,0	30,4	60,3
	3,0	16,1	146,0		1,0	15,5	60,7		2,0	13,2	133,2
	6,0	91,4	60,2		3,5	100,7	34,8		2,5	110,7	20,9
	23,0	13,9	1307,9		12,0	19,9	548,3		16,0	27,2	512,8
	10,5	23,7	394,1		6,0	14,7	378,4		7,0	23,6	263,8
					58,0	64,5	844,9		120,0	65,5	1669,9
					40,0	64,1	522,6		65,0	57,4	820,0
					5,0	55,0	89,5		5,0	43,1	108,1
					30,0	49,9	570,2		40,0	37,3	914,7
					115,0	78,1	1352,9		145,0	92,5	1457,6
					18,1	102,0	169,2		35,0	109,7	296,5
					18,0	48,6	332,3		20,0	57,4	287,5
					30,0	57,6	508,5		40,0	54,6	699,5
					3,5	52,4	65,6		4,5	67,9	64,2
					15,0	54,4	260,9		25,0	26,3	899,7
					2,0	54,2	36,0		Fused	58,5	with EPL
					50,0	194,3	240,4		100,0	192,0	496,9
					25,0	37,9	571,8		30,0	31,2	743,1
					20,0	25,4	729,4		40,0	26,3	1114,1
					6,0	47,3	126,7		7,0	59,5	117,7
					Absent				Absent		
					5,0	44,4	104,8		15,0	37,7	379,1
					Absent				Absent		
					18,5	55,7	315,9		40,0	37,5	926,8

Pp9	V (mm3)	FL (mm)	PCSA (mm2)	Pt1	V (mm3)	FL (mm)	PCSA (mm2)	Hs1	V (mm3)	FL (mm)	PCSA (mm2)
	7,5	27,9	256,7		16,0	42,6	354,8		6,0	58,0	103,5
	Fused with APB and OPP				Fused	48,4	APB and OPP		3,5	48,2	72,7
	7,0	38,7	161,3		3,0	48,2	55,2		17,0	51,4	330,7
	Fused with APB and FPB				Fused with APB and FPB				4,5	50,6	88,9
	2,5	29,0	82,6		8,0	40,9	191,8		10,0	95,5	104,7
	2,5	23,9	102,0		6,0	50,9	114,9		Fused with ADM		
	1,5	23,9	62,4		4,0	30,4	131,7		3,0	44,3	67,7
	4,0	92,0	43,5		8,0	108,7	73,6		4,0	74,0	54,0
	19,0	26,7	673,5		25,0	35,9	632,6		12,0	62,8	191,0
	6,5	26,7	232,8		12,0	62,4	178,0		7,0	62,3	112,3
	52,0	83,5	595,2		131,0	85,5	1456,4		94,0	75,7	1184,6
	34,5	95,0	358,8		60,0	81,0	638,1		26,4	62,9	403,3
	2,0	32,5	60,9		3,0	42,4	69,2		Absent		
	34,5	52,5	610,1		59,0	53,3	984,1		34,0	99,1	321,8
	97,0	63,9	1463,6		193,0	101,4	1757,6		116,9	111,1	1004,1
	19,5	89,4	215,2		40,0	131,4	278,3		82,0	160,5	499,0
	20,0	69,5	270,2		44,0	62,9	606,5		82,0	160,5	499,0
	30,0	127,5	232,9		73,0	85,0	813,4		46,0	66,4	640,5
	5,0	77,3	64,5		Fused with ED				Fused with ED		
	19,0	88,2	212,2		30,0	49,7	561,0		25,0	44,7	541,8
	3,5	72,1	47,9		6,0	76,6	74,0		5,0	90,0	55,6
	28,5	187,2	142,4		99,0	267,3	355,3		45,0	263,0	171,1
	19,0	42,4	437,1		52,0	29,0	1608,8		37,0	70,0	528,8
	31,0	57,0	544,2		58,0	39,2	1250,7		18,0	75,7	237,7
	6,0	48,2	124,6		13,0	52,8	246,3		12,0	38,0	315,8
	Absent				Absent				33,0	75,6	424,0
	6,0	61,7	96,0		10,0	66,3	144,3		10,5	61,9	167,9
	Absent				Absent				1,5	57,7	26,0
	15,0	73,6	197,6		40,0	49,2	723,8		17,0	50,7	322,5

S5: An overview of muscle fascicle lengths in the bonobo hand and forearm muscles

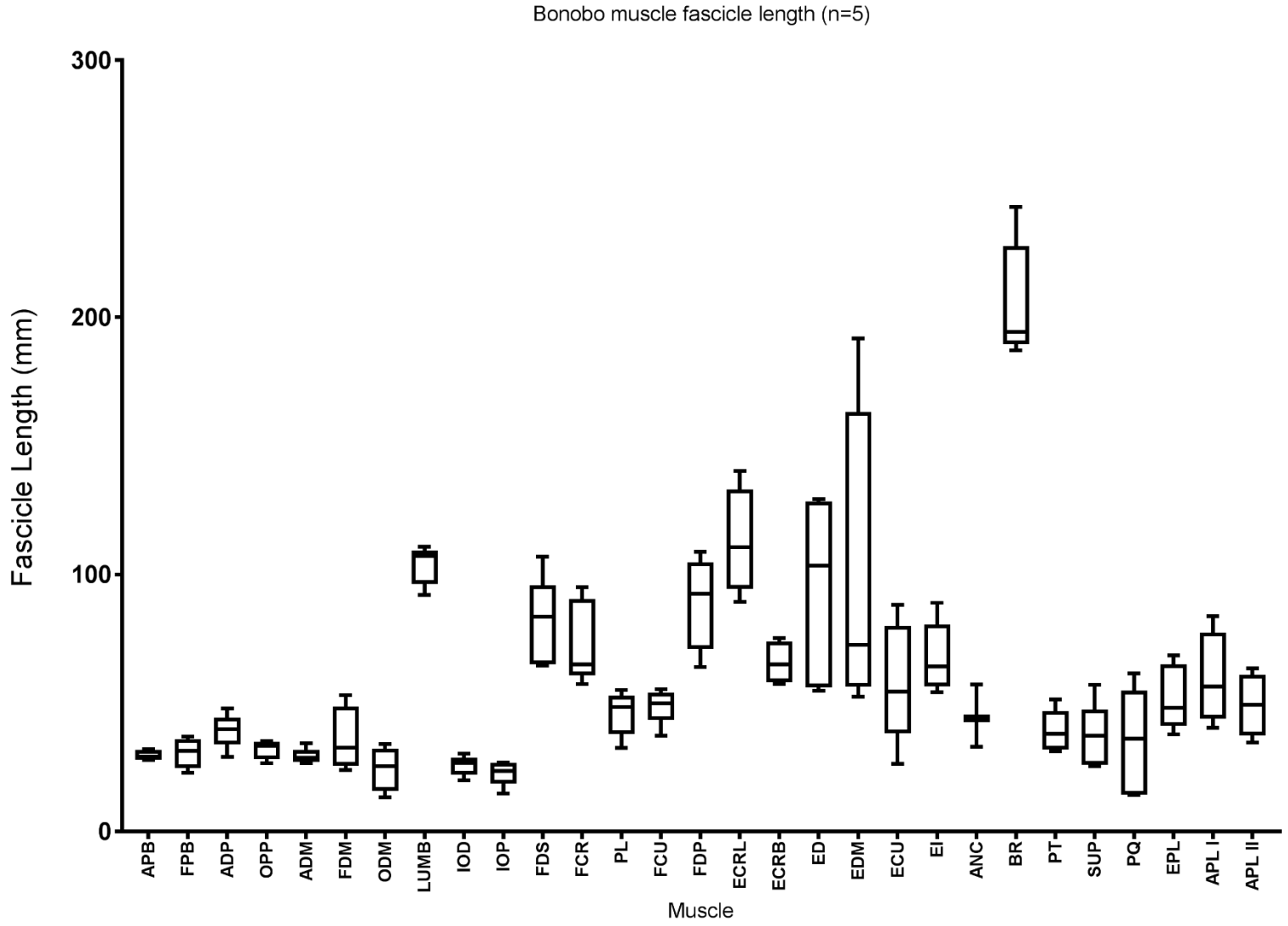

S6: An overview of muscle pennation angles in the bonobo hand and forearm muscles

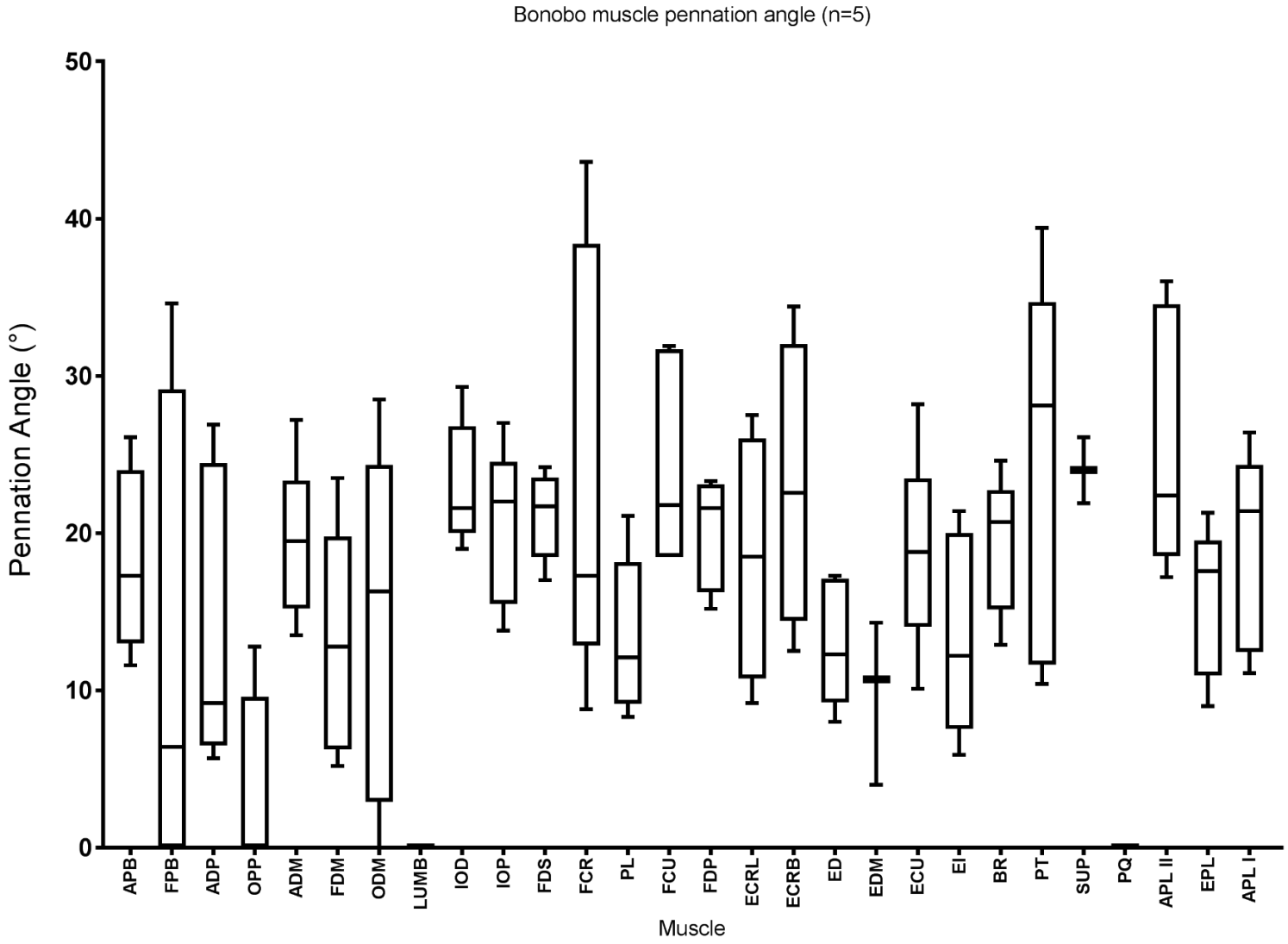

References

Alba, D. M., Moya-Sola, S. and Kohler, M. (2003) 'Morphological affinities of the Australopithecus afarensis hand on the basis of manual proportions and relative thumb length', *Journal of Human Evolution*, 44(2), pp. 225–254. doi: 10.1016/s0047-2484(02)00207-5.

Almécija, S., Smaers, J. B. and Jungers, W. L. (2015) 'The evolution of human and ape hand proportions', *Nature Communications*, 6(1), p. 7717. doi: 10.1038/ncomms8717.

Aversi-Ferreira, T. A. *et al.* (2010) 'Comparative anatomical study of the forearm extensor muscles of Cebus libidinosus (Rylands et al., 2000; primates, cebidae), modern humans, and other primates, with comments on primate evolution, phylogeny, and manipulatory behavior', *Anatomical Record*, 293(12), pp. 2056–2070. doi: 10.1002/ar.21275.

Bardo, A. *et al.* (2016) 'Behavioral and functional strategies during tool use tasks in bonobos', *American Journal of Physical Anthropology*, 161(1), pp. 125–140. doi: 10.1002/ajpa.23015.

Boesch, C., Head, J. and Robbins, M. M. (2009) 'Complex tool sets for honey extraction among chimpanzees in Loango National Park, Gabon', *Journal of Human Evolution*, 56(6), pp. 560–569. doi: 10.1016/j.jhevol.2009.04.001.

Breuer, T., Ndoundou-Hockemba, M. and Fishlock, V. (2005) 'First observation of tool use in wild gorillas', *PLoS Biology*, 3(11), pp. 2041–2043. doi: 10.1371/journal.pbio.0030380.

Butterworth, G. and Itakura, S. (1998) 'Development of precision grips in chimpanzees', *Developmental Science*, 1(1), pp. 39–43. doi: 10.1111/1467-7687.00010.

Carlson, N. S. and Lowe, N. K. (2006) 'CenteringPregnancy: A new approach in prenatal care', *MCN The American Journal of Maternal/Child Nursing*, 31(4), pp. 218–223. doi: 10.1007/s10329-005-0166-4.

Channon, A. J. *et al.* (2009) 'Mechanical constraints on the functional morphology of the gibbon hind limb.', *Journal of Anatomy*, 215(4), pp. 383–400. doi: 10.1111/j.1469-7580.2009.01123.x.

Christel, M. I., Kitzel, S. and Niemitz, C. (1998) 'How precisely do bonobos (Pan paniscus) grasp small objects?', *International Journal of Primatology*, 19(1), pp. 165–193. doi: 10.1023/A:1020319313219.

Colell, M., Segarra, M. D. and Pi, J. S. (1995) 'Hand preferences in chimpanzees (Pan troglodytes), bonobos (Pan paniscus), and orangutans (Pongo pygmaeus) in food-reaching and other daily activities', *International Journal of Primatology*, 16(3), pp. 413–434. doi: 10.1007/BF02735795.

Coolidge, H. J. and Shea, B. T. (1982) 'External body dimensions of Pan paniscus and Pan troglodytes chimpanzees', *Primates*, 23(2), pp. 245–251. doi: 10.1007/BF02381164.

Crast, J. *et al.* (2009) 'Dynamic in-hand movements in adult and young juvenile chimpanzees (Pan troglodytes)', *American Journal of Physical Anthropology*. Wiley-Blackwell, 138(3), pp. 274–285. doi: 10.1002/ajpa.20925.

Diogo, R. *et al.* (2017) *Photographic and Descriptive Musculoskeletal Atlas of Bonobos*. 1st edn. Springer International Publishing. doi: 10.1007/978-3-319-54106-8.

Diogo, R., Molnar, J. L. and Wood, B. (2017) 'Bonobo anatomy reveals stasis and mosaicism in chimpanzee evolution, and supports bonobos as the most appropriate extant model for the common ancestor of chimpanzees and humans', *Scientific Reports*. Springer US, 7(1), pp. 1–8. doi: 10.1038/s41598-017-00548-3.

Diogo, R., Potau, J. M. and Pastor, J. F. (2013) *Photographic and Descriptive Musculoskeletal Atlas of Chimpanzees: With Notes on the Attachments, Variations, Innervation, Function and Synonymy and Weight of the Muscles*. CRC Press.

Feix, T. *et al.* (2015) 'Estimating thumb-index finger precision grip and manipulation potential in extant and fossil primates', *Journal of The Royal Society Interface*, 12(106), pp. 20150176–20150176. doi: 10.1098/rsif.2015.0176.

Fragaszy, D. *et al.* (2004) 'Wild capuchin monkeys (Cebus libidinosus) use anvils and stone pounding tools', *American Journal of Primatology*, 64(4), pp. 359–366. doi: 10.1002/ajp.20085.

Furuichi, T. and Thompson, J. (2008) *The Bonobos*, *Behavior, Ecology, and Conservation*. Edited by Takeshi Furuichi and Jo Thompson. New York, NY: Springer New York. doi: 10.1007/978-0-387-74787-3.

Gumert, M. D., Hoong, L. K. and Malaivijitnond, S. (2011) 'Sex differences in the stone tool-use behavior of a wild population of burmese long-tailed macaques (Macaca fascicularis aurea)', *American Journal of Primatology*, 73(12), pp. 1239–1249. doi: 10.1002/ajp.20996.

Hamrick, M. W. (1998) 'Functional and adaptive significance of primate pads and claws: Evidence from New World anthropoids', *American Journal of Physical Anthropology*, 106(2), pp. 113–127. doi: 10.1002/(SICI)1096-8644(199806)106:2<113::AID-AJPA2>3.0.CO;2-R.

Ingmanson, E. J. (1998) 'Tool-using behaviour in wild Pan paniscus: Social and ecological considerations', in Russon, A. E., Bard, K. A., and Parker, S. T. (eds) *Reaching Into Thought: The Minds of the Great Apes*. Cambridge University Press, p. 464.

Inouye, S. E. (1992) 'Ontogeny and allometry of African ape manual rays', *Journal of Human Evolution*, 23(2), pp. 107–138. doi: 10.1016/0047-2484(92)90103-G.

Jordan, C. (1982) 'Object manipulation and tool-use in captive pygmy chimpanzees (Pan paniscus)', *Journal of Human Evolution*, 11(1), pp. 35–39. doi: 10.1016/S0047-2484(82)80029-8.

Kivell, T. L. (2015) 'Evidence in hand: recent discoveries and the early evolution of human manual manipulation', *Philosophical Transactions of the Royal Society B: Biological Sciences*, 370(1682), p. 20150105. doi: 10.1098/rstb.2015.0105.

Kuhlwilm, M. *et al.* (2016) 'Evolution and demography of the great apes', *Current Opinion in Genetics and Development*, 41, pp. 124–129. doi: 10.1016/j.gde.2016.09.005.

Lesnik, J. J., Sanz, C. M. and Morgan, D. B. (2015) 'The interdigital brace and other grips for termite nest perforation by chimpanzees of the Goualougo Triangle, Republic of Congo', *American Journal of Physical Anthropology*, 157(2), pp. 252–259. doi: 10.1002/ajpa.22706.

Marzke, M. W. (1997) 'Precision grips, hand morphology, and tools', *American Journal of Physical Anthropology*, 102(1), pp. 91–110. doi: 10.1002/(SICI)1096-8644(199701)102:1<91::AID-AJPA8>3.0.CO;2-G.

Marzke, M. W. *et al.* (1998) 'EMG study of hand muscle recruitment during hard hammer percussion manufacture of Oldowan tools', *American Journal of Physical Anthropology*, 105(3), pp. 315–332. doi: 10.1002/(SICI)1096-8644(199803)105:3<315::AID-AJPA3>3.0.CO;2-Q.

Marzke, M. W. and Marzke, R. F. (2000) 'Evolution of the human hand: Approaches to acquiring, analysing and interpreting the anatomical evidence.', *Journal of Anatomy*, 197, pp. 121–140. doi: 10.1046/j.1469-7580.2000.19710121.x.

Marzke, M. W., Wullstein, K. L. and Viegas, S. F. (1992) 'Evolution of the power ("squeeze") grip and its morphological correlates in hominids', *American Journal of Physical Anthropology*, 89(3), pp. 283–298. doi: 10.1002/ajpa.1330890303.

Medler, S. (2002) 'Comparative trends in shortening velocity and force production in skeletal muscles', *American Journal of Physiology-Regulatory, Integrative and Comparative Physiology*. American Physiological Society, 283(2), pp. R368–R378. doi: 10.1152/ajpregu.00689.2001.

Miller, R. (1952) 'The musculature of Pan paniscus', *American Journal of Anatomy*, 91, pp. 183–232.

Myatt, J. P. *et al.* (2012) 'Functional adaptations in the forelimb muscles of non-human great apes', *Journal of Anatomy*, 220(1), pp. 13–28. doi: 10.1111/j.1469-7580.2011.01443.x.

Neufuss, J. *et al.* (2017) 'Nut-cracking behaviour in wild-born, rehabilitated bonobos (Pan paniscus): a comprehensive study of hand-preference, hand grips and efficiency', *American Journal of Primatology*, 79(2), pp. 1–16. doi: 10.1002/ajp.22589.

Oishi, M. *et al.* (2009) 'Dimensions of forelimb muscles in orangutans and chimpanzees', *Journal of Anatomy*, 215(4), pp. 373–382. doi: 10.1111/j.1469-7580.2009.01125.x.

Pouydebat, E. *et al.* (2009) 'Biomechanical study of grasping according to the volume of the object: Human versus non-human primates', *Journal of Biomechanics*, 42(3), pp. 266–272. doi: 10.1016/j.jbiomech.2008.10.026.

Prado-Martinez, J. (2013) 'Great ape genetic diversity and population history', *Nature*, 499(7459), pp. 471–475. doi: 10.1038/nature12228.Great.

Prüfer, K. *et al.* (2012) 'The bonobo genome compared with the chimpanzee and human genomes', *Nature*, 486(7404), pp. 527–531. doi: 10.1038/nature11128.

Schindelin, J. *et al.* (2012) 'Fiji: an open-source platform for biological-image analysis', *Nature Methods*, 9, p. 676.

Simpson, S. W., Latimer, B. and Lovejoy, C. O. (2018) 'Why Do Knuckle-Walking African Apes Knuckle-Walk?', *The Anatomical Record*. Wiley-Blackwell, 301(3), pp. 496–514. doi: 10.1002/ar.23743.

Skinner, M. M. *et al.* (2015) 'Human evolution. Human-like hand use in Australopithecus africanus.', *Science (New York, N.Y.)*, 347(6220), pp. 395–9. doi: 10.1126/science.1261735.

Spinozzi, G., Truppa, V. and Laganà, T. (2004) 'Grasping behavior in tufted capuchin monkeys (Cebus apella): Grip types and manual laterality for picking up a small food item', *American Journal of Physical Anthropology*, 125(1), pp. 30–41. doi: 10.1002/ajpa.10362.

Susman, R. L. (1998) 'Hand function and tool behavior in early hominids', *Journal of*

Human Evolution, 35(1), pp. 23–46.

Susman, R. L. and Stern, J. T. (1980) 'EMG of the interosseous and lumbrical muscles in the chimpanzee (Pan troglodytes) hand during locomotion', *American Journal of Anatomy*, 157(4), pp. 389–397. doi: 10.1002/aja.1001570407.

Takeshita, H. and Walraven, V. (1996) 'A comparative study of the variety and complexity of object manipulation in captive chimpanzees (Pan troglodytes) and bonobos (Pan paniscus)', *Primates*, 37(4), pp. 423–441. doi: 10.1007/BF02381377.

Thorpe, S. K. S. *et al.* (1999) 'Dimensions and moment arms of the hind- and forelimb muscles of common chimpanzees (Pan troglodytes)', *American Journal of Physical Anthropology*, 110(2), pp. 179–199. doi: 10.1002/(SICI)1096-8644(199910)110:2<179::AID-AJPA5>3.0.CO;2-Z.

Tocheri, M. W. *et al.* (2008) 'The evolutionary history of the hominin hand since the last common ancestor of Pan and Homo', *Journal of Anatomy*, 212(4), pp. 544–562. doi: 10.1111/j.1469-7580.2008.00865.x.

Toth, N. *et al.* (1993) 'Pan the Tool-Maker: Investigations into the Stone Tool-Making and Tool-Using Capabilities of a Bonobo (Pan paniscus)', *Journal of Archaeological Science*, 20(1), pp. 81–91. doi: 10.1006/jasc.1993.1006.

Tuttle, R. H. (1969) 'Quantitative and functional studies on the hands of the anthropoidea. I. The Hominoidea', *Journal of Morphology*, 128(3), pp. 309–363. doi: 10.1002/jmor.1051280304.

Vereecke, E. E. *et al.* (2005) 'Functional analysis of the foot and ankle myology of gibbons and bonobos.', *Journal of anatomy*, 206(5), pp. 453–76. doi: 10.1111/j.1469-7580.2005.00412.x.

Visalberghi, E. *et al.* (2009) 'Selection of Effective Stone Tools by Wild Bearded Capuchin Monkeys', *Current Biology*, 19(3), pp. 213–217. doi: 10.1016/j.cub.2008.11.064.

Wells, J. B. (1965) 'Comparison of mechanical properties between slow and fast mammalian muscles', *The Journal of Physiology*, 178(2), pp. 252–269. doi: 10.1113/jphysiol.1965.sp007626.

Williams, E. M., Gordon, A. D. and Richmond, B. G. (2010) 'Upper limb kinematics and the role of the wrist during stone tool production', *American Journal of Physical Anthropology*, 143(1), pp. 134–145. doi: 10.1002/ajpa.21302.

Wolfe, S. W. *et al.* (2006) 'The Dart-Throwing Motion of the Wrist: Is It Unique to Humans?', *Journal of Hand Surgery*, 31(9), pp. 1429–1437. doi: 10.1016/j.jhsa.2006.08.010.

Young, N. M. *et al.* (2015) 'Fossil hominin shoulders support an African ape-like last common ancestor of humans and chimpanzees', *Proceedings of the National Academy of Sciences*, 112(38), pp. 11829–11834. doi: 10.1073/pnas.1511220112.

Zihlman, A. L. and Bolter, D. R. (2015) 'Body composition in *Pan paniscus* compared with *Homo sapiens* has implications for changes during human evolution', *Proceedings of the National Academy of Sciences*, 112(24), pp. 7466–7471. doi: 10.1073/pnas.1505071112.

Part 2.
Form and function of the TMC joint

In this part I address the form and function of the thumb at the level of the TMC joint. Morphological and kinematic analyses based on medical imaging are used to assess the shape and principal capabilities of the TMC joint. This part comprises two chapters; **Chapter 2** provides insight in these areas in the bonobo with the inclusion of a chimpanzee and human specimen, while **Chapter 3** expands this work to the gibbon and macaque. This part addresses *objective 1, objective 2,* and *objective 3* of the thesis

Objective 1: To document the forelimb soft and hard tissue morphology through detailed dissections and medical imaging in order to provide a detailed anatomical dataset for bonobos, gibbons, and macaques.

Objective 2: To compare morphological differences related to thumb function between the primate taxa.

Objective 3: To investigate and compare the functional capabilities of the TMC joint in bonobos, gibbons and macaques.

Chapter 2.

Mobility and structural constraints of the bonobo trapeziometacarpal joint

Timo van Leeuwen[1], Maarten Vanneste[1], Faes D. Kerkhof[1], Priscilla D'Agostino[1], Marie J.M. Vanhoof[1], Jeroen M.G. Stevens[2,3], G. Harry van Lenthe[4], Evie E. Vereecke[1]

[1]Department of Development and Regeneration, KU Leuven, Belgium

[2]Centre for Research and Conservation, Royal Zoological Society Antwerp, Belgium

[3]Behavioural Ecology and Ecophysiology Group, University of Antwerp, Belgium

[4]Biomechanics Section, Department of Mechanical Engineering, University of Leuven, Leuven, Belgium

Published as:

van Leeuwen, T., Vanneste, M., Kerkhof, F. D., D'agostino, P., Vanhoof, M. J. M., Stevens, J. M. G., van Lenthe, G. H., and Vereecke E. E. 2019 *Mobility and structural constraints of the bonobo trapeziometacarpal joint*. Biological Journal of the Linnean Society. 127, 3, pp. 681-693.

Abstract

The human thumb is specialised for manual tasks as it is no longer typically involved in locomotion. However, members of the genus *Pan* – the closest extant relatives to modern humans – also have a highly mobile thumb which allows complex manual tasks such as tool-crafting and use. Here, we investigate the thumb kinematics of bonobos (*Pan paniscus*) in relation to the morphology of their trapeziometacarpal joint using unembalmed bonobo specimens and compare that with the human condition. We use CT-based models of skeletal elements of the thumb during positions of maximum abduction/adduction and flexion/extension to determine the kinematics of the first metacarpal in bonobos and healthy human volunteers. In addition, the 3D geometry of the trapeziometacarpal joint is quantified and, together with assessment of the ligaments surrounding the joint, is related to the obtained kinematics of the first metacarpal. Our results show a similar trapezial 3D morphology and similar kinematics of the first metacarpal in bonobos and humans, with a markedly higher extension of the first metacarpal in humans. This study provides an integrated analysis of thumb anatomy and kinematics in a unique sample of bonobo specimens.

Keywords: primate anatomy, thumb, *Pan paniscus,* trapeziometcarpal joint, thumb ligaments

Introduction

Due to its frequent interaction with the environment, the structure of the hand reflects adaptations related to its use and the level of dexterity of the animal. The thumb is a key component of the hand, with a less mobile thumb having more stability to withstand forces associated with locomotion, whereas a more mobile thumb allows better manipulation and grasping skills (Marzke *et al.*, 2010). The human thumb is a prime example of a highly mobile structure capable of excellent manual dexterity, however, several non-human primate species possess a similarly mobile thumb and display advanced manipulative capabilities (Christel, 1993; Colell, Segarra and Pi, 1995; Christel, Kitzel and Niemitz, 1998; Spinozzi, Truppa and Laganà, 2004; Breuer, Ndoundou-Hockemba and Fishlock, 2005; Gumert, Hoong and Malaivijitnond, 2011). Members of the genus *Pan*, human's closest extant relatives, express a range of complex grip types, e.g. forceful power grips, in-hand manipulations, and dextrous precision grips, as well as thumb opposition, similar to humans (Marzke, 1997; Butterworth and Itakura, 1998; Christel, Kitzel and Niemitz, 1998; Pouydebat *et al.*, 2009; Feix *et al.*, 2015; Bardo *et al.*, 2016). Moreover, like humans, bonobos (*Pan paniscus*) and chimpanzees (*Pan troglodytes*) are capable of tool use, a feature that requires relatively complex thumb utilisation (Jordan, 1982; Toth *et al.*, 1993; Takeshita and Walraven, 1996; Ingmanson, 1998; Neufuss, Humle, *et al.*, 2017). Yet, unlike humans, bonobos and chimpanzees also use their hands during both arboreal and terrestrial locomotion. During terrestrial knuckle-walking, however, the thumb is not typically engaged with the substrate because of its relatively short length (Tuttle, 1967; Wunderlich and Jungers, 2009). How bonobos and chimpanzees use their thumb during arboreal locomotion is not well documented. Recently, behavioural observations by Neufuss et al. showed that the thumb is important during vertical climbing in wild chimpanzees (and mountain gorillas) (Neufuss, Robbins, *et al.*, 2017), but lab-based pressure measurements during vertical climbing in captive bonobos indicates that the pressure underneath the thumb is minimal (Samuel *et al.*, 2018). Such use patterns indicate that the bonobo (and chimpanzee) thumb may be used more for manipulation than previously thought, and might therefore show adaptive signals towards thumb mobility converging to that of the human thumb (Marzke *et al.*, 2015).

The mobility of the thumb and the degree to which it can serve as a prehensile organ is determined by a set of morphological parameters: the position of the trapezium in the carpal complex (which determines the orientation of the distal trapezial joint facet and thus the orientation of the thumb relative to the fingers), the length of the thumb (relative to finger length), the thumb musculature, the trapeziometacarpal joint ligaments, the 3D geometry of the metacarpophalangeal (MCP), interphalangeal (IP) and, in particular, the trapeziometacarpal (TMC) joint (Napier, 1952, 1955, 1960; Rose, 1992). The morphology of the TMC or basal thumb joint has been associated with the range of motion of the thumb

and, as a result, with grip capability in different primate species (Rose, 1992). In hominids, the TMC joint is a saddle-shaped joint (Marzke, 1971; Lewis, 1977; Tocheri *et al.*, 2003, 2005; Marzke *et al.*, 2010), the physiological equivalent of a universal joint with two degrees of freedom (Cooney and Chao, 1977). The majority of movement is guided along the two principal directions of movement of the thumb; abduction-adduction and flexion-extension, and is passively constrained particularly by the ligaments crossing the TMC joint, stabilizing the first metacarpal (MC1).

As the modern human's closest extant relatives, members of the genus *Pan* are essential for interpreting the fossil record and have thus been incorporated in many studies of fossil hominin and hominoid morphology (Rafferty, 1990; Tocheri *et al.*, 2008; Marzke *et al.*, 2010; Almécija, Alba and Moyà-Solà, 2012; Feix *et al.*, 2015; Skinner *et al.*, 2015; Marchi *et al.*, 2017). However, relatively little is known about the morphology and functional capacity of the thumb in either chimpanzees and, especially, bonobos. In a recent study (van Leeuwen et al. 2018), we used a series of bonobo cadavers to document and quantify extrinsic and intrinsic hand musculature. The anatomical data indicated a similar muscle configuration and force-generating capacity at the level of the TMC joint in bonobos and humans, however, TMC ligament configuration and 3D joint geometry were not included in the study. The human TMC joint ligament configuration has been studied in detail and comprises a dorsal ligament complex (*dorsal radial ligament* (DRL), *dorsal central ligament* (DCL), and *posterior oblique ligament* (POL)) that reinforces the TMC against dorsal subluxing forces that are associated with power grips and pinches, volar ligaments (*anterior oblique ligament* (AOL) and *ulnar collateral ligament* (UCL)) which stabilize the thumb during extension and prevent palmar subluxation, and ulnar ligaments (*intermetacarpal ligament* (IML) and *deep intermetacarpal ligament* (DIML) that stabilize the MC1 (Bettinger *et al.*, 1999; Ladd, Lee and Hagert, 2012; D'Agostino *et al.*, 2014; Komatsu and Lubahn, 2018). In comparison, relatively little is known about non-human primate thumb ligament structures (but see Lewis (1977) and Shrewsbury (2003)) and configurations in different primates need to be further studied.

Here, we investigate both the functional capabilities and the morphology of the bonobo TMC joint in comparison to that of humans. The study primarily investigates the kinematics of the bonobo first metacarpal during the principal movements of the thumb, the geometry of the trapezial articular surface that facilitates movement of the thumb, and the surrounding ligaments that passively restrain the TMC joint. These are subsequently compared to the kinematics and morphology of the human thumb and related to both species' manual capabilities. We hypothesize that the bonobo thumb has a large range of motion in both planes (flexion-extension, abduction-adduction), approaching the level of mobility of the human thumb, to allow for the dextrous manual abilities described in literature (Marzke, 1997; Butterworth and Itakura, 1998; Christel, Kitzel and

Niemitz, 1998; Pouydebat *et al.*, 2009; Feix *et al.*, 2015; Bardo *et al.*, 2016). We expect to see this reflected in the geometry of the joint; a saddle-shaped joint comparable to that of humans, as well as in the ligaments, that should be sufficiently developed to provide passive tension when required but that do not impede heavily on the mobility of the thumb.

Materials and methods

Specimen acquisition

Cadaver specimens of five adult bonobos were obtained in collaboration with various European zoos (**Table 1**). One cadaveric human specimen, obtained via the Human Body Donation Program of the University of Leuven, Belgium, was included for comparison of the anatomical features between bonobo and human. The specimens included the entire forearm and hand and were stored at -18 degrees Celsius. The bonobo and human specimens have been included in a previous study focussing on extrinsic and intrinsic hand musculature (van Leeuwen *et al.*, 2018). All individuals died of natural causes.

Table 1: Cadaveric specimen details. Pp: *Pan paniscus*, Hs: *Homo sapiens*, F: female, M: male, L: left arm + hand, R: right arm + hand, *Specimen code in van Leeuwen et al. (2018); **wild born

Code	Previous Code*	Subject Identifier	Sex	Age	Sample	Origin	Analysis
Pp1	Pp2	Zorba** 8365526	M	adult 35yr	L	Wilhelma Zoo, Stuttgart, Germany	Anatomy/ Kinematics
Pp2	Pp5	Jasiri 15295295	F	subadult 8yr	L	Royal Zoological Society Antwerp, Belgium	Anatomy/ Kinematics
Pp3	Pp7	Ludwig MIG12-29882197	M	adult 32yr	R	Zoo Frankfurt, Germany	Anatomy/ Kinematics
Pp4	Pp8	Kirembo SB:177	M	adult 24yr	R	La Vallée des Singes, Le Gureau, France	Anatomy/ Kinematics
Pp5	Pp9	Hermien** 27641621	F	adult 39yr	L	Wilhelma Zoo, Stuttgart, Germany	Anatomy/ Kinematics
Hs1	Hs1	692	M	adult 60yr	L	University of Leuven, Kortrijk, Belgium	Anatomy

CT scanning and image segmentation

The specimens were CT-scanned using a 64 slice Discovery HD 750 CT scanner (GE Healthcare, Little Chalfont, UK; Display Field of View (DFOV): 250 mm; slice thickness: 0.625 mm; voxel size: 0.15 mm^3; 100 kV; 180 mA; image size: 512x512 pixels). Each specimen was scanned in a set of static functional positions including thumb abduction, adduction, flexion, and extension, using a custom-designed radiolucent rig according to a protocol adapted from (Crisco et al. 2015; D'Agostino et al. 2017a).

The CT-scans were segmented manually using Mimics 19.0 (Mimics for Research 19.0, Materialise, Leuven, Belgium) and the bone elements involved in thumb motion (i.e. the radius, scaphoid, trapezium, and first metacarpal (MC1)) were reconstructed into 3D surface models for each position.

Human volunteers

CT scan data from five healthy human volunteers from a previous study on human thumb kinematics (Kerkhof *et al.*, 2018) were used in our analysis for comparison. Subject details are provided in **Table 2**. Static CT scans of the functional positions mentioned above were collected using the same radiolucent rig and with a similar protocol as used to collect the bonobo data. CT-scan segmentation and reconstruction followed the same protocol as used for the bonobo scans.

Table 2: Human volunteer details. F: female, M: male; R: right arm + hand, L: left arm + hand

Code	Subject identifier	Sex	Age	Sample	Analysis
Hs2	Patient 10	F	30	R	Kinematics
Hs3	Patient 11	F	25	L	Kinematics
Hs4	Patient 12	F	37	R	Kinematics
Hs5	Patient 18	F	55	R	Kinematics
Hs6	Patient 19	M	26	R	Kinematics

Kinematic analysis and 3D joint geometry

We used custom Matlab (Mathworks, Natick, MA) scripts to register the bonobo and human 3D bone models from each static functional position onto their counterpart (i.e. flexion-extension, abduction-adduction) to determine the kinematics of the involved bone elements during thumb flexion and abduction. An iterative closest point (ICP) algorithm was applied to calculate the transformation matrix (i.e. rotation and translation) between the bone models of each investigated thumb motion by minimizing the squared distances between model vertices (Bergström et al. 2011; Bergström & Edlund 2017; D'Agostino et al. 2017a). Movements of the MC1 during thumb motion are expressed in a local coordinate system, relative to the trapezium, while the movements of the scaphoid and trapezium are expressed in a radius-based coordinate system.

The local coordinate system is represented by the principal axes of the TMC joint (**Fig. 1**). As the trapezium articulates with the MC1 through a saddle-shaped joint surface, the two principal directions of the saddle represent the two principal movements of the thumb, adduction-abduction and flexion-extension. A fifth-degree polynomial was fitted to the joint surface of the trapezium to determine the saddle point (i.e. where the slope in both principal directions is zero, see below) and the principal directions of curvature, which represent the two orthogonal axes of the joint surface that define the coordinate system (Halilaj *et al.*, 2013). The radii of curvature of a 25-point grid in a 2.25 mm radius around the saddle point were averaged in each principal direction of the coordinate system, corresponding to the functional axes of the trapezium, to represent joint surface curvature of each direction.

Movements of the trapezium and scaphoid are expressed relative to a radius-based coordinate system, which is defined using manual point registration at the radiocarpal joint using the radial styloid process and ulnar notch as landmarks (Orr et al. 2010; D'Agostino et al. 2017a). The coordinate system is in line with the International Society of Biomechanics (ISB) convention (Wu and Cavanagh, 1995; Wu *et al.*, 2005), with dorsoventral being the x-axis, proximo-distal the y-axis, and radio-ulnar the z-axis. Each bone element is fitted onto its counterpart within the same principal motion of the thumb using the ICP algorithm as described above. By using the radius as an anchor point, the rotation and translation of each bone element relative to the radius are determined for thumb flexion and abduction. Subsequently, by subtracting the movements of the previous element in the chain (radius – scaphoid – trapezium – MC1), movements of each element with respect to the previous element are calculated.

In addition, the trapezium-based coordinate system was used relative to the radius-based coordinate system to determine the orientation of the trapezium within the hand. The *saddle point* of the trapezium is determined within the radius-based coordinate system, standardized to the radial styloid, to represent the location of the trapezium. The trapezium-based coordinate system's normal, perpendicular to the distal trapezial articular surface, and the proximodistal axis of the radius were aligned. The trapezium's offset from the proximodistal axis was determined and described as angles in both the mediolateral plane, *azimuth,* and the dorsoventral plane, *elevation* (**Fig. 1**). Given the small sample size, we evaluated potential differences between bonobos and humans visually using scatter-dot plots.

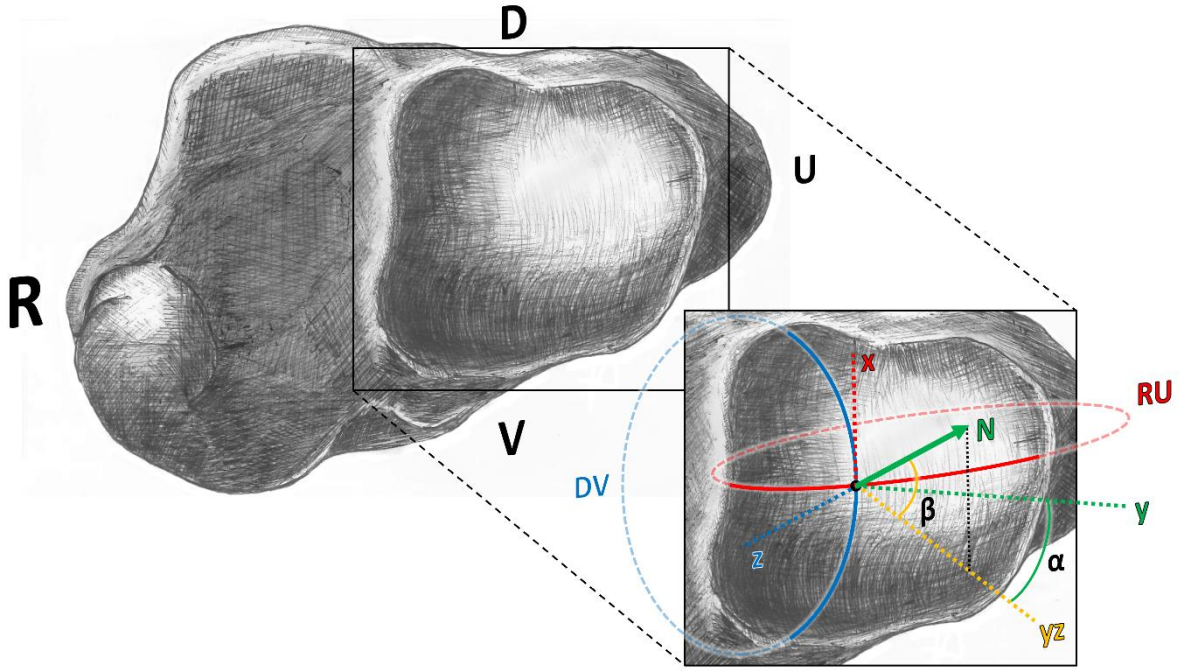

Figure 1: The trapezium coordinate system depicted on a bonobo left hand trapezium, where **R**, **U**, **D** and **V** are the trapezium's radial, ulnar, dorsal and volar sides, respectively. The local coordinate system is defined by DV, the dorsal–volar, N, the proximal–distal, and RU, the radial–ulnar axis. Rotation along DV results in thumb abduction or adduction, along RU in flexion or extension, and along N in rotation of the MC1. Joint surface curvature is quantified as the radius that describes the circles DV and RU that describe the curvature in each of the trapezium's principal directions of movement. **N** is defined by the saddle point's normal, its relative deviation to the radial coordinate system, here defined by *x* (radial–ulnar), *y* (proximal–distal) and *z* (dorsal–volar), and describes the orientation of the trapezium's distal facet. This deviation is a product of the radial deviation, defined by the azimuth (**α**), and the volar deviation, defined by the elevation (**β**).

Dissection of the TMC joint ligaments

After the removal of the muscle tissue (van Leeuwen *et al.*, 2018), the TMC ligament structure was dissected according to the technique of Berger et al. (2001), and ligament origin and insertion were identified and photographed in situ. Subsequently, the individual ligaments were extracted and documented using a remote-controlled digital camera set-up.

Results

Kinematics of the first metacarpal during thumb abduction and flexion

Kinematic analysis of the MC1 range of motion with respect to the trapezium during thumb abduction and flexion indicates that bonobos are capable of similar ranges of MC1 motion as humans during thumb abduction, while the human range of MC1 motion during thumb flexion far exceeds that of bonobos, with the exception of one individual (**Fig. 2**). The mean range of motion of the MC1 in bonobos about the dorsoventral (x) axis during thumb abduction is 31.4 ± 6.5°, similar to the observed human range of movement of 33.0 ± 4.5°. In contrast, during thumb flexion, the range of motion of the MC1 about the mediolateral (z) axis in bonobos is 9.5 ± 2.9° (after exclusion of outlier Pp2 with a range of MC1 motion of 53.0°) while that of humans is 38.7 ± 3.9°. Visual evaluation of the maximum thumb positions indicates that the substantial difference in flexion-extension range of motion between bonobos and humans is due by the capability of higher extension of the human MC1 (**Fig. 3**). Furthermore, the analysis shows that in addition to MC1 rotation about the principal axis during either thumb abduction or flexion, rotation along the other two axes occurs as well. That is, during thumb flexion, MC1 flexion is combined with abduction and external rotation of the MC1, while during thumb abduction, rotation about the other two axes is more variable, such that either MC1 flexion or extension may occur with either internal or external rotation of the MC1 (**Fig. 2**).

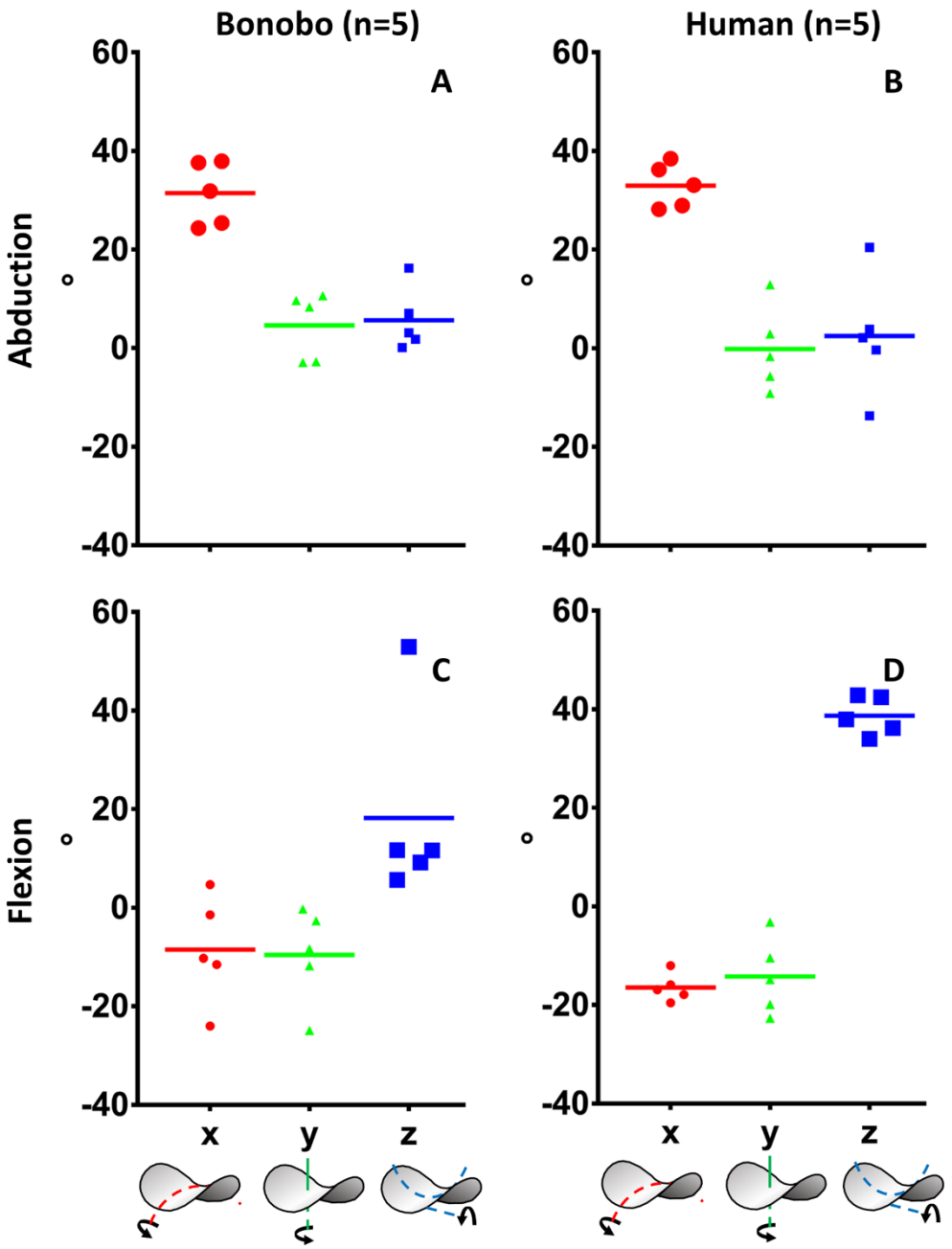

Figure 2. Thumb range of motion represented by rotational angles about the principal axes of the trapezium (x = dorsal–volar, y = proximal–distal, and z = radial–ulnar), during thumb abduction (**A**, **B**) and thumb flexion–extension (**C**, **D**), in bonobos ($N = 5$) (**A**, **C**) and humans ($N = 5$) (**B**, **D**). Positive rotations about x reflect MC1 abduction, positive rotations about y reflect MC1 exo-rotation, and positive rotations about z reflect MC1 flexion.



Figure 3: Example of maximal MC1 extension in one bonobo specimen (Pp5) and a human volunteer (Hs4). Note the markedly larger MC1 extension in the human subject.

Curvature of the distal articular facet of the trapezium

The curvature of the distal articular facet of the trapezium (**Fig. 4**) is similar between humans and bonobos in the dorsoventral plane, with a convex radius of curvature of 4.1 ± 1.2 mm in bonobos, and 4.3 ± 0.8 mm in humans. However, visual inspection of the curvature along the entire facet shows that the radius of curvature at the level of the saddle point does not describe the curvature of the entire distal facet in the direction of thumb flexion/extension. Instead, the dorsoventral profile of the trapezium's joint surface appears to level off at the most dorsal and most volar aspects of the facet in both bonobos and humans, causing its profile to resemble more of a bell curve than a circle. In contrast, the joint surface curvature of the entire facet in the mediolateral plane is shown to be well represented by the radius of curvature at the saddle point, both in bonobos and humans. In this direction of thumb abduction/adduction, we do see a difference in curvature between bonobos and humans, where the former has a concave radius of curvature of 7.1 ± 1.5 mm and the latter 11.1 ± 1.0 mm.

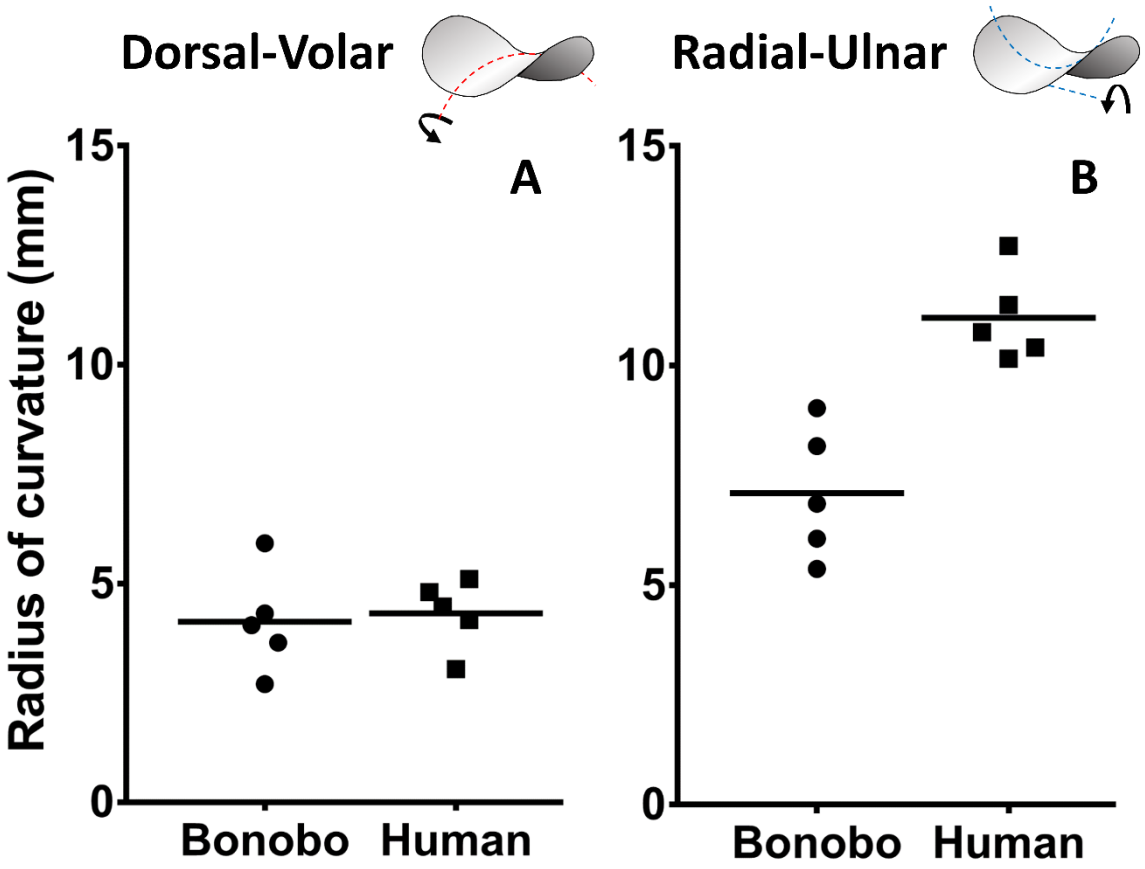

Figure 4: Radii of curvature that describe the circle that lies tangential to the curvature in the trapezium principal directions of movement, flexion (**A**) and abduction (**B**), in both bonobos and humans. A larger radius describes a larger circle, and thus a less curved surface.

Orientation and position of the trapezium relative to the radial styloid

No clear distinction can made in orientation and/or position of the trapezium in the carpal complex between bonobos and humans (**Fig. 5**). The saddle point of the bonobo trapezium is located 11.2 ± 5.7 mm lateral, 19.5 ± 4.1, mm distal, and 6.7 ± 2.2 volar relative to the radial styloid process. Similarly, the human's trapezial saddle point is located 8.7 ± 4.3 mm lateral, 17.7 ± 1.4 mm distal, and 6.7 ± 2.4 volar to the styloid. Likewise, the orientation of both species' trapezial articular surfaces are similar, with the normal in the trapezial saddle point facing volarly and radially. Radial deviation from the proximodistal axis of the forearm (*azimuth*) is 33.9 ± 9.2° in bonobos and 39.4 ± 1.3° in humans, while deviation towards the volar side of the hand (*elevation*) in bonobos is 26.0 ± 22.3°, and 20.5 ± 13.2° in humans.

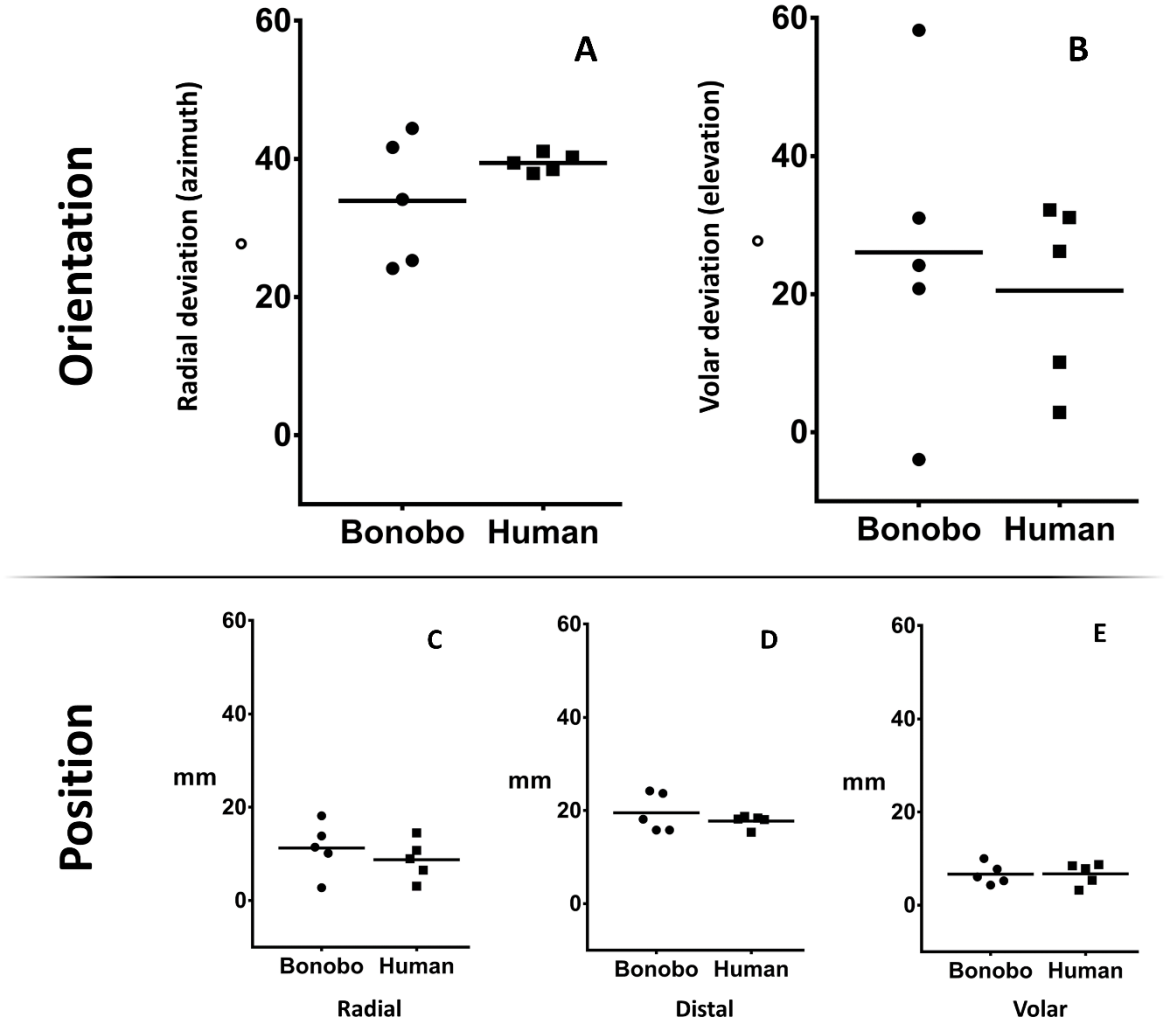

Figure 5: Orientation and position of the trapezium within the bonobo and human hand. The orientation of the trapezium distal facet is defined as the angle deviation of the trapezium normal from the proximal–distal axes of the radius, which is along the arm. Its deviation can be defined using two angles, one in the radialulnar plane, or azimuth (**A**), and the other in the dorsal–volar plane, elevation (**B**). The position of the trapezium saddle point is defined relative to the radial styloid, described in a 3D, radius-based, coordinate system with the styloid defined as origin. The trapezium saddle point is subsequently found a distance more radial (**C**), more distal (**D**) and more volar (**E**) to this point.

Functional anatomy of the TMC joint ligaments

From our observations on the TMC ligament configurations (**Fig. 6**), we conclude that our single human specimen does conform to the standard descriptions of the TMC ligaments (Bettinger *et al.*, 1999; D'Agostino *et al.*, 2014). We observe a prominent dorso-radial ligament (DRL), originating from the trapezium's dorso-radial tubercle and inserting on the dorsal edge of the MC1 base. The posterior oblique ligament (POL) originates just medially to the DRL, from the dorso-ulnar aspect of the trapezium and inserts onto the dorso-ulnar side of the MC1 and towards the palmar-ulnar tubercle. As reported in the literature, the anterior oblique ligament (AOL) originates from the volar tubercle of the trapezium and inserts onto the volar beak of MC1. The AOL in our specimen is translucent, frail and under-developed compared to the dorsal ligaments, which is consistent with previous reports (Bettinger *et al.*, 1999; D'Agostino *et al.*, 2014). The intermetacarpal ligament (IML) that stabilizes the MC1 runs from the base MC2 to the base of MC1, corresponding to the descriptions in the literature (Bettinger *et al.*, 1999; D'Agostino *et al.*, 2014).

In bonobos, the DRL is thin compared to the human DRL, but with a similar origin and insertion. The DRL is characterized by the clearly distinguishable direction of its collagen fibres, in bonobos, however, these fibres are more widely spaced compared to humans, adding to its thin appearance. The POL configuration in bonobos is similar to that of humans but relatively well developed when compared to the adjacent DRL. In contrast to the human configuration, the AOL is more prominent in bonobos, compared to the other TMC ligaments and compared to the human AOL. Its origin and insertion are the same as in humans, but it is a thick, non-translucent structure. The IML in bonobos is similar to that of humans in its origin, insertion, and its dimensions.

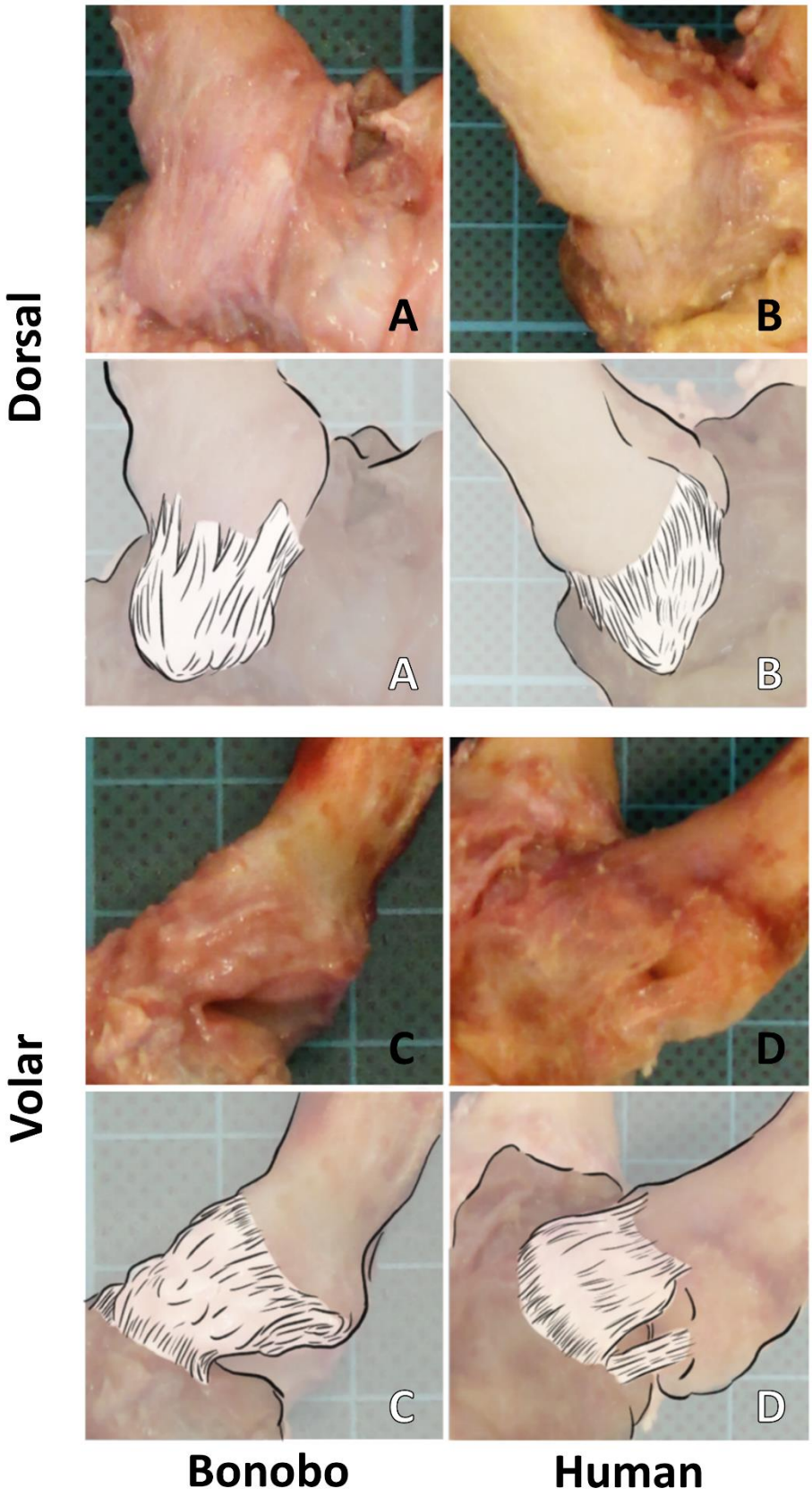

Figure 6: Pictures and illustrations of TMC joint ligament configurations in bonobos (**A**, **C**) compared to that of humans (**B**, **D**). Dorsally (**A**, **B**) we see the DRL and POL, and on the volar side (**C**, **D**) we see the AOL.

Discussion

Our results show that the anatomy and kinematics of the bonobo thumb display many similarities with the human thumb, which can be expected given the close phylogenetic relationship between the two species. However, we do observe differences in mechanical capabilities, articular surface geometry and ligament configuration which might be related to dissimilar daily use of the thumb and overall dexterity.

The kinematic analysis shows that bonobos display a smaller range of MC1 motion during thumb flexion than during thumb abduction. Moreover, the range of motion of the MC1 during thumb flexion is markedly lower than observed in humans, displaying a limitation of close to 30°, which may lead to more restricted thumb mobility. Evaluation of the positions of maximum flexion and extension in both species indicates that the larger range of motion of the human MC1 in the dorsoventral plane can be attributed to the human's capacity to further extend the MC1 compared to bonobos (**Fig. 3**). Orientation of the trapezium does not explain this higher extension potential of the human MC1 given that the position and orientation of the trapezium in the carpal complex is similar between bonobos and humans. Also, surface curvature analysis shows no specific differences between bonobos and humans that could explain a larger range of motion of the MC1 during thumb flexion (i.e. the dorsoventral radius of curvature is similar in the bonobo and human trapezium). However, dissections of the ligaments surrounding the TMC joint do show relatively well developed volar ligaments in bonobos. The human configuration mostly displays a prominent dorso-radial ligament (DRL) that plays a significant role in TMC joint stability (Bettinger *et al.*, 1999; D'Agostino *et al.*, 2014) especially relative to the less prominent and weaker anterior oblique ligament (AOL). During thumb extension in bonobos, the relatively prominent volar AOL may restrict the range of motion compared to humans where the relatively weak AOL cannot provide such restraint. Inversely, during flexion, the relatively weak dorso-radial ligament found in bonobos may not result in the same increase in range of motion due to additional restriction from the interaction of the first metacarpal's volar beak with the trapezium joint surface. Quantification of the 3D geometry of the distal trapezial facet shows that the TMC joint in both bonobos and humans is not a true saddle joint, as the dorsoventral aspect is not fully convex. Instead, the surface in this direction resembles more of a bell curve; levelling off near the periphery on both sides of the facet. Here, the distal trapezial surface captures the volar or dorsal protuberances of the first metacarpal, restricting the range of motion during flexion and extension. This ensues foremost at the volar base of the facet due to the explicitly protruding volar beak of the MC1 in bonobos and humans. The triangular-shaped human volar beak is particularly interesting due to its implications for combined movements of the thumb. The apex of the volar beak limits MC1 flexion because it interacts with the volar aspect of the trapezium. At the same time, the triangular shape of the volar beak

will facilitate mediolateral motions (abduction and adduction) during thumb flexion, allowing thumb opposition. In contrast, the bonobo's rounded volar beak would impede such combined motion, as noted previously in literature (Marzke, 1992; Tocheri *et al.*, 2003), a phenomenon that also occurs during MC1 extension in *Pan* and *Gorilla* (Rafferty, 1990).

In the mediolateral plane, the human distal trapezial articular surface has a larger radius of curvature than in bonobos, but nevertheless, the range of motion of the MC1 during thumb abduction is similar in both species. A larger radius of curvature does, however, provide a more suitable facet for combined movements (e.g. thumb opposition by the combined efforts of MC1 flexion, adduction, and internal rotation), divergent from the principal axes of the trapezium, which are required to facilitate thumb opposition. The relatively 'flat' articular surface of the human trapezium has been associated with facilitating thumb opposition before (Marzke, 1992). However, a flat facet is more vulnerable to subluxation and non-human primates may, in order to stabilize the TMC against relatively high pressures involved in locomotion, require stronger ligaments, or, as described in many non-human primates, a deeper trapezial facet (Marzke *et al.*, 2010). In our bonobo specimens, we can only discern four TMC joint ligaments (i.e. AOL, DRL, POL, IML), a similar amount as has been described for chimpanzees (Lewis, 1977). In humans, additional ligaments crossing the TMC joint have been described (e.g. ulnar collateral ligament (UCL), deep intermetacarpal ligament (DIML) (Imaeda *et al.*, 1993; Bettinger *et al.*, 1999; Cardoso *et al.*, 2009) which might suggest that the human TMC joint requires more extrinsic stabilisation (e.g. due to flatter articular surfaces and/or higher joint loading).

In humans, the proximal articular facet of the MC1 has a smaller radius of curvature than the distal articular facet of the trapezium, which together mean that the mediolateral plane of the TMC joint is incongruent in a neutral position (Napier 1955; D'Agostino et al. 2017b). During either abduction or adduction, however, the proximal facet on the MC1 is rotated and aligned with the distal facet on the trapezium to ensure relative congruency at the end of the movement (Napier, 1955; Rafferty, 1990). In bonobos, the more curved distal trapezial articular surface could achieve such a congruency earlier, which would limit the range of abduction-adduction of the MC1, but this is not observed in our study. Perhaps, the more curved distal trapezial facet is met with a sufficiently curved MC1 articular surface that allows for the similar range of MC1 abduction-adduction as humans. The MC1 range of motion is, however, not only determined by the radius of curvature of the articular facets, but also by the 3D geometry and surrounding soft-tissue (i.e. ligaments, tendons and muscles). In addition to the TMC joint ligaments discussed above, the joint is also reinforced radially by the tendon of the *abductor pollicis longus* muscle which is positioned adjacent to the DRL. This tendon (or tendons, as multiple parallel

tendons occur in humans) inserts on the base of the MC1, but the muscle typically has a second tendon that inserts on the trapezium both in bonobos and humans (van Oudenaarde, 1991; van Leeuwen *et al.*, 2018). The second APL insertion on the trapezium is variable, and additional tendon slips spanning (and reinforcing) the TMC joint can occur (van Oudenaarde, 1991).

Comparison of our results with other studies is difficult, given that this is the first study that quantifies the kinematics of the MC1 using intact cadaveric bonobo specimens. For example, Tocheri et al. (2003) investigated the orientation of trapezial articular surfaces in extant primates and fossil hominins by studying the bony morphology of the trapezium in isolation, while our study uses in situ cadaveric specimens. Furthermore, Tocheri et al. (2003) did not quantify the curvature of the distal metacarpal facet of the trapezium. Rafferty (1990) investigated the functional morphology of the TMC joint in a large skeletal sample of extant primates, including *Pan* and humans, by tracing the articular facets of both the trapezium and MC1. Her results did not include any quantification of curvature but did show joint incongruity in both *Pan* and humans, but increased joint congruency during MC1 extension in *Pan* only. The single study we know of that quantified the MC1 range of motion in bonobos, is the study by Rose (1992) who used dry skeletal museum specimens that were put in positions of maximum flexion-extension and abduction-adduction. The range of MC1 motion obtained during thumb abduction corresponds well for bonobos (31.4 ± 6.5° versus Rose's (1992) 34.9 ± 4.5°), but less so for humans (33.0 ± 4.5° versus Rose's (1992) 46.3 ± 4.9°). While the range of MC1 motion during thumb flexion corresponds well for humans (38.7 ± 3.9° versus Rose's (1992) 37.6 ± 5.3°) and the bonobo range of MC1 motion deviates markedly from Rose's (1992) observations (9.5 ± 2.9° versus Rose's (1992) 32.8 ±5.3°). The lack of correspondence between these studies most likely is the result of methodological differences. Rose (1992) determined range of motion by aligning the articular surfaces of the trapezium and MC1 from one position to the other using dry skeletal material. Our kinematic analysis, however, was performed using intact cadaver specimens (including articular cartilage, ligaments, tendons, muscles) without being based on subjective limitations the way visual alignment does. As mentioned before, the well-developed anterior oblique ligament (AOL) may be responsible for notable restriction of bonobo thumb extension, possibly causing overestimation of the range of MC1 motion during thumb flexion and extension in the study of Rose (1992). As Rose (1992) acknowledged, soft-tissues will influence the biomechanics of the TMC joint, however, it is also clear that such influences may vary. Our study shows kinematic differences between bonobos and humans that cannot be related to the 3D geometry of the skeletal elements. This has important implications for studies on fossil remains, as these differences are most likely related differences in soft-tissue which are typically lacking in the fossil record. When studying extant apes, where both the functional capabilities and

the morphology can be studied, it is important to investigate and understand the effects of all types of tissue in biomechanical analyses of joint systems as this can contribute to a more accurate interpretation of fossil remains.

This study provides a quantification of MC1 kinematics of bonobos in comparison to humans, and is important to help our understanding of the functional abilities of the bonobo thumb and hand. Some limitations should, however, be taken into account, such as the small sample size and the use of cadaver specimens for the bonobo analysis. Bonobos are an endangered species (Fruth *et al.*, 2016) and specimens are difficult to obtain because the captive population is small. The small sample size does not allow us to take into account intra- and interspecific variations or to investigate sex or age differences. As such, we cannot comment on the relatively large variability displayed by the one subadult specimen. Furthermore, the use of cadaver specimens might also influence the kinematics obtained for the bonobos and might hamper the comparison with the human data set which was obtained from healthy volunteers (e.g. active versus passive positioning, muscle activity, etc.). This issue is, however, difficult to circumvent given that CT scan acquisition of living bonobos is not possible.

Another limiting factor of the study is that curvatures of the distal trapezial facet were determined using 3D bone models reconstructed from CT scans, which excludes information on articular cartilage. Although little is known about the distribution of articular cartilage in the bonobo TMC joint, articular cartilage has been shown to be distributed non-uniformly in the human TMC joint (Dourthe *et al.*, 2018). The actual joint curvature might therefore deviate slightly from the curvatures we measured based on the CT-based bone models.

Finally, we used a standardized rig to position the bonobo and human thumb in maximum flexion-extension and maximum abduction-adduction. Although this approach ensures sufficient standardization between specimens and between humans and bonobos, we cannot ascertain that we have effectively determined the maximum range of motion in each plane. For example, the orientation of the trapezium was quantified in the position of maximum thumb extension. The amount of extension varies between specimens, resulting in a high variation in calculated elevation angle (standard deviation of ±22.3° and ± 13.2° in bonobos and humans respectively). The other parameter, the azimuth, shows much lower variation as this was defined in the abduction-adduction plane which was more constrained.

In our current analysis, we focus on the TMC joint and movements and mechanics of the MC1, however, the used protocol yields information of the entire kinematic chain of the thumb (i.e. movements of the scaphoid, trapezium, and MC1 relative to the radius) and could be further expanded to incorporate other areas of the wrist and hand in future

analysis. This study is an example of the potential of using a combination of anatomical data, both hard and soft tissues, and biomechanical analyses.

Conclusions

The present study uses anatomical and kinematic data to provide new information on thumb mobility, specifically the trapeziometacarpal complex, of the bonobo, a hominid with a fully opposable thumb and high dexterity. We show that the anatomy and kinematics of the bonobo thumb are similar to that of humans, however, we do observe differences in mechanical capabilities, articular surface geometry and ligament configuration. Most importantly, we find that humans are capable of extending their first metacarpal considerably more than bonobos which might be related to their higher level of dexterity. Furthermore, we find kinematic differences between bonobos and humans that cannot solely be related to 3D geometry of the skeletal elements. It appears that trapeziometacarpal joint biomechanics are influenced by both the articular surface geometry and its associated soft-tissue, and both should be studied in greater detail when investigating the functional ability of the TMC joint system or any other anatomical structure. It is important to investigate and understand the effects of all types of tissue in biomechanical analyses of joint systems as this can contribute to a more accurate interpretation of fossil remains.

Acknowledgements

This paper was a contribution to a European Federation for Primatology symposium on "What an interdisciplinary approach can tell us about the evolution of grasping and manipulation" held on August 21–25, 2017 at the University of Strasbourg in France and organised by Emmanuelle Pouydebat and Ameline Bardo, the proceedings of which have been collated as a Special Issue of the Biological Journal of the Linnean Society (2018).

The authors thank the *Bonobo Morphology Initiative* organized in January 2016 by dr. Nauwelaerts and dr. Pereboom from the Centre for Research and Conservation (Royal Zoological Society Antwerp, Belgium) that enabled access to a large part of the bonobo specimens and allowed dissection of these specimens by an international team of anatomists. We are also grateful to the different zoos which provided additional bonobo specimens: Jean-Pascal Guéry (La Vallée des Singes, Romagne, France), Christina Geiger (Zoo Frankfurt, Germany), and Martina Balz (Wilhelma Zoo, Stuttgart, Germany. Furthermore, we thank dr. Olivier Vanovermeire and Henk Lacaeyse from the Medical Imaging Department, AZ Groeninge (Kortrijk, Belgium) for CT-scanning the specimens. Lastly, we thank our reviewers; dr. Tracy Kivell and dr. Biren Patel, for their valuable input. Funding for this project was obtained from KU Leuven (project number: C14/16/082).

Author contributions

TvL conceived the study; EEV and TvL further designed the study; JS provided the specimens and assisted in data collection; TvL, MJMV, FDK, PDA, and EEV performed the dissections; MV and TvL created the analysis; TvL, and EEV analysed the data and wrote the manuscript; HvL provided feedback to the final draft; all authors reviewed and approved the article. Illustrations by TvL.

References

Almécija, S., Alba, D. M. and Moyà-Solà, S. (2012) 'The thumb of Miocene apes: New insights from Castell de Barberà (Catalonia, Spain)', *American Journal of Physical Anthropology*, 148(3), pp. 436–450. doi: 10.1002/ajpa.22071.

Bardo, A. *et al.* (2016) 'Behavioral and functional strategies during tool use tasks in bonobos', *American Journal of Physical Anthropology*, 161(1), pp. 125–140. doi: 10.1002/ajpa.23015.

Berger, R. A. (2001) 'The Anatomy of the Ligaments of the Wrist and Distal Radioulnar Joints', *Clinical Orthopaedics and Related Research*, 383, pp. 32–40. doi: 10.1097/00003086-200102000-00006.

Bergström, P. and Edlund, O. (2017) 'Robust registration of surfaces using a refined iterative closest point algorithm with a trust region approach', *Numerical Algorithms*, 74(3), pp. 755–779. doi: 10.1007/s11075-016-0170-3.

Bergström, P., Edlund, O. and Söderkvist, I. (2011) 'Repeated surface registration for on-line use', *The International Journal of Advanced Manufacturing Technology*, 54(5–8), pp. 677–689. doi: 10.1007/s00170-010-2950-6.

Bettinger, P. C. *et al.* (1999) 'An Anatomic Study of the Stabilizing Ligaments of the Trapezium and Trapeziometacarpal Joint', *The Journal of Hand Surgery*, 24(4), pp. 786–798. doi: 10.1053/jhsu.1999.0786.

Breuer, T., Ndoundou-Hockemba, M. and Fishlock, V. (2005) 'First observation of tool use in wild gorillas', *PLoS Biology*, 3(11), pp. 2041–2043. doi: 10.1371/journal.pbio.0030380.

Butterworth, G. and Itakura, S. (1998) 'Development of precision grips in chimpanzees', *Developmental Science*, 1(1), pp. 39–43. doi: 10.1111/1467-7687.00010.

Cardoso, F. N. *et al.* (2009) 'Imaging the Ligaments of the Trapeziometacarpal Joint: MRI Compared with MR Arthrography in Cadaveric Specimens', *American Journal of Roentgenology*, 192(1), pp. W13–W19. doi: 10.2214/AJR.07.4010.

Christel, M. (1993) 'Grasping techniques and hand preferences in Hominoidea', in Preuschoft, H. and Chivers, D. J. (eds) *Hands of Primates*. Vienna: Springer Vienna, pp. 91–108. doi: 10.1007/978-3-7091-6914-8_7.

Christel, M. I., Kitzel, S. and Niemitz, C. (1998) 'How precisely do bonobos (Pan paniscus) grasp small objects?', *International Journal of Primatology*, 19(1), pp. 165–193. doi: 10.1023/A:1020319313219.

Colell, M., Segarra, M. D. and Pi, J. S. (1995) 'Hand preferences in chimpanzees (Pan troglodytes), bonobos (Pan paniscus), and orangutans (Pongo pygmaeus) in food-reaching and other daily activities', *International Journal of Primatology*, 16(3), pp. 413–434. doi: 10.1007/BF02735795.

Cooney, W. P. and Chao, E. Y. (1977) 'Biomechanical analysis of static forces in the thumb during hand function.', *The Journal of bone and joint surgery. American volume*, 59(1), pp. 27–36.

Crisco, J. J. *et al.* (2015) 'In vivo kinematics of the trapeziometacarpal joint during thumb extension-flexion and abduction-adduction', *Journal of Hand Surgery*. Elsevier Inc, 40(2), pp. 289–296. doi: 10.1016/j.jhsa.2014.10.062.

D'Agostino, P. *et al.* (2014) 'Comparison of the Anatomical Dimensions and Mechanical Properties of the Dorsoradial and Anterior Oblique Ligaments of the Trapeziometacarpal Joint', *The Journal of Hand Surgery*, 39(6), pp. 1098–1107. doi: 10.1016/j.jhsa.2014.02.025.

D'Agostino, P., Dourthe, B., Kerkhof, F., Harry Van Lenthe, G., *et al.* (2017) 'In vivo biomechanical behavior of the trapeziometacarpal joint in healthy and osteoarthritic subjects', *Clinical Biomechanics*, 49, pp. 119–127. doi: 10.1016/j.clinbiomech.2017.09.006.

D'Agostino, P., Dourthe, B., Kerkhof, F., Stockmans, F., *et al.* (2017) 'In vivo kinematics of the thumb during flexion and adduction motion: Evidence for a screw-home mechanism', *Journal of Orthopaedic Research*, 35(7), pp. 1556–1564. doi: 10.1002/jor.23421.

Dourthe, B. *et al.* (2018) 'Assessment of healthy trapeziometacarpal cartilage properties using indentation testing and contrast-enhanced computed tomography', *Clinical Biomechancics*, Manuscript.

Feix, T. *et al.* (2015) 'Estimating thumb-index finger precision grip and manipulation potential in extant and fossil primates', *Journal of The Royal Society Interface*, 12(106), pp. 20150176–20150176. doi: 10.1098/rsif.2015.0176.

Fruth, B. *et al.* (2016) 'Pan paniscus', *The IUCN Red List of Threatened Species 2016*. doi: 10.2305.

Gumert, M. D., Hoong, L. K. and Malaivijitnond, S. (2011) 'Sex differences in the stone tool-use behavior of a wild population of burmese long-tailed macaques (Macaca fascicularis aurea)', *American Journal of Primatology*, 73(12), pp. 1239–1249. doi: 10.1002/ajp.20996.

Halilaj, E. *et al.* (2013) 'A thumb carpometacarpal joint coordinate system based on articular surface geometry', *Journal of Biomechanics*, 46(5), pp. 1031–1034. doi: 10.1016/j.jbiomech.2012.12.002.

Imaeda, T. *et al.* (1993) 'Anatomy of trapeziometacarpal ligaments', *The Journal of Hand Surgery*, 18(2), pp. 226–231. doi: 10.1016/0363-5023(93)90352-4.

Ingmanson, E. J. (1998) 'Tool-using behaviour in wild Pan paniscus: Social and ecological considerations', in Russon, A. E., Bard, K. A., and Parker, S. T. (eds) *Reaching Into Thought: The Minds of the Great Apes*. Cambridge University Press, p. 464.

Jordan, C. (1982) 'Object manipulation and tool-use in captive pygmy chimpanzees (Pan paniscus)', *Journal of Human Evolution*, 11(1), pp. 35–39. doi: 10.1016/S0047-2484(82)80029-8.

Kerkhof, F. D. *et al.* (2018) 'Trapeziometacarpal stabilization through dorsoradial ligament reconstruction: An early post-surgery in vivo biomechanical analyses', *Journal of Orthopaedic Research®*, Manuscript. doi: 10.1002/jor.24103.

Komatsu, I. and Lubahn, J. D. (2018) 'Anatomy and Biomechanics of the Thumb Carpometacarpal Joint', *Operative Techniques in Orthopaedics*, 28(1), pp. 1–5. doi: 10.1053/j.oto.2017.12.002.

Ladd, A. L., Lee, J. and Hagert, E. (2012) 'Macroscopic and Microscopic Analysis of the Thumb Carpometacarpal Ligaments', *The Journal of Bone and Joint Surgery-American Volume*, 94(16), pp. 1468–1477. doi: 10.2106/JBJS.K.00329.

van Leeuwen, T. *et al.* (2018) 'Insights into the musculature of the bonobo hand', *Journal of Anatomy*, 233(3), pp. 328–340. doi: 10.1111/joa.12841.

Lewis, O. J. (1977) 'Joint remodelling and the evolution of the human hand.', *Journal of Anatomy*, 123(Pt 1), pp. 157–201.

Marchi, D. *et al.* (2017) 'Morphological correlates of the first metacarpal proximal articular surface with manipulative capabilities in apes, humans and South African early hominins', *Comptes Rendus Palevol*, 16(5–6), pp. 645–654. doi: 10.1016/j.crpv.2016.09.002.

Marzke, M. W. (1971) 'Origin of the human hand', *American Journal of Physical Anthropology*, 34(1), pp. 61–84. doi: 10.1002/ajpa.1330340106.

Marzke, M. W. (1992) 'Evolutionary development of the human thumb.', *Hand clinics*, 8(1), pp. 1–8.

Marzke, M. W. (1997) 'Precision grips, hand morphology, and tools', *American Journal of Physical Anthropology*, 102(1), pp. 91–110. doi: 10.1002/(SICI)1096-8644(199701)102:1<91::AID-AJPA8>3.0.CO;2-G.

Marzke, M. W. *et al.* (2010) 'Comparative 3D quantitative analyses of trapeziometacarpal joint surface curvatures among living catarrhines and fossil hominins.', *American journal of physical anthropology*. United States, 141(1), pp. 38–51. doi: 10.1002/ajpa.21112.

Marzke, M. W. *et al.* (2015) 'Grips and hand movements of chimpanzees during feeding in Mahale Mountains National Park, Tanzania', *American Journal of Physical Anthropology*, 156(3), pp. 317–326. doi: 10.1002/ajpa.22651.

Napier, J. R. (1952) 'The attachments and function of the abductor pollicis brevis.', *Journal of anatomy*, 86(4), pp. 335–41.

Napier, J. R. (1955) 'The form and function of the carpo-metacarpal joint of the thumb.', *Journal of anatomy*, 89(3), pp. 362–9.

Napier, J. R. (1960) 'Studies of the hands of living primates', *Proceedings of the Zoological Society of London*, 134, pp. 647–657.

Neufuss, J., Robbins, M. M., *et al.* (2017) 'Comparison of hand use and forelimb posture during vertical climbing in mountain gorillas (Gorilla beringei beringei) and chimpanzees (Pan troglodytes)', *American Journal of Physical Anthropology*, 164(4), pp. 651–664. doi: 10.1002/ajpa.23303.

Neufuss, J., Humle, T., *et al.* (2017) 'Nut-cracking behaviour in wild-born, rehabilitated bonobos (Pan paniscus): a comprehensive study of hand-preference, hand grips and efficiency', *American Journal of Primatology*, 79(2), pp. 1–16. doi: 10.1002/ajp.22589.

Orr, C. M. *et al.* (2010) 'Studying Primate Carpal Kinematics in Three Dimensions Using a Computed-Tomography-Based Markerless Registration Method', *The Anatomical Record: Advances in Integrative Anatomy and Evolutionary Biology*, 293(4), pp. 692–709. doi: 10.1002/ar.21137.

van Oudenaarde, E. (1991) 'Structure and function of the abductor pollicis longus muscle.', *Journal of Anatomy*, 174, pp. 221–227.

Pouydebat, E. *et al.* (2009) 'Biomechanical study of grasping according to the volume of the object: Human versus non-human primates', *Journal of Biomechanics*, 42(3), pp. 266–272.

doi: 10.1016/j.jbiomech.2008.10.026.

Rafferty, K. L. (1990) *The Functional and Phylogenetic Significance of the Carpometacarpal Joint of the Thumb in Anthropoid Primates*. New York University.

Rose, M. D. (1992) 'Kinematics of the trapezium-1st metacarpal joint in extant anthropoids and Miocene hominoids', *Journal of Human Evolution*, 22(4–5), pp. 255–266. doi: 10.1016/0047-2484(92)90058-H.

Samuel, D. S. *et al.* (2018) 'Hand pressures during arboreal locomotion in captive bonobos (Pan paniscus)', *The Journal of Experimental Biology*, 221(8), p. jeb170910. doi: 10.1242/jeb.170910.

Shrewsbury, M. (2003) 'Pollical oblique ligament in humans and non-human primates', *Journal of Anatomy*, 202(4), pp. 397–407. doi: 10.1046/j.1469-7580.2003.00172.x.

Skinner, M. M. *et al.* (2015) 'Human evolution. Human-like hand use in Australopithecus africanus.', *Science (New York, N.Y.)*, 347(6220), pp. 395–9. doi: 10.1126/science.1261735.

Spinozzi, G., Truppa, V. and Laganà, T. (2004) 'Grasping behavior in tufted capuchin monkeys (Cebus apella): Grip types and manual laterality for picking up a small food item', *American Journal of Physical Anthropology*, 125(1), pp. 30–41. doi: 10.1002/ajpa.10362.

Takeshita, H. and Walraven, V. (1996) 'A comparative study of the variety and complexity of object manipulation in captive chimpanzees (Pan troglodytes) and bonobos (Pan paniscus)', *Primates*, 37(4), pp. 423–441. doi: 10.1007/BF02381377.

Tocheri, M. W. *et al.* (2003) 'Functional capabilities of modern and fossil hominid hands: Three-dimensional analysis of trapezia', *American Journal of Physical Anthropology*, 122(2), pp. 101–112. doi: 10.1002/ajpa.10235.

Tocheri, M. W. *et al.* (2005) 'A 3D quantitative comparison of trapezium and trapezoid relative articular and nonarticular surface areas in modern humans and great apes', *Journal of Human Evolution*, 49(5), pp. 570–586. doi: 10.1016/j.jhevol.2005.06.005.

Tocheri, M. W. *et al.* (2008) 'The evolutionary history of the hominin hand since the last common ancestor of Pan and Homo', *Journal of Anatomy*, 212(4), pp. 544–562. doi: 10.1111/j.1469-7580.2008.00865.x.

Toth, N. *et al.* (1993) 'Pan the Tool-Maker: Investigations into the Stone Tool-Making and Tool-Using Capabilities of a Bonobo (Pan paniscus)', *Journal of Archaeological Science*, 20(1), pp. 81–91. doi: 10.1006/jasc.1993.1006.

Tuttle, R. H. (1967) 'Knuckle-walking and the evolution of hominoid hands', *American Journal of Physical Anthropology*, 26(2), pp. 171–206. doi: 10.1002/ajpa.1330260207.

Wu, G. *et al.* (2005) 'ISB recommendation on definitions of joint coordinate systems of various joints for the reporting of human joint motion—Part II: shoulder, elbow, wrist and hand', *Journal of Biomechanics*, 38(5), pp. 981–992. doi: 10.1016/j.jbiomech.2004.05.042.

Wu, G. and Cavanagh, P. R. (1995) 'ISB recommendations for standardization in the reporting of kinematic data', *Journal of Biomechanics*, 28(10), pp. 1257–1261. doi: 10.1016/0021-9290(95)00017-C.

Wunderlich, R. E. and Jungers, W. L. (2009) 'Manual digital pressures during knuckle-walking in chimpanzees (Pan troglodytes)', *American Journal of Physical Anthropology*,

139(3), pp. 394–403. doi: 10.1002/ajpa.20994.

Chapter 3.

Trapeziometacarpal joint mobility in gibbons (fam. Hylobatidae) and rhesus macaques (*Macaca mulatta*).

Timo van Leeuwen[1]; Maarten Vanneste[1]; Priscilla D'Agostino[1,2]; Evie E. Vereecke[1]

[1]Dept. Development and Regeneration, Biomedical Sciences Group, KU Leuven, Belgium

[2]Louise Medical Center, Hand Clinic, Brusseles, Belgium

Resubmitted for revision for publication in the *American Journal of Physical Anthropology* as:

van Leeuwen, T., Vanneste, M., D'Agostino, P., and Vereecke, E. E., 2021, *Trapeziometacarpal joint mobility in gibbons (fam. Hylobatidae) and rhesus macaques (Macaca mulatta).* American Journal of Physical Anthropology, In Revision.

Abstract

Objectives

The purpose of this study is to investigate the differences in 3D kinematics of the trapeziometacarpal (TMC) joint between gibbons (fam. Hylobatidae) and macaques (*Macaca mulatta*), two non-human primate groups with a distinct locomotor behaviour, but a similar capacity for advanced manipulative tasks. Gibbons are highly arboreal species that do not use the thumb in brachiation, while macaques load their thumb in palmigrade quadrupedalism and climbing. Here, we investigate the mobility and structural constraints of the TMC joint in both primates and evaluate the hypothesis that differences in locomotor mode are reflected in differences in joint structure and function.

Materials and methods

We have developed an innovative software suite allowing quantification of in situ 3D kinematics based on medical imaging of the primate TMC joint using a unique sample of eight gibbons and seven macaques. These analyses are further supported by detailed dissection of the surrounding ligaments. We furthermore integrate data from a previous study on human and bonobo TMC joint mobility to interpret the data in a broader evolutionary context.

Results

The data demonstrate distinct differences in TMC joint mobility between gibbons and macaques, with a wide range of motion in the gibbon TMC joint and restricted movement in macaques. Furthermore, the dissections show little differences in ligament anatomy that could be associated with the differences in TMC joint capabilities.

Conclusion

We conclude that gibbons possess a highly mobile TMC joint and the ball-and-socket morphology allows for large ranges of motion, on par with that of the human thumb and beyond that of bonobos or macaques. This type of morphology, however, does not offer much inherent stabilisation, and we find no indications that the gibbon ligament anatomy is any different from that of macaques, bonobos, or humans to make up for the joint instability. This relative lack of structural joint reinforcement suggests that gibbons may have difficulty in performing any type of power grasp with high loads, without risking dislocation of the thumb. Macaques, on the other hand, are shown to have a considerably reinforced TMC joint, which is likely related to the habitual loading of the thumb during

locomotion. The restricted mobility of the TMC joint in macaques requires recruitment of the more distal joints in manual tasks involving larger ranges of thumb motion.

Introduction

The thumb is a critical structure in the study of human evolution. The development of a strong and highly mobile thumb is a key factor in the enhanced manual dexterity required for tool production and use, one of the major characteristics that define modern humans (e.g. Jones, 1920; Napier, 1956; Lewis, 1977, 1989; Susman, 1988; Napier *et al.*, 1993; Marzke and Marzke, 2000). As a distinctly relevant structure during daily activities, both in modern human and hominin societies, thumb morphology and biomechanics have been widely studied (e.g. Napier, 1956; Rafferty, 1990; Rose, 1992; Marzke *et al.*, 2010; van Leeuwen *et al.*, 2018, 2019). Albeit, thumb biomechanics have primarily been studied from a clinical perspective in modern populations. In the paleo-anthropological context, hand use in hominins is inferred from morphological studies. Such implications are then further derived into general behaviour and locomotion (e.g. in the arboreal versus bipedal paradigm). By the intrinsic nature of these studies, however, soft-tissue components are largely overlooked. Investigating both thumb soft- and hard tissue in non-human primates to expand the context in which we look at fossil data is therefore of critical importance. Enhanced dexterity characterizes primates, and similar to modern humans many extant non-human primates possess highly dexterous hands with mobile thumbs that are capable of advanced manual tasks and even tool production and use (e.g. Christel, 1993; Toth *et al.*, 1993; Fragaszy *et al.*, 2004; Malaivijitnond *et al.*, 2007; Gumert, Hoong and Malaivijitnond, 2011; Bardo *et al.*, 2016; Liu, Xiong and Hu, 2016; Neufuss *et al.*, 2017), while also including the hand in locomotion. However, compared to our understanding of the human thumb, the anatomy and biomechanics of the non-human primate thumb remains poorly understood (Tuttle, 1969; Diogo *et al.*, 2009). In particular, thumb biomechanics are underrepresented in the literature (Napier, 1960; Thompson, 2020), as is the relation between functional capability and musculoskeletal anatomy. Several paleo-anthropological studies do include interpretations of non-human primate biomechanics (Rafferty, 1990; Rose, 1992; Marzke *et al.*, 2010), but these interpretations are based on fossil collections which, again, include only bony material and lack the soft-tissue context of the joint which has been shown to be of relevance in determining joint function (van Leeuwen *et al.*, 2019; Thompson, 2020).

In this study we expand on our efforts to investigate the kinematic capabilities of the non-human primate thumb in taxa that employ different modes of locomotion. We focus on the basal thumb, or trapeziometacarpal (TMC) joint, which is most relevant for thumb mobility (Napier, 1955; Rose, 1992). Here, we study TMC joint range of motion for the first time in direct association with the soft-tissue anatomy surrounding the joint. We focus on the arboreal gibbon (fam. Hylobatidae, inclusion of four genera) and the semi-terrestrial rhesus macaque (*Macaca mulatta*) and interpret these in the context of previous data on the bonobo and modern human (van Leeuwen *et al.*, 2019). This previous study has shown that the bonobo TMC joint is highly mobile, similar even to humans, with the exception of thumb extension which is more restricted. The ligaments surrounding the bonobo TMC joint, the passive soft tissue that resists joint dislocation, also show many similarities to the configuration reported in humans (Bettinger *et al.*, 1999), but with emphasis on palmar reinforcement (van Leeuwen *et al.*, 2019). By expanding this work to Hylobatidae and *Macaca mulatta*, we bring a novel line of evidence in the investigation of thumb motion in non-human primates which will further inform work on fossil taxa.

Gibbons are highly arboreal, hominoid primates that use brachiation as their dominant locomotor mode (van Horn, 1972; Cannon and Leighton, 1994). During brachiation and suspensory locomotion, they form a hook-grip with their long fingers, excluding the thumb (van Horn, 1972). Loading of the thumb is therefore limited and occurs mainly during the less frequent vertical climbing, if during locomotion at all, where they use wide power grasps that make use of the mobile thumb (Carpenter, 1941; van Horn, 1972). In manipulative tasks, wide grasps are used handling food (Carpenter, 1941; van Horn, 1972), and in precision grasping gibbons prefer a thumb tip to radial aspect of the index digit's proximal interphalangeal joint to manipulate smaller objects (Christel, 1993). Perhaps due to the lack of habitual loading, the gibbon TMC joint is shaped as a ball-and-socket (Marzke, 1971), in contrast to other extant primate species, including humans, and macaques, who are characterized by a saddle-shaped TMC joint (Napier, 1955). A saddle-shaped joint is the physiological equivalent of a universal joint , which due to its inverse concavo-convex surfaces inhibit axial rotation while allowing flexion-extension and abduction-adduction. Rhesus macaques are predominantly terrestrial palmigrade and/or digitigrade quadrupeds, although they are also frequently observed in arboreal locomotion, where they navigate the environment through arboreal quadrupedalism and vertical climbing (e.g. Dunbar, 1989; Rawlins, 1993; Wells and Turnquist, 2001; Roos and Zinner, 2015). Locomotor modes and hand use varies across macaque species but most include some type of substrate interaction of the thumb and/or thenar pad (e.g. Hayama,

Chatani and Nakatsukasa, 1994; Macfarlane and Graziano, 2009; Aversi-Ferreira *et al.*, 2016; Thompson, 2020). During vertical climbing, a small repertoire of relatively simple hand wraps and hooks is used (Macfarlane and Graziano, 2009). Yet, in object manipulation a large variety of grasps are employed, including multiple power grasps and advanced precision grips (Macfarlane and Graziano, 2009).

To quantify the functional capacity of the TMC joint in gibbons and macaques we combine medical imaging based kinematic analyses with detailed dissection of the TMC joint ligaments. Given the substantial differences in thumb loading between both primate groups, we hypothesize that there will be considerable differences in the functionality of the TMC joint. Gibbons are expected to show a high degree of TMC joint mobility, based on their low locomotor-related loading, as well as the ball-and-socket morphology of the TMC joint. To avoid dislocation of such a mobile structure with relatively little bony restrictions, well-developed ligaments are expected to stabilize the TMC joint. In contrast, the macaque TMC joint is expected to show relatively low joint mobility, as proper stabilisation is required for loading of the joint during locomotion. The passive soft tissue is expected to reflect this through a well-developed envelope of TMC joint ligaments, possibly with particularly reinforced palmar ligaments to combat palmar subluxation and hyperextension of the first metacarpal during quadrupedal locomotion.

Methodology

Specimens

Cadaveric forearms of a total of eight (sub)adult of members of the Hylobatidae family (further referred to as gibbons) and seven rhesus macaques (*Macaca mulatta,* further referred to as macaques) were obtained in collaborations with various European zoos and institutes (**Table 1**). All forelimbs were disarticulated either at the glenohumeral joint or at the scapulothoracic joint, and stored at -18°C. All forelimb specimens were thawed at room temperature preceding the imaging protocol.

Table 1: Specimen details. F = female, M = male, unknown sex. Exact age information is unknown but the specimens could be identified as adult (A) or subadult (sA) based on bone growth plate progression. Sample refers to the side used; L = left, R = right.

Subject	Species	Sex	Age	Sample	Collection
G1	*Hylobates lar*	F	sA	L	NMS, Edingburgh, Scotland
G2	*Hylobates lar*		sA	R	NMS, Edingburgh, Scotland
G3	*Hylobates lar*		sA	R	Ghent University, Merelbeke, Belgium
G4	*Hylobates pileatus*	M	A	R	NMS, Edingburgh, Scotland
G5	*Nomascus concolor*	M	A	L	Pakawi Park, Olmen, Belgium
G6	*Nomascus leucogenys*	M	A	R	Zoo Mulhouse, Mulhouse, France
G7	*Symphalanges syndactylus*	M	A	R	Zoo Antwerp, Antwerp, Belgium
G8	*Symphalanges syndactylus*	M	A	L	NMS, Edingburgh, Scotland
M1	*Macaca mulatta*		A	R	Ghent University, Merelbeke, Belgium
M2	*Macaca mulatta*	F	A	L	Ghent University, Merelbeke, Belgium
M3	*Macaca mulatta*		A	L	Ghent University, Merelbeke, Belgium
M4	*Macaca mulatta*		A	L	Ghent University, Merelbeke, Belgium
M5	*Macaca mulatta*		A	L	Ghent University, Merelbeke, Belgium
M6	*Macaca mulatta*	M	A	L	Ghent University, Merelbeke, Belgium
M7	*Macaca mulatta*		A	R	KU Leuven, Leuven, Belgium

Imaging protocol

Each specimen was imaged in four terminal positions of principal thumb motion, i.e. palmar abduction, palmar adduction, extension, and flexion. The terminal positions were standardized using a radio-translucent rig following a previous protocol (van Leeuwen *et al.*, 2019) based on Crisco et al. (2015) and D'Agostino et al. (2016). Scans were conducted using a 64-slice Discovery HD 750 CT scanner (GE Healthcare, Little Chalfont, UK) at AZ Groeninge, Kortrijk, Belgium (DFOV: 250 mm; slice thickness: 0.625 mm; voxel size: 0.15 mm3; 100 kV; 180 mA; image size: 512 × 512 pixels). In each scan, the trapezium and first metacarpal were segmented semi-automatically using Mimics Research 21.0 (Materialise, Leuven, Belgium), and reconstructed as triangular STL meshes.

Kinematic analysis

A custom-developed, Python (3.6)-based joint kinematic analysis suite (JOKE) was used to quantify the range of motion during thumb abduction and thumb extension by calculating the motion between the corresponding terminal positions of each principal thumb motion (i.e. abduction-adduction, and flexion-extension). The method has been adapted from previous kinematic analyses in the bonobo TMC joint (van Leeuwen *et al.*, 2019). JOKE was further used to calculate the TMC joint articular surfaces' radii of curvature along the principal axes of motion. TMC joint range of motion angles are defined in a joint coordinate system that is defined based specimen's articular surface 3D geometry. Articular surface meshes were extracted from the trapezium and MC1 bone meshes by selecting the surface along the articulation periphery, visible as bone landmarks, and storing them as separate STL meshes. The coordinate system of the macaque's saddle-shaped TMC joint was computed according to a method developed for the human TMC joint (Halilaj *et al.*, 2013), where a fifth-order polynomial was fitted to the extracted reciprocal TMC joint surfaces to determine both saddle points. Subsequently, the principal directions of curvature were computed to orient the axes of each side. The trapezium and MC1 coordinate systems were combined to generate the TMC joint coordinate system, in line with the International Society of Biomechanics (ISB) convention (Wu and Cavanagh, 1995; Wu *et al.*, 2005; Halilaj *et al.*, 2013); In this TMC joint coordinate system, the z-axis (Z) represents the radio-ulnar plane and is defined by the average of both the trapezium and MC1 vectors in the radio-ulnar plane; the TMC joint y-axis (Y) represents the proximodistal plane and is defined by the cross-product of Z and the vector average of the trapezium and MC1 in the dorsopalmar plane; the x-axis

(X) represents the dorso-palmar plane and is defined by the cross-product of Y and Z (Halilaj *et al.*, 2013).

The coordinate system for gibbon's ball-and-socket joint shaped TMC joint was determined by an adapted version of the above, using a least squares optimised sphere fit to the extracted reciprocal TMC articular surfaces instead of the fifth-order polynomial. As the ball-and-socket joint lacks distinct directional features, manually selected bone landmarks (i.e. the proximal articular surface, the radio-palmar tubercle, and ulnar tubercle) were used to orient the trapezium. Despite the distinct shape of the articular facets, the overall shape of the gibbon trapezium is similar to that humans, allowing the axes of both reciprocal articular surfaces to be aligned in a combined TMC joint coordinate system in line with the International Society of Biomechanics (ISB) convention (Wu and Cavanagh, 1995; Wu *et al.*, 2005).

The curvatures of the articular facets were defined by (1) inverting the eigenvalues of the trapezium and first metacarpal principal curvatures in both planes (flexion – extension, abduction -adduction) to yield radii for the surface corresponding circles, and (2) the optimising a sphere fit to both the trapezium and first metacarpal articular surface, calculating the fitted sphere radii for each surface. We use the ratio between the trapezium and the MC1 curvature as an indication of joint congruence, defined in **Table 2** as the congruence factor.

The transformation matrices of the MC1 during thumb abduction-adduction and flexion-extension were calculated by iterative closest point fitting the terminal positions of the MC1 in each movement set. In this process the trapezium was considered to be fixed while the MC1 was moving. The rotation angles along each axis (x, y, z) were extracted from the transformation matrices to represent range of motion during each thumb movement. Range of motion was defined as the angle between the terminal MC1 position pairs. For abduction-adduction that means the rotation angle along the dorsopalmar (x) axis, for flexion-extension it is rotation along the radio-ulnar (z) axis, and rotation along the proximodistal (y) axis defines axial rotation of the MC1. Ranges of motion were compared between gibbons, macaques, and existing data on the range of motion of the TMC joint in bonobos (*Pan paniscus*) and humans from a previous study (van Leeuwen *et al.*, 2019) using an ANOVA and Tukey test in R ($\alpha = 0.05$) (R Core Team, 2017).

Ligament anatomy

The forearm specimens of the gibbon and macaque sample were used in a parallel study where the musculature was dissected and quantified (Vanhoof, van Leeuwen and

Vereecke, 2020). After removal of all muscle tissue, the ligaments surrounding the TMC joint were documented following Berger (Berger, 2001), and interpreted in the context of the human and bonobo TMC ligament configuration (Bettinger *et al.*, 1999; Berger, 2001; D'Agostino *et al.*, 2014; van Leeuwen *et al.*, 2019).

Results

Articular surface curvature

In the dorsopalmar plane, the trapezial facet of macaques has a convex curvature with an average of 6.6 mm (± 4.2 mm), and a concave curvature with an average radius of 4.1 mm (± 1.2 mm) on the MC1 facet (**Fig. 1a, b, Table 2**). In the radioulnar plane, the trapezial facet has an average concave radius of 2.3 mm (± 0.4 mm) and the MC1 facet has an average convex radius of 2.2 mm (± 0.2 mm). The average congruence factor between trapezium and MC1 curvature, used as an indication for joint congruency, is 1.5 (± 0.5) and 1.1 (± 0.2) in the dorsopalmar and radioulnar planes respectively.

In gibbons, the average curvature of the articular facet of the trapezium is 3.2 mm (± 0.5 mm) and 12.1 mm (± 19.5 mm) for the MC1 (**Fig. 1c, Table 2**), with an average congruency factor of 0.6 (± 0.3). However, after the elimination of an outlier (G2), the average sphere radii are 3.3 mm (± 0.4 mm) for the trapezium and 5.2 mm (± 1.7 mm) for the MC1, with an average congruency factor of 0.7 (± 0.2).

Table 2: Macaque radii of trapezium and first metacarpal joint surface curvature in the dorsovolar (flexion-extension) and radioulnar (abduction-adduction) plane. Cong. refers to the congruence factor; the ratio between trapezium and MC1 curvature as an indication of joint congruence.

Macaques	**Dorsovolar curvature (mm)**			**Radioulnar curvature (mm)**		
Specimen	**Trapezium**	**MC1**	**Cong.**	**Trapezium**	**MC1**	**Cong.**
M1	14.49	-6.24	-2.32	-2.16	2.17	-1.00
M2	5.31	-4.69	-1.13	-2.70	2.51	-1.07
M3	4.56	-3.30	-1.38	-2.27	2.29	-0.99
M4	10.15	-4.44	-2.29	-1.86	2.03	-0.92
M5	3.57	-3.06	-1.16	-2.17	1.90	-1.14
M6	3.37	-3.60	-0.94	-3.13	2.28	-1.37
M7	4.76	-3.03	-1.57	-2.06	2.36	-0.87

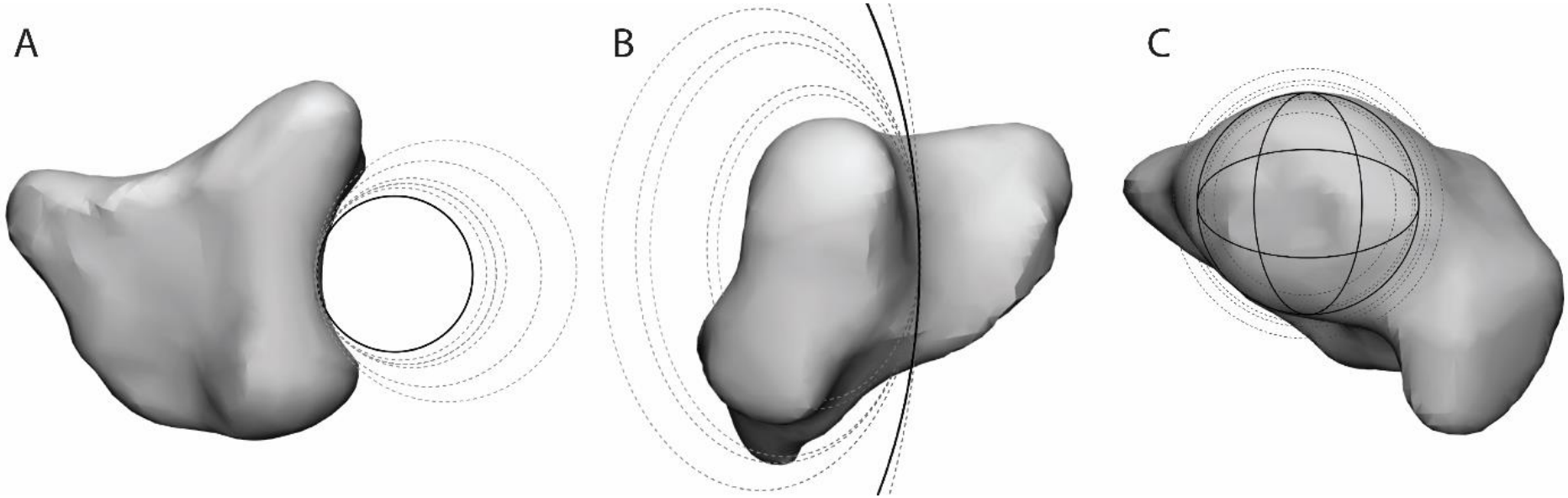

Figure 1: Articular surface curvatures in macaques and gibbons. **A** and **B** respectively visualize the macaque radio-distal and dorsal view of the total trapezium curvatures (**table 2**) in dotted lines, all depicted on one bone model (specimen M4) with its corresponding curvature indicated by the **bold** line. **C** visualizes the distal view of the gibbon trapezium fitted spheres with the total calculated radii (**table 3**) in dotted lines, all depicted on one bone model (specimen G1) with its corresponding sphere indicated by the **bold** lines.

Kinematic analysis

Results from the kinematic analysis confirm a highly mobile TMC joint in gibbons, disparate from the restricted joint found in macaques (**Fig. 2**). The gibbons TMC joint has an average range of motion of 47.3° (± 12.1°) in the principal plane during thumb abduction-adduction, and of 43.5° (± 8.2°) during thumb flexion-extension. In contrast, the average range of motion of the macaque TMC joint in the principal planes are 7.1° (± 2.1°) during thumb abduction-adduction, and 8.0° (± 5.9°) during flexion-extension. In addition, relatively high axial rotation of the MC1 occurs during thumb abduction-adduction and flexion-extension, in both gibbons and macaques. The axial rotation in the gibbon MC1 amounts on an average to 16.2° (± 11.6°) and 26.7° (± 14.6°), during thumb abduction-adduction and flexion-extension respectively. In macaques, MC1 axial rotation amounts to an average of 10.3° (± 12.5°) and 10.9° (± 10.0°) respectively during the same thumb movements.

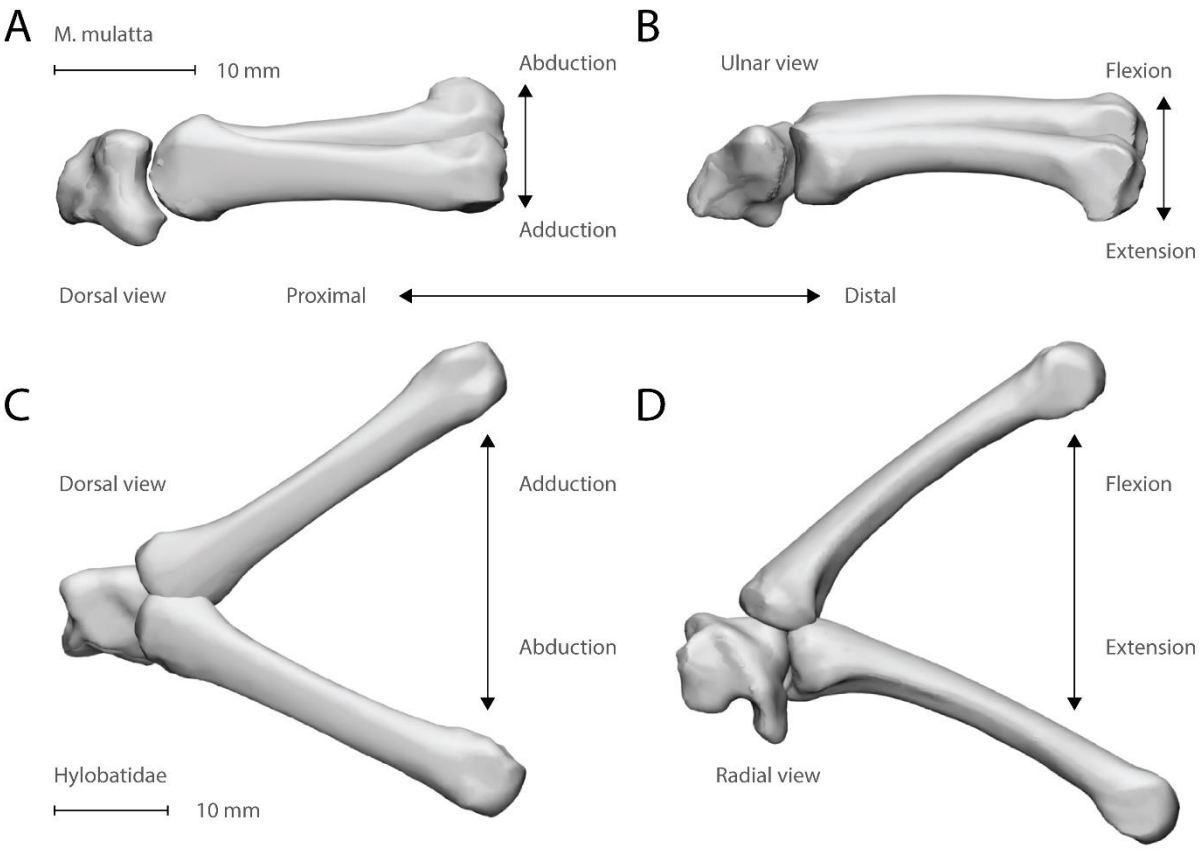

Figure 2: Range of motion in macaques (**A** and **B**) and gibbons (**C** and **D**), during abduction-adduction (**A** and **C**, dorsal view) and flexion-extension (**B**, ulnar view, and **D**, radial view). Specimens visualized: macaque M3 (mirrored for visualisation purposes) and gibbon G8.

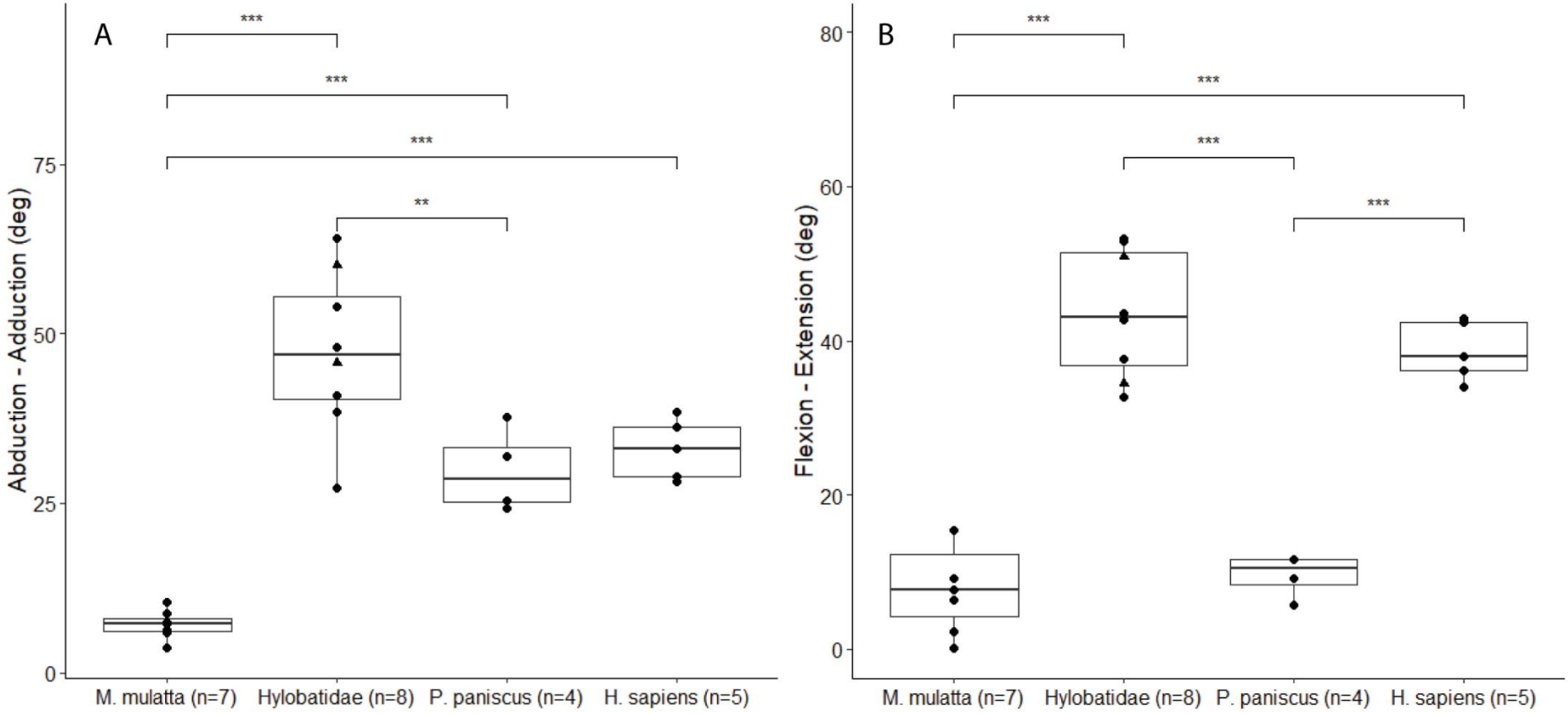

Figure 3: Range of motion of the TMC during thumb abduction-adduction (**A**) and thumb flexion-extension (**B**) in rhesus macaques, gibbons, bonobos, and humans. Plotted as boxplots with the median and quartiles, * = p-value = 0.01 to α (0.05), **: p-value = 0.001 to 0.01, ***: p-value < 0.001. In the gibbon sample triangles represent the two, larger sized, siamangs (*Symphalanges syndactylus*) in the sample.

The range of motion of the macaque TMC joint is low compared to both modern humans and gibbons (**Fig. 3**) and is also significantly lower than in bonobos during thumb abduction-adduction (p-value < 0.001), but not flexion-extension (p-value = 0.98). Gibbon TMC joint mobility is significantly higher compared to bonobos and macaques (p-values < 0.001, p-value < 0.01 during abduction-adduction), but not statistically distinct from the human TMC joint range of motion (p-value = 0.54 during flexion-extension, p-value = 0.22 during abduction-adduction).

Ligament anatomy

The anterior oblique ligament (AOL) inserts onto the palmar aspect of the MC1's palmar (volar) beak in both macaques and gibbons (**Fig.4a, d**). It originates from the palmar ridge of the trapezium's distal articular surface, from the palmar radial tubercle towards the palmar ulnar aspect of the distal facet. The ligament is well developed in both primate groups.

The dorsoradial ligament (DRL) originates from the dorsoradial tubercle of the trapezium, from which it fans out to insert dorsally at the base of MC1 (**Fig.4b, c, e, f**). The DRL has the same origin and insertion in both macaques and gibbons, situated adjacent to the posterior oblique ligament (POL), it is a well-developed ligament in both primate groups.

The POL (**Fig.4b, c, e, f**) originates dorsally from the trapezium, directly adjoining the DRL on the ulnar side (**Fig.4b, c, e, f**). Its fibres insert obliquely onto the dorsoulnar ridge of the MC1 in both macaques and gibbons, however, a more distal insertion, on the MC1 shaft, was observed in one gibbon specimen (G4). Notable is that where in humans the POL is described to also insert on the palmar aspect of the MC1 (Bettinger et al., 1999), deep with respect to the dorsal intermetacarpal ligament (DIML), this deep insertion is not clearly present in either macaques or gibbons. The POL is a pronounced ligament in both macaques and gibbons, relatively more so compared to the DRL, especially in macaques, where the POL is clearly the most prominent ligament.

The intermetacarpal ligament (IML) connects the dorsoradial aspect of the MC2 base and the ulnar ridge of the palmar beak on the MC1 (**Fig. 4c, f**). In humans, the IML is accompanied by a dorsally situated dorsal intermetacarpal ligament (DIML), which connects dorsally to the POL on the MC1 base (Bettinger et al., 1999). This ligament, however, does not appear to be present in macaques or gibbons.

In macaques, the ulnar collateral ligament (UCL) (**Fig. 4a**) originates from the palmar and palmo-ulnar aspect of the trapezium and distal trapezial ridge. The fibres insert on

the ulnar side of the palmar beak adjacent to the IML. In gibbons, no separate UCL could be identified, it can either be part of the AOL or not present at all, as the ulnar side of the AOL does not reflect a morphology corresponding to that of the UCL.

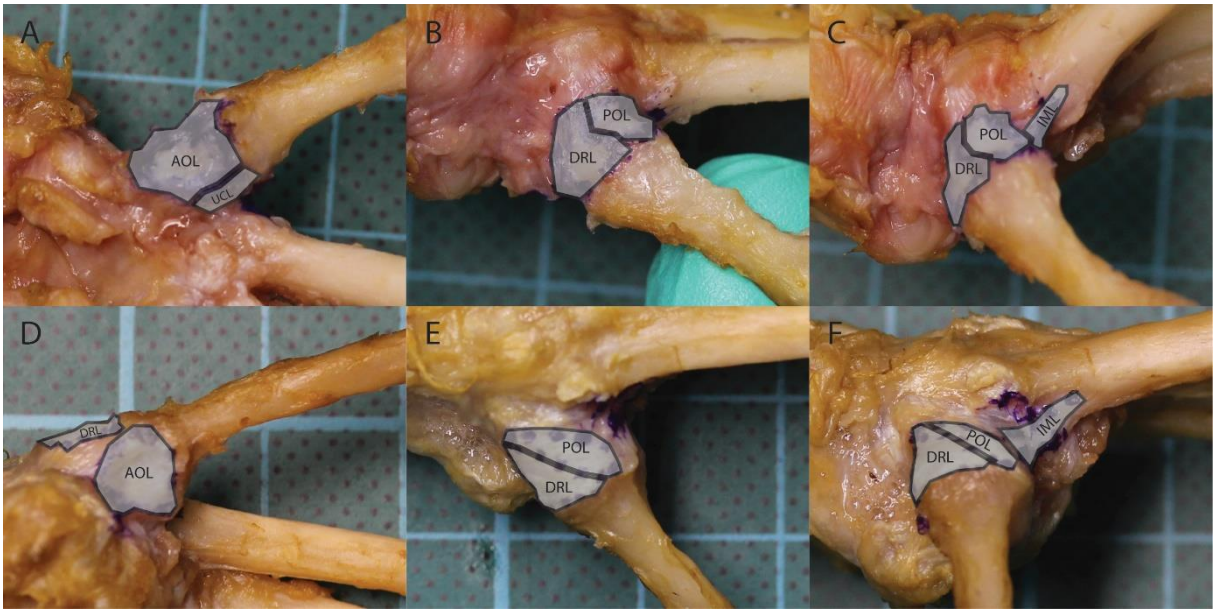

Figure 4: TMC ligaments in macaques (**A, B, C**) and gibbons (**D, E, F**). The anterior oblique ligament (AOL) (**A** and **D**), the dorsoradial ligament (DRL) (**B**, **C**, **D**, **E**, and **F**) and posterior oblique ligament (POL) (**B**, **C**, **E**, and **F**), the intermetacarpal ligament (IML) (**C** and **F**), and the ulnar collateral ligament (UCL) (**A**). Specimens visualized: macaque M5 and gibbon G5.

Discussion

The purpose of this study was to investigate the in-situ kinematics of the TMC joint in members of the Hylobatidae family and *Macaca mulatta*, two non-human primate groups that display highly disparate locomotor behaviour but are both capable of advanced manipulative tasks (Carpenter, 1941; van Horn, 1972; Dunbar, 1989; Christel, 1993; Macfarlane and Graziano, 2009). To interpret the data in an evolutionary context, we have also included data from a previous study on *in-situ* kinematics of the human and bonobo TMC joint (van Leeuwen *et al.*, 2019). We also document the ligament configuration of the gibbon and macaque TMC joint to supplement the under-represented anatomical knowledge on non-human primate hands in the literature, and furthermore allowing us to include the influence of the passive soft-tissue in the interpretation of primate TMC joint capabilities.

The data demonstrate distinct differences in TMC joint mobility between gibbons and macaques, with a wide range of motion in the gibbon and considerably restricted movement in macaques. When bonobo and human data are taken into consideration, we find that gibbons and macaques represent the high and low mobility extremes in this sample, respectively. The ball-and-socket configuration of the gibbon's TMC joint places their mobility on par with that of humans. It appears that the low habitual thumb loading in gibbons allows for a TMC joint morphology that imposes low structural constraints. Due to the lack of axial stabilisation, the ball-and-socket morphology in gibbons is inherently less stable when compared to the saddle-shaped version found in most other primates. But it also excludes a screw home mechanism, present in the saddle-shaped joint, that further increases joint congruency during opposition, stabilizing the joint during forceful gripping (D'Agostino *et al.*, 2017). Furthermore, there is no indication of increased reinforcement of the inherently unstable TMC joint by means of a strongly developed soft-tissue envelope. Not only the ligaments, but also the thenar muscles do not show any indications that imply a relatively high reliance on soft-tissue stabilisation of the TMC joint (Vanhoof, van Leeuwen and Vereecke, 2020). It appears that the joint allows for too many degrees of freedom to function in the same manner as the human TMC joint does. The gibbon TMC joint mobility is not only characterised by a large range of motion in the principal planes, but our results also indicate that high degrees of MC1 axial rotation can occur during thumb flexion-extension and abduction-adduction (See supplementary material **S1**). This can likely be attributed to the morphology of the gibbon MC1 (**Fig. 5**), which shows variable degrees of axial torsion. This can affect the terminal positions of the thumb in the

rig, and individuals with high may present high axial rotation of the MC1 during thumb movements.. Axial rotation of the MC1 has been document before in other apes and was reportedly particularly high in orangutans (Drapeau, 2015), this was speculated to have be in relation to the set of the trapezium with respect to the other carpals (Lewis, 1977; Sarmiento, 1994; Tocheri *et al.*, 2005). Drapeau also pointed out that the combined inversion of the MC1 and eversion of the MC2 shares similarities with the torted first and second metatarsi in apes, which relates to grasping and vertical climbing (Drapeau and Harmon, 2013). However, coevolution of the hands and feet should also be considered (Rolian, Lieberman and Hallgrímsson, 2010).

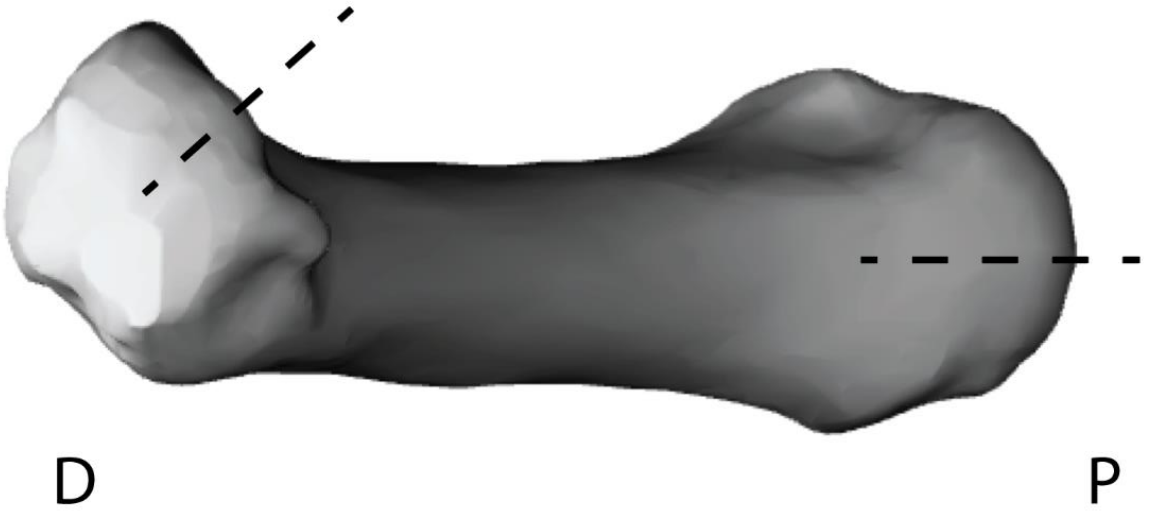

Figure 5: Visualisation of torsion in the gibbon first metacarpal. The distal (**D**) head is rotated with respect to the proximal (**P**) base of the MC1. Palmar view of gibbon specimen G8.

The macaque TMC joint maximum range of motion is highly restricted in both planes, even more so than reported values for Cercopithecines by Rose (1992) (± 21.4° in flexion-extension, 18.1° in abduction-adduction). Although those values include a broader range of species. This restriction occurs while the curvature ratio in macaques is close to one, indicating high congruence, especially in the radio-ulnar plane. Highly corresponding articular curvatures have been associated with high joint mobility (Hamrick, 1996), but as was indicated by Hamrick this may not be the case for all joint types and taxa. From the TMC joint surface morphology we can discern that although the surface curvature in the saddle-point of the macaque joint is more curved compared to that of gibbons, bonobos, and humans, this strong curvature does not persist towards the periphery of the articular surface (particularly clear in **Fig. 3b**). As the curvature progressively flattens out, trapeziometacarpal interactions start to resemble those of planar joints like the carpometacarpal joints in the other digits of the hand. A relatively flat articular surface curvature has been described in the closely related *Papio*, where the flattened radio-ulnar curvature causes the saddle to be cylinder shaped (Marzke *et al.*, 2010). Yet, this low curvature is relatively well sustained throughout the radio-ulnar surface, allowing for accurate fitting using a quadratic shape (Tocheri *et al.*, 2006; Marzke *et al.*, 2010; Matsuura, Ogihara and Nakatsukasa, 2010). The macaque articular curvature fitted here, however, appears more complex, with fluctuations in curvature describing its shape. While we used the fitting of quantic shape to account for just that, our current approach only allows for accurate curvature description at the centre of the articulation. In gibbons, a consistent surface curvature is better maintained, allowing the surface fit to more accurately describe the curvature of the joint. Therefore, in order to accurately describe the full interaction of the more complex macaque TMC joint surfaces, a more intricate joint surface analysis than presented here is required.

Although high structural stability is to be expected of a joint that is loaded in locomotion, it does present issues for thumb mobility during advanced manual tasks, of which the macaque is certainly capable (Macfarlane and Graziano, 2009). From CT scan reconstructions of the entire macaque hand we were able to visually discern that a large extent of their thumb mobility can be attributed to the more distal metacarpophalangeal (MCP) joint (**Fig. 6**). The MCP joint, however, is considered to be primarily a hinge joint, mainly allowing for thumb flexion-extension. Yet, abduction-adduction has been shown to occur in the macaque MCP (Thompson, 2020). We do find that the macaque joint less congruent in the flexion-extension plane, which causes the TMC joint morphology to diverge from a true universal joint. This likely allows some axial rotation of the MC1,

facilitating opposition of the thumb. We see this occur in our analysis, where axial rotation of the MC1 is present in the movements of the macaque thumb.

The overall qualitative configuration of the TMC ligaments is similar in gibbons, macaques, bonobos, and humans alike, despite marked differences in the geometry of the TMC joint. We see that in gibbons, macaques, in addition to bonobos, the POL is more developed compared to the DRL (van Leeuwen *et al.*, 2019). This is in contrast to the human configuration where the DRL plays a key role in joint stabilisation (D'Agostino *et al.*, 2014). The individual DIML present in humans, could not be identified in either gibbons, macaques, or bonobos. The main difference between gibbons and humans is that fewer individual structures can be identified in gibbons, and instead a more unified structure is present. This same, relatively simple, configuration corresponds with what was reported by van Horn (1972). It is therefore likely that although gibbons can match humans in terms of TMC joint mobility, they are likely not able to do so in terms of grip strength. It should, however, be noted information on the mechanical properties of the ligaments are needed to draw conclusions about ligament function, as even though the ligament configuration may appear qualitatively similar, it can be functionally different.

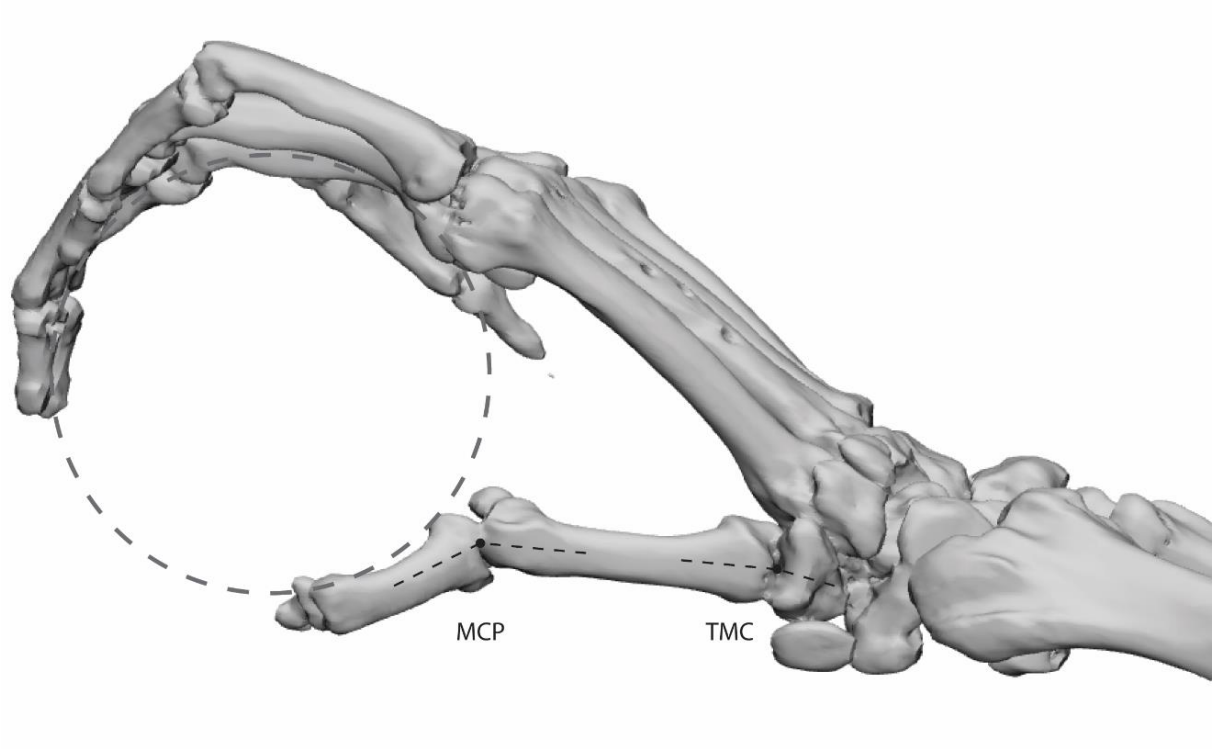

Figure 6: Visualisation of metacarpophalangeal (specimen M1) (MCP) joint mobility compared to trapeziometacarpal joint mobility during a small diameter power grasp. Note the recruitment of the MCP joint in order to achieve the range of motion for a full grasp. This image is a rough CT scan segmentation from a currently unpublished, parallel study on gripping in macaques by van Leeuwen and others.

The macaque TMC joint is further reinforced by a generally well defined ligament structure. Their configuration is similar to that of gibbons, bonobos, and humans. Like gibbons and bonobos, the POL is more developed in comparison to the DRL, and no individual DIML can be identified. The macaque configuration is, however, characterised by the presence of an individual UCL. This ligament likely reinforces the AOL in preventing palmar subluxation during thumb extension, which can particularly be relevant for palmigrade locomotion where the TMC joint may be loaded in extension. In humans, an individual UCL is also present, where it stabilizes thumb extension and prevents palmar subluxation (Bettinger *et al.*, 1999). This may be related to the relatively large degree of thumb extension that humans are capable of, which was shown to be largely attributed to the increased extension of the MC1 in humans (van Leeuwen *et al.*, 2019).

This study provides insight into the *in-situ* capabilities of the TMC joint in a limited, but unique sample of gibbons and macaques, along with detailed documentation of the surrounding ligaments. Our findings on TMC joint mobility and stability correspond well with our expectations based on the loading regimes associated with locomotor behaviour. The relatively disencumbered thumb of the arboreal gibbon is capable of a large range of MC1 motion. Their morphology appears adapted to low degrees of habitual loading, due to the ball-and-socket joint morphology without apparent soft-tissue reinforcement. The TMC joint of semi-terrestrial macaques, in contrast, is heavily restricted, so much so that the metacarpophalangeal joint is recruited to accommodate the thumb with the mobility required for advanced manual tasks. Future work should increase the sample size, both in terms of specimens and species, so that we can provide a larger framework in which we study adaptation of the primate hand and thumb as a basis for evolutionary interpretation.

Acknowledgements

The authors are deeply grateful to Georg Hantke of the National Museum of Scotland (NMS), Edinburgh, Scotland, Pieter Cornillie of Ghent University, campus Merelbeke, Belgium, Koen Nelissen, of KU Leuven, campus Gasthuisberg, Belgium, Robby Van der Velden of Pakawi Park, Olmen, Belgium, François Druelle of the Zoological and Botanical Park of Mulhouse, France, , and Jeroen Stevens of Zoo Antwerp, Belgium for collaborating on this study by granting access to this unique sample of primate specimens. We are further indebted to Olivier Vanovermeire and Henk Lacaeyse of AZ Groeninge, Kortrijk, Belgium, for providing access and technical support during the imaging procedures. We would like to thank Elaine Kozma, Nathan Thompson, Caley Orr, Tracy Kivell, and Jos Snoeks for their valuable manuscript feedback. Lastly, we would like to acknowledge KU Leuven for granting funding for this study (grant RQ1-D1114-C14/16/082).

Supplementary material

Gibbon (Hylobatidae)																								
Specimen	G1			G2			G3			G4			G5			G6			G7			G8		
Axis	**x**	y	z	**x**	y	z	**x**	y	z	**x**	y	z	**x**	y	z	**x**	y	z	**x**	y	z	**x**	y	z
Movement	**Abduction - Adduction**																							
Rotation (°)	38.41	-14.21	-2.59	53.99	-5.68	-1.64	48.01	34.54	-6.64	27.19	-30.01	4.79	40.89	-14.86	0.29	64.02	-10.30	14.75	45.68	19.61	6.26	60.15	0.35	12.96
Translation (mm)	0.07	-0.73	0.74	0.18	-1.33	1.49	0.40	-0.01	-0.34	0.07	-0.94	-1.46	0.17	-0.57	0.21	0.34	-0.45	1.66	-0.67	0.86	1.70	0.49	-0.62	0.98
Movement	**Flexion - Extension**																							
Rotation (°)	-7.25	21.49	42.73	1.13	13.77	53.21	-4.83	21.08	32.61	-9.50	-23.03	52.86	8.04	41.34	37.64	-7.80	20.64	43.51	-2.44	-56.36	34.47	-5.49	15.63	50.94
Translation (mm)	0.19	0.07	0.08	-0.16	1.10	-0.68	0.36	0.77	2.06	0.08	-0.17	-1.67	-1.01	0.22	-0.18	0..22	0.07	0.45	0.88	0.30	0.74	0.30	0.48	0.13
Macaque (*Macaca mulatta*)																								
Specimen	M1			M2			M3			M4			M5			M6			M7					
Axis	x	y	**z**	x	y	**z**	x	y	**z**	x	y	**z**	x	y	**z**	x	y	**z**	x	y	**z**			
Movement	**Abduction - Adduction**																							
Rotation (°)	10.44	0.19	-0.81	7.28	37.31	0.05	5.99	8.85	-4.77	7.40	9.97	-3.49	3.73	8.82	-3.75	6.38	5.67	-3.58	8.72	-1.27	0.74			
Translation (mm)	-0.23	-0.05	0.44	-0.79	0.01	1.04	-0.58	-0.09	0.68	0.13	0.04	0.56	-2.00	0.55	-0.38	-0.05	0.02	0.59	-0.22	0.52	0.33			
Movement	**Flexion - Extension**																							
Rotation (°)	0.20	1.90	2.20	-12.79	27.06	9.07	0.13	4.06	0.13	-7.20	21.41	15.42	3.59	8.61	7.70	-5.69	11.88	15.47	-3.28	-1.36	6.27			
Translation (mm)	0.10	0.18	-0.20	-0.62	-0.29	0.38	0.17	0.05	-0.15	-1.23	-0.41	0.28	-1.50	0.99	-0.37	-0.49	-0.45	0.40	-0.06	-0.26	-0.22			

S1: Full dataset of MC1 transformations with respect to the trapezium in gibbons (Hylobatidae) and rhesus macaques (*Macaca mulatta*). Rotation angles (in degrees °) and translation (in mm) are reported for each axis; x, y, and z represent the axes of the TMC joint. x: the dorsopalmar axis, rotation about x results in thumb abduction (-) - adduction (+), positive translation along x results in palmar translation; y: the proximodistal axis, rotation about y results in axial rotation (internal +, external -) of the MC1, positive translation along y results in proximal translation; z: the radioulnar axis, rotation about z results in flexion (+) – extension (-), positive translation along z results in radial translation. Axes in **bold** indicate the relevant rotation axis during each movement; **x** for abduction – adduction, **z** for flexion – extension.

References

Aversi-Ferreira, T. A. *et al.* (2016) 'Comparative anatomy of the arm muscles of the Japanese monkey (Macaca fuscata) with some comments on locomotor mechanics and behavior', *Journal of Medical Primatology*, 45(4), pp. 165–179. doi: 10.1111/jmp.12222.

Bardo, A. *et al.* (2016) 'Behavioral and functional strategies during tool use tasks in bonobos', *American Journal of Physical Anthropology*, 161(1), pp. 125–140. doi: 10.1002/ajpa.23015.

Berger, R. A. (2001) 'The Anatomy of the Ligaments of the Wrist and Distal Radioulnar Joints', *Clinical Orthopaedics and Related Research*, 383, pp. 32–40. doi: 10.1097/00003086-200102000-00006.

Bettinger, P. C. *et al.* (1999) 'An Anatomic Study of the Stabilizing Ligaments of the Trapezium and Trapeziometacarpal Joint', *The Journal of Hand Surgery*, 24(4), pp. 786–798. doi: 10.1053/jhsu.1999.0786.

Cannon, C. H. and Leighton, M. (1994) 'Comparative locomotor ecology of gibbons and macaques: Selection of canopy elements for crossing gaps', *American Journal of Physical Anthropology*, 93(4), pp. 505–524. doi: 10.1002/ajpa.1330930409.

Carpenter, C. R. (1941) *A field study in Siam of the behavior and social relations of the gibbon (Hylobates lar)*. Baltimore, Md.: The Johns Hopkins Press.

Christel, M. I. (1993) 'Grasping techniques and hand preferences in Hominoidea', (January 1993), pp. 91–108. doi: 10.1007/978-3-7091-6914-8.

Crisco, J. J. *et al.* (2015) 'In vivo kinematics of the trapeziometacarpal joint during thumb extension-flexion and abduction-adduction', *Journal of Hand Surgery*. Elsevier Inc, 40(2), pp. 289–296. doi: 10.1016/j.jhsa.2014.10.062.

D'Agostino, P. *et al.* (2014) 'Comparison of the Anatomical Dimensions and Mechanical Properties of the Dorsoradial and Anterior Oblique Ligaments of the Trapeziometacarpal Joint', *The Journal of Hand Surgery*, 39(6), pp. 1098–1107. doi: 10.1016/j.jhsa.2014.02.025.

D'Agostino, P. *et al.* (2016) 'In vivo kinematics of the thumb during flexion and adduction motion: Evidence for a screw-home mechanism', *Journal of Orthopaedic Research*, pp. 1–9. doi: 10.1002/jor.23421.

D'Agostino, P. *et al.* (2017) 'In vivo kinematics of the thumb during flexion and adduction motion: Evidence for a screw-home mechanism', *Journal of Orthopaedic Research*, 35(7), pp. 1556–1564. doi: 10.1002/jor.23421.

Diogo, R. *et al.* (2009) 'From fish to modern humans - comparative anatomy, homologies and evolution of the pectoral and forelimb musculature', *Journal of Anatomy*. Wiley/Blackwell (10.1111), 214(5), pp. 694–716. doi: 10.1111/j.1469-7580.2009.01067.x.

Drapeau, M. S. M. (2015) 'Metacarpal torsion in apes, humans, and early Australopithecus: implications for manipulatory abilities', *PeerJ*, 3, p. e1311. doi: 10.7717/peerj.1311.

Drapeau, M. S. M. and Harmon, E. H. (2013) 'Metatarsal torsion in monkeys, apes, humans and australopiths', *Journal of Human Evolution*, 64(1), pp. 93–108. doi:

10.1016/j.jhevol.2012.10.008.

Dunbar, D. C. (1989) 'Locomotor behavior of rhesus macaques (Macaca mulatta) on Cayo Santiago.', *Puerto Rico health sciences journal*, 8(1), pp. 79–85.

Fragaszy, D. *et al.* (2004) 'Wild capuchin monkeys (Cebus libidinosus) use anvils and stone pounding tools', *American Journal of Primatology*, 64(4), pp. 359–366. doi: 10.1002/ajp.20085.

Gumert, M. D., Hoong, L. K. and Malaivijitnond, S. (2011) 'Sex differences in the stone tool-use behavior of a wild population of burmese long-tailed macaques (Macaca fascicularis aurea)', *American Journal of Primatology*, 73(12), pp. 1239–1249. doi: 10.1002/ajp.20996.

Halilaj, E. *et al.* (2013) 'A thumb carpometacarpal joint coordinate system based on articular surface geometry', *Journal of Biomechanics*, 46(5), pp. 1031–1034. doi: 10.1016/j.jbiomech.2012.12.002.

Hamrick, M. W. (1996) 'Articular size and curvature as determinants of carpal joint mobility and stability in strepsirhine primates', *Journal of Morphology*, 230(2), pp. 113–127. doi: 10.1002/(SICI)1097-4687(199611)230:2<113::AID-JMOR1>3.0.CO;2-I.

Hayama, S., Chatani, K. and Nakatsukasa, M. (1994) 'The Digitigrade Hand and Terrestrial Adaptation in Japanese Macaques', *Anthropological Science*, 102(Supplement), pp. 115–125. doi: 10.1537/ase.102.Supplement_115.

van Horn, R. N. (1972) 'Structural Adaptations to Climbing in the Gibbon Hand', *American Anthropologist*, 74(3), pp. 326–334. doi: 10.1525/aa.1972.74.3.02a00050.

Jones, F. W. (1920) *The principles of anatomy as seen in the hand*. J. & A. Churchill.

van Leeuwen, T. *et al.* (2018) 'Insights into the musculature of the bonobo hand', *Journal of Anatomy*, 233(3), pp. 328–340. doi: 10.1111/joa.12841.

van Leeuwen, T. *et al.* (2019) 'Mobility and structural constraints of the bonobo trapeziometacarpal joint', *Biological Journal of the Linnean Society*, 127(3), pp. 681–693. doi: 10.1093/biolinnean/bly162.

Lewis, O. J. (1977) 'Joint remodelling and the evolution of the human hand.', *Journal of Anatomy*, 123(Pt 1), pp. 157–201.

Lewis, O. J. (1989) *Functional morphology of the evolving hand and foot*. Oxford University Press, USA.

Liu, M.-J., Xiong, C.-H. and Hu, D. (2016) 'Assessing the manipulative potentials of monkeys, apes and humans from hand proportions: implications for hand evolution', *Proceedings of the Royal Society B: Biological Sciences*, 283(1843), p. 20161923. doi: 10.1098/rspb.2016.1923.

Macfarlane, N. B. W. and Graziano, M. S. A. (2009) 'Diversity of grip in Macaca mulatta', *Experimental Brain Research*, 197(3), pp. 255–268. doi: 10.1007/s00221-009-1909-z.

Malaivijitnond, S. *et al.* (2007) 'Stone-tool usage by Thai long-tailed macaques (Macaca fascicularis)', *American Journal of Primatology*, 69(2), pp. 227–233. doi: 10.1002/ajp.20342.

Marzke, M. W. (1971) 'Origin of the human hand', *American Journal of Physical Anthropology*, 34(1), pp. 61–84. doi: 10.1002/ajpa.1330340106.

Marzke, M. W. *et al.* (2010) 'Comparative 3D quantitative analyses of trapeziometacarpal joint surface curvatures among living catarrhines and fossil hominins.', *American journal of physical anthropology*. United States, 141(1), pp. 38–51. doi: 10.1002/ajpa.21112.

Marzke, M. W. and Marzke, R. F. (2000) 'Evolution of the human hand: Approaches to acquiring, analysing and interpreting the anatomical evidence.', *Journal of Anatomy*, 197, pp. 121–140. doi: 10.1046/j.1469-7580.2000.19710121.x.

Matsuura, Y., Ogihara, N. and Nakatsukasa, M. (2010) 'A Method for Quantifying Articular Surface Morphology of Metacarpals Using Quadric Surface Approximation', *International Journal of Primatology*, 31(2), pp. 263–274. doi: 10.1007/s10764-010-9397-3.

Napier, J. *et al.* (1993) *Hands*. Princeton University Press (Natural science).

Napier, J. R. (1955) 'The form and function of the carpo-metacarpal joint of the thumb.', *Journal of anatomy*, 89(3), pp. 362–9.

Napier, J. R. (1956) 'The Prehensile Movements of the Human Hand', *The Journal of Bone and Joint Surgery. British volume*, 38-B(4), pp. 902–913. doi: 10.1302/0301-620X.38B4.902.

Napier, J. R. (1960) 'Studies of the hands of living primates', *Proceedings of the Zoological Society of London*, 134, pp. 647–657.

Neufuss, J. *et al.* (2017) 'Nut-cracking behaviour in wild-born, rehabilitated bonobos (Pan paniscus): a comprehensive study of hand-preference, hand grips and efficiency', *American Journal of Primatology*, 79(2), pp. 1–16. doi: 10.1002/ajp.22589.

R Core Team, R. (2017) 'R: A language and environment for statistical com-puting'. Vienna, Austria: R Foundation for Statistical Computing. Retrieved from ….

Rafferty, K. L. (1990) *The Functional and Phylogenetic Significance of the Carpometacarpal Joint of the Thumb in Anthropoid Primates*. New York University.

Rawlins, R. G. (1993) 'Locomotive and manipulative use of the hand in the Cayo Santiago macaques (Macaca mulatta)', in *Hands of Primates*. Vienna: Springer Vienna, pp. 21–30. doi: 10.1007/978-3-7091-6914-8_3.

Rolian, C., Lieberman, D. E. and Hallgrímsson, B. (2010) 'The Coevolution Of Human Hands And Feet', *Evolution*, 64(6), pp. 1558–1568. doi: 10.1111/j.1558-5646.2009.00944.x.

Roos, C. and Zinner, D. (2015) 'Diversity and Evolutionary History of Macaques with Special Focus on Macaca mulatta and Macaca fascicularis', in *The Nonhuman Primate in Nonclinical Drug Development and Safety Assessment*. Elsevier, pp. 3–16. doi: 10.1016/B978-0-12-417144-2.00001-9.

Rose, M. D. (1992) 'Kinematics of the trapezium-1st metacarpal joint in extant anthropoids and Miocene hominoids', *Journal of Human Evolution*, 22(4–5), pp. 255–266. doi: 10.1016/0047-2484(92)90058-H.

Sarmiento, E. E. (1994) 'Terrestrial traits in the hands and feet of gorillas. American Museum novitates; no. 3091'. New York, NY: American Museum of Natural History.

Susman, R. L. (1988) 'Hand function and tool behavior in early hominids', *Academic Press Journal of Human Evolution*, 35, pp. 23–36. doi: 10.1006/jhev.1998.0220.

Thompson, N. E. (2020) 'The biomechanics of knuckle-walking: 3-D kinematics of the chimpanzee and macaque wrist, hand and fingers', *The Journal of Experimental Biology*, 223(14), p. jeb224360. doi: 10.1242/jeb.224360.

Tocheri, M. W. *et al.* (2005) 'A 3D quantitative comparison of trapezium and trapezoid relative articular and nonarticular surface areas in modern humans and great apes', *Journal of Human Evolution*, 49(5), pp. 570–586. doi: 10.1016/j.jhevol.2005.06.005.

Tocheri, M. W. *et al.* (2006) 'Quadric-based metrics for shape analysis of three-dimensional osteological surfaces', *Am J Phys Anthropol*, 129, pp. 177–178.

Toth, N. *et al.* (1993) 'Pan the Tool-Maker: Investigations into the Stone Tool-Making and Tool-Using Capabilities of a Bonobo (Pan paniscus)', *Journal of Archaeological Science*, 20(1), pp. 81–91. doi: 10.1006/jasc.1993.1006.

Tuttle, R. H. (1969) 'Quantitative and functional studies on the hands of the anthropoidea. I. The Hominoidea', *Journal of Morphology*, 128(3), pp. 309–363. doi: 10.1002/jmor.1051280304.

Vanhoof, M. J. M., van Leeuwen, T. and Vereecke, E. E. (2020) 'The forearm and hand musculature of semi-terrestrial rhesus macaques (Macaca mulatta) and arboreal gibbons (Fam. Hylobatidae). Part I. Description and comparison of the muscle configuration', *Journal of Anatomy*. John Wiley & Sons, Ltd, n/a(n/a). doi: 10.1111/joa.13222.

Wells, J. P. and Turnquist, J. E. (2001) 'Ontogeny of locomotion in rhesus macaques (Macaca mulatta): II. Postural and locomotor behavior and habitat use in a free-ranging colony', *American Journal of Physical Anthropology*, 115(1), pp. 80–94. doi: 10.1002/ajpa.1059.

Wu, G. *et al.* (2005) 'ISB recommendation on definitions of joint coordinate systems of various joints for the reporting of human joint motion—Part II: shoulder, elbow, wrist and hand', *Journal of Biomechanics*, 38(5), pp. 981–992. doi: 10.1016/j.jbiomech.2004.05.042.

Wu, G. and Cavanagh, P. R. (1995) 'ISB recommendations for standardization in the reporting of kinematic data', *Journal of Biomechanics*, 28(10), pp. 1257–1261. doi: 10.1016/0021-9290(95)00017-C.

Part 3.

Trapezial morphology and load distribution

In this part, I address the form and function of the TMC joint at the level of the trapezium. I assess joint interaction, and how stress and strain are distributed within the joint and trapezial internal bony architecture as a result of different types of grasping. This part comprises three chapters; **Chapter 4** is the development of the parametric finite element (FE) approach to assess intra articular stress distributions on the bonobo trapezium articular surface during grasping. **Chapter 5** further implements these stress patterns into an integrated μFE workflow that calculates internal strain distribution in the bonobo trapezium as a result of these different grasps. **Chapter 6** uses this combined FE/μFE approach to assess the stress/strain distributions in the gibbon and macaque trapezium during the same grasps as the bonobo. This part addresses objective 1, objective 4, objective 5, and objective 6

Objective 1: To document the forelimb soft and hard tissue morphology through detailed dissections and medical imaging in order to provide a detailed anatomical dataset for bonobos, gibbons, and macaques.

Objective 4: To design and develop an integrated workflow to study trapezium internal stress distribution from simulated grasping positions.

Objective 5: To determine how forces are distributed within the TMC joint during grasping, and how morphology influences the resulting stress patterns.

Objective 6: To investigate and compare morphological adaptation of the trapezium internal bone architecture to grasping.

Chapter 4.

Stress distribution in the bonobo (*Pan paniscus*) trapeziometacarpal joint during grasping

Timo van Leeuwen[1,2], G. Harry van Lenthe[2], Evie E. Vereecke[1], Marco T.Y. Schneider[3]

[1]Department of Development and Regeneration, KU Leuven KULAK, Kortrijk, Belgium

[2]Department of Mechanical Engineering, University of Leuven, Leuven, Belgium

[3]Auckland Bioengineering Institute, The University of Auckland, Auckland, New Zealand

Resubmitted for revision for publication in *PeerJ:*

van Leeuwen, T., van Lenthe, G.H., Vereecke, E. E., and Schneider, M.T.Y., 2021, *Stress distribution in the bonobo (Pan paniscus) trapeziometacarpal joint during grasping.* PeerJ. In Revision.

Abstract

The primate thumb plays a central role in grasping and the basal trapeziometacarpal (TMC) joint is critical to its function. The TMC joint morphology varies across primates, yet little is known about form-function interaction within in the TMC joint. The purpose of this study was to investigate how stress distributions within the joint differ between five grasping types commonly employed by bonobos (*Pan paniscus*). Five cadaveric bonobo forearms were CT scanned in five standardized positions of the hand as a basis for the generation of parametric finite element models to compare grasps. We have developed a novel approach to finite element analysis (FEA) to investigate stress distribution patterns in the TMC joint associated with each grasp type. We hypothesized that the simulated stress distributions for each position would correspond with the patterns expected from a saddle-shaped joint. However, we also expected there to be differences in stress patterns arising from intraindividual variations in morphology. The models showed a high agreement between simulated and expected stress patterns for each of the five grasps (86% of successful simulations), while partially (52%) and fully (16%) diverging patterns were also encountered. We identified individual variations of key morphological features in the bonobo TMC joint that account for the diverging stress patterns and emphasized the effect of inter-individual variation on joint functioning. This study gives unprecedented insight in the form-function interactions in the TMC joint of the bonobo. We provides an innovative FEA approach to modelling intra-articular stress distributions; a valuable tool for the study of the primate thumb that can facilitate the expansion of our knowledge on primate joint biomechanics.

Introduction

The combination of high thumb mobility and forceful grasping is considered a unique modern human hallmark (Napier, 1956, 1960; Napier and Napier, 1967; Marzke, 1997; Susman, 1998). The high mobility of the modern human thumb predominantly originates from the morphology of the basal thumb or trapeziometacarpal (TMC) joint (**Fig. 1**) (Napier, 1955). The TMC joint is a reciprocal saddle-shaped joint, the physiological equivalent of a universal joint which allows motion in two planes (flexion-extension, abduction-adduction) (Cooney and Chao, 1977). The shape allows for large ranges of motion of the first metacarpal (MC1), but also offers the stability required for forceful grasping (Napier, 1955; Rose, 1992; D'Agostino *et al.*, 2017). The morphology of the TMC joint varies across primates (Lewis, 1977; Rafferty, 1990; Marzke *et al.*, 2010), but how this relates to specific thumb function in these primates remains unclear. Where many studies focus on the human TMC joint, especially from a clinical point of view (Haines, 1944; Kuczynski, 1974; Ladd *et al.*, 2013, 2014; Crisco *et al.*, 2015; Schneider *et al.*, 2015; Dourthe *et al.*, 2016; Kerkhof *et al.*, 2018)., far less is known about form-function relations in the non-human primate thumb. In this study, we investigate the effect of different grip types on the stress distribution in their TMC joint in bonobos (*Pan paniscus*, Fam. *Hominidea*) (**Fig. 2A**). Bonobos are both arboreal and terrestrial, and they use their hands during locomotion, manipulation, including cases of tool use that have been observed in captivity. (Jordan, 1982; Christel, Kitzel and Niemitz, 1998; Ingmanson, 1998; Crast *et al.*, 2009; Feix *et al.*, 2015; Bardo *et al.*, 2016; Neufuss *et al.*, 2017). Common grasp types used by bonobos include various types of power grasps as well as a key pinch precision grip (**Fig. 2**) (Napier, 1956; Christel, 1993; Christel, Kitzel and Niemitz, 1998; Neufuss *et al.*, 2017). In addition, bonobos use their thumb in vertical climbing and clambering, to grasp trunks or branches, but the thumb is not loaded during knuckle-walking (Tuttle, 1967; Inouye, 1992; Wunderlich and Jungers, 2009; Samuel *et al.*, 2018).

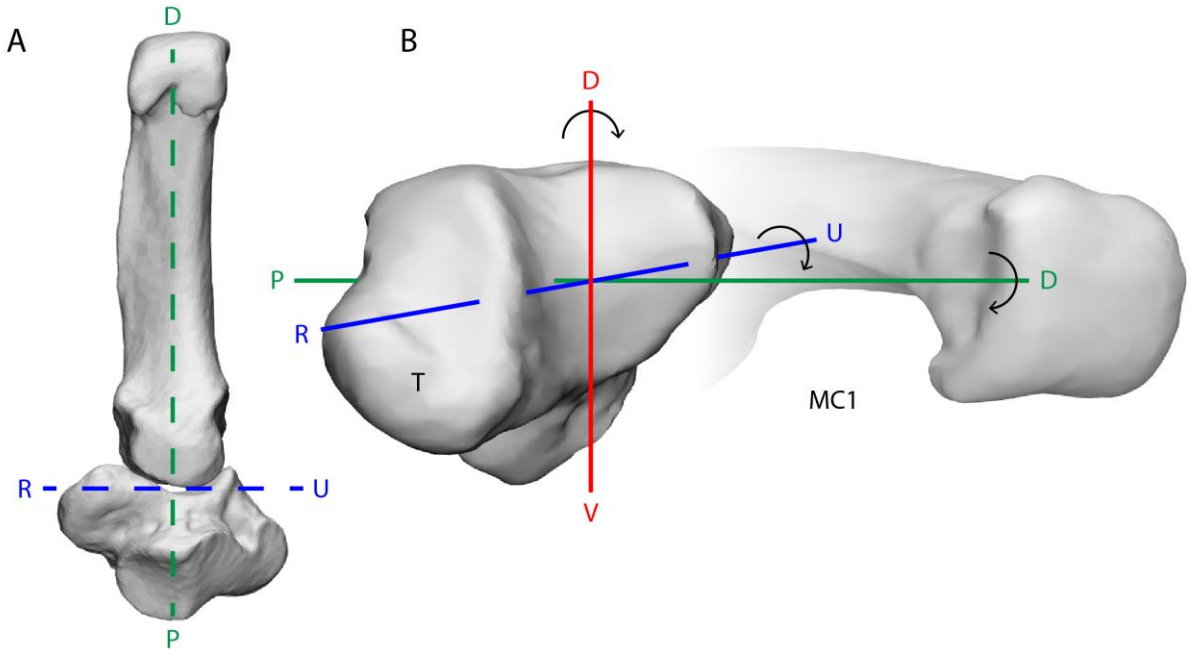

Figure 1: The bonobo trapeziometacarpal (TMC) joint, from a ventral (palmar) view (**A**) and a radiodistal view (**B**) view. Its reciprocal surfaces are saddle-shaped. The distal articular surface of the trapezium (**T**) has a convex curvature along the dorsal-palmar (**D-V**) axis, and makes contact with the concave curvature of the first metacarpal (**MC1**), while the trapezial articular surface along the radio-ulnar (**R-U**) axis is concave, to match the convex curvature of the MC1. The principal movements of the thumb align with rotation about one of three axes of the joint; rotation about the **D-V** axis results in palmar abduction-adduction, rotation about the **R-U** axis results in thumb flexion-extension, and rotation about the proximal-distal (**P-D**) axis results in axial rotation of the thumb. The depicted bone models are trapezium and MC1 surface meshes reconstructed from CT scanning Pp5 in a neutral position of the thumb.

Bonobos, like humans, possess a saddle-shaped TMC joint, and have a very similar soft-tissue configuration, i.e. the surrounding muscles and ligaments, to that of humans (van Leeuwen *et al.*, 2018, 2019). Such morphology is not unique to hominids. In fact the saddle-shape is also present in New World monkeys (Lewis, 1977; Rafferty, 1990), some of which who are also highly dextrous (Parker and Gibson, 1977). In bonobos, the TMC joint is highly curved even when compared to humans (Marzke, 1997), allowing for wide ranges of motion in particular during adduction and adduction of the thumb. Our previous research on the kinematics of the primate TMC joint has shown that the mobility of the bonobo thumb is similar to that of humans, but thumb extension is limited by the presence of a strong anterior oblique ligament which reinforces the palmar side of the TMC joint (van Leeuwen *et al.*, 2019). Based on these findings, we expect that the force distribution within the TMC joint will reflect signals of the specific joint morphology. Recently, Schneider et al. (2017) developed a finite element (FE) approach to model stress distribution in the human TMC joint. Here, we build upon this work and propose a derived model-based method to investigate the stress distribution in the bonobo TMC joint.

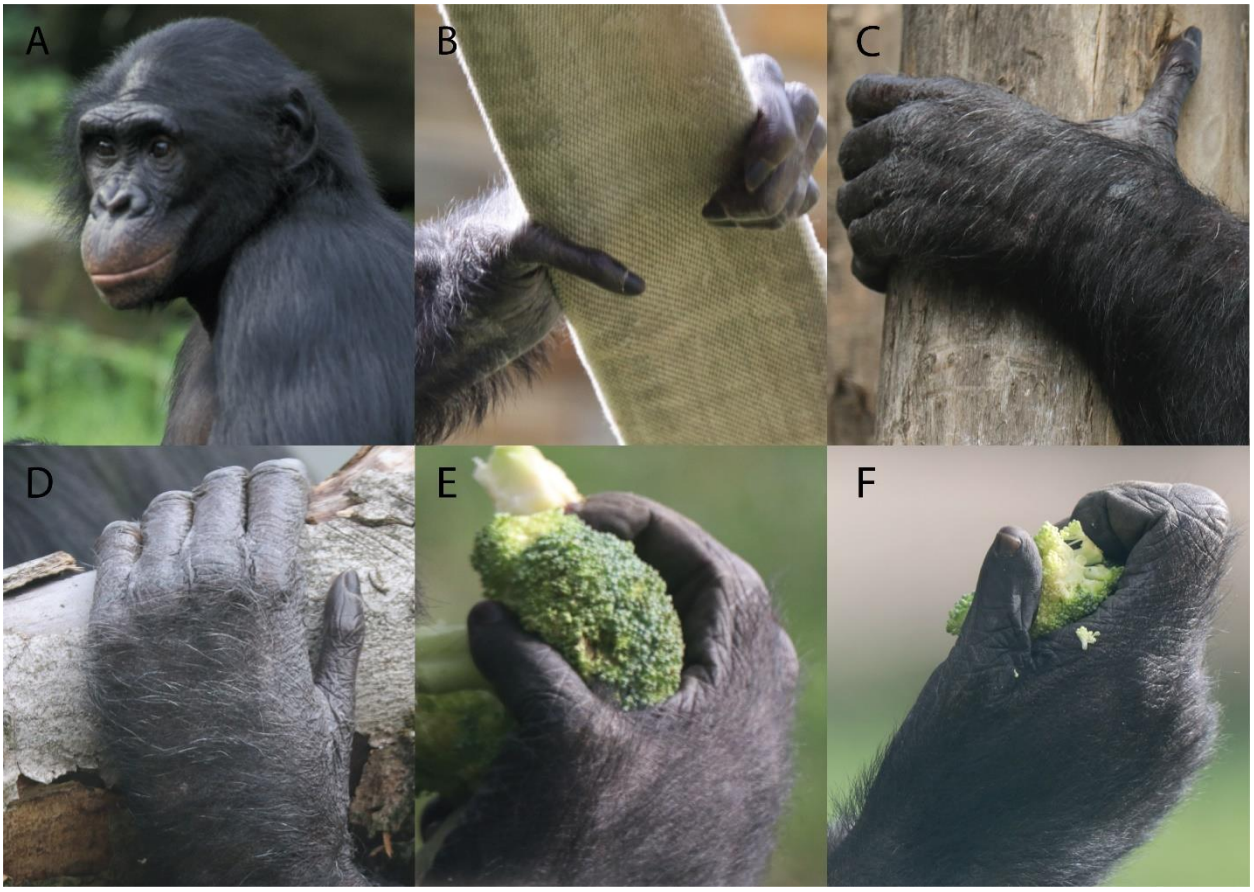

Figure 2: Depiction of the different grasping types observed in bonobos. **A**: an adult male bonobo, **B**: large diameter power grip with thumb abducted (*powerL*), **C**: large diameter power grip with thumb extended (*powerLE*), **D**: large diameter power grip with thumb abducted (*powerLA*), **E**: small diameter power grip (*powerS*), **F**: pad-to-side precision grip or keypinch (*pinch*). Photography by courtesy of Marie Vanhoof and prof. Kristiaan D'Aout.

In total, we investigate five types of grasps commonly used by bonobos (Christel, 1993; Samuel *et al.*, 2018). Out of these, three are large diameter power grasps, one with the thumb abducted, one with the thumb extended, and one with an adducted thumb. The abducted type, further referred to as *powerL* (**Fig. 2B**), is characterized by a wide grip and an abducted and externally rotated thumb that is still radioulnarly in line with the trapezium. Stresses are expected to be diverted to the radio-central aspect of the articular facet of the trapezium during *powerL*. The large diameter power grasp with extended thumb (*powerLE*) (**Fig. 2C**) extends the thumb near the maximal excursion of the TMC joint, but in line with the dorsopalmar plane of the trapezium. Stress peaks are therefore expected in the dorsal-central aspect of the articular facet of the trapezium. The large diameter power grasp with thumb adducted (*powerLA*) (**Fig. 2D**) places the thumb in line with the other digits of the hand. The thumb is adducted and externally rotated. Here, the opposite of the grasps with abducted thumb is expected; high stress in the ulnar-central articular facet of the trapezium. The small diameter power grasp (*powerS*) (**Fig. 2E**) is

similar to the large diameter variant, but in contrast, the amount of thumb abduction is less extreme. Stress is expected to concentrate centrally on the articular facet, with a radial tendency. The key *pinch* (**Fig. 2F**) is characterized by a relatively straight thumb and trapeziometacarpal joint. External thumb tip force is exerted downwards towards the radial side of the middle phalanx of a flexed index finger. As a result, forces are expected to be diverted towards to the central-palmar aspect of the trapezial facet, creating stress peaks in this area. A visual representation of the expected stress patterns is included in the Results section (see **Fig. 5**, top row).

Materials & Methods

In this study, we use an FE approach to model TMC joint stress distributions during various types of grasps employed by bonobos in manipulation and arboreal locomotion. The focus of this study is on the distribution of stress within the TMC joint during each grasp, the localisation of stress peaks, and how stress distributions may be influenced by individual TMC joint morphology. We use an optimised parametric finite element approach to model trapeziometacarpal joints of five cadaveric bonobo hands in five functional positions.

Specimens

Five cadaveric forearms of (sub)adult bonobos were obtained opportunistically via collaboration with five European zoos (**Table 1**). The forearms were disarticulated either at the glenohumeral joint or at the elbow joint and stored at -18 °C shortly after decease. All specimens were part of parallel studies on bonobo forelimb morphology and thumb biomechanics (van Leeuwen *et al.*, 2018, 2019). Specimen Pp2 was a sub-adult with a TMC joint that was not fully mature, presenting incomplete epiphysial fusion of the MC1 and a relatively smooth articular periphery (without pronounced bony ridges). The specimen has been included in the sample as the articular surfaces were sufficiently developed to present the reciprocal saddle-shape of the adult TMC joint. No articular pathologies were observed at the TMC joint in any of the specimens used for this study.

Table 1: Specimen information, *Master specimen, **Scanned in 4 positions only, ***Wild born but raised in captivity, SB: studbook number, M: male, F: female, R: right, L: left.

Code	Subject ID	Age	Sex	Sample	Origin	Zoo
Pp1	8365526	35	M	L	Wild born***	Wilhelma Zoo, Stuttgart, Germany
Pp2	15295295 SB: 295	8	F	L	Captive born	Royal Zoological Society Antwerp, Belgium
Pp3	MIG12-29882197 SB: 126	32	M	R	Captive born	Zoo Frankfurt, Germany
Pp4*	SB:177 CITES:79209	24	M	R	Captive born	La Vallée des Singes, Le Gureau, France
Pp5**	SB: 88 27641621	39	F	L	Wild born***	Wilhelma Zoo, Stuttgart, Germany

Imaging protocol

Each specimen was thawed at room temperature over a period of 24 hours before being imaged using a 64-slice Discovery HD 750 CT scanner [GE Healthcare, Little Chalfont, UK; display field of view (DFOV): 173 mm; slice thickness: 0.625 mm; pixel spacing: 0.338/0.338 mm, voxel size: 0.071 mm^3; 100 kV; 180 mA; image size: 512 × 512 pixels). A radio-translucent rig with a small (50mm) and large diameter peg (125m) was used to standardize each hand in the five functional grip positions (i.e. *powerL, powerLA, powerLE, powerS,* and *pinch*). This resulted in a total of 24 scan positions, as we were unable to position specimen Pp5 in a *powerL* grasp. Each trapezium and the first metacarpal was segmented separately using Mimics Research 20.0 (Materialise, Leuven, Belgium) and exported as triangular meshes.

Parametric meshing

Parametric FE meshes for 24 TMC joint models were generated in two steps by aligning all specimen-position combinations to a template set of TMC meshes and fitting the discretised master meshes to the 23 remaining specimen-position combinations.

Step 1: Mesh alignment

For each specimen, the trapezium and MC1 STL meshes of one specific grasp (*pinch*) were selected and designated as template meshes (**Fig. 3A**). A master TMC set template mesh (**Fig. 3A**) was selected and reoriented to a TMC-based coordinate system where the principal directions of motion of the thumb (i.e. abduction-adduction, extension-flexion, and axial rotation) are aligned with the cartesian coordinate system using a method based

on Halilaj et al. (2013; van Leeuwen *et al.*, 2019). The individual template sets for the remaining specimens were aligned with the master mesh in the same coordinate system by rigid body registration fitting the trapezium to the master trapezium template, and transforming the corresponding MC1 (**Fig. 3B**). The MC1s of all remaining specimen-position combinations were aligned with their respective template trapezium by rigid body registration fitting each combination's respective trapezium and transforming the first metacarpal along the resulting rotation matrix. This yields five aligned triangular trapezium meshes, one per specimen, each with five corresponding triangular metacarpal meshes, one per grasp (with the exception of Pp5, which has four) (**Fig. 3C**).

Step 2: Mesh fitting

The trapezium and first metacarpal master template triangular meshes were discretized into quadrilateral meshes using Instant Meshes software (Jakob *et al.*, 2015) (**Fig. 3D**). The reciprocal subchondral articular surfaces of the TMC joint were identified on both bones from bone landmarks, and delineated via local meshing using Instant Meshes' Position Field and Orientation Field tools. To ensure the subchondral surface mesh quality, Instant Meshes' Singularity tools were used to reduce mesh irregularities, minimize element distortion and increase mesh Jacobian values (Burkhart, Andrews and Dunning, 2013). The delineated subchondral elements were extracted using MeshLab software (v2016.12) (Cignoni *et al.*, 2008) and exported as separate quadrilateral meshes. Custom Python (3.6) scripts were used to generate quadrilateral template TMC meshes for each individual specimen. The discretised master trapezium, first metacarpal, and their respective cartilage meshes were fitted to the vertices of each specimen's triangular template mesh using Radial Basis Function (RBF) fitting (**Fig. 3E**). A three-layer, hexahedral cartilage layer mesh was generated for each specimen by lofting the extracted subchondral meshes along the surface node normal using a custom Python script based on Schneider et al. (2017). As cartilage information for the bonobo TMC joint was lacking, the cartilage layer was generated at a thickness of 0.5 mm, somewhat lower than the 0.6-0.7 mm thickness reported for human TMC joint cartilage (Dourthe *et al.*, 2018) to account for the relatively smaller bone size. MC1 quadrilateral meshes for the remaining grasps of each specimen were generated by rigid body registration fitting their quadrilateral MC1 template mesh to each position (**Fig. 3F**), and using the resulting transformation matrices to transform the corresponding hexahedral cartilage meshes. This yields five quadrilateral trapezium meshes, one per specimen, each with five (with the exception of Pp5) corresponding quadrilateral first metacarpal meshes (**Fig. 3G**), one per position, and hexahedral cartilage meshes for all bone meshes.

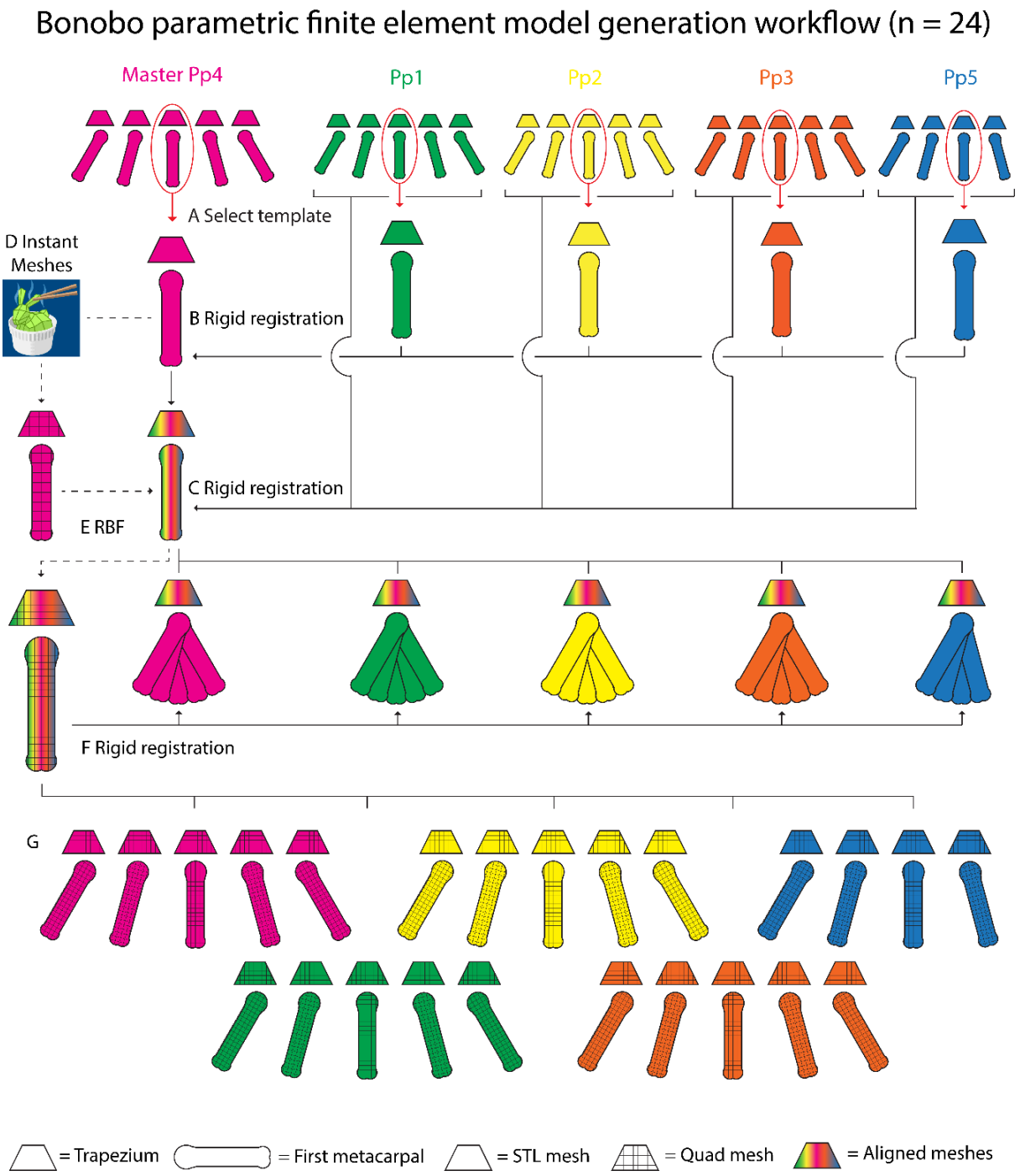

Figure 3: A schematic representation of the parametric finite element model generation pipeline. Template TMC meshes are selected for each specimen, one set is designated as the master mesh (**A**). All template meshes are aligned with the master mesh using rigid body registration of the trapezia, and transforming the MC1s onto the master meshes (**B**). The remaining MC1 positions for each specimen are aligned with their corresponding template set, again using rigid body registration of the trapezia and transforming the MC1s (**C**). The master template mesh is discretized into quadrilateral meshes (**D**), the articular surfaces are identified, extracted as quadrilateral meshes, and lofted into hexahedral cartilage meshes (not visualized). The quadrilateral bone and hexahedral cartilage (not visualized) master templates are fitted to the morphology of each specimen's template set using Radial Basis Function (RBF) fitting (**E**). The master MC1 template meshes are fitted to the remaining grasping positions in each specimen using rigid body registration (**F**). The workflow yields discretized quadrilateral meshes for all five specimens, for each of the five (four in the case of Pp5) positions (**G**).

FE model generation

All FE models were generated and solved using FEBio Software Suite (Maas et al., 2012). A master model (**Fig. 4**) was manually set up in FEBio Preview (v2.1.3) to be solved by the FEBio solver (v.2.9.0). The quadrilateral bone surface meshes were modelled as rigid bodies, and connected to their respective hexahedral cartilage meshes, modelled as a neo-Hookean material (Young's modulus = 18 MPa, Poisson's ratio = 0.45) (Black and Hastings, 2013). The trapezium mesh was constrained in all degrees of freedom, while the MC1 was given three degrees of freedom, allowing it to translate but not rotate.

As the imaging was performed on cadaveric material, the resulting bone meshes were situated in unloaded positions. To account for this, the model was set up as a two-step, force-driven model. The first step serves to bring the elements into contact, facilitated by nonlinear springs, exerting 1N of force each, corresponding to the bonobo TMC joint ligaments (van Leeuwen et al., 2019). Step two introduces the applied force vector. We performed a 2D static force analysis, based on Cooney and Chao (1977), to estimate the magnitude of the resultant force vector applied on the MC1. In the static force analysis, the initial thumb tip force was estimated at 50N, based on muscle PCSA, and muscle attachment information was based on detailed dissections published by our research group (van Leeuwen *et al.*, 2018). The analysis yielded a force vector magnitude of about 300N, which was applied to the MC1 for all positions. Successful model termination was achieved when the FEBio solver was capable of executing all steps of the force application process without any elements collapsing.

The remaining 23 models were generated using a custom Python script that substitutes the master mesh data with the parametric mesh data and adapted the force vector orientation to conform to the first metacarpal orientation for each specimen-position combination.

To simulate the five grasping positions of the thumb, the models were optimized to bring the position after loading in close agreement with the scanned positions of the thumb. This was done using a Python-based function that optimizes the orientation of the force vector to yield a loaded terminating position that closely resembles the unloaded, scanned position of the MC1 by reducing the root mean square (RMS) error between these positions. As RMSE gives a relatively high weight to larger errors, it helps guide the optimiser towards the optimal position of the MC1. The proximo-distal difference between the loaded and unloaded state was accounted for in the final RMSE calculation by excluding the articular gap distance.

Distal trapezial articular surface Von Mises stresses were normalized and plotted for each individual model. The location of stress peaks and the overall stress distributions were compared to the expected patterns for each position.

Results

Out of 24 simulated models, 21 terminated successfully. Two grips of Pp2 (*powerL* and *powerS)*, and one grip of Pp5 (*powerLA)* were unable to successfully terminate using our method due to issues discussed below. Average RMS errors for the successfully terminated models were 1.364 mm for *pinch*, and below 0.7mm for the power grasp simulations (0.516 mm for *powerL*, 0.307 mm for *powerLA*, 0.514 mm for *powerLE*, and 0.667 mm for *powerS).*

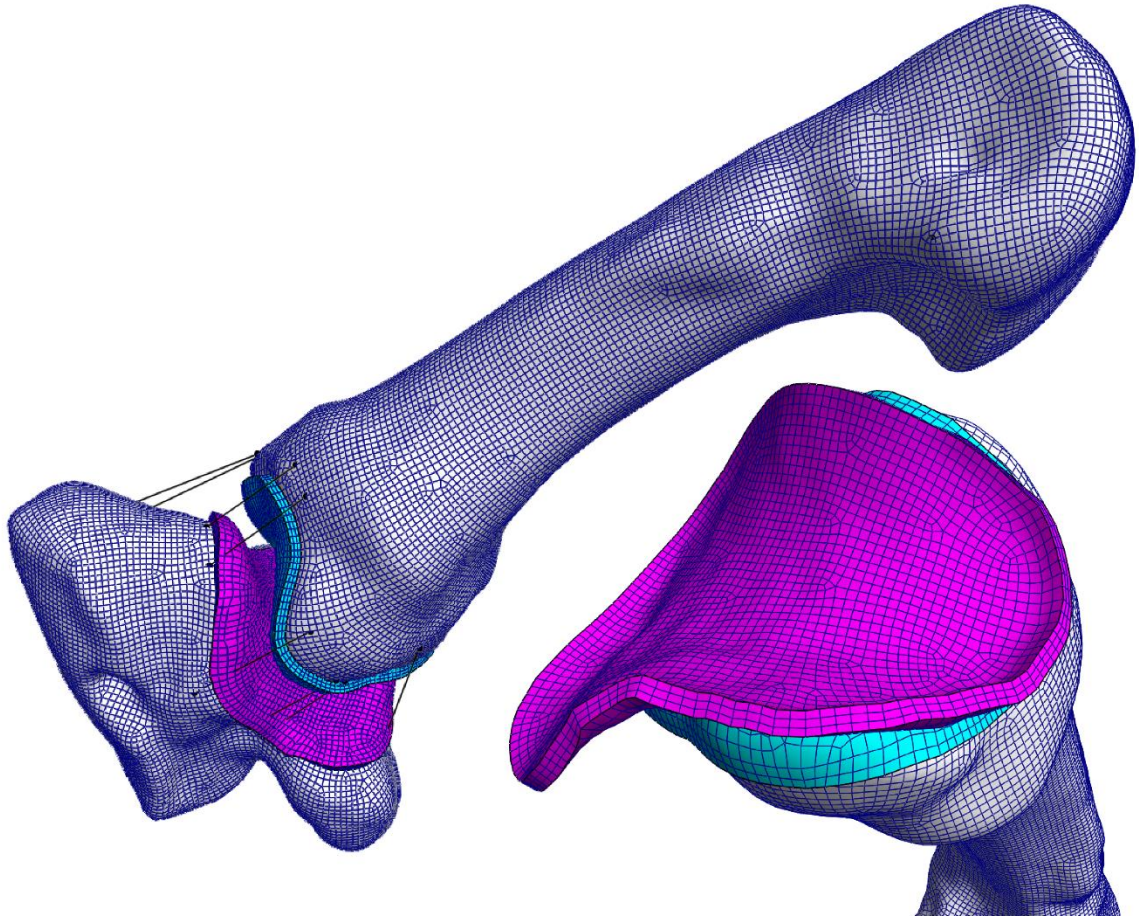

Fig 4: The TMC joint FE model in the large diameter power grasp with extended thumb (*powerLE*). The coloured surfaces represent the cartilage layers on the trapezium (pink) and MC1 (blue), black lines indicate non-linear springs and correspond to ligament positions. Shown here is the FE model based on the morphology of Pp4.

Individual stress distribution plots (**Fig. 5**) show indications of the expected stress patterns in 18 out of the 21 simulations. During *pinch*, stress peaks are located centrally and palmarly when compared to the other positions in the same individual, cases of palmar edge loading occur in 3/5 individuals. During *powerL*, radial stress distributions are present in two-thirds of the simulations. During *powerLA,* forces are directed to the ulnar side in the four successful simulations. The *powerLE* position displays high stress on the dorsal aspect of the articulation in all five simulations. During *powerS*, forces are diverted to the far radial side in one simulation, to the central-radial side in another simulation, and to a combination of both the central and far radial aspect of the articular surface in a third.

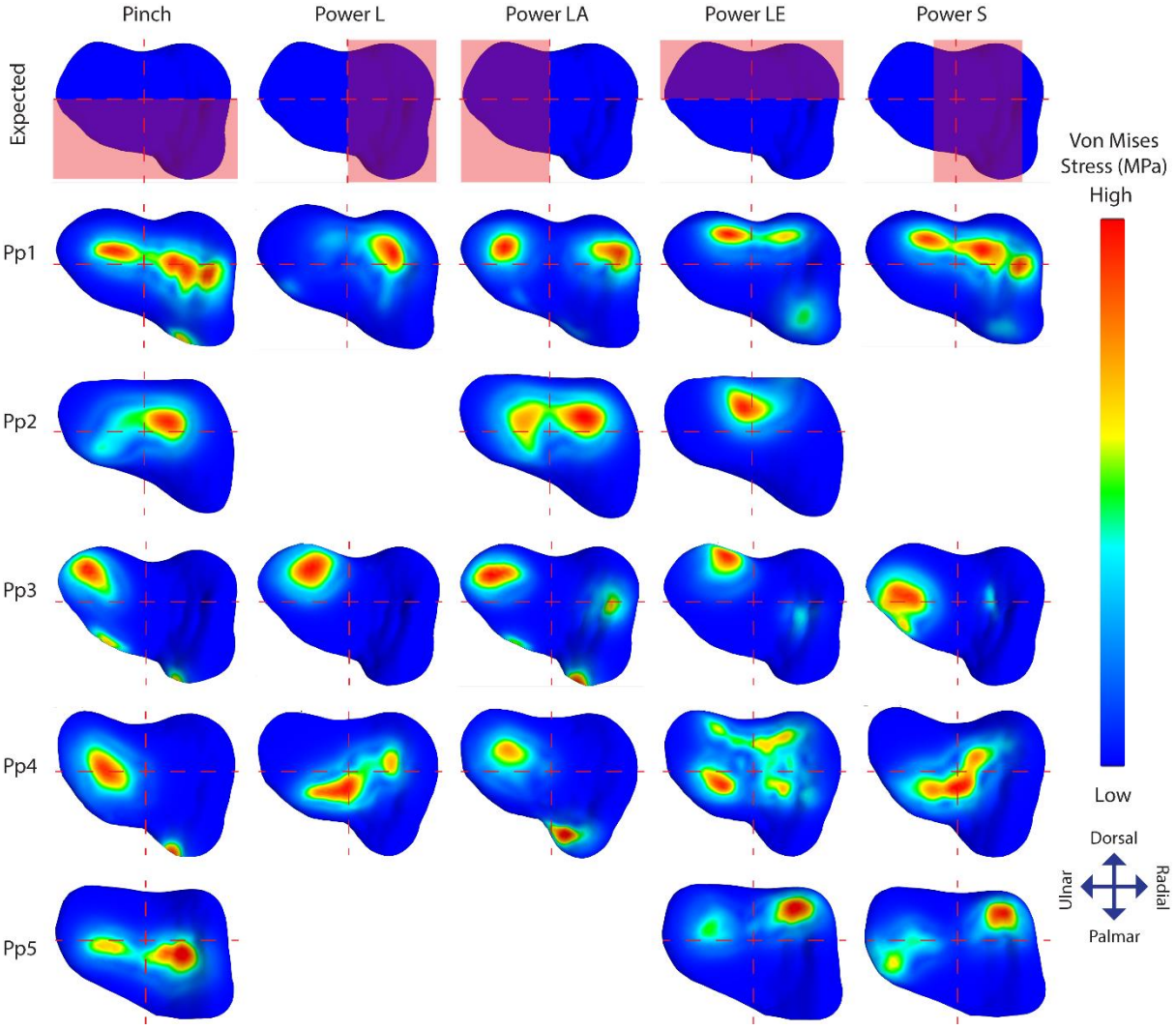

Figure 5: TMC joint Von Mises stress distributions plotted on a distal view of the isolated trapezium distal articular surfaces. The top row displays the quadrants where stress distribution is expected in red for each position. Empty slots represent unsuccessful scans or simulations.

Stress distributions diverging from the expected patterns are present in 14 simulations; 11 show divergent patterns in addition to the expected patterns, and three show divergent patterns only (**Fig. 5**). Pp1 shows divergent patterns on the ulnar aspect of the articular facet during *pinch* and *powerS*, as well as on the radial aspect during *powerLA*. Pp2 shows high stress peaks radio-centrally during all three successful positions; *pinch*, *powerLA*, and *powerLE*, but during *powerLE* it is part of the expected location. Pp3 shows divergent stress peaks on the dorso-ulnar aspect of the articular facet during *pinch, powerL,* and *powerS,* these peaks are also present during the other two positions, but in those cases they are part of the expected pattern. In addition, Pp3 shows divergent indications of contact on the radial side during *powerLA*. Pp4 shows stress peaks located ventrally on the articular surface in all five positions, although these are only expected during *pinch*. Stress distributions in Pp5 are directed ulnarly in all three of the successful simulations, but this is only unexpected during *powerS*.

Discussion

The purpose of this study was to simulate functional grasps commonly used by bonobos and to investigate how stress distributions within TMC joint vary between these activities. We applied a computational modelling approach using parametric meshes to compare stress distributions across five individuals using five grasping tasks. The magnitude of the resultant force vectors were set to 300N and the direction of the resultant force vectors were optimised in force-driven FE simulations for the 24 simulation cases. Of the 24 simulations, 21 simulations converged to an average RMSE of 0.673 mm ± 0.364 mm. We hypothesized that the simulated stress distributions for each position would correspond with the patterns expected from a saddle-shaped joint. However, we also expected there to be differences in stress patterns arising from individual variations in morphology.

Overall, the results appear to correspond with our predictions for each position, 21 of the 24 simulations showing stress distributions largely matching the expected distributions for a universal type joint. Out of these, there are 11 cases where additional patterns of stress distribution can be recognized, while the remaining three simulations show patterns fully diverging from the expected stress distributions. In summary, the results show that grip type influences the stress distributions in the expected manner, but variations in joint morphology interfere with this expected pattern. Most likely, morphological variations cause the joint to function less like a universal joint. A perfect

universal joint consists of a double hinge that allows for rotation in two planes only, while restricting axial rotation (Cooney and Chao, 1977). This strict functionality is by virtue of the shape of the joint and is lost when the morphology varies. In the current bonobo sample, such variations are prevalent and consequently, stress patterns appear to vary more between individuals than between grip types. A detailed interpretation of the individual differences is given below. Most of the deviations from the expected stress patterns can be explained by differences in joint morphology.

Our results give an indication of the influence of an individual's morphology on joint stress distribution (**Fig. 5**). The divergent patterns in Pp1 show high stress peaks on the dorsal aspect. Furthermore, there are indications of palmar contact during *powerLE* and *powerS*. When inspecting the TMC joint morphology of Pp1, these patterns coincide with the relatively protruding dorsal ridge and palmar beak of its MC1 (**Fig. 6a**), which come in contact with the dorsal and palmar parts of the articular surface of the trapezium upon loading. Pp2 shows stress peaks in the central-radial aspect of the articular surface in all three successful positions, while it was only expected in *powerLA*. This may be attributed to the dorsal ridge of its MC1 articular surface, which is more asymmetrical than in the other specimens. In Pp2, the most proximal point of the dorsal ridge is slightly offset to the radial side of facet. This causes contact with the trapezium, which symmetrical shape does not accommodate for the offset protrusion (**Fig. 6b**). During *pinch*, the asymmetrical dorsal ridge aspect may initiate contact before the palmar beak. Furthermore, Pp2 is a sub-adult with a TMC joint that is not fully mature, resulting in a smoother articular periphery and in particular less pronounced dorsal and palmar ridges. . This affects the shape of the TMC articular surfaces and appears to influence the interaction between the palmar beak and palmar aspect of the trapezium during *pinch* particularly, possibly causing it to not show the expected stress peaks in the palmar region during this grasp. Pp3 shows relatively high average stress peaks on the dorso-ulnar aspect of the articular facet in all positions. Upon visual assessment of this specimen it is clear that its joint morphology is relatively robust compared to the other specimens, i.e. the morphological features of the trapezium and MC1 are more strongly developed. The dorso-ulnar periphery of the trapezium's distal facet protrudes heavily (**Fig. 6c**), interacting with the MC1 in every modelled scenario. All positions collide heavily on the ulnar aspect of the facet, causing high stress in that area for each position. Two of the three divergent patterns (that do not also show an expected pattern) are Pp3's *powerL* and *powerS*, which are both power grips with the thumb abducted. These two grips show the same divergent stress patterns. It appears that in these cases, the MC1 loads the protruding dorso-ulnar aspect

of the trapezial facet's periphery instead of initiating contact on the radial side of the trapezial articular surface as expected for these grasps. This causes the protrusion to function as a 'bony stop', for which bone is not intended (Simpson, Latimer and Lovejoy, 2018). Such loading of the articular surface periphery may be the result of a self-perpetuating cycle where the high loads cause inflammation and pathological bone responses. Despite the absence of osteophytes, the protrusion may be an early sign of osteoarthritis (Wilson, McWalter and Johnston, 2008), although reports of hand osteoarthritis are rare in non-human primates. Also during *pinch*, high stresses are observed in the dorso-ulnar region, which can be explained by the protrusion on the articular periphery. Pp3's divergent stress patterns further show loading on the radial aspect of the trapezial articular facet during *powerLA*, *powerLE*, and *powerS*, as well as on the palmar edge during *powerLA*. This is likely due to the pronounced dorsal ridge and palmar beak on the MC1. The divergent stress patterns in Pp4 indicate loading on the palmar aspect of the articular facet. The trapezial morphology shows that the palmar aspect of the articular surfaces flattens out relatively fast towards the palmar aspect (**Fig. 6d**). At the bottom, the surface shows light indications of indenture, which may capture the palmar beak during loaded positions (**Fig. 6d**). Pp5 shows divergent stress patterns on the ulnar side of the trapezial facet. This appears to be caused by a protrusion of the trapezial facet's ulnar periphery, as seen in Pp3 (**Fig. 6c**). The protrusion, however, is not as explicit as in the case of Pp3, which may explain the lower stress peaks in Pp5.

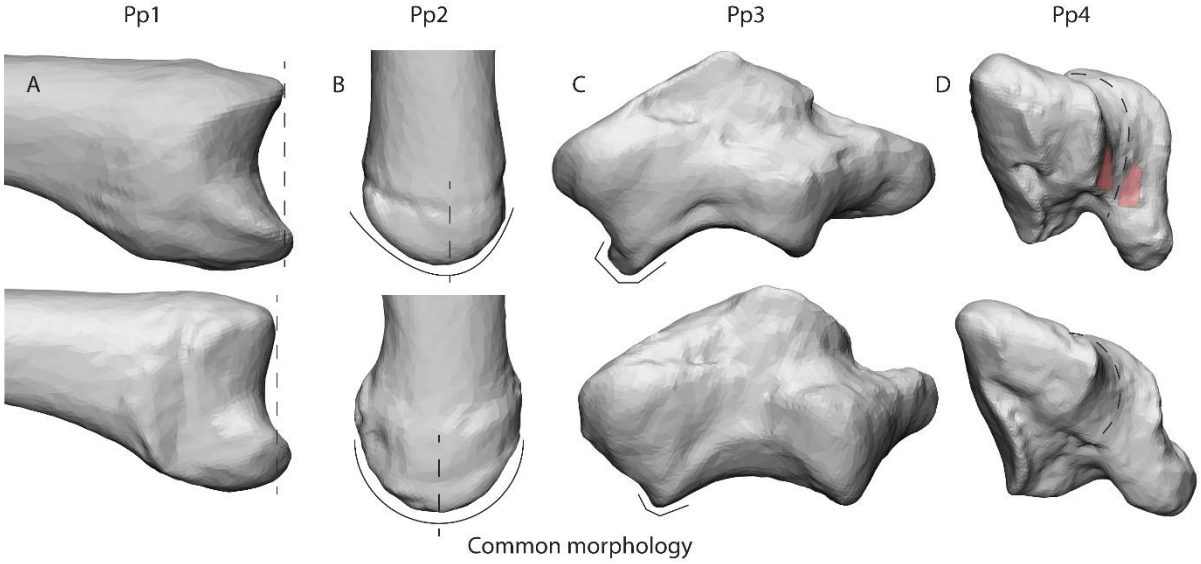

Figure 6: Deviating morphologies in specimens Pp1-4 in the top row in comparison to more common morphologies of the remaining specimens in the bottom row. **A**: Radial view of the protruding dorsal ridge and volar beak of Pp1's MC1 base. **B**: Dorsal view of the asymmetrical dorsal ridge of Pp2's MC1 base. **C**: Dorsal view of Pp3's protruding dorso-ulnar periphery of the trapezial articular facet. **D**: Disto-ulnar view of the Pp4's flattened palmar trapezial articular facet, as well as the palmar indentures highlighted in red.

The bonobo is a primate species underrepresented in literature. Due to its remote and scarce population (Prüfer *et al.*, 2012), academic focus on the bonobo has been limited in in comparison to its sister taxon; the chimpanzee (*Pan troglodytes*). Studies on the functional anatomy of the bonobo remain limited (Miller, 1952; Vereecke *et al.*, 2005; Payne *et al.*, 2006a; Payne *et al.*, 2006b; Myatt *et al.*, 2012; Diogo *et al.*, 2017), and most literature including *Pan* only make use of chimpanzees (Lewis, 1977; Rafferty, 1990; Rose, 1992; Marzke *et al.*, 2010). Claims have been made that due to evolutionary stasis, the bonobo may be the most suitable model for the *Pan – Homo* last common ancestor (Diogo, Molnar and Wood, 2017). Whether such a model exists in extant species is still debated, but it does indicate that the bonobo is a relevant piece of the evolutionary puzzle. Our previous research on the bonobo thumb revealed that their TMC joint is highly similar to that of humans, both in form and function (van Leeuwen *et al.*, 2018, 2019). These similarities are further supported in the current study as the intra articular stress patterns encountered correspond well similar grasps tested in humans (Schneider *et al.*, 2017). Chimpanzees also possess a similarly shaped TMC joint (Lewis, 1977; Rafferty, 1990; Marzke *et al.*, 2010), with a likely similar capacity for mobility (Rose, 1992), and so homologous joint loading patterns may be expected. However, caution should be taken when making such assumptions considering the behavioural differences between both species of *Pan* (Manson, Perry and Parish, 1997; Hare, Wobber and Wrangham, 2012). Bonobos are reportedly more arboreal (Doran, 1993), while chimpanzees appear to engage in tool use more often than bonobos (Neufuss *et al.*, 2017). Yet these differences in reported locomotor and tool use behaviour may also be a reflection of the offset in study frequency between these taxa and need to be studied in detail. It would certainly be interesting to apply our FEA approach to a broader set of primate taxa, including not only the closely related chimpanzee but also primates displaying variations on the saddle-shaped TMC joint (e.g. *Gorilla, Pongo, Papio, Macaca*), as well as those that display a completely different joint shape (e.g. *Hylobatidae*) (Rafferty, 1990). To that end, this study provides a suitable FEA method to investigate joint interactions and stress patterns within these morphologies for future work.

We have developed an innovative modelling workflow for the estimation of intra-articular stress distributions in a joint, and demonstrated its performance in the bonobo TMC joint. We want to stress that, rather than aiming to provide accurate estimations of stress distributions in the bonobo TMC joint, our aim was to compare stress distribution patterns between grip types and between individuals. To increase the accuracy of the model, detailed information on non-human primate tissue properties and dimensions is needed.

Since such information is still lacking, we make several assumptions when building our models. First of all, a simplified cartilage layer was included in our FE model as we were unable to obtain accurate cartilage dimensions for the studied specimens and had to rely on human-based studies. Furthermore, we modelled the cartilage layer as a layer with a constant thickness, while it has been shown that cartilage varies in thickness across the articular surface in the human TMC joint, be it only slightly (<10%) (Koff *et al.*, 2003; Dourthe *et al.*, 2019). In future modelling, we would recommend to include known dimensions of the cartilage layer as variations in cartilage thickness across the articular surface are likely to influence joint congruency and stress distributions. Inclusion of an accurate, non-uniform cartilage layer may affect the morphology of the TMC articular surfaces so that a more accurate representation of the stress distribution in the joint can be achieved. Our modelling approach has been designed with a modular cartilage layer to ensure that available information on TMC joint cartilage can be included in future studies. Secondly, the cartilage layer elastic properties were selected based on the previous human models (Schneider *et al.*, 2017), and tuned within the range of human literature to the current values (Young's modulus = 18 MPa, Poisson's ratio = 0.45) (Black and Hastings, 2013). This to increase the robusticity of the modelling, and to ensure a higher success ratio throughout the large amount of models tested in various positions of the MC1. We expect that our choice for the parameters minimally affects the results of the study, as we compare differences in the distribution of stress, as opposed to load magnitude, for which the exact properties have been shown to be less relevant (Gil Espert, Marcé Nogué and Sánchez, 2015).

While the sample size for this study was small due to inherent limitations in obtaining cadaver material from bonobos, a critically endangered species with a small captive population (Fruth *et al.*, 2016), our approach allowed us to perform an in depth analysis of form-function relation surpassing the level of detail of existing studies on non-human primates. We did, however, observe some sensitivity to joint model shape during certain wide grasps in our approach. Due to this sensitivity, not all models were able to terminate successfully and we had to eliminate three simulations during our analysis. Pp5's *powerLA* position was excluded due to severe cases of edge loading in the later stages of the simulation. Edge loading occurs as a result of the lofting approach used to simulate the TMC cartilage layer, where the edge of the cartilage is artificially high compared to the surrounding bone. This mainly presents an issue during simulations of extreme MC1 excursions where the only remaining contact with the trapezium is maintained directly onto this artificial cartilage edge. Such extreme loading on the edge cause the peripheral

elements of the mesh to collapse, and the simulation to fail. We furthermore had to exclude two grasp types of the sub-adult specimen Pp2. The relatively smooth morphology of the articulating bones presented difficulties in simulating grasps with an abducted thumb (*powerL* and *powerS)* and these positions could not be successfully terminated using our approach. Despite the low sample size, the open source finite element method presented here is widely applicable for the study of stress distributions in joints, regardless of species or joint system.

This study yields biomechanical insight in the bonobo thumb, moreover it provides subchondral stress distributions of the TMC joint which will be included in future research on joint morphology in bonobos. The exact locations and magnitudes of these forces will be applied to investigate if the orientation of the trabecular microarchitecture of the bonobo trapezium correlates with the stress distributions estimated here. This to investigate how the bonobo thumb morphology is adapted to different types of manual activities and for interpretations of hand use in the fossil record.

Conclusions

The present study applies a parametric finite element approach to simulate stress distributions in the TMC joint of bonobos with the aim of investigating how stress distribution differs during five grasps commonly employed in captive populations. We find that the simulated stress patterns correspond well with the expected patterns during the modelled grasps, and the divergent signals can be attributed to the individual joint morphology. We conclude that inter-individual variation in joint morphology has a strong influence on articular stress distributions and should always be considered when modelling joint interactions. The results demonstrate that this modelling workflow is suitable to estimate TMC joint stress distributions and can be a valuable tool for the study of primate joint biomechanics in future work.

Acknowledgements

The authors are indebted to Jeroen Stevens for his initiative taken in the collection of bonobo specimens and his courtesy in collaborating with our lab to make this study possible. We are thankful to Maarten Vanneste, Ted Yeung, Nynke Rooks, and Mousa Kazemi for their expertise and input on modelling and programming. We extend our gratitude to Olivier Vanovermeire and Henk Lacaeyse at the Medical Imaging Department, AZ Groeninge (Kortrijk, Belgium) for providing us with the means and assistance for the imaging protocol. Furthermore, we thank Marie Vanhoof and Kristiaan D'Aout for their courtesy in supplying us with primate images. The authors thank Johanna Neufuss, Tracy Kivell, and one anonymous reviewer for their valuable input which greatly helped with the improvement of this manuscript.

References

Bardo, A. *et al.* (2016) 'Behavioral and functional strategies during tool use tasks in bonobos', *American Journal of Physical Anthropology*, 161(1), pp. 125–140. doi: 10.1002/ajpa.23015.

Black, J. and Hastings, G. (2013) *Handbook of biomaterial properties*. Springer Science & Business Media.

Burkhart, T. A., Andrews, D. M. and Dunning, C. E. (2013) 'Finite element modeling mesh quality, energy balance and validation methods: A review with recommendations associated with the modeling of bone tissue', *Journal of Biomechanics*, 46(9), pp. 1477–1488. doi: 10.1016/j.jbiomech.2013.03.022.

Christel, M. (1993) 'Grasping techniques and hand preferences in Hominoidea', in Preuschoft, H. and Chivers, D. J. (eds) *Hands of Primates*. Vienna: Springer Vienna, pp. 91–108. doi: 10.1007/978-3-7091-6914-8_7.

Christel, M. I., Kitzel, S. and Niemitz, C. (1998) 'How precisely do bonobos (Pan paniscus) grasp small objects?', *International Journal of Primatology*, 19(1), pp. 165–193. doi: 10.1023/A:1020319313219.

Cignoni, P. *et al.* (2008) 'MeshLab: an Open-Source Mesh Processing Tool', in *Eurographics Italian Chapter Conference*, pp. 129–136.

Cooney, W. P. and Chao, E. Y. (1977) 'Biomechanical analysis of static forces in the thumb during hand function.', *The Journal of bone and joint surgery. American volume*, 59(1), pp. 27–36.

Crast, J. *et al.* (2009) 'Dynamic in-hand movements in adult and young juvenile chimpanzees (Pan troglodytes)', *American Journal of Physical Anthropology*. Wiley-Blackwell, 138(3), pp. 274–285. doi: 10.1002/ajpa.20925.

Crisco, J. J. *et al.* (2015) 'In vivo kinematics of the trapeziometacarpal joint during thumb extension-flexion and abduction-adduction', *Journal of Hand Surgery*. Elsevier Inc, 40(2), pp. 289–296. doi: 10.1016/j.jhsa.2014.10.062.

D'Agostino, P. *et al.* (2017) 'In vivo kinematics of the thumb during flexion and adduction motion: Evidence for a screw-home mechanism', *Journal of Orthopaedic Research*, 35(7), pp. 1556–1564. doi: 10.1002/jor.23421.

Diogo, R. *et al.* (2017) *Photographic and Descriptive Musculoskeletal Atlas of Bonobos*. 1st edn. Springer International Publishing. doi: 10.1007/978-3-319-54106-8.

Diogo, R., Molnar, J. L. and Wood, B. (2017) 'Bonobo anatomy reveals stasis and mosaicism in chimpanzee evolution, and supports bonobos as the most appropriate extant model for the common ancestor of chimpanzees and humans', *Scientific Reports*. Springer US, 7(1), pp. 1–8. doi: 10.1038/s41598-017-00548-3.

Doran, D. M. (1993) 'Comparative locomotor behavior of chimpanzees and bonobos: The influence of morphology on locomotion', *American Journal of Physical Anthropology*, 91(1), pp. 83–98. doi: 10.1002/ajpa.1330910106.

Dourthe, B. *et al.* (2016) 'In vivo contact biomechanics in the trapeziometacarpal joint using finite deformation biphasic theory and mathematical modelling', *Medical Engineering &*

Physics, 38(2), pp. 108–114. doi: 10.1016/j.medengphy.2015.11.003.

Dourthe, B. *et al.* (2018) 'Assessment of healthy trapeziometacarpal cartilage properties using indentation testing and contrast-enhanced computed tomography', *Clinical Biomechancics*, Manuscript.

Dourthe, B. *et al.* (2019) 'Assessment of healthy trapeziometacarpal cartilage properties using indentation testing and contrast-enhanced computed tomography', *Clinical Biomechanics*, 61, pp. 181–189. doi: 10.1016/j.clinbiomech.2018.12.015.

Feix, T. *et al.* (2015) 'Estimating thumb-index finger precision grip and manipulation potential in extant and fossil primates', *Journal of The Royal Society Interface*, 12(106), pp. 20150176–20150176. doi: 10.1098/rsif.2015.0176.

Fruth, B. *et al.* (2016) 'Pan paniscus', *The IUCN Red List of Threatened Species 2016*. doi: 10.2305.

Gil Espert, L., Marcé Nogué, J. and Sánchez, M. (2015) 'Insights into the controversy over materials data for the comparison of biomechanical performance in vertebrate', *Palaeontologia Electronica*. doi: 10.26879/509.

Haines, R. W. (1944) 'The mechanism of rotation at the first carpo-metacarpal joint.', *Journal of anatomy*, 78(Pt 1-2), pp. 44–6.

Halilaj, E. *et al.* (2013) 'A thumb carpometacarpal joint coordinate system based on articular surface geometry', *Journal of Biomechanics*, 46(5), pp. 1031–1034. doi: 10.1016/j.jbiomech.2012.12.002.

Hare, B., Wobber, V. and Wrangham, R. (2012) 'The self-domestication hypothesis: evolution of bonobo psychology is due to selection against aggression', *Animal Behaviour*, 83(3), pp. 573–585. doi: 10.1016/j.anbehav.2011.12.007.

Ingmanson, E. J. (1998) 'Tool-using behaviour in wild Pan paniscus: Social and ecological considerations', in Russon, A. E., Bard, K. A., and Parker, S. T. (eds) *Reaching Into Thought: The Minds of the Great Apes*. Cambridge University Press, p. 464.

Inouye, S. E. (1992) 'Ontogeny and allometry of African ape manual rays', *Journal of Human Evolution*, 23(2), pp. 107–138. doi: 10.1016/0047-2484(92)90103-G.

Jakob, W. *et al.* (2015) 'Instant field-aligned meshes', *ACM Transactions on Graphics*, 34(6), pp. 1–15. doi: 10.1145/2816795.2818078.

Jordan, C. (1982) 'Object manipulation and tool-use in captive pygmy chimpanzees (Pan paniscus)', *Journal of Human Evolution*, 11(1), pp. 35–39. doi: 10.1016/S0047-2484(82)80029-8.

Kerkhof, F. D. *et al.* (2018) 'Trapeziometacarpal stabilization through dorsoradial ligament reconstruction: An early post-surgery in vivo biomechanical analyses', *Journal of Orthopaedic Research*®, Manuscript. doi: 10.1002/jor.24103.

Koff, M. F. *et al.* (2003) 'Sequential wear patterns of the articular cartilage of the thumb carpometacarpal joint in osteoarthritis', *The Journal of Hand Surgery*, 28(4), pp. 597–604. doi: 10.1016/S0363-5023(03)00145-X.

Kuczynski, K. (1974) 'Carpometacarpal joint of the human thumb.', *Journal of anatomy*, 118(Pt 1), pp. 119–26.

Ladd, A. L. *et al.* (2013) 'The thumb carpometacarpal joint: anatomy, hormones, and biomechanics.', *Instructional course lectures*, 62, pp. 165–79.

Ladd, A. L. *et al.* (2014) 'The 2014 ABJS Nicolas Andry Award: The Puzzle of the Thumb: Mobility, Stability, and Demands in Opposition', *Clinical Orthopaedics and Related Research®*, 472(12), pp. 3605–3622. doi: 10.1007/s11999-014-3901-6.

van Leeuwen, T. *et al.* (2018) 'Insights into the musculature of the bonobo hand', *Journal of Anatomy*, 233(3), pp. 328–340. doi: 10.1111/joa.12841.

van Leeuwen, T. *et al.* (2019) 'Mobility and structural constraints of the bonobo trapeziometacarpal joint', *Biological Journal of the Linnean Society*, 127(3), pp. 681–693. doi: 10.1093/biolinnean/bly162.

Lewis, O. J. (1977) 'Joint remodelling and the evolution of the human hand.', *Journal of Anatomy*, 123(Pt 1), pp. 157–201.

Maas, S. A. *et al.* (2012) 'FEBio: Finite Elements for Biomechanics', *Journal of Biomechanical Engineering*, 134(1), p. 011005. doi: 10.1115/1.4005694.

Manson, J. H., Perry, S. and Parish, A. R. (1997) 'Nonconceptive Sexual Behavior in Bonobos and Capuchins', *International Journal of Primatology*, 18(5), pp. 767–786. doi: 10.1023/A:1026395829818.

Marzke, M. W. (1997) 'Precision grips, hand morphology, and tools', *American Journal of Physical Anthropology*, 102(1), pp. 91–110. doi: 10.1002/(SICI)1096-8644(199701)102:1<91::AID-AJPA8>3.0.CO;2-G.

Marzke, M. W. *et al.* (2010) 'Comparative 3D quantitative analyses of trapeziometacarpal joint surface curvatures among living catarrhines and fossil hominins.', *American journal of physical anthropology*. United States, 141(1), pp. 38–51. doi: 10.1002/ajpa.21112.

Miller, R. A. (1952) 'The musculature of pan paniscus', *American Journal of Anatomy*, 91(2), pp. 183–232. doi: 10.1002/aja.1000910202.

Myatt, J. P. *et al.* (2012) 'Functional adaptations in the forelimb muscles of non-human great apes', *Journal of Anatomy*, 220(1), pp. 13–28. doi: 10.1111/j.1469-7580.2011.01443.x.

Napier, J. R. (1955) 'The form and function of the carpo-metacarpal joint of the thumb.', *Journal of anatomy*, 89(3), pp. 362–9.

Napier, J. R. (1956) 'The Prehensile Movements of the Human Hand', *The Journal of Bone and Joint Surgery. British volume*, 38-B(4), pp. 902–913. doi: 10.1302/0301-620X.38B4.902.

Napier, J. R. (1960) 'Studies of the hands of living primates', *Proceedings of the Zoological Society of London*, 134, pp. 647–657.

Napier, J. R. and Napier, P. H. (1967) *A Handbook of Living Primates: Morphology, Ecology and Behaviour of Nonhuman Primates*. Academic P.

Neufuss, J. *et al.* (2017) 'Nut-cracking behaviour in wild-born, rehabilitated bonobos (Pan paniscus): a comprehensive study of hand-preference, hand grips and efficiency', *American*

Journal of Primatology, 79(2), pp. 1–16. doi: 10.1002/ajp.22589.

Parker, S. T. and Gibson, K. R. (1977) 'Object manipulation, tool use and sensorimotor intelligence as feeding adaptations in cebus monkeys and great apes', *Journal of Human Evolution*, 6(7), pp. 623–641. doi: 10.1016/S0047-2484(77)80135-8.

Payne, R. C., Crompton, R. H., Isler, K., Savage, R., Vereecke, E. E., Günther, M. M., *et al.* (2006) 'Morphological analysis of the hindlimb in apes and humans. I. Muscle architecture', *Journal of Anatomy*, 208(6), pp. 709–724. doi: 10.1111/j.1469-7580.2005.00433.x-i1.

Payne, R. C., Crompton, R. H., Isler, K., Savage, R., Vereecke, E. E., G??nther, M. M., *et al.* (2006) 'Morphological analysis of the hindlimb in apes and humans. II. Moment arms', *Journal of Anatomy*, 208(6), pp. 725–742. doi: 10.1111/j.1469-7580.2006.00564.x.

Prüfer, K. *et al.* (2012) 'The bonobo genome compared with the chimpanzee and human genomes', *Nature*, 486(7404), pp. 527–531. doi: 10.1038/nature11128.

Rafferty, K. L. (1990) *The Functional and Phylogenetic Significance of the Carpometacarpal Joint of the Thumb in Anthropoid Primates*. New York University.

Rose, M. D. (1992) 'Kinematics of the trapezium-1st metacarpal joint in extant anthropoids and Miocene hominoids', *Journal of Human Evolution*, 22(4–5), pp. 255–266. doi: 10.1016/0047-2484(92)90058-H.

Samuel, D. S. *et al.* (2018) 'Hand pressures during arboreal locomotion in captive bonobos (Pan paniscus)', *The Journal of Experimental Biology*, 221(8), p. jeb170910. doi: 10.1242/jeb.170910.

Schneider, M. T. Y. *et al.* (2015) 'Men and women have similarly shaped carpometacarpal joint bones', *Journal of Biomechanics*, 48(12), pp. 3420–3426. doi: 10.1016/j.jbiomech.2015.05.031.

Schneider, M. T. Y. *et al.* (2017) 'Trapeziometacarpal joint contact varies between men and women during three isometric functional tasks', *Medical Engineering & Physics*, 50, pp. 43–49. doi: 10.1016/j.medengphy.2017.09.002.

Simpson, S. W., Latimer, B. and Lovejoy, C. O. (2018) 'Why Do Knuckle-Walking African Apes Knuckle-Walk?', *The Anatomical Record*. Wiley-Blackwell, 301(3), pp. 496–514. doi: 10.1002/ar.23743.

Susman, R. L. (1998) 'Hand function and tool behavior in early hominids', *Journal of Human Evolution*, 35(1), pp. 23–46.

Tuttle, R. H. (1967) 'Knuckle-walking and the evolution of hominoid hands', *American Journal of Physical Anthropology*, 26(2), pp. 171–206. doi: 10.1002/ajpa.1330260207.

Vereecke, E. E. *et al.* (2005) 'Functional analysis of the foot and ankle myology of gibbons and bonobos.', *Journal of anatomy*, 206(5), pp. 453–76. doi: 10.1111/j.1469-7580.2005.00412.x.

Wilson, D. R., McWalter, E. J. and Johnston, J. D. (2008) 'The Measurement of Joint Mechanics and their Role in Osteoarthritis Genesis and Progression', *Rheumatic Disease Clinics of North America*, 34(3), pp. 605–622. doi: 10.1016/j.rdc.2008.05.002.

Wunderlich, R. E. and Jungers, W. L. (2009) 'Manual digital pressures during knuckle-walking

in chimpanzees (Pan troglodytes)', *American Journal of Physical Anthropology*, 139(3), pp. 394–403. doi: 10.1002/ajpa.20994.

Chapter 5.

The effect of different grasping types on the strain distributions in the trapezium in bonobos (*Pan paniscus*)

Timo van Leeuwen[1,3], Marco T.Y. Schneider[2], G. Harry van Lenthe[3], Evie E. Vereecke[1],

[1]Department of Development and Regeneration, University of Leuven Campus Kortrijk, Kortrijk, Belgium

[2]Auckland Bioengineering Institute, The University of Auckland, Auckland, New Zealand

[3]Department of Mechanical Engineering, University of Leuven, Leuven, Belgium

Submitted for publication in *Journal of Biomechanics* as:

van Leeuwen, T., Schneider, M.T.Y, van Lenthe, G.H., and Vereecke, E. E., 2021, *The effect of different grasping types on the strain distributions in the trapezium in bonobos (Pan paniscus).* Journal of Biomechanics, In review.

Abstract

The thumb has played a key role in primate evolution due to its involvement in grasping and manipulation. A large component of this wide functionality is by virtue of the uniquely shaped trapeziometacarpal (TMC) joint. This basal thumb joint allows for a broad range of functional positions, but how the bone structure is adapted to withstand the variety of loading regimes associated with a multitude of grasps is poorly understood. In this study, we investigate the bone functional adaptation of trapezium in five bonobo specimens (*Pan paniscus*), one of modern humans closest living relatives. We have developed a novel, integrated finite element-micro finite element (FE-μFE) workflow for the analysis of strain distributions across the internal bone architecture of the trapezium. We evaluate the strain distribution of five loading regimes, calculated from grasping positions used by bonobos in the wild, and furthermore assess how the joint forces are transferred through the bone microstructure. Our results show the absence of strain peaks associated with bone failure, moreover, we report that the strain distributions between the simulated grasps are highly similar, and mainly load the same proximoulnar cluster of trabeculae regardless of trapezial morphology. This study presents an innovative FE-μFE approach to simulating joint strain distributions, and yields insight in the functional adaptation of the TMC joint in bonobos.

Introduction

Where humans use their hands almost exclusively for manipulation, other primate species also employ their hands in many types of locomotor modes in addition to manipulation (Napier and Napier, 1967; Doran, 1993; Larson, 2018). This broader functionality of the hand in nonhuman primates results in a broad range of loading regimes. As the thumb plays a key role in hand function, it is also subjected to a large variability in loading, but how its morphology is geared towards withstanding the different stresses involved in varying loading scenarios is poorly understood.

It is expected that bone adapts in response to habitual loading regimes. According to Wolff's Law, currently referred to as bone functional adaptation (Kivell, 2016), bone is a dynamic tissue and habitual loading regimes are expected to reshape and reorganize the internal bony architecture. Bone deposition or resorption occurs in response to the presence or absence of mechanical stimuli (Cowin, 2003; Ruff, Holt and Trinkaus, 2006; Currey, 2012; Schulte *et al.*, 2013; Christen *et al.*, 2014), optimizing the micro-architecture to withstand frequently experienced loading patterns. This adaptive response to habitual loading is used to infer manipulative behaviour in our hominin ancestors (Tsegai *et al.*, 2013; Kivell, 2016; Dunmore *et al.*, 2019; Synek, Dunmore, *et al.*, 2019). However, how joint loading is transferred through the internal bony architecture under different loading regimes remains poorly studied. We want to address this knowledge gap by investigating the strain distribution in the trapezium under different loading conditions of the thumb.

Here, we focus on bonobos (*Pan paniscus*) who are closely related to humans and are characterized by a human-like basal thumb joint or trapeziometacarpal (TMC) joint. Bonobos have a high dexterity and are capable of a large repertoire of grasps and pinches (Christel, 1993; Christel, Kitzel and Niemitz, 1998; Neufuss *et al.*, 2017). Bonobos are knuckle-walkers, during which the thumb remains unloaded, but they also regularly engage in vertical climbing and clambering, during which the thumb is used for grasping (Doran, 1993; D'Aout *et al.*, 2004; Samuel *et al.*, 2018).

Both in bonobos and modern humans, the TMC joint is a reciprocal, saddle-shaped articulation between the trapezium and first metacarpal (MC1) that, theoretically, allows for flexion-extension and palmar abduction-adduction only (Cooney and Chao, 1977). However, the human TMC joint does allow for internal rotation of the MC1 which has been shown to be an important component of thumb opposition (Napier, 1955, 1956; Cooney *et al.*, 1981; Marzke, 1997; Odgers and Rayan, 2018). In the previous chapter (**Chapter 4**), we simulated five positions of the thumb corresponding to grasp types used by bonobos.

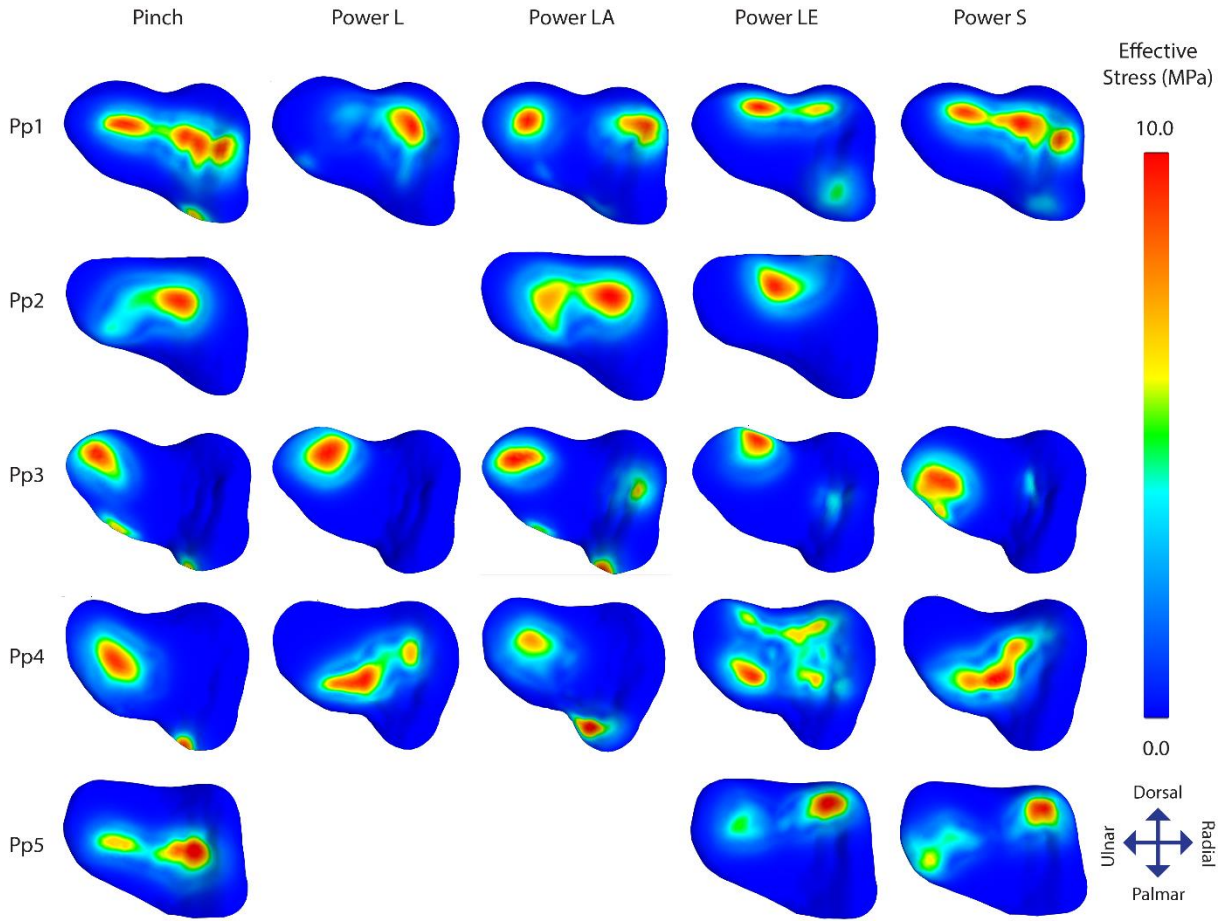

Figure 1: Trapezium distal articular surface subchondral loading regimes for each specimen and position of the thumb (van Leeuwen *et al.*, 2021). These regimes are applied as boundary conditions to the trapezium bone volume mesh to generate three to five µFE models per specimen. The specimen/grasp combinations not represented are unsuccessful simulations related to either technical or anatomical restrictions for which we refer to the original article.

Using a finite-element (FE) approach, we found that the articular surface of the trapezium was loaded differently across grasping types (**Figure 1**). In the present study, we use these pressure patterns to investigate how strain is transmitted across the microstructure of the trapezium during these grasps. More specifically, we evaluate if the bonobo TMC joint is well adapted to execute each of the tested grasping positions. As these grasping positions correspond to grasps that are used during daily activities of captive and wild bonobos (Christel, 1993; Christel, Kitzel and Niemitz, 1998; Neufuss et al., 2017), we expect that the bonobo TMC joint will be well adapted to the applied loading regimes. Bone functional adaptation occurs in response to habitual loading, so the loading process needs to be repeatable without compromising the bone. As such the indicator for bone failure in this context is the amount of deformation that may occur before the bone material properties are affected in an irreversible manner. This occurs at the yield strain (ε_{yield}) value of bone;

so the condition for failure is $\varepsilon \geq \varepsilon_{yield}$. We hypothesize (H1) that the strain distribution in the trapezium will be substantially smaller than bone yield strain (ε_{yield}) in each of the simulated grasps. Furthermore, we expect that strain distributions between grasps will be different, while the trapezium morphology is expected to be equally adapted to each pattern. We therefore test if (H2.1) the strain distribution patterns differ between grasps, and if (H2.2) mean strain values are similar between each grasp.

Methodology

We used an integrated finite element (FE) and micro-FE (μFE) approach to apply functionally representative loads to the trapezial trabecular architecture during five different grasps. Micro-FE models are often characterised by simplified or arbitrary boundary conditions. Here, we implement a method that integrates morphologically-relevant boundary conditions to more accurately simulate the stress and strain distribution within the bone.

Specimen information and scan protocol

Trapezia of five bonobo specimens, that were obtained in the context of previous studies (**Table 1**), were scanned using μCT (SkyScan 1272, Bruker, Kontich, Belgium) at a voxel size of 20.0 μm. The individual trapezia were extracted from the carpal complex and stored at -18°C until scanning was performed. The data were reconstructed using NRecon software (Bruker). The reconstructed images were preprocessed in CTAn (Bruker) using the Thresholding and Despeckle functions. No animals were sacrificed for these studies, but were collected opportunistically via collaboration with European zoos. All specimens were part of studies on bonobo thumb morphology and biomechanics (van Leeuwen *et al.*, 2018, 2019).

Table 1: Bonobo specimen information, SB: studbook number, M: male, F: female; R: right, L: left.

Code	Subject ID	Age	Sex	Sample	Origin	Zoo
Pp1	8365526	35	M	L	Wild born	Wilhelma Zoo, Stuttgart, Germany
Pp2	15295295 SB: 295	8	F	L	Captive born	Royal Zoological Society Antwerp, Belgium
Pp3	MIG12-29882197 SB: 126	32	M	R	Captive born	Zoo Frankfurt, Germany
Pp4	SB:177 CITES:79209	24	M	R	Captive born	La Vallée des Singes, Le Gureau, France
Pp5	SB: 88 27641621	39	F	L	Wild born	Wilhelma Zoo, Stuttgart, Germany

FE model integration

The subchondral pressure distribution on the trapezium was calculated in a previous study (van Leeuwen *et al.*, 2021) and was integrated in the µFE workflow. In short, the cadaveric bonobo hands were CT scanned in five positions of the thumb used by bonobos during locomotion and manipulation. The positions include three types of large diameter power grasps, (i.e thumb abducted (*power L*), thumb adducted (*power LA*), and thumb extended (*power LE*)), a small diameter power grasp (*power S*), and a key pinch precision grip (*pinch*). Stress distributions were modelled with an estimated applied force of 300N (Cooney and Chao, 1977) and solved using FEBio Software Suite (Maas *et al.*, 2012). To allow for intuitive interpretation of the data, the FE model has been designed with the trapezium in a TMC joint coordinate system. Here the [x, y, z] planes are aligned with the principal operations of the trapezium; thumb flexion-extension, abduction-adduction, and axial rotation. For this, a method based on Halilaj et al. was used (Halilaj *et al.*, 2013; van Leeuwen *et al.*, 2019). Trapezial subchondral nodal positions and reaction forces were extracted from the FEBio solution using custom Python scripts (**Fig. 1**).

Model generation

The trapezium µFE models were generated using a series of custom Python scripts that import the µCT image and re-orient it to align with the intuitive, trapezium-based coordinate system. For each specimen, we fitted the µCT image to the morphology of the FE model and associated the subchondral nodal reaction forces with the subchondral nodes of the µCT image. This was done for each loading regime, generating three to five µFE models per specimen.

In Python, the 3D µCT image is imported at a 20.0 µm voxel resolution. A copy is downsampled using a mean-based block reduction function to match the FE model morphology resolution of 0.625 mm (**Fig. 2A**). A surface mesh is generated from the downsampled point cloud using a Lewiner marching cubes algorithm module (Lewiner *et al.*, 2003) (**Fig. 2B**). This surface mesh is fitted onto the FE model using rigid body fitting (GIAS2 module (Zhang, 2020)) to obtain the transformation matrix between the two morphologies (**Fig. 2C**). The µCT image is rotated using the transformation matrix and reconstructed in the TMC-based coordinate system using inverse rotation (Heurtebiese and Thon, 2006) (**Fig. 2D**). The rotated mesh is again downsampled to 0.625 mm resolution point cloud (**Fig. 2E**) to allow for a K-dimensional (K-D) tree closest point analysis (**Fig. 2F**). This associates the FE model subchondral node reaction forces with the corresponding subchondral morphology on the downsampled point cloud (Bentley, 1975; Hou *et al.*, 2018). In parallel, a custom image processing script based on OpenCV modules (Bradski and Kaehler, 2000) was used on the rotated high resolution image to generate an image outline that extracts the cortical bone (**Fig. 2G**). The associated subchondral nodal information is then 3D interpolated to 20.0 µm resolution by expanding each individual point into a 3D point cube with a step size of 20.0 µm. The applied force for the individual node is divided over the amount of points in the cube that correspond to bone applied to the subchondral cortical bone of the rotated image by using the cortical bone image outline as a mask. The same process is used to apply restrictive boundary conditions. The nodal information of the proximal articulations of the trapezium were included in the FE model output, boundary nodes were identified and their the x, y and z components were set to zero using a separately generated, boundary K-D tree closest point analysis (**Fig. 2F**). All detailed morphology operations are executed using custom Python scripts unless the relevant Python module is indicated.

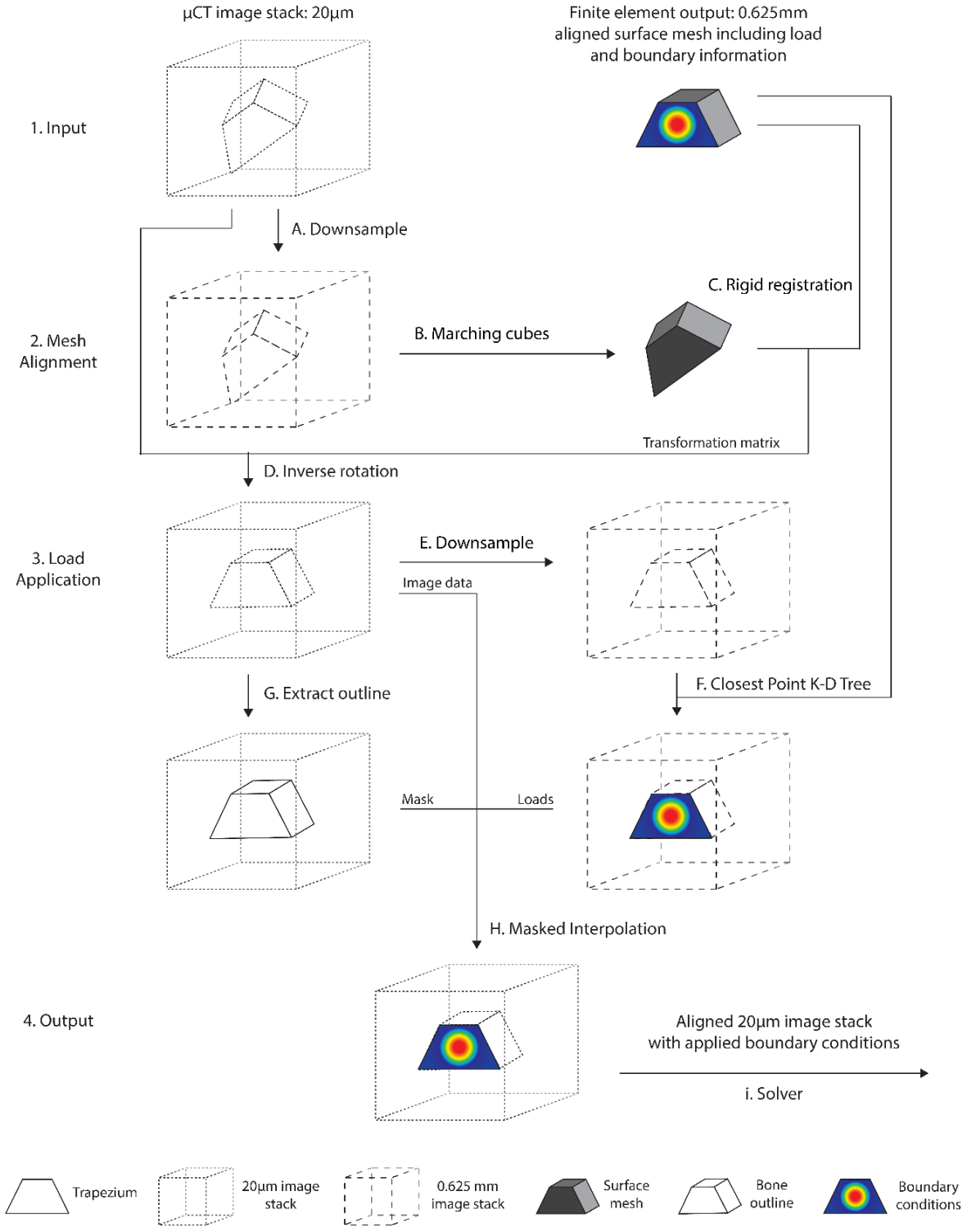

Figure 2: Illustration of the µFE model generation. See *model generation* for workflow description.

The rotated image and boundary conditions were exported in a HDF5 format, and solved using ParOSol (Flaig and Arbenz, 2011) on the supercomputer Piz Daint at the Swiss National Supercomputing Centre (CSCS). (**Fig. 2i**). By modelling the internal trabecular architecture the anisotropic nature of the trabecular bone is taken into account (van Lenthe and Müller, 2006). The individual elements were modelled as a homogenous, isotropic material with constant Young's moduli and Poisson's ratios (Ladd *et al.*, 1998; Kabel *et al.*, 1999). Individual bone properties were based on material properties in human bone; the Poisson's ratio was set at 0.3 (Wirtz *et al.*, 2000), and the Young's moduli of the individual elements of trabecular bone were assumed to be similar to that of human cortical bone and set to 18 GPa (Rho, Ashman and Turner, 1993). The 3D location of the one element and their corresponding effective stresses (Von Mises stress) were extracted from the solution, and the distributions were analysed per amount of bone volume. Effective strain was calculated from the Von Mises stress per element using the Young's modulus. The mean and peak strain values were extracted per grasp. As peak strain values are affected by the voxelized nature of the mesh, the top percentile of the peak strain value was excluded and determination of the peak strain value was based on the 99% value instead (Tomaszewski *et al.*, 2010). We report the 99-percentile peak strain values in **Table 2**. We addressed (H1) by assessing if peak strain values induced bone failure. As repeated loading of the structure is required in order for the bone to function during habitual loading, we use yield strain (ε_{yield}) as an indicator for bone failure. As such failure was assumed to occur at $\varepsilon \geq \varepsilon_{yield}$.

We visualize the localisations of strain by associating the bone element data with the corresponding nodal data and heatmapping the strain per element (**Fig. 3**). We assessed strain distribution patterns (H2.1) using image stack heatmap visualisations. Furthermore, we provide statistical context by testing for strain differences between grasps. We use a single factor ANOVA (R, $\alpha = 0.05$) to test if the mean strain values are similar between grasps (H2.2) (R Core Team, 2017).

Results

The data show that the mean strain values for the five grasp types, across all five specimens, are well below the strain values associated with bone failure. The average mean strain across all simulations amounted to 62.11 με ± 18.05 με. The highest strain value encountered was 578.36 με, which is reported for specimen Pp3 during the *pinch* position. The average peak strain over all simulations was 333.72 με ± 128.77 με. **Table 2** reports the individual mean and maximal strain values for each position, as well as averages over grasps and specimens. ANOVA-based comparisons show that mean strain distributions between grasps are not statistically different ($F(4,16) = 0.43$, $p = 0.78$). Figure 3 shows the strain distribution in one slice of the dorsopalmar plane of the trapezium for each of the simulated positions. Strain distributions image stacks in GIF format are to be published as e-supplementary (**S1**) material of the submitted work.

Table 2: Mean effective strain (M) values with standard deviation and peak strain (Max) at the 99th percentile per simulation, and average values per grasp and per specimen. Strain values are reported in με.

Bonobo		**Pinch**	**PowerL**	**PowerLA**	**PowerLE**	**PowerS**	**Mean ± SD**
Pp1	M	72.07 ± 74.92	61.21 ± 78.91	70.88 ± 60.74	55.78 ± 50.62	85.17 ± 76.49	69.02 ± 68.34
	Max	419.17	448.15	341.85	277.15	425.77	382.42 ± 71.20
Pp2	M	47.72 ± 46.66		45.52 ± 44.59	57.05 ± 60.11		50.10 ± 50.45
	Max	248.81		237.64	322.02		269.49 ± 45.84
Pp3	M	93.89 ± 104.78	81.81 ± 95.49	86.11 ± 81.06	65.11 ± 73.71	96.79 ± 106.91	84.74 ± 92.39
	Max	578.36	510.86	455.87	390.13	574.20	501.88 ± 80.26
Pp4	M	46.44 ± 46.01	56.37 ± 47.04	61.17 ± 49.89	51.90 ± 43.05	50.94 ± 41.78	53.36 ± 45.55
	Max	271.76	259.22	281.96	227.38	227.71	253.61 ± 25.12
Pp5	M	43.34 ± 46.01			37.20 ± 43.05	37.75 ± 41.78	39.43 ± 43.61
	Max	191.29			152.40	166.39	170.03 ± 19.70
Mean ± SD	M	60.69 ± 63.68	66.46 ± 73.82	65.92 ± 59.07	53.41 ± 54.11	67.66 ± 66.74	
Max ± SD	Max	341.88 ± 156.65	406.08 ± 130.99	329.33 ± 94.55	273.82 ± 90.50	348.52 ± 186.78	

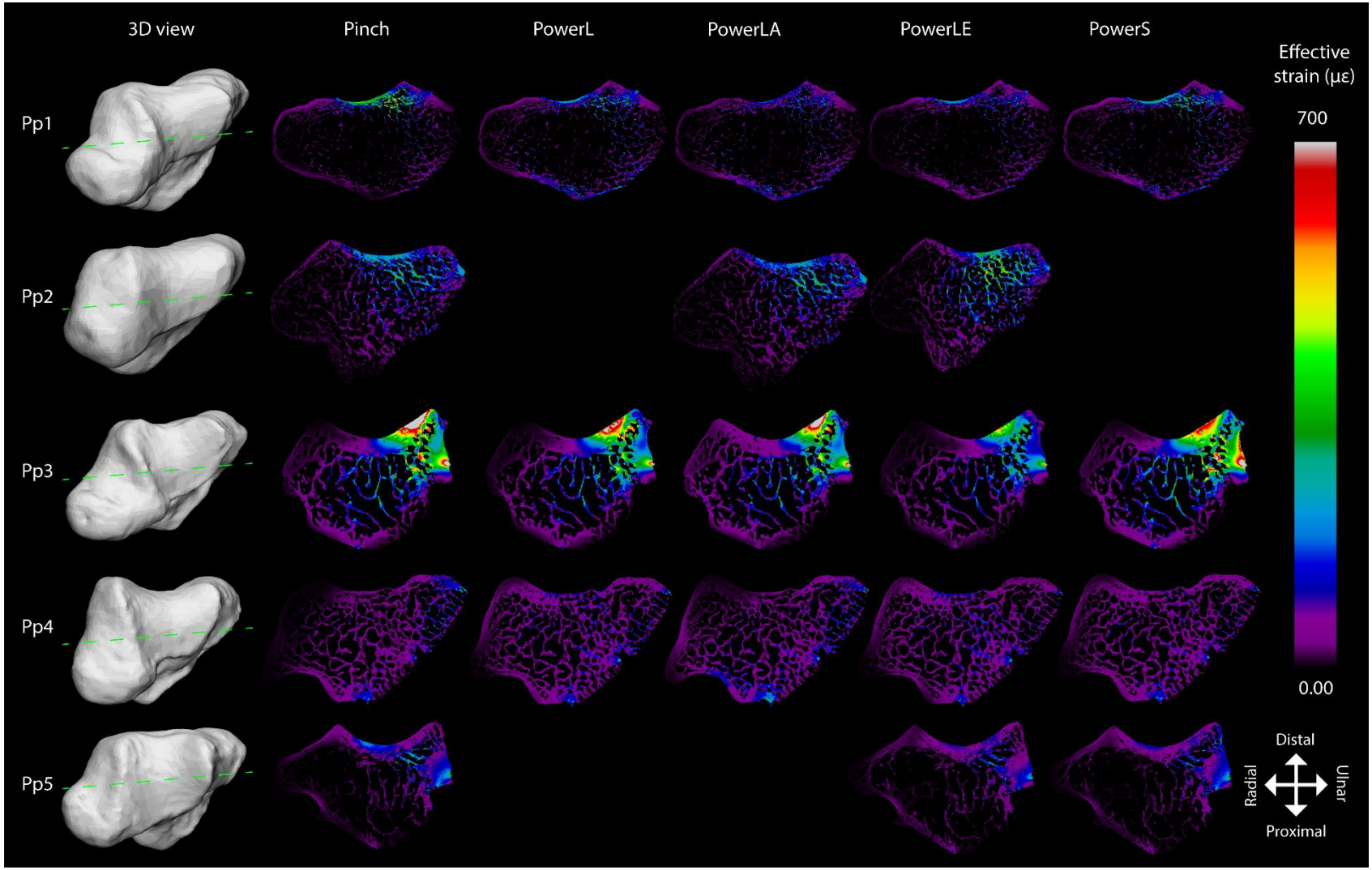

Figure 3: Visualization of effective strain (με) distributions per specimen and per grasp. View of a slice in the dorsopalmar plane, indicated by the green dashed line on the radiodistally oriented 3D view. The maximum heatmap value equals to 10% of ε_{yield} = 7000 με to improve contrast. Full GIF format visualization of image stacks are available in the supplementary material.

Discussion

The purpose of this study was to integrate TMC joint force distributions from FE models in the development of μFE models to investigate internal strain distributions in the bonobo trapezium during different functional grasps. We investigate how the varying subchondral force regimes are distributed within the trapezium bone, and if the bony architecture is well adapted to withstand the internal strains that arise for each of the tested grasping positions. We hypothesized that (H1) the strain values across the trapezium would be substantially smaller than bone yield strain (ε_{yield}) in each simulated grasp. Furthermore, we hypothesized that (H2.1) the strain distribution patterns would differ between grasps, but that (H2.2) mean strain values would be similar across grasps. We find supporting evidence for H1 and H2.2, but not for H2.1. The heatmap visualisations show that strain is distributed towards the proximoulnar aspect of the trapezium through the same cluster of trabeculae in all simulations, and the quantitative analysis of mean strain also points towards a high similarity in strain values between grasps.

The highest reported peak strain value did not exceed 10% of the ε_{yield},, thus supporting H1. Our results show that the bonobo trapezium is well adapted to withstand the joint loads involved in each of the simulated grasping positions. With the exception of one specimen (Pp3), the loading regimes result in relatively uniform strain distributions. Heatmap visualisations of the strain patterns (**Fig.3**, **S1**) allow us to evaluate how strain is distributed through the internal architecture, as well as to localise strain peaks. The overall strain distribution pattern shows that the applied loads are being directed from the distal articular surface of the trapezium (facet for the first metacarpal) along trabeculae oriented towards the proximo-ulnar cortical bone, regardless of specimen or grasping type. While the subchondral loading patterns varied between grasp types, no large variations in strain were reported. The distribution of strain across the trapezium always appears to occur via the same ulnar trabecular cluster regardless of grasping type, unlike what we predicted (H2.1). Visual inspection shows that the trabecular morphology in the ulnar side of the trapezium is more dense and less isotropic when compared to the radial side. Especially the radial tubercle, which is situated radiopalmarly on the trapezium, remains virtually unloaded in all simulations. In two of the older specimens (Pp1 and Pp5), the central and radial trabecular architecture not only remains unloaded, but it appears as if these trabeculae have been resorbed, possibly due to low adaptive stimuli. The successful distribution of loads towards the proximo-ulnar aspect of the trapezium, the articulations with the trapezoid and scaphoid, shows that applied loads are

distributed further along the carpal complex via these trabeculae. Even with diminished central and radial trabeculae, the architecture appears to be sufficiently adapted to withstand the tested loading regimes, without overloading the morphology.

The main outliers to the strain distribution pattern directed to the articulation with the carpal complex are the strain peaks in Pp3, which are also the highest peak strain values encountered in all simulations. These are likely related to the subchondral forces that were applied to the Pp3 models, which in its turn are affected by the morphology of the TMC joint. As presented in the FE study (van Leeuwen *et al.*, 2021), the trapezium of Pp3 has a protrusion at the distal articular surface periphery that causes increased loading, particularly at the dorsoulnar aspect of the facet. This high joint loading leads to high subchondral strain at that same aspect in the volumetric model, as visible in **Fig. 3**. Although these estimated strain values are still far below values associated with bone yield, we suspect that loading of the TMC joint was likely pathological in this specimen, and might have affected its daily usage of the thumb. Inspection of the affected area on CT and 3D bone mesh show early signs of osteoarthrosis.

Assessing bone failure is not straightforward as the conditions for failure rely on the mechanical properties of bone which are dependent on many factors across the multiple hierarchical levels of tissue (e.g. macro, micro-, nanoscale) (Weiner and Wagner, 1998). Trabecular yield strain, for instance, is dependent a variety of factors including; trabecular thickness, anisotropy, bone density, load orientation (on- or off-axis), and type of loading (compressive or tensile) (Kopperdahl and Keaveny, 1998; Tomaszewski *et al.*, 2010). Information on bone material properties in bonobos is lacking in literature, but elastic moduli for chimpanzee cranial cortical bone have been shown to resemble that of humans (Gharpure et al., 2016). Reported E and ε_{yield} values vary greatly across human bone tissue as well as between studies (Rho, Ashman and Turner, 1993; Schwartz-Dabney and Dechow, 2003; Wolfram and Schwiedrzik, 2016; Wu *et al.*, 2018). Despite reported E values often being between 10.0 and 14.0 GPa, particularly in long bones, (Rho, Ashman and Turner, 1993), values as low as 2.16 GPa have been reported in healthy human vertebral bone (Busse *et al.*, 2009). When such low elastic moduli are accounted for, we would obtain strain levels ranging between 1720 με and 5200 με in the bonobo trapezium, which can be classified as bone in an adapted or overloaded state. However, these bone mechanical response classifications, and also ε_{yield}, vary depending on the study (Frost, 1987, 2003; Wolfram and Schwiedrzik, 2016; Pivonka, Park and Forwood, 2018), with ε_{yield} ranging between 3500 με - 13,000 με in human cortical bone (Wolfram and Schwiedrzik, 2016). When the more conservative E for human bone (E = 18.0 GPa), is evaluated against a

frequently reported yield value of ε_{yield} 7000 με (Wolfram and Schwiedrzik, 2016), the highest peak strain encountered across all simulations (Pp3 *pinch* at 578.36 με) is at 8.26% of the bone yield value. These are strain levels more commonly associated with low-end stimuli for the physiological, adapted state of bone, even venturing into stimuli levels of bone disuse and remodelling (Frost, 1987; Pivonka, Park and Forwood, 2018). Furthermore, this maximum value was found in Pp3, whose peak strain values across all grasps are some of the highest peak strain encountered across all simulations. The averaged peak strain across all simulation was even lower at 4.77% ± 1.84% of ε_{yield}. The lack of potentially harmful strain values across all five simulated grasps suggests that the bonobo trapezium is capable of withstanding the strain values to which it is subjected during habitual activities and hand use. Moreover, the relatively low values with respect to the stimuli required for bone to remain in the adapted state (approx. 200 με to 2000 με) may imply that the trapezium is functionally adapted to higher loads. This appears to be in line with bone modelling and bone gain in other animals which were shown to occur during more vigorous activities rather than at walking speeds (Fritton, McLeod and Rubin, 2000; Yang, Brüggemann and Rittweger, 2011). Yet, the reported strain levels here are relatively low compared to the functional strains induced at walking speeds in other animals, including humans, at approx. 200 με to 1000 με (Lanyon and Smith, 1970; Burr *et al.*, 1996; Fritton, McLeod and Rubin, 2000; Yang, Brüggemann and Rittweger, 2011). In light of this, the relatively low strain values in bonobos may indicate that the elastic moduli for the bonobo trapezium bone is generally lower than 18.0 GPa. This is particularly likely in the specimens that show a well-defined internal trabecular architecture, although we do observe signs of trabecular bone loss in two specimens (Pp1 and Pp5).

The above further stresses the importance of testing the bone response to a broader range of applied loading for future research. Achieving this involves the assessment of bonobo grip strength during multiple stages of locomotion and gaits (Samuel *et al.*, 2018), as well as the potential development of a specific primate hand and/or thumb musculoskeletal model to aid in the accurate estimation of various loading scenarios (Mirakhorlo *et al.*, 2018; Synek, Lu, *et al.*, 2019). The incorporation of these steps will yield broader insight in the functional adaptation of the bonobo trapezium, TMC joint, and thumb as a whole. To that end, the presented methodology and results, combined with the CT and μCT datasets acquired for this research, provide an excellent dataset for future research.

Conclusion

This study presents an integrated finite-element micro-finite-element (FE-μFE) workflow for the calculation of internal bone strain distributions. We use FE-based loading regimes in the bonobo TMC joint in five grasping positions as input in the μFE analysis to evaluate if and how the trabecular architecture of the trapezium is adapted to withstand the loads associated with each grasping type. We conclude that these grasps produce strain levels sufficiently below any values associated with bone failure. Furthermore, we conclude that the distribution of loads, and the further distribution along the internal bony architecture, follows similar patterns regardless of applied loading regime.

Acknowledgements

The authors thank dr. Jeroen Stevens of the Royal Zoological Society Antwerp, Belgium, for facilitating access to this unique sample of bonobo specimens. We further thank Steffi Van Hees, Amelie Sas, and dr. Karen Mys from the Department of Mechanical Engineering, University of Leuven, Leuven, Belgium, Maarten Vanneste, Marie Vanhoof, and dr. Elaine Kozma from the Biomedical Sciences Group, University of Leuven, Kortrijk, Belgium, and prof. Thor Besier, dr. Ted Yeung, Nynke Rooks, and dr. Mousa Kazemi from the Auckland Bioengineering Institute, University of Auckland, New Zealand, for their individual involvement in the various design stages of the integrated FE-μFE approach. This project was funded by the KU Leuven – the University of Leuven, Belgium (grant RQ1-D1114-C14/16/082), and supported by the Swiss National Supercomputing Centre (CSCS) under project ID 841, allowing access to the supercomputer Piz Daint at CSCS. KU Leuven had no further involvement in the study outside of funding the project.

References

Bentley, J. L. (1975) 'Multidimensional binary search trees used for associative searching', *Communications of the ACM*, 18(9), pp. 509–517. doi: 10.1145/361002.361007.

Bradski, G. and Kaehler, A. (2000) 'OpenCV', *Dr. Dobb's journal of software tools*, 3.

Burr, D. B. *et al.* (1996) 'In vivo measurement of human tibial strains during vigorous activity', *Bone*, 18(5), pp. 405–410. doi: 10.1016/8756-3282(96)00028-2.

Busse, B. *et al.* (2009) 'Increased calcium content and inhomogeneity of mineralization render bone toughness in osteoporosis: Mineralization, morphology and biomechanics of human single trabeculae', *Bone*, 45(6), pp. 1034–1043. doi: 10.1016/j.bone.2009.08.002.

Christel, M. (1993) 'Grasping techniques and hand preferences in Hominoidea', in Preuschoft, H. and Chivers, D. J. (eds) *Hands of Primates*. Vienna: Springer Vienna, pp. 91–108. doi: 10.1007/978-3-7091-6914-8_7.

Christel, M. I., Kitzel, S. and Niemitz, C. (1998) 'How precisely do bonobos (Pan paniscus) grasp small objects?', *International Journal of Primatology*, 19(1), pp. 165–193. doi: 10.1023/A:1020319313219.

Christen, P. *et al.* (2014) 'Bone remodelling in humans is load-driven but not lazy', *Nature Communications*, 5(1), p. 4855. doi: 10.1038/ncomms5855.

Cooney, W. P. *et al.* (1981) 'The kinesiology of the thumb trapeziometacarpal joint.', *The Journal of Bone & Joint Surgery*, 63(9), pp. 1371–1381. doi: 10.2106/00004623-198163090-00002.

Cooney, W. P. and Chao, E. Y. (1977) 'Biomechanical analysis of static forces in the thumb during hand function.', *The Journal of bone and joint surgery. American volume*, 59(1), pp. 27–36.

Cowin, S. C. (2003) 'Adaptive Elasticity: A Review and Critique of a Bone Tissue Adaptation Model', *Engineering Transactions*, Vol. 51, i, pp. 113–193.

Currey, J. D. (2012) 'The structure and mechanics of bone', *Journal of Materials Science*, 47(1), pp. 41–54. doi: 10.1007/s10853-011-5914-9.

D'Aout, K. *et al.* (2004) 'Locomotion in bonobos (Pan paniscus): differences and similarities between bipedal and quadrupedal terrestrial walking, and a comparison with other locomotor modes', *Journal of Anatomy*, 204(5), pp. 353–361. doi: 10.1111/j.0021-8782.2004.00292.x.

Doran, D. M. (1993) 'Comparative locomotor behavior of chimpanzees and bonobos: The influence of morphology on locomotion', *American Journal of Physical Anthropology*, 91(1), pp. 83–98. doi: 10.1002/ajpa.1330910106.

Dunmore, C. J. *et al.* (2019) 'Metacarpal trabecular bone varies with distinct hand-positions used in hominid locomotion', *Journal of Anatomy*, p. Epub. doi: 10.1111/joa.12966.

Flaig, C. and Arbenz, P. (2011) 'A scalable memory efficient multigrid solver for micro-finite element analyses based on CT images', *Parallel Computing*, 37(12), pp. 846–854. doi: 10.1016/j.parco.2011.08.001.

Fritton, S. P., McLeod, K. J. and Rubin, C. T. (2000) 'Quantifying the strain history of bone: spatial uniformity and self-similarity of low-magnitude strains', *Journal of Biomechanics*, 33(3), pp. 317–325. doi: 10.1016/S0021-9290(99)00210-9.

Frost, H. M. (1987) 'Bone "mass" and the "mechanostat": A proposal', *The Anatomical Record*, 219(1), pp. 1–9. doi: 10.1002/ar.1092190104.

Frost, H. M. (2003) 'Bone's mechanostat: A 2003 update', *The Anatomical Record*, 275A(2), pp. 1081–1101. doi: 10.1002/ar.a.10119.

Gharpure, P. *et al.* (2016) 'Elastic Properties of Chimpanzee Craniofacial Cortical Bone', *The Anatomical Record*, 299(12), pp. 1718–1733. doi: 10.1002/ar.23466.

Halilaj, E. *et al.* (2013) 'A thumb carpometacarpal joint coordinate system based on articular surface geometry', *Journal of Biomechanics*, 46(5), pp. 1031–1034. doi: 10.1016/j.jbiomech.2012.12.002.

Heurtebiese, X. and Thon, S. (2006) 'Discrete Tools for Virtual Sculpture', in *Proceedings of the First International Conference on Computer Graphics Theory and Applications*. SciTePress - Science and and Technology Publications, pp. 415–422. doi: 10.5220/0001354604150422.

Hou, W. *et al.* (2018) 'An Advanced k Nearest Neighbor Classification Algorithm Based on KD-tree', in *2018 IEEE International Conference of Safety Produce Informatization (IICSPI)*. IEEE, pp. 902–905. doi: 10.1109/IICSPI.2018.8690508.

Kabel, J. *et al.* (1999) 'The role of an effective isotropic tissue modulus in the elastic properties of cancellous bone', *Journal of Biomechanics*, 32(7), pp. 673–680. doi: 10.1016/S0021-9290(99)00045-7.

Kivell, T. L. (2016) 'A review of trabecular bone functional adaptation: what have we learned from trabecular analyses in extant hominoids and what can we apply to fossils?', *Journal of Anatomy*, 228(4), pp. 569–594. doi: 10.1111/joa.12446.

Kopperdahl, D. L. and Keaveny, T. M. (1998) 'Yield strain behavior of trabecular bone', *Journal of Biomechanics*, 31(7), pp. 601–608. doi: 10.1016/S0021-9290(98)00057-8.

Ladd, A. J. C. *et al.* (1998) 'Finite-element modeling of trabecular bone: Comparison with mechanical testing and determination of tissue modulus', *Journal of Orthopaedic Research*, 16(5), pp. 622–628. doi: 10.1002/jor.1100160516.

Lanyon, L. E. and Smith, R. N. (1970) 'Bone strain in the tibia during normal quadrupedal locomotion', *Acta Orthopaedica Scandinavica*. Taylor & Francis, 41(3), pp. 238–248.

Larson, S. G. (2018) 'Nonhuman Primate Locomotion', *American Journal of Physical Anthropology*, 165(4), pp. 705–725. doi: 10.1002/ajpa.23368.

van Leeuwen, T. *et al.* (2018) 'Insights into the musculature of the bonobo hand', *Journal of Anatomy*, 233(3), pp. 328–340. doi: 10.1111/joa.12841.

van Leeuwen, T. *et al.* (2019) 'Mobility and structural constraints of the bonobo trapeziometacarpal joint', *Biological Journal of the Linnean Society*, 127(3), pp. 681–693. doi: 10.1093/biolinnean/bly162.

van Leeuwen, T. *et al.* (2021) 'Stress distribution and the influence of morphology during grasping in the bonobo (Pan paniscus) trapeziometacarpal joint', *PeerJ*, p. In review.

van Lenthe, G. H. and Müller, R. (2006) 'Prediction of failure load using micro-finite element analysis models: Toward in vivo strength assessment', *Drug Discovery Today: Technologies*, 3(2), pp. 221–229. doi: 10.1016/j.ddtec.2006.06.001.

Lewiner, T. *et al.* (2003) 'Efficient Implementation of Marching Cubes' Cases with Topological Guarantees', *Journal of Graphics Tools*, 8(2), pp. 1–15. doi: 10.1080/10867651.2003.10487582.

Maas, S. A. *et al.* (2012) 'FEBio: Finite Elements for Biomechanics', *Journal of Biomechanical Engineering*, 134(1). doi: 10.1115/1.4005694.

Marzke, M. W. (1997) 'Precision grips, hand morphology, and tools', *American Journal of Physical Anthropology*, 102(1), pp. 91–110. doi: 10.1002/(SICI)1096-8644(199701)102:1<91::AID-AJPA8>3.0.CO;2-G.

Mirakhorlo, M. *et al.* (2018) 'A musculoskeletal model of the hand and wrist: model definition and evaluation', *Computer Methods in Biomechanics and Biomedical Engineering*, 21(9), pp. 548–557. doi: 10.1080/10255842.2018.1490952.

Napier, J. R. (1955) 'The form and function of the carpo-metacarpal joint of the thumb.', *Journal of anatomy*, 89(3), pp. 362–9.

Napier, J. R. (1956) 'The Prehensile Movements of the Human Hand', *The Journal of Bone and Joint Surgery. British volume*, 38-B(4), pp. 902–913. doi: 10.1302/0301-620X.38B4.902.

Napier, J. R. and Napier, P. H. (1967) : *A Handbook of Living Primates: Morphology, Ecology and Behaviour of Nonhuman Primates.*, *American Anthropologist*. Academic P.

Neufuss, J. *et al.* (2017) 'Nut-cracking behaviour in wild-born, rehabilitated bonobos (Pan paniscus): a comprehensive study of hand-preference, hand grips and efficiency', *American Journal of Primatology*, 79(2), pp. 1–16. doi: 10.1002/ajp.22589.

Odgers, R. A. and Rayan, G. M. (2018) 'Axial Rotation Test for Trapeziometacarpal Joint Hypermobility in the Normal Population', *The Journal of Hand Surgery (Asian-Pacific Volume)*, 23(03), pp. 351–355. doi: 10.1142/S2424835518500352.

Pivonka, P., Park, A. and Forwood, M. R. (2018) 'Functional Adaptation of Bone: The Mechanostat and Beyond BT - Multiscale Mechanobiology of Bone Remodeling and Adaptation', in Pivonka, P. (ed.). Cham: Springer International Publishing, pp. 1–60. doi: 10.1007/978-3-319-58845-2_1.

R Core Team, R. (2017) 'R: A language and environment for statistical com-puting'. Vienna, Austria: R Foundation for Statistical Computing.

Rho, J. Y., Ashman, R. B. and Turner, C. H. (1993) 'Young's modulus of trabecular and cortical bone material: Ultrasonic and microtensile measurements', *Journal of Biomechanics*, 26(2), pp. 111–119. doi: 10.1016/0021-9290(93)90042-D.

Ruff, C., Holt, B. and Trinkaus, E. (2006) 'Who's afraid of the big bad Wolff?: "Wolff's law" and bone functional adaptation', *American Journal of Physical Anthropology*, 129(4), pp. 484–498. doi: 10.1002/ajpa.20371.

Samuel, D. S. *et al.* (2018) 'Hand pressures during arboreal locomotion in captive bonobos (Pan paniscus)', *The Journal of Experimental Biology*, 221(8), p. jeb170910. doi: 10.1242/jeb.170910.

Schulte, F. A. *et al.* (2013) 'Local Mechanical Stimuli Regulate Bone Formation and Resorption in Mice at the Tissue Level', *PLoS ONE*. Edited by K. Kupczik, 8(4), p. Epub. doi: 10.1371/journal.pone.0062172.

Schwartz-Dabney, C. L. and Dechow, P. C. (2003) 'Variations in cortical material properties throughout the human dentate mandible', *American Journal of Physical Anthropology*, 120(3), pp. 252–277. doi: 10.1002/ajpa.10121.

Synek, A., Dunmore, C. J., *et al.* (2019) 'Inverse remodelling algorithm identifies habitual manual activities of primates based on metacarpal bone architecture', *Biomechanics and Modeling in Mechanobiology*, 18(2), pp. 399–410. doi: 10.1007/s10237-018-1091-y.

Synek, A., Lu, S.-C., *et al.* (2019) 'Musculoskeletal models of a human and bonobo finger: parameter identification and comparison to in vitro experiments', *PeerJ*, 7, p. Epub. doi: 10.7717/peerj.7470.

Tomaszewski, P. K. *et al.* (2010) 'A Comparative Finite-Element Analysis of Bone Failure and Load Transfer of Osseointegrated Prostheses Fixations', *Annals of Biomedical Engineering*, 38(7), pp. 2418–2427. doi: 10.1007/s10439-010-9966-9.

Tsegai, Z. J. *et al.* (2013) 'Trabecular bone structure correlates with hand posture and use in hominoids', *PLoS ONE*, 8(11). doi: 10.1371/journal.pone.0078781.

Weiner, S. and Wagner, H. D. (1998) 'The material bone: structure-mechanical function relations', *Annual review of materials science*. Annual Reviews 4139 El Camino Way, PO Box 10139, Palo Alto, CA 94303-0139, USA, 28(1), pp. 271–298.

Wirtz, D. C. *et al.* (2000) 'Critical evaluation of known bone material properties to realize anisotropic FE-simulation of the proximal femur', *Journal of Biomechanics*, 33(10), pp. 1325–1330. doi: 10.1016/S0021-9290(00)00069-5.

Wolfram, U. and Schwiedrzik, J. (2016) 'Post-yield and failure properties of cortical bone', *BoneKEy Reports*, 5. doi: 10.1038/bonekey.2016.60.

Wu, D. *et al.* (2018) 'Young's modulus of trabecular bone at the tissue level: A review', *Acta Biomaterialia*, 78, pp. 1–12. doi: 10.1016/j.actbio.2018.08.001.

Yang, P., Brüggemann, G.-P. and Rittweger, J. (2011) 'What do we currently know from in vivo bone strain measurements in humans?', *Journal of Musculoskeletal and Neuronal Interactions*. International Society of Musculoskeletal and Neuronal Interactions, 11(1), pp. 8–20.

Zhang, J. (2020) 'GIAS2 (Geometry Image-Analysis Statistics)'. Available at: https://bitbucket.org/jangle/gias2/downloads/.

Chapter 6.

The effect of grasping on stress and strain distributions in the trapezium of hylobatids (fam. Hylobatidae) and rhesus macaques (*Macaca mulatta*).

Timo van Leeuwen[1,3], Marco T.Y. Schneider[2], G. Harry van Lenthe[3], Evie E. Vereecke[1],

[1]Department of Development and Regeneration, KU Leuven Campus Kortrijk, Kortrijk, Belgium

[2]Auckland Bioengineering Institute, The University of Auckland, Auckland, New Zealand

[3]Department of Mechanical Engineering, KU Leuven, Leuven, Belgium

Currently not submitted for publication

Abstract

The primate thumb plays a key role during manipulation. Non-human primates, however, also employ their hands and thumbs for a large variety of locomotor modes. How the different morphologies of the thumb, and in particular its unique trapeziometacarpal (TMC) joint, in these species are capable of withstanding the varying loading regimes involved in this broad functionality is poorly understood. Here, we employ an integrated finite element – micro finite element approach to simulate various functional grasps in gibbons and macaques, two species with drastically different locomotor repertoires, in order to investigate stress and strain distributions in the trapezium. We use FE to simulate the intra-articular stress distributions during each grasp, and μFE to calculate how the resulting strain is transmitted across the microarchitecture of the trapezium. We investigate if the trapezium is functionally adapted to execute common primate grasps. Our results show that the gibbon TMC joint is loaded with great variation between the modelled grasps. Gibbons also show great variation in how the internal strain is distributed, but appear to be capable of executing the simulated grasps without resulting in high strain peaks. The macaque TMC joint, in contrast, is highly constrained and, is loaded in a similar way across all grasp types. Consequently, the internal strain distribution is similar across grasp types. The trapezium micro-architecture seems capable of withstanding the forces involved in the simulated grasps, and the enlarged prepollex that is present in macaques appears to reinforce the trapezium within the carpal complex.

Introduction

The modern human hand is known for its advanced manipulation capabilities and powerful opposable thumb (Napier and Napier, 1967; Marzke, 1997; Samuel *et al.*, 2018), which plays a critical role in grasping and in-hand manipulation (Napier, 1956; Crast *et al.*, 2009; Fragaszy and Crast, 2016). This is reflected in the morphology of the human thumb, which is highly mobile and yet has the required stability to perform strong power grasps. Humans, however, are not the only primate species that are capable of complex manual tasks, yet their habitual bipedalism is unique among primates. As the hands are no longer involved in habitual locomotion in modern humans this means that, in principle, the hands have been free to adapt mainly towards manipulation and other non-locomotory activities (e.g. dart-throwing) (Wolfe *et al.*, 2006; Kivell, 2015). In other primate species, the hand is subjected to selective pressures related to both locomotion and manipulation. Furthermore, locomotor modes vary significantly across primate taxa, even among closely related species (Napier and Napier, 1967; Larson, 2018). The differences in locomotor mode as well as in manual dexterity across closely related primates are particularly interesting for the study of functional adaptation of primate hand morphology.

Gibbons and macaques are prime examples of two closely-related primate taxa with distinct functional repertoires. Genetically separated about 25 million years ago (Kumar and Hedges, 1998; Perelman *et al.*, 2011; Carbone *et al.*, 2014), these two primates are still closely related in evolutionary measures. Yet the niches they inhabit, and their adopted locomotor modes, are completely different. Hylobatids (fam. *Hylobatidae*) – hereafter referred to as 'gibbons' - are highly arboreal apes that inhabit the rainforests of South and South-East Asia (Matsudaira and Ishida, 2010). They navigate the forest canopy by means of brachiation, or arm-swinging, using hook-like grasps on the superstratum without involvement of the thumb (Napier and Napier, 1967; van Horn, 1972; Rumbaugh, 1976; Michilsens *et al.*, 2009). Gibbons are capable of advanced manual tasks, such as precision grips with a tip-to-side between index and thumb (Christel, 1993), as well as power grasps, which are used during vertical climbing (van Horn, 1972). In contrast, macaques (genus *Macaca*) are palmigrade/digitigrade quadrupeds that are widespread in North Africa, Asia and Southern Europe (Gibraltar), where they inhabit terrestrial, arboreal, and urban areas (Lewis and Prongay, 2015; Roos and Zinner, 2015). Vertical climbing is observed in these animals, but even in arboreal environments they often employ digitigrade quadrupedal walking similar to their terrestrial quadrupedalism when on top of the branches (Hayama, Chatani and Nakatsukasa, 1994). Macaques are capable of many

types of grasps, including multiple power grasps and advanced precision grips (Macfarlane and Graziano, 2009).

Adaptation towards both manual dexterity and a specific locomotor repertoire will affect the gibbon and macaque thumb in different ways. In humans, much of the interplay between mobility and stability of the thumb occurs at the basal thumb or trapeziometacarpal (TMC) joint (Napier, 1956; Cooney *et al.*, 1981; Crisco *et al.*, 2015; D'Agostino *et al.*, 2017). In most primates, including humans and macaques, the TMC joint is saddle-shaped (Rafferty, 1990). This type of reciprocal concave-convex articular surface allows for considerable mobility of the thumb due to the unrestricted flexion/extension and palmar adduction/abduction planes, while simultaneously offering stability by limiting axial rotation and increased joint congruency upon muscle activation (Napier, 1955; Cooney and Chao, 1977). In rhesus macaques (*Macaca mulatta*), the joint curvatures are substantially more shallow than in modern humans (**Chapter 3**). This flattened out TMC joint morphology significantly restricts the mobility of the joint in macaques, in comparison to the human TMC joint. In contrast, the ball-and-socket morphology of the TMC joint in gibbons is drastically different from that of other primates. Such a highly mobile joint allows gibbons to reach ranges of motion that exceed even the mobility of the human thumb **(Chapter 3**). However, in contrast to other ball-and-socket joint morphologies, such as the hip and shoulder (Kammel, El Bitar and Leber, 2021), the gibbon TMC joint appears to lack significant soft-tissue restrictions to provide joint stability (van Leeuwen *et al.*, 2018, 2019; Vanhoof *et al.*, 2020; Vanhoof, van Leeuwen and Vereecke, 2020).

These differences in locomotor function and overall TMC joint morphology between gibbons and macaques are expected to yield different joint loading regimes. As bone functional adaptation occurs in response to habitual mechanical stimuli (Huiskes *et al.*, 2000; Eriksen, 2010), the internal bony architecture is likely to be different. A well-adapted morphology distributes the experienced loads across the bony microarchitecture in a manner that avoids local stress peaks that may strain the bone to the point of bone failure. An indicator for bone functional adaptation is the amount of deformation that may occur before the bone material properties are affected in an irreversible manner, which is the yield strain value (ε_{yield}) (Kopperdahl and Keaveny, 1998). In the previous chapter (**Chapter 5**), we investigated how different functional loading regimes are distributed throughout the bonobo trapezium during different functional grasps. We found that the bonobo is not only well adapted to different loading patterns, as the maximum strains encountered are well below ε_{yield}, but also that the different grasps result in similar strain

distribution patterns towards the proximal ulnar articulation with the rest of the carpal complex. However, whether or not the same adaptational response of the TMC joint also applies to other primates with a distinct joint morphology and loading regime, such as the gibbon and macaque, remains unknown.

In this chapter, we investigate stress distributions within the gibbon and macaque trapezium during the five functional grasps. We use a similar approach of integrated finite element (FE) – micro finite element (μFE) modelling to calculate the intra-articular stress distribution during these grasps in gibbons and macaques. The resulting joint forces are subsequently integrated in the μFE model to determine strain distributions across the internal architecture of the trapezium. We analyse the resulting strain distribution to investigate if the trapezium of gibbons and macaques is adapted to execute each of the five grasp types. Our first set of hypotheses address how stress is distributed in the TMC joint of gibbons and macaques. Gibbons have a larger TMC joint mobility compared to that of bonobos, while the macaque joint is severely restricted. We therefore hypothesize that (H1.1) the gibbon stress distribution patterns will be similar in orientation to the bonobo and macaque patterns, but with larger excursions (i.e. the patterns are more expanded towards the periphery of the articular surface, and there is less pattern overlap). While (H1.2) the stress distribution patterns on the macaque TMC articulation will be more constrained, with more pattern overlap between grasps. We also expect small differences in stress distribution patterns between different types of grasps, as visualized in **Fig. 2.**. For example; during *powerLE,* we expect that the stress distribution in gibbons will occur highly dorsally on the facet due to their capability for extreme thumb extension. In contrast, we expect the stress pattern to be located slightly more dorsally compared to a neutral loaded position in macaques.

As both gibbons and macaques are capable of precision pinching and power grasps, we expect the trabecular architecture of the trapezium to be adapted to withstand the loading regimes associated with these grips. We therefore hypothesize that (H2) the strain distribution pattern in both the gibbon and macaque trapezium will not lead to peak strains associated with bone failure. Our following hypotheses address how well the trapezium of gibbons and macaques is adapted to the loading regimes associated with different types of grasping. As both species use their hands in a wide variety of grasps (van Horn, 1972; Christel, 1993; Macfarlane and Graziano, 2009), we expect both taxa to be well adapted to multiple loading regimes. Based on our previous findings in bonobos, where strain distribution patterns inside the trapezium were largely similar across grasp types, we hypothesize that (H3) the strain is distributed similarly across all five grasps in

gibbons (H3.1) and in macaques (H3.2). Furthermore, we hypothesize that (H4) the mean strain is similar between grasps in both gibbons (H4.1) and macaques (H4.2), as was observed in bonobos.

Methodology

Overview

In this study, we use the integrated FE-μFE approach (introduced in **Chapters 4** and **5**) to model how loading on the articular surface of the trapezium is dissipated throughout its micro-architecture during five functional grasps. We use standardized medical imaging in cadaveric specimens of gibbons and macaques to generate CT-based 3D reconstructions of the TMC joint in five grasping positions. These reconstructions are used to generate FE models of the TMC joint to calculate stress distribution on the articular surface of the trapezium. High-resolution μCT scans are used to make volumetric reconstructions of the trapezium bone, which are used to generate μFE models. The FE-derived stress distributions are used as loading cases representing each grasp and applied to the trapezium volumetric model to calculate the stress distributions and strain levels inside the trapezium. The strain levels are compared to those associated with bone failure to assess the adaptation of the trapezium to each grasp.

Specimen information

Cadaveric forearm specimens of eight gibbons and seven rhesus macaques were obtained opportunistically in collaboration with five European zoos (**Table 1**). All specimens were disarticulated at the glenohumeral joint and stored at -18 °C. After the CT scanning protocol described below, the soft-tissue morphology was removed (Vanhoof *et al.*, 2020; Vanhoof, van Leeuwen and Vereecke, 2020) and the individual trapezia were extracted from the carpal complex for μCT scanning.

Table 1: Specimen details. *Code from previous study (**Chapter 3)**. [a]Wildborn, F = female, M = male, U = unknown sex. Exact age information is unknown but the specimens could be identified as adult (A) or subadult (sA) based on bone growth plate progression. Sample refers to the side used; L = left, R = right.

Code*	Species	Sex	Age	Sample	Collection
G1	*Hylobates lar*	F	sA	L	National Museum of Scotland, Edinburgh, Scotland
G2	*Hylobates lar*	U	sA	R	National Museum of Scotland, Edinburgh, Scotland
G3	*Hylobates lar*	U	sA	R	Ghent University, campus Merelbeke, Belgium
G4	*Hylobates pileatus*	M	A	R	National Museum of Scotland, Edinburgh, Scotland
G5	*Nomascus concolor*	M	A	L	Pakawi Park, Olmen, Belgium
G6[a]	*Nomascus leucogenys*	M	A	L	Zoological and Botanical Park of Mulhouse, France
G7	*Symphalanges syndactylus*	M	A	R	National Museum of Scotland, Edinburgh, Scotland
G8	*Symphalanges syndactylus*	M	A	L	National Museum of Scotland, Edinburgh, Scotland
M1	*Macaca mulatta*	U	A	R	Ghent University, campus Merelbeke, Belgium
M2	*Macaca mulatta*	F	A	L	Ghent University, campus Merelbeke, Belgium
M3	*Macaca mulatta*	U	A	L	Ghent University, campus Merelbeke, Belgium
M4	*Macaca mulatta*	U	A	L	Ghent University, campus Merelbeke, Belgium
M5	*Macaca mulatta*	U	A	L	Ghent University, campus Merelbeke, Belgium
M6	*Macaca mulatta*	M	A	L	Ghent University, campus Merelbeke, Belgium
M7	*Macaca mulatta*	U	A	R	KU Leuven, campus Gasthuisberg, Belgium

Imaging protocols

Before imaging, all specimens were thawed at room temperature. The specimens were placed in a radio-translucent rig with variable diameter cylinders (multiple options for small and large, depending on species and hand size) to standardize the five grasping types (**Fig. 1**): The key pinch precision grasp (*pinch*), the small diameter power grasp (*powerS*), and the three large diameter power grasps, thumb abducted (*powerL*), adducted (*powerLA*), and extended (*powerLE*). CT imaging was done using a 64-slice Discovery HD 750 CT scanner [GE Healthcare, Little Chalfont, UK; display field of view (DFOV): 173 mm; slice thickness: 0.625 mm; pixel spacing: 0.338/0.338 mm, voxel size: 0.071 mm^3; 100 kV; 180 mA; image size: 512 × 512 pixels). Image segmentation was done semi-automatically using Mimics Research 20.0 (Materialise, Leuven, Belgium) and the trapezium and MC1 were exported as triangular meshes.



Figure 1: Radio-translucent rig based standardized grasps in the *powerL* position in gibbon (**A**) and macaque (**B**).

After soft-tissue removal and the extraction from the carpal complex, the trapezia were individually scanned using a micro-CT SkyScan 1172 (Bruker, Kontich. Belgium) at a voxel size of 20.0 µm. The data were reconstructed using NRecon software (Bruker). The reconstructed images were pre-processed in CTAn (Bruker) using the Thresholding and Despeckle functions.

FE model generation

A parametric meshing approach (**Chapter 4**, fig. 3) was used to generate FE models for both gibbons and macaques. For each specimen, a grasp (*pinch*) is selected to serve as a template mesh. A master template was selected per species, and its trapezium and MC1 meshes were aligned with a TMC joint based coordinate system, where the principal axes of motion were aligned with the cartesian coordinate system. This was done separately for the gibbon and the macaque using two different methods adapted from Halilaj et al. (2013), presented in **Chapter 3**. For each specimen, the remaining template meshes were aligned with the master template by using rigid body registration of each trapezium to its master trapezium. The corresponding MC1 for each pair was transformed to match its respective trapezium using the transformation matrix resulting from the fit.

For each specimen, Instant Meshes (Jakob *et al.*, 2015) was used to discretize the master template trapezium and MC1 triangular meshes into quadrilateral meshes, to delineate the TMC joint articular surfaces for extraction, and to ensure mesh quality by reducing mesh irregularities, element distortion, and increasing mesh Jacobian values (Burkhart, Andrews and Dunning, 2013). The quadrilateral articular surfaces were extracted using MeshLab software (Cignoni *et al.*, 2008). Each specimen's master template quadrilateral meshes were fitted onto their remaining position models using Radial Basis Function (RBF) fitting, and the separated surface meshes were lofted into hexahedral volumetric mesh using Python scripts based on Schneider et al. (2017). Accurate cartilage information for these species is unknown, therefore, a uniform cartilage layer thickness of 0.3 mm was used based on the intra-articular distance derived from CT images. The master trapezium quadrilateral and hexahedral meshes were used for each individual position, while the master MC1 quadrilateral and hexahedral meshes were fitted to each triangular MC1 position. This yields a quadrilateral trapezium and MC1 mesh pair, each with corresponding hexahedral cartilage layer meshes, for all scanned positions per specimen.

All FE models were generated, solved, and visualized using FEBio Software Suite (Maas *et al.*, 2012). The cadaveric specimens were scanned in unloaded grasping positions. The FE models were set up as two-step, force-driven simulations of each grasping position.

First, we simulated joint contact by means of nonlinear springs exerting 1N of force each. Next, the second step introduced the applied force vector for the actual simulation of joint stresses. The thumb tip forces were based on 2D static force analyses of the gibbon and macaque TMC joint (Cooney and Chao, 1977), based on their respective muscle PCSA, thumb muscle-tendon data, and MC1 and phalanx proportions, assessed in **Part 1** of this thesis (Vanhoof *et al.*, 2020; Vanhoof, van Leeuwen and Vereecke, 2020). Both the acquired gibbon and macaque applied force vector approximated 30 N and were thus set at 30 N. Bone proportions were measured from CT images, while soft-tissue data were obtained from dissection data (Vanhoof *et al.*, 2020; Vanhoof, van Leeuwen and Vereecke, 2020).

As part of the parametric approach, only a master model was manually designed in FEBio Preview (v2.1.3). The quadrilateral bone surface meshes were modelled as rigid bodies, and connected to their respective hexahedral cartilage meshes, modelled as a neo-Hookean material (Young's modulus = 18.0 MPa, Poisson's ratio = 0.45). The proximal articulations of the trapezium with the carpal complex were selected and included in the FE nodal data for boundary assignments in the μFE procedure. As the modelled positions closely resembled the intended terminating position in terms of translation, the trapezium mesh was fully constrained while the MC1 was allowed to translate only to come into contact and terminate successfully. The remaining models per species were generated by swapping out the parametric meshes using custom Python scripts. This yields successfully initiating launching models in the correct position for each grasp in each specimen. The models were solved using the FEBio solver (v.2.9.0). The successfully terminating simulations were further optimized to resemble the intended grasping positions by means of a custom, Python-based optimizer function. Here, the terminating position of the loaded simulation is brought in close proximity to the initial scan that represents that intended grasp by optimising the orientation of the applied force vector. Optimal positions are achieved by minimizing the root mean square error (RMSE) between the simulated and targeted position. RMSE values always included the interarticular distance. The stress distributions from successful simulations were visualised and compared to the expected patterns for each position (**Fig. 2**). Subchondral coordinates and loading information were extracted from the simulations and imported in Python for integration in the μFE approach.

μFE model generation

The entire μFE model generation procedure is executed in Python, unless specified otherwise. All scripts are custom designs, with the exception of specific Python modules

which are credited accordingly. The procedure is described in detail in **Chapter 5** (for a visualisation refer to **Chapter 5**, **Fig. 2**).

The reconstructed, CTan-processed, µCT image stack was imported in Python. A copy was downsampled and used to generate a surface mesh (Lewiner *et al.*, 2003) of equal resolution (0.625 mm) to the FE trapezium mesh. The downsampled mesh was fitted to the FE mesh (Zhang, 2020), and the obtained transformation matrix is used to transform the original high resolution image stack into the same TMC joint based coordinate system as the FE mesh (Heurtebiese and Thon, 2006; Halilaj *et al.*, 2013; Zhang, 2020). This new, TMC joint aligned, high-resolution image stack was similarly downsampled and surface meshed. The nodal information for subchondral loading and boundary restrictions were extracted from the FE model and the location of the equivalent nodes were identified on the downsampled point cloud. The corresponding loads from the FE models were applied to the TMC articulation, and the loads at the location of boundary restriction (proximal articulations of the trapezium) were set to zero (Bentley, 1975; Hou *et al.*, 2018). The downsampled point cloud, including the applied loads, was upscaled back to a 20 µm resolution. In this process, a bone outline (Bradski and Kaehler, 2000) was used as a mask to ensure loads were only applied to the cortical bone layer of the articular surfaces.

The rotated image and boundary conditions are exported in a HDF5 format, and solved using ParOSol (Flaig and Arbenz, 2011) on the supercomputer Piz Daint at the Swiss National Supercomputing Centre (CSCS). As in the previous chapter, the individual mesh elements were modelled as a homogenous, isotropic material with constant Young's moduli (18 GPa) and Poisson's ratios (0.3) (Rho, Ashman and Turner, 1993; Ladd *et al.*, 1998; Kabel *et al.*, 1999; Wirtz *et al.*, 2000). Nodal coordinates and corresponding effective stress values were extracted from the solution and processed using Python. Maximum stress value was extracted at the 99th percentile of data to exclude the influence of mesh imperfections (Tomaszewski *et al.*, 2010). Maximum effective strain values were calculated per grasp based on Von Mises stress for a Young's modulus (E) 18.0 GPa. An ANOVA was used to test for differences in mean effective strain between grasps. Heatmap visualisation was used to discern the course of effective strain distribution.

Results

Successful simulations

Out of 75 FE simulated models, 40 for gibbons and 35 for macaques, only 25 simulations in four gibbons and one macaque initiated and terminated successfully. I identified the majority of the encountered problems as being related to the initial CT scanning resolution and segmentation. Unfortunately, these could not be solved. Scan resolution and mesh quality are important points of attention for the FE workflow in particular for future use.

Out of the 25 successful FE simulations, three more grasps had to be excluded. One gibbon specimen (G4) could not be positioned in the *powerL* grasp due to insufficient thumb mobility. In addition, simulations of *powerLE* and *powerL* in two other gibbon specimens (G6 and G8 , resp) could not be terminated successfully as a direct result of the very high MC1 excursion in these specimens. In the simulation, the MC1 travelled beyond the limitations of the simulated cartilage layer rendering the model unsolvable within the conditions set for this step in the workflow. Average RMS errors for the remaining, successfully terminated models were 0.924 mm for *pinch,* 1.01 mm for *powerL*, 0.942 mm for *powerLA*, 0.890 mm for *powerLE*, and 1.04 mm for *powerS*. An overview of the successfully terminating simulations and their corresponding RMSE values can be found in the supplementary material (**S1**). Despite the low sample size of the final study, the interpretation of the data can be used as a proof of concept for the integrated FE-μFE approach.

Stress distribution on the articular surface of the trapezium

The FE results (**Fig. 2**) show marked differences between the stress distribution on the trapezial joint surface of gibbons and macaque. The macaque shows similar stress patterns during each simulated grasp. Peak stresses are found at the palmar-ulnar aspect of the articular facet, as well as at the dorsoradial aspect. In gibbons, the simulated stress distributions are more variable than in macaques and correspond well to the expected quadrants in all of the simulated gibbon grasps (17/17). Yet, stress distributions that deviate from the expected patterns are also present (9/17). However, no simulations showed fully divergent patterns.

The stress distribution patterns during *powerL, powerLE,* and *powerS* correspond closely to the predicted patterns. During both *powerL* and *powerS,* the stress is situated radially of the articular facet, while a dorsal distribution is found during *powerLE*. During *powerLA,* we do see a more ulnarly yet still rather centrally located positioned distribution of stress.

Although the stress distributions during *pinch* and *powerLA* partly correspond with the expected pattern, additional articular regions subjected to high stress were observed in each of these simulations. During *pinch*, the stress distribution was indeed found on the palmar aspect, and also in particular on the radiopalmar aspect, of the articular surface. But dorsal loading is also observed in all gibbon *pinch* simulations. During *powerLA*, the stress distribution is situated on the ulnar quadrants as expected, but we also observe a more centrally located loading.

Trapezial internal strain distribution

The data show that the average mean strain value for the five grasping types is 9.68 με ± 6.29 με in gibbons, and 9.26 με ± 1.93 με in the macaque. The highest reported strain in the gibbon specimens amounts to 125.34 με (in G6) during *powerLA*, while the maximum in the macaque specimen (M3) was observed during *pinch* (46.44 με). **Table 2** reports the individual mean and maximal strain values for each specimen calculated for E = 18.0 GPa. ANOVA-based comparisons show that mean strain does not differ significantly between different grasp types ($F(4,12) = 0.52$, $p = 0.78$).

Figure 3 shows the distribution of strain in one slice of the dorsal to palmar plane of the trapezium for each of the simulated positions. It shows the localisation of high strain areas in response to the loading conditions.

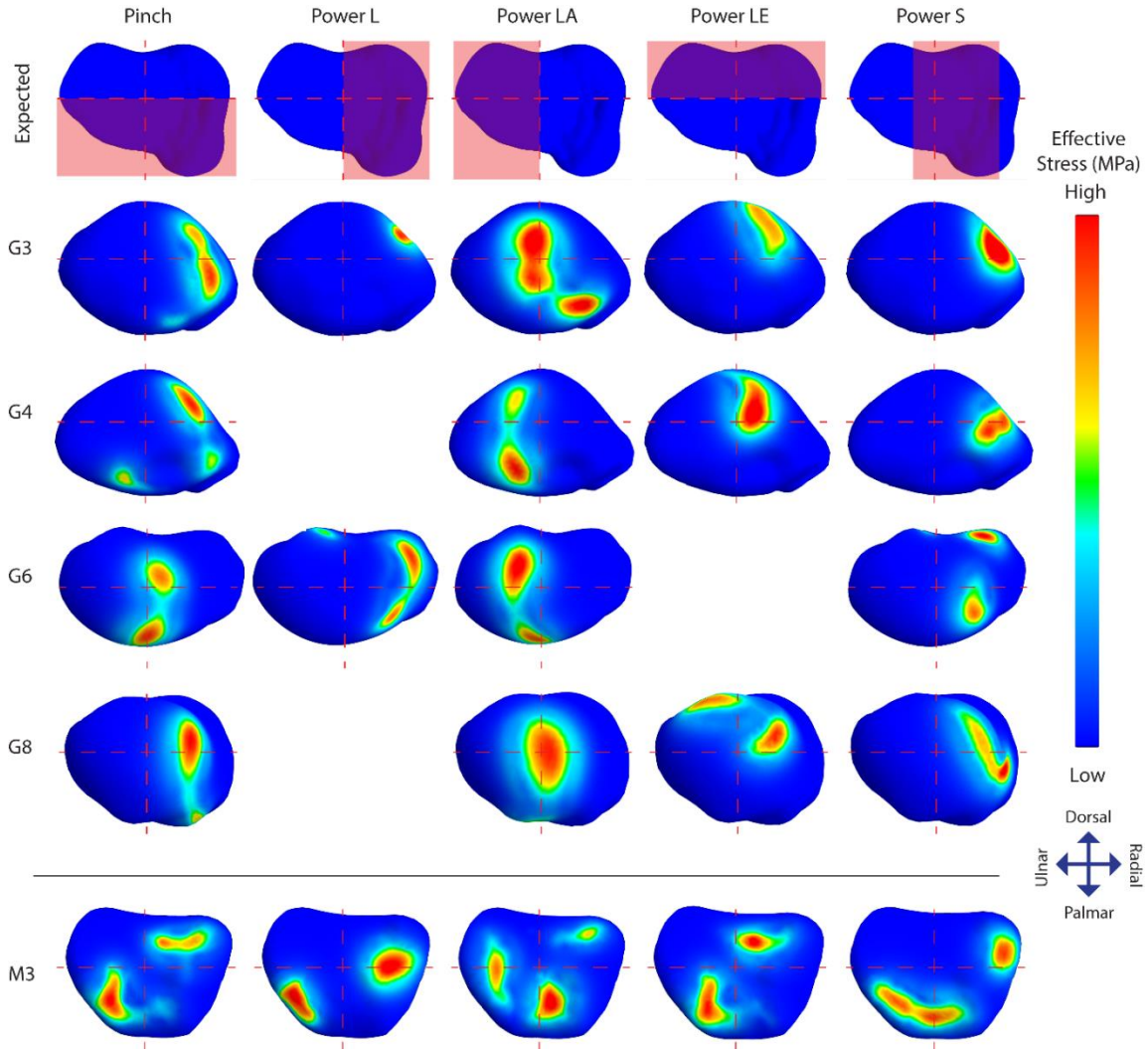

Figure 2: TMC joint effective stress distribution plotted on a distal view of the isolated trapezium distal articular surfaces in gibbons (**G**) and macaque (**M**). The top row displays the quadrants where stress distribution is expected in red for each position, visualised on a bonobo trapezial articular surface morphology.

Table 2: Mean strain (M) with standard deviation, and maximum strain (Max) at the first 99 percentile with a Young's modulus of 18 GPa. Strain values are reported in micro strain (με).

Gibbon	**με**	**Pinch**	**PowerL**	**PowerLA**	**PowerLE**	**PowerS**	**Average**
G3	M	4.61 ± 4.02	6.33 ± 5.82	7.96 ± 7.63	3.29 ± 2.95	10.17 ± 10.56	6.47 ± 6.19
	Max	23.91	31.21	39.69	16.78	57.40	33.80 ± 15.70
G4	M	4.89 ± 4.11		7.07 ± 7.05	4.09 ± 3.73	5.20 ± 4.69	5.31 ± 4.89
	Max	20.49		38.57	19.27	23.22	25.39 ± 8.94
G6	M	19.07 ± 15.64	16.68 ± 12.70	25.74 ± 24.02		12.07 ± 9.70	18.39 ± 15.51
	Max	75.70	63.59	125.34		48.82	78.36 ± 33.19
G8	M	5.73 ± 4.18		5.66 ± 4.59	7.85 ± 8.17	13.70 ± 9.87	8.23 ± 6.70
	Max	19.78		21.80	44.42	45.82	32.95 ± 14.08
Average	M	8.57 ± 6.99	11.50 ± 9.26	11.61 ± 10.82	5.08 ± 4.95	10.29 ± 8.70	
	Max	34.97 ± 26.26	47.40 ± 11.45	56.35 ± 45.46	26.82 ± 12.90	43.81 ± 11.65	
Macaque		**Pinch**	**PowerL**	**PowerLA**	**PowerLE**	**PowerS**	**Average**
M3	M	10.93 ± 8.67	6.76 ± 5.77	7.64 ± 5.65	10.88 ± 8.53	10.06 ± 7.98	9.26 ± 7.32
	Max	46.44	29.30	27.91	45.08	40.60	37.87 ± 8.74

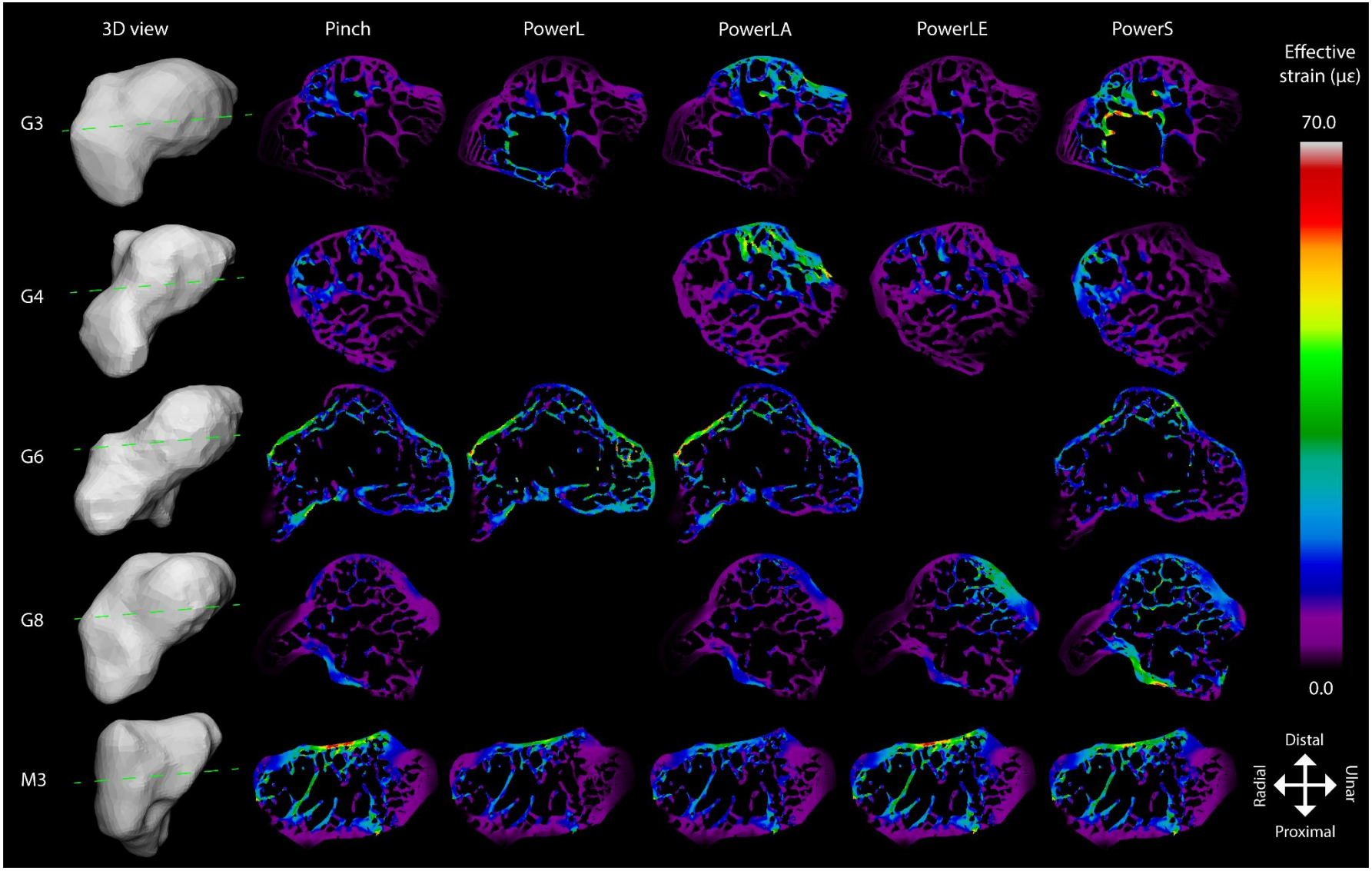

Figure 3: Visualization of effective strain (με) distributions per grasp in gibbons (**G**) and macaque (**M**). View of a slice in the dorsal – palmar plane, indicated by the green dashed line on the radiodistal oriented 3D view. Heatmap colors are scaled to 70 με.

Discussion

The purpose of this study was to simulate the effect of different functional grasps on TMC joint loading in gibbons and macaques, and to investigate the further transmission of internal strain across the trapezium microarchitecture. We applied an integrated FE-μFE workflow to address hypotheses regarding (H1) stress distribution patterns on the trapezial distal articular surface, (H2) how well the trapezium internal bony architecture is adapted to withstand the resulting loading regimes, (H3) the differences in the course of the internal strain distributions between grasps, specimens, and primate taxa, and (H4) differences in mean strain values between grasps.

The integrated FE-μFE workflow was first developed for the bonobo (*Pan paniscus*) (**Chapters 4** and **5**), and its implementation to smaller species such as the gibbon and macaque did present some difficulties. These issues are foremost related to mesh quality problems as a direct result of insufficient CT scan resolution with respect to the size of the specimens. Despite this, 22 successful simulations were achieved for this study, 17 of which converged to an average RMSE of 1.00 mm ± 0.30 mm in four gibbon specimens, and five simulations averaged at a RMSE of 0.83 mm ± 0.12 mm in one macaque. The FE results support H1.1 as the stress patterns in gibbons corresponded to the expected patterns in all of the successfully terminated simulations. However, during *pinch* and *powerLA*, unanticipated regions were loaded in addition to the expected areas. In the macaque, H1.2 was partially supported, as stress patterns were indeed a reflection of a constrained joint, but more so than expected as the simulated patterns showed highly similar stress distributions in each of the five grasps, but did not match the expected patterns. However, as we were only able to simulate stress patterns for one macaque specimen, we should be careful in drawing conclusions.

The μFE analyses show that both in gibbons and in the macaque, the micro-architecture of the trapezium is able to withstand the stresses and strains induced by the applied loading regimes. The maximum encountered strain value is 225.62 με in gibbons and 83.59 με in macaque. Bone failure occurs when strain levels affect the bone material properties in an irreversible manner as a result of the accumulation of microdamage. This is a gradual process that reportedly starts to occur around 3000 με (Biewener, 1993; Frost, 2003). The estimated strain values are well below critical strain values in both gibbons and macaques and lack peak strains that would be associated with bone failure, confirming H2.

The distribution of strain in the gibbon trapezium differs between grasp types, countering H3.1 that strain distribution would occur similarly throughout the trapezial microarchitecture regardless of grasp type. Despite this, the mean strain values between these grasps are similar within each specimen. This supports H4.1 and indicates that the gibbon trapezium is capable of withstanding the different loading regimes of the five tested grasps. However, the strain distributions, although similar in some specimen/grasp combinations, are also often dissimilar between gibbon specimens.

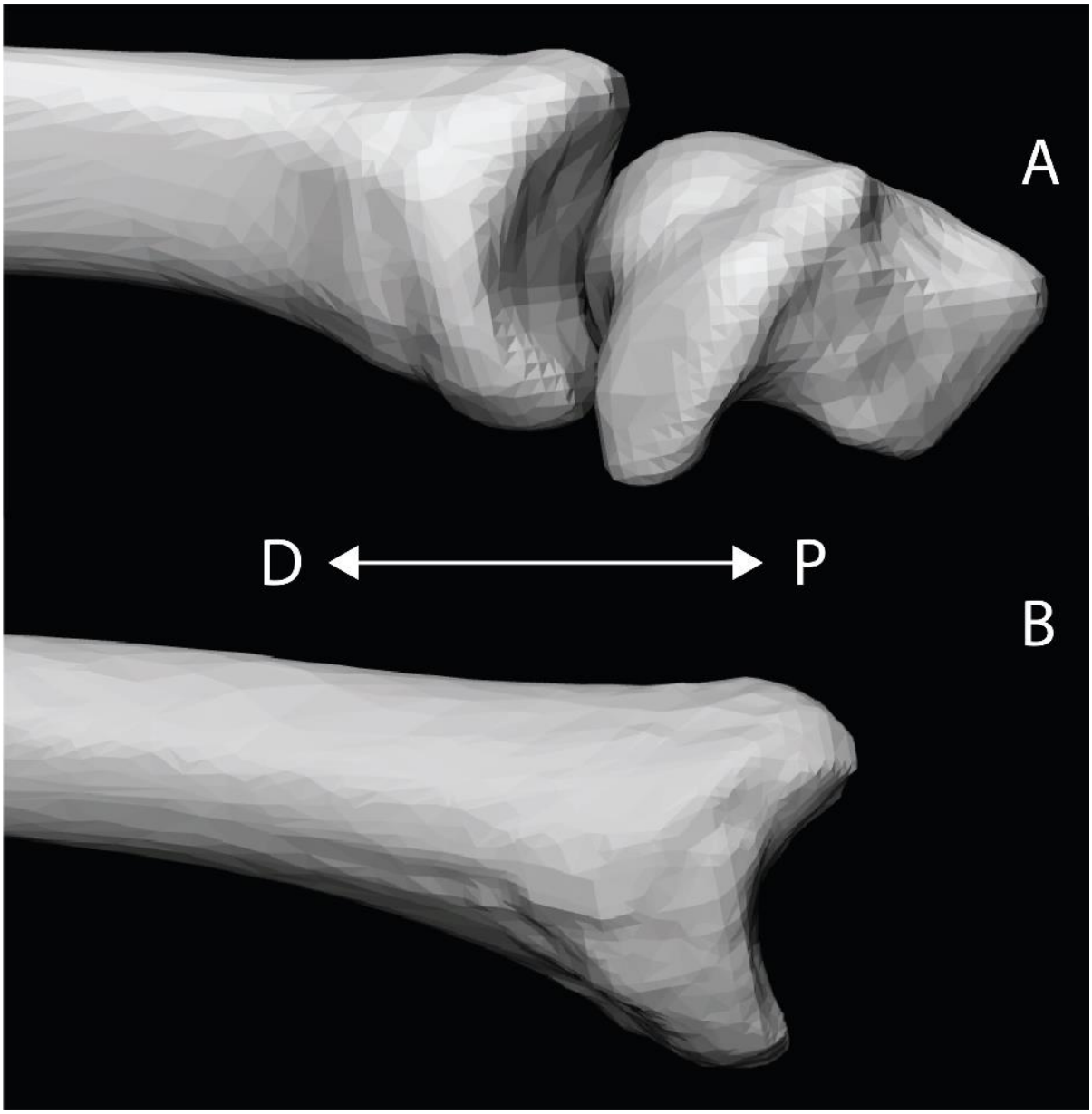

Figure 4: Gibbon morphology of the TMC. (**A**) Radial view of the TMC joint (G3). A relatively large socket of the MC1 in comparison to the smaller trapezial ball, the difference in congruency between dorsopalmar and radioulnar, and the volar and dorsal beak (**B**) ulnar view of the more extreme dorsal beak in G6. **D** = distal, **P** = proximal.

Interpretation of stress distribution on the articular surface of the trapezium

In gibbons, the estimated the resulting stress patterns correspond relatively well to the expected patterns in particular during the *powerL, powerLE* and *powerS*. We do, however, find some deviating patterns which may be related to the ball-and-socket joint morphology. Most notably, all cases of *pinch* do not only include the expected loading of the palmar aspect of the articular surface, but they also show loading on the dorsal aspect. This pattern, where the load is distributed along a large portion of the facet in the dorsopalmar plane, but only along a fraction of the facet in the radioulnar plane, occurs in other grasps as well but is not classified as a diverging pattern. This dorsopalmar loading pattern originates from the relatively large MC1 socket with respect to the ball of the MC1, in combination with the difference in joint congruency in the dorsopalmar plane and the radioulnar plane. The joint is more congruent in the former, terminating at both the dorsal and palmar periphery in a morphology that is similar to the volar (palmar) beak in humans (**Fig. 4a**). This causes the joint to maintain contact dorsopalmarly, while radioulnarly the curvature flattens out towards the periphery, keeping only a fraction of the surface in contact. The prominent dorsal 'beak' in one specimen (G6) (**Fig. 4b**) also explains the marked dorsoulnar loading that occurs during *powerL*.

Overall, the stress distributions in the macaque are highly similar in all five grasps, which might be due to high joint congruency and mechanical constraints. Our previous research (**Chapter 3**) already showed that the range of motion of the MC1 is severely limited in the macaque TMC joint by hard and soft tissue constraints. We suggest that these constraints also restrict the variability in loading regimes, causing the joint the be loaded similarly despite using different grasps.

Trapezial internal strain

In three out of four tested gibbons the strain distribution varies between grasps. This is most likely due to the wide variety in the applied loads. The ball and socket morphology requires the trapezial 'ball' internal architecture to withstand loading regimes with potentially over 180 degrees of force vector orientations, in both the dorsopalmar and radioulnar plane. This situation is different from the hip ball-and-socket joint. Despite large variations in loading occurring during various activities and movements of the hip, the overall most important load vectors are relatively unidirectional as a result of the gravitational component (Bergmann *et al.*, 2016). While the experienced loading regimes are multidirectional in the gibbon trapezium, the loading of a relatively flat, saddle-shaped TMC joint, as seen in macaques, is mostly unidirectional (distoproximal). Consequently,

the resultant force vector in most load cases will have a relatively high-magnitude component in parallel to the axial axis. Bone adaptation will be more anisotropic in response to unidirectional habitual loading patterns, while bone that is subjected to varied loading patterns will be more isotropic and present a more variable architecture.

Overall, the gibbon trapezium appears to be loaded multi-directionally over different grasps. The internal trabecular architecture diverts these patterns in varying ways, even across specimens. This is reflected in the differences in external trapezial morphology (**Fig. 3**, 3D view), and can also be expected from the internal architecture. Yet the wide variety in loading regimes resulting from the tested grasps is also more likely to reflect adaptation to individual preferences in grasps.

In the macaque, the distribution of strain occurs similarly between all five grasps. From heatmap visualisations we see increased strain values towards the proximoulnar articulation in the palmar aspect of the trapezium, similar to that seen in bonobos (**Chapter 4**). However, unlike bonobos, we see strain dissipation to the radial side of the trapezium (**Fig. 3**) in macaques. This may be related to the prepollex bone that is situated proximal and radial to the trapezium (**Fig. 5**). The macaque prepollex is relatively large when compared to that of gibbons and bonobos, while in humans, a prepollex is usually absent (Le Minor, 1994). The prepollex in macaques may function as a radial connection for load transference to the more proximal scaphoid.

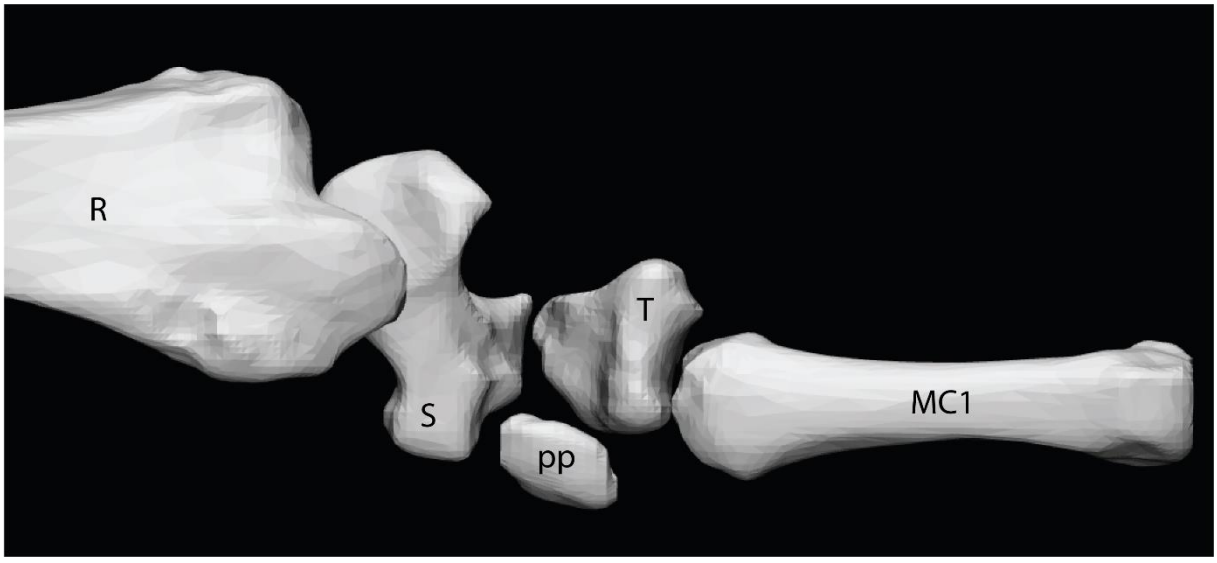

Figure 5: Dorsal view of the macaque wrist's radial ray: radius (**R**) with the relatively large prepollex (**pp**), and the TMC joint comprising the trapezium (**T**) and **MC1**, the proximal connection to the scaphoid (**S**), but also the radial connection via the **pp**.

Critical considerations

The assumptions made about the thickness and uniformity of the cartilage layer are expected to have an impact on the stress distributions calculated by the FE mode, influencing not only the resulting stress pattern itself but likely also the terminating position of the model. Specimen-specific cartilage layer information would likely increase the efficacy of the model optimiser. This would more accurately simulate the MC1 terminating position, and the estimated loading patterns. Thanks to the modular nature of the workflow, cartilage information can be included in the model when it becomes available.

The mean and maximum strain values encountered were 9.68 με ± 6.29 με and 125.34 με in gibbons, and 9.26 με ± 1.93 and 46.44 με in macaques. These values are typically associated with bone that is in a state disuse and resorption (< -200 με). As these bones are not likely to be in a state of resorption, other factors need to be taken under consideration. First, the 2D static model based estimation of the applied force may be an underestimation of the actual forces that drive adaptation. This could be due to the fact that we modelled relatively passive functional strains, while bone functional adaptation takes place in response to more intensive activities (Lanyon and Smith, 1970; Burr *et al.*, 1996; Fritton, McLeod and Rubin, 2000; Yang, Brüggemann and Rittweger, 2011). To gain a better understanding of the forces involved in such activities, we suggest to use joint forces obtained from musculoskeletal modelling in the future. Second, the bone material properties, and in particular the Young's modulus we used in the simulations, may be an overestimation of the actual material properties which remain unknown for these species. 18.0 GPa is at the high end for trabecular bone, as values as low as 2.1 GPa have been reported in humans alone (Busse *et al.*, 2009). A correct assessment of bone material properties for gibbons and macaques is expected to greatly improve the accuracy of the trapezial strain estimations. For this study, parameters based on human data were used. This is likely a good approximation, as cortical elastic properties of the rhesus macaques mandible have been shown to be similar to humans (Dechow, Panagiotopoulou and Gharpure, 2017), however, elastic properties of rhesus macaque craniofacial cortical bone were shown to vary between functional areas, some differing from humans (Wang and Dechow, 2006).

Conclusions

This study provides a proof of concept for the application of an integrated FE-μFE workflow to investigate joint stress distributions on both the macro and the micro level. We studied the stress distribution patterns on the articular surface of the trapezium during five functional grasps in gibbons and macaques, as well as the subsequent effect of the loading regimes on the strain distribution in the trapezium. We conclude that the stress distribution on the trapezial ball of the gibbon TMC joint varies widely across different types of grasping, and that the distribution of strain within the trapezium is highly different between grasps. Yet, the gibbon trapezium seems adapted to withstand the multidirectional loading regimes encountered in these grasps. We further conclude that the macaque TMC joint is a constrained joint, showing similar articular stress patterns regardless of the executed grasp type. Consequently, the strain distribution within the trapezium occurs in a similar way between grasps, possibly even employing the relatively large prepollex bone to facilitate strain distribution through a radial chain of load transference

Acknowledgments

The authors are grateful to Georg Hantke of the National Museum of Scotland (NMS), Edinburgh, Scotland, Pieter Cornillie of Ghent University, campus Merelbeke, Belgium, Koen Nelissen of Pakawi Park, Olmen, Belgium, François Druelle of the Zoological and Botanical Park of Mulhouse, France, Robby Van der Velden of the University of Leuven, campus Gasthuisberg, Leuven, Belgium, and Jeroen Stevens of Zoo Antwerp, Belgium for granting us access to this unique sample of primate specimens. We thanks Maarten Vanneste, dr. Ted Yeung, Nynke Rooks, and Mousa Kazemi for respective roles in the development of the FE-μFE approach. We thank Marie Vanhoof for her overall assistance and support. We furthermore extend our gratitude to Dr Olivier Vanovermeire and Henk Lacaeyse at the Medical Imaging Department, AZ Groeninge (Kortrijk, Belgium) for providing access and technical support during the imaging procedures. This work was supported by the Swiss National Supercomputing Centre under project ID 841, and funded by the KU Leuven – the University of Leuven, Belgium (grant RQ1-D1114-C14/16/082)

Supplementary material

S1: Table of successful simulation RMS errors in mm for this study. **X** = unsuccessful simulation

RMSE (mm)	Pinch	PowerL	PowerLA	PowerLE	PowerS
G3	1.50	1.31	1.67	1.04	1.42
G4	0.68	X	0.9	0.78	0.87
G6[a]	0.71	0.86	0.67	X	0.96
G8	0.99	X	0.79	0.89	0.98
M3	0.74	0.86	0.68	0.89	0.97

References

Bentley, J. L. (1975) 'Multidimensional binary search trees used for associative searching', *Communications of the ACM*, 18(9), pp. 509–517. doi: 10.1145/361002.361007.

Bergmann, G. *et al.* (2016) 'Standardized Loads Acting in Hip Implants', *PLOS ONE*. Edited by M. A. Pérez, 11(5), p. e0155612. doi: 10.1371/journal.pone.0155612.

Biewener, A. A. (1993) 'Safety factors in bone strength', *Calcified Tissue International*, 53(S1), pp. S68–S74. doi: 10.1007/BF01673406.

Bradski, G. and Kaehler, A. (2000) 'OpenCV', *Dr. Dobb's journal of software tools*, 3.

Burkhart, T. A., Andrews, D. M. and Dunning, C. E. (2013) 'Finite element modeling mesh quality, energy balance and validation methods: A review with recommendations associated with the modeling of bone tissue', *Journal of Biomechanics*, 46(9), pp. 1477–1488. doi: 10.1016/j.jbiomech.2013.03.022.

Burr, D. B. *et al.* (1996) 'In vivo measurement of human tibial strains during vigorous activity', *Bone*, 18(5), pp. 405–410. doi: 10.1016/8756-3282(96)00028-2.

Busse, B. *et al.* (2009) 'Increased calcium content and inhomogeneity of mineralization render bone toughness in osteoporosis: Mineralization, morphology and biomechanics of human single trabeculae', *Bone*, 45(6), pp. 1034–1043. doi: 10.1016/j.bone.2009.08.002.

Carbone, L. *et al.* (2014) 'Gibbon genome and the fast karyotype evolution of small apes', *Nature*, 513(7517), pp. 195–201. doi: 10.1038/nature13679.

Christel, M. (1993) 'Grasping techniques and hand preferences in Hominoidea', in Preuschoft, H. and Chivers, D. J. (eds) *Hands of Primates*. Vienna: Springer Vienna, pp. 91–108. doi: 10.1007/978-3-7091-6914-8_7.

Cignoni, P. *et al.* (2008) 'MeshLab: an Open-Source Mesh Processing Tool', in *Eurographics Italian Chapter Conference*, pp. 129–136.

Cooney, W. P. *et al.* (1981) 'The kinesiology of the thumb trapeziometacarpal joint.', *The*

Journal of Bone & Joint Surgery, 63(9), pp. 1371–1381. doi: 10.2106/00004623-198163090-00002.

Cooney, W. P. and Chao, E. Y. (1977) 'Biomechanical analysis of static forces in the thumb during hand function.', *The Journal of bone and joint surgery. American volume*, 59(1), pp. 27–36.

Crast, J. *et al.* (2009) 'Dynamic in-hand movements in adult and young juvenile chimpanzees (Pan troglodytes)', *American Journal of Physical Anthropology*. Wiley-Blackwell, 138(3), pp. 274–285. doi: 10.1002/ajpa.20925.

Crisco, J. J. *et al.* (2015) 'In vivo kinematics of the trapeziometacarpal joint during thumb extension-flexion and abduction-adduction', *Journal of Hand Surgery*. Elsevier Inc, 40(2), pp. 289–296. doi: 10.1016/j.jhsa.2014.10.062.

D'Agostino, P. *et al.* (2017) 'In vivo kinematics of the thumb during flexion and adduction motion: Evidence for a screw-home mechanism', *Journal of Orthopaedic Research*, 35(7), pp. 1556–1564. doi: 10.1002/jor.23421.

Dechow, P. C., Panagiotopoulou, O. and Gharpure, P. (2017) 'Biomechanical implications of cortical elastic properties of the macaque mandible', *Zoology*, 124, pp. 3–12. doi: 10.1016/j.zool.2017.06.008.

Eriksen, E. F. (2010) 'Cellular mechanisms of bone remodeling', *Reviews in Endocrine and Metabolic Disorders*, 11(4), pp. 219–227. doi: 10.1007/s11154-010-9153-1.

Flaig, C. and Arbenz, P. (2011) 'A scalable memory efficient multigrid solver for micro-finite element analyses based on CT images', *Parallel Computing*, 37(12), pp. 846–854. doi: 10.1016/j.parco.2011.08.001.

Fragaszy, D. M. and Crast, J. (2016) 'Functions of the hand in primates', in *The evolution of the primate hand*. Springer, pp. 313–344.

Fritton, S. P., McLeod, K. J. and Rubin, C. T. (2000) 'Quantifying the strain history of bone: spatial uniformity and self-similarity of low-magnitude strains', *Journal of Biomechanics*, 33(3), pp. 317–325. doi: 10.1016/S0021-9290(99)00210-9.

Frost, H. M. (2003) 'Bone's mechanostat: A 2003 update', *The Anatomical Record*, 275A(2), pp. 1081–1101. doi: 10.1002/ar.a.10119.

Halilaj, E. *et al.* (2013) 'A thumb carpometacarpal joint coordinate system based on articular surface geometry', *Journal of Biomechanics*, 46(5), pp. 1031–1034. doi: 10.1016/j.jbiomech.2012.12.002.

Hayama, S., Chatani, K. and Nakatsukasa, M. (1994) 'The Digitigrade Hand and Terrestrial Adaptation in Japanese Macaques', *Anthropological Science*, 102(Supplement), pp. 115–125. doi: 10.1537/ase.102.Supplement_115.

Heurtebiese, X. and Thon, S. (2006) 'Discrete Tools for Virtual Sculpture', in *Proceedings of the First International Conference on Computer Graphics Theory and Applications*. SciTePress - Science and and Technology Publications, pp. 415–422. doi: 10.5220/0001354604150422.

van Horn, R. N. (1972) 'Structural Adaptations to Climbing in the Gibbon Hand', *American Anthropologist*, 74(3), pp. 326–334. doi: 10.1525/aa.1972.74.3.02a00050.

Hou, W. *et al.* (2018) 'An Advanced k Nearest Neighbor Classification Algorithm Based on KD-tree', in *2018 IEEE International Conference of Safety Produce Informatization (IICSPI)*. IEEE, pp. 902–905. doi: 10.1109/IICSPI.2018.8690508.

Huiskes, R. *et al.* (2000) 'Effects of mechanical forces on maintenance and adaptation of form in trabecular bone', *Nature*, 405(6787), pp. 704–706. doi: 10.1038/35015116.

Jakob, W. *et al.* (2015) 'Instant field-aligned meshes', *ACM Transactions on Graphics*, 34(6), pp. 1–15. doi: 10.1145/2816795.2818078.

Kabel, J. *et al.* (1999) 'The role of an effective isotropic tissue modulus in the elastic properties of cancellous bone', *Journal of Biomechanics*, 32(7), pp. 673–680. doi: 10.1016/S0021-9290(99)00045-7.

Kammel, K. R., El Bitar, Y. and Leber, E. H. (2021) *Posterior Shoulder Dislocations*, *StatPearls*.

Kivell, T. L. (2015) 'Evidence in hand: recent discoveries and the early evolution of human manual manipulation', *Philosophical Transactions of the Royal Society B: Biological Sciences*, 370(1682), p. 20150105. doi: 10.1098/rstb.2015.0105.

Kopperdahl, D. L. and Keaveny, T. M. (1998) 'Yield strain behavior of trabecular bone', *Journal of Biomechanics*, 31(7), pp. 601–608. doi: 10.1016/S0021-9290(98)00057-8.

Kumar, S. and Hedges, S. B. (1998) 'A molecular timescale for vertebrate evolution', *Nature*, 392(6679), pp. 917–920. doi: 10.1038/31927.

Ladd, A. J. C. *et al.* (1998) 'Finite-element modeling of trabecular bone: Comparison with mechanical testing and determination of tissue modulus', *Journal of Orthopaedic Research*, 16(5), pp. 622–628. doi: 10.1002/jor.1100160516.

Lanyon, L. E. and Smith, R. N. (1970) 'Bone strain in the tibia during normal quadrupedal locomotion', *Acta Orthopaedica Scandinavica*. Taylor & Francis, 41(3), pp. 238–248.

Larson, S. G. (2018) 'Nonhuman Primate Locomotion', *American Journal of Physical Anthropology*, 165(4), pp. 705–725. doi: 10.1002/ajpa.23368.

van Leeuwen, T. *et al.* (2018) 'Insights into the musculature of the bonobo hand', *Journal of Anatomy*, 233(3), pp. 328–340. doi: 10.1111/joa.12841.

van Leeuwen, T. *et al.* (2019) 'Mobility and structural constraints of the bonobo trapeziometacarpal joint', *Biological Journal of the Linnean Society*, 127(3), pp. 681–693. doi: 10.1093/biolinnean/bly162.

Lewiner, T. *et al.* (2003) 'Efficient Implementation of Marching Cubes' Cases with Topological Guarantees', *Journal of Graphics Tools*, 8(2), pp. 1–15. doi: 10.1080/10867651.2003.10487582.

Lewis, A. D. and Prongay, K. (2015) 'Basic Physiology of Macaca mulatta', in *The Nonhuman Primate in Nonclinical Drug Development and Safety Assessment*. Elsevier, pp. 87–113. doi: 10.1016/B978-0-12-417144-2.00006-8.

Maas, S. A. *et al.* (2012) 'FEBio: Finite Elements for Biomechanics', *Journal of Biomechanical Engineering*, 134(1), p. 011005. doi: 10.1115/1.4005694.

Macfarlane, N. B. W. and Graziano, M. S. A. (2009) 'Diversity of grip in Macaca mulatta',

Experimental Brain Research, 197(3), pp. 255–268. doi: 10.1007/s00221-009-1909-z.

Marzke, M. W. (1997) 'Precision grips, hand morphology, and tools', *American Journal of Physical Anthropology*, 102(1), pp. 91–110. doi: 10.1002/(SICI)1096-8644(199701)102:1<91::AID-AJPA8>3.0.CO;2-G.

Matsudaira, K. and Ishida, T. (2010) 'Phylogenetic relationships and divergence dates of the whole mitochondrial genome sequences among three gibbon genera', *Molecular Phylogenetics and Evolution*, 55(2), pp. 454–459. doi: 10.1016/j.ympev.2010.01.032.

Michilsens, F. *et al.* (2009) 'Functional anatomy of the gibbon forelimb: Adaptations to a brachiating lifestyle', *Journal of Anatomy*, 215(3), pp. 335–354. doi: 10.1111/j.1469-7580.2009.01109.x.

Le Minor, J. M. (1994) 'The Sesamoid Bone of Musculus abductor pollicis longus (Os radiale externum or Prepollex) in Primates', *Cells Tissues Organs*, 150(3), pp. 227–231. doi: 10.1159/000147623.

Napier, J. R. (1955) 'The form and function of the carpo-metacarpal joint of the thumb.', *Journal of anatomy*, 89(3), pp. 362–9.

Napier, J. R. (1956) 'The Prehensile Movements of the Human Hand', *The Journal of Bone and Joint Surgery. British volume*, 38-B(4), pp. 902–913. doi: 10.1302/0301-620X.38B4.902.

Napier, J. R. and Napier, P. H. (1967) : *A Handbook of Living Primates: Morphology, Ecology and Behaviour of Nonhuman Primates.*, *American Anthropologist*. Academic P.

Perelman, P. *et al.* (2011) 'A Molecular Phylogeny of Living Primates', *PLoS Genetics*. Edited by J. Brosius, 7(3), p. e1001342. doi: 10.1371/journal.pgen.1001342.

Rafferty, K. L. (1990) *The Functional and Phylogenetic Significance of the Carpometacarpal Joint of the Thumb in Anthropoid Primates*. New York University.

Rho, J. Y., Ashman, R. B. and Turner, C. H. (1993) 'Young's modulus of trabecular and cortical bone material: Ultrasonic and microtensile measurements', *Journal of Biomechanics*, 26(2), pp. 111–119. doi: 10.1016/0021-9290(93)90042-D.

Roos, C. and Zinner, D. (2015) 'Diversity and Evolutionary History of Macaques with Special Focus on Macaca mulatta and Macaca fascicularis', in *The Nonhuman Primate in Nonclinical Drug Development and Safety Assessment*. Elsevier, pp. 3–16. doi: 10.1016/B978-0-12-417144-2.00001-9.

Rumbaugh, D. M. (1976) 'Suspensory behavior, locomotion, and other behaviors of captive gibbons, Gibbon and Siamang, a series of volumes on Lesser apes, vol. 4'. Karger, Basel, 316p.

Samuel, D. S. *et al.* (2018) 'Hand pressures during arboreal locomotion in captive bonobos (Pan paniscus)', *The Journal of Experimental Biology*, 221(8), p. jeb170910. doi: 10.1242/jeb.170910.

Schneider, M. T. Y. *et al.* (2017) 'Trapeziometacarpal joint contact varies between men and women during three isometric functional tasks', *Medical Engineering & Physics*, 50, pp. 43–49. doi: 10.1016/j.medengphy.2017.09.002.

Tomaszewski, P. K. *et al.* (2010) 'A Comparative Finite-Element Analysis of Bone Failure

and Load Transfer of Osseointegrated Prostheses Fixations', *Annals of Biomedical Engineering*, 38(7), pp. 2418–2427. doi: 10.1007/s10439-010-9966-9.

Vanhoof, M. J. M. *et al.* (2020) 'The forearm and hand musculature of semi-terrestrial rhesus macaques (Macaca mulatta) and arboreal gibbons (fam . Hylobatidae). Part II. Quantitative analysis', *Journal of Anatomy*, p. joa.13314. doi: 10.1111/joa.13314.

Vanhoof, M. J. M., van Leeuwen, T. and Vereecke, E. E. (2020) 'The forearm and hand musculature of semi-terrestrial rhesus macaques (Macaca mulatta) and arboreal gibbons (Fam. Hylobatidae). Part I. Description and comparison of the muscle configuration', *Journal of Anatomy*. John Wiley & Sons, Ltd, n/a(n/a). doi: 10.1111/joa.13222.

Wang, Q. and Dechow, P. C. (2006) 'Elastic properties of external cortical bone in the craniofacial skeleton of the rhesus monkey', *American Journal of Physical Anthropology*, 131(3), pp. 402–415. doi: 10.1002/ajpa.20438.

Wirtz, D. C. *et al.* (2000) 'Critical evaluation of known bone material properties to realize anisotropic FE-simulation of the proximal femur', *Journal of Biomechanics*, 33(10), pp. 1325–1330. doi: 10.1016/S0021-9290(00)00069-5.

Wolfe, S. W. *et al.* (2006) 'The Dart-Throwing Motion of the Wrist: Is It Unique to Humans?', *Journal of Hand Surgery*, 31(9), pp. 1429–1437. doi: 10.1016/j.jhsa.2006.08.010.

Yang, P., Brüggemann, G.-P. and Rittweger, J. (2011) 'What do we currently know from in vivo bone strain measurements in humans?', *Journal of Musculoskeletal and Neuronal Interactions*. International Society of Musculoskeletal and Neuronal Interactions, 11(1), pp. 8–20.

Zhang, J. (2020) 'GIAS2 (Geometry Image-Analysis Statistics)'. Available at: https://bitbucket.org/jangle/gias2/downloads/.

General Discussion

The overarching aim of this dissertation is to contribute to our understanding of the evolutionary relationship between form and function in the primate thumb. To that end I have used broad-to-detailed, multi-levelled studies of functional morphology and biomechanics of the thumb in three non-human primate taxa of close phylogenetic relationship and with different locomotor repertoires yet high manual dexterity. The project yields detailed morphological insights for primate taxa that are underrepresented in the literature. I shed light on the mechanics of the TMC joint with respect to different hand functionalities, and the implications for functional adaptation of the thumb in these taxa.

Findings and conclusions per part

Findings and conclusions of Part 1: Musculature of the forearm, hand, and thumb

The findings in this part support the hypothesis that the thumb musculature of the bonobo, gibbon, and macaque is well developed and shows morphological differences that can be related to their specific locomotor mode. I found differences in the relative force generating capacities of different functional muscle groups in addition to the specific morphology of each group.

The comparative anatomical analyses of primate forelimb morphology were done on multiple levels. As part of this thesis, a complete quantitative and qualitative documentation of the broad forelimb muscular anatomy of eight bonobos (*Pan paniscus*), one chimpanzee (*Pan troglodytes*), and one human was provided, while the same data on eight gibbons (fam. *Hylobatidae*) and seven rhesus macaques (*Macaca mulatta*) was documented in the context of another PhD thesis (Vanhoof *et al.*, 2020; Vanhoof, van Leeuwen and Vereecke, 2020). Further detailed analyses of the thenar and external thumb muscles were performed in these specimens.

The overall configuration of forelimb muscle morphology in bonobos, gibbons, and macaques is highly similar, and is comparable to that of humans. I found a high degree of intra-specific variation, in particular in the bonobo sample, which may be related to mild selective pressure and may indicate evolutionary stasis (Diogo, Molnar and Wood, 2017). Gibbons also show some intra-specific variation, in particular in the intermediate intrinsic hand musculature where both bonobos and gibbons display variable amounts of fusion. Macaques do not display such intraspecific variety, possibly indicating that the present configuration is optimized for positioning during palmigrade and digitigrade quadrupedal

gaits. Yet this may also be refuted due to sample bias as the amount of specimens was limited and originated from the same institution. The main differences in the forelimb musculature are found not in the configuration of the muscles, but in the parameters of the different functional groups. Force generating capacity ratios in these groups likely reflect differences in locomotion. All three primate taxa show highly developed flexors and rotators when compared to humans. In gibbons (Vanhoof *et al.*, 2020; Vanhoof, van Leeuwen and Vereecke, 2020), this especially concerns the digital flexors and the large force-generating capacity of the elbow flexors and *m. biceps brachii*, which are related to brachiation (Michilsens *et al.*, 2010). Macaques, in contrast, show a relatively well developed *m. triceps brachii* in addition to the particularly well developed wrist flexors, which appear to be related to their quadrupedal gait mechanics (Manter, 1938; Demes *et al.*, 1998).

Humans in comparison, have proportionally large forearm extensors which may be related to tool making and use (Williams, Gordon and Richmond, 2010). A highly relevant difference between the studied primate specimens and humans is the degree of functional coupling between muscles. Individual muscles in bonobos, gibbons, and macaques are more often coupled, either by muscle belly fusion or connections between tendons, compared to humans. This results in either co-contraction of the bellies, or at least concerted action between structures that in humans can be individually operated. Such coupling is found throughout the forelimb, but in particularly in the flexors of the first and second digit. Marzke and colleagues reported the effects of this during muscle activations in the chimpanzee, describing it as secondary muscle functions (Marzke *et al.*, 1998; Mary W Marzke *et al.*, 1999). We conclude that this increased muscle individualisation in the human forelimb and hand plays a key role in the high manual dexterity found in humans.

Functional coupling is also prevalent when investigating the detailed anatomy of the thumb. Bonobos, gibbons, and macaques have comparatively less individualisation in the thenar muscles. Bonobos and macaques fully lack a separation between the deep and superficial short thumb flexor (*m. flexor pollicis brevis*). No individual long thumb flexor exists in bonobos, gibbons, and macaques (*m. flexor pollicis longus*), instead it is part of the deep digital flexor (*m. flexor digitorum profundus*). The short thumb extensor (*m. extensor pollicis brevis*) is lacking in all non-human primates. The ratio of force generating capacity in the thenar muscles with respect to the rest of the intrinsic muscles is high in humans, in particular when compared to the ratio found in bonobos. However, capability for force generation within the TMC joint was calculated to be high in bonobos, mostly due to the geometry of the TMC joint articular surfaces rather than differences in PCSA. A

similar effect was reported when calculating muscle torque in chimpanzees in comparison to humans, where moment arms were the main defining factor (Marzke *et al.*, 1999). In bonobos, the intermediate muscles have a particularly high PCSA, yet the thenar musculature is also strongly developed. The intra-articular pressure in the TMC joint as a result of contraction of the thenar muscles in bonobos is comparable with that of humans. The relatively high PCSA of the bonobo intermediate intrinsic muscles may be related to their function of adducting the mid-hand under the compressive pressures on the distal metacarpals during knuckle-walking (Wunderlich and Jungers, 2009). I conclude that bonobos, gibbons, and macaques possess a well-developed thumb musculature capable of considerable force generation, while at the same type presenting a higher degree of functional coupling compared to humans.

Findings and conclusions of Part 2: Form and function of the TMC joint

In Part 2, I documented the TMC joint morphology by performing detailed dissections of the TMC joint to document the surrounding ligament tissue and by analysing digital CT datasets of the hand and thumb of five bonobos, eight gibbons, and seven macaques. This was compared to datasets of human volunteers (Kerkhof *et al.*, 2018). TMC joint congruency was assessed by calculating surface curvatures as well as the persistence of this curvature along the reciprocal articular facets of the TMC joint, in combination with visual (mesh based and FE joint contact modelling) assessment of the morphology to determine joint congruency. I assessed TMC joint function through kinematic analyses to determine the basic capabilities of the TMC joint present in bonobos, gibbons, and macaques.

Morphology of the TMC joint

The TMC joint morphology of bonobos and macaques is saddle-shaped, but there are striking differences between them. The bonobo TMC joint is highly similar to that of humans, which itself functions like a universal joint (Cooney and Chao, 1977). In bonobos, the joint is relatively incongruent and joint surface curvatures are maintained sufficiently well, yet during flexion its mobility is restricted palmarly due to interaction between trapezium and the volar beak of the MC1. The shape corresponds with that reported in the chimpanzee (Rafferty, 1990), and the low congruence is likely to allow for axial rotation of the thumb, and thus opposition (Napier, 1955). The location and orientation of the trapezium within the carpal complex was also shown to be similar to humans. This orientation has been shown to be different between humans and chimpanzees (Sarmiento, 1994), and brings the trapezium more in line with the radio-ulnar plane to accommodate

larger loads on the palmar aspect (Lewis, 1977; Tocheri *et al.*, 2005; Drapeau, 2015). I furthermore found a broad range of morphological variation particularly at the periphery of the articular facet, ranging from indentures on the outer facet to protrusions and asymmetries on the articular periphery. Yet, none of these morphologies were consistently present in the specimens. The surrounding ligament structure is well developed and highly similar to that of humans. The main deviation is the prominence of the palmarly situated anterior oblique ligament (AOL), compared to that of the dorsal ligaments (POL and DRL), a situation which is reversed in humans as the dorsal ligaments play a significant role in TMC joint stability in humans (Bettinger *et al.*, 1999; D'Agostino *et al.*, 2014). Furthermore, where the dorsoradial ligament (DRL) in humans is the dominant dorsal ligament, in bonobos the posterior oblique ligament (POL) is more developed than the DRL. The DRL is involved in withstanding dorsal subluxation at the TMC joint during movements where the thumb is not extended, but it also tightens during thumb flexion, preventing pronation and reinforcing thumb opposition (Bettinger *et al.*, 1999). In contrast, the POL is more involved in reinforcing the TMC joint during abduction, opposition, and supination (Bettinger *et al.*, 1999), a combination which is relevant in wide power grips (Napier, 1955). Comparatively, it appears that the human dorsal ligamenture is geared more towards stabilizing positions where the thumb is opposed and closer to the palm, such as during in-hand manipulation, while the dominating POL appears to be geared towards wide power grasps, relevant in climbing. The overall morphology of the bonobo TMC joint show the possibility for considerable joint mobility in terms of curvature and congruency, but also a combination of the inherent soft- and hard-tissue mechanisms for stability.

The macaque TMC joint morphology, in contrast, invariably shows a hybrid between the saddle-shaped morphology and a planar arthrodial joint found in the other carpometacarpal joints in hominids (Selby, Simpson and Lovejoy, 2016). The surface curvature, although concavo-convex with considerable curvature at the centre of the facet, progressively flattens out towards the periphery. In addition, the joint shows a high degree of congruency in particular in the radioulnar plane, while the dorsovolar plane allows for more clearance. Previous analyses of primate TMC joint articular surface curvature do not mention the declining curvature towards the periphery, and they indicate that cercopithecids, in general, show lower congruency in the radioulnar plane (Rafferty, 1990). Yet, a more shallow and congruent type of concavo-convex TMC joint morphology is present in New World Monkeys (parvorder *Platyrrhini*), suggesting that it is more primitive version of the less congruent saddle-shaped TMC joint found in bonobos and

humans (Rafferty, 1990). And, although not all of platyrrhine species are capable of advanced manual tasks like catarrhines, capuchin monkeys in the genus *Cebus* in particular are highly dexterous and capable of tool use (Parker and Gibson, 1977).

The relatively flat TMC joint in macaques may be similarly geared towards resisting angular movement when the thumb is loaded during palmigrade/digitigrade locomotion, as a flat, planar joint does (Ayhan and Ayhan, 2020). While the lower joint congruency in the dorsovolar plane may allow for some axial rotation, a planar joint type does allow for sliding and axial rotation. Furthermore, where a fully planar morphology will leave the joint susceptible to sheer forces, this may be less the case in the macaque TMC joint as the overall joint retains some of its saddle-shape to prevent translational sliding. Translation of the joint will be furthermore contained by the well-developed ligament structure in the macaque. The configuration is again highly similar to that of humans and bonobos. As in humans, the dorsal ligaments are well developed in macaques, however, similar to bonobos, the POL is the more dominant dorsal ligament. Again, this may be related to climbing, but in macaques the abducted thumb can also benefit from the stabilisation that a well-developed POL offers during digitigrade terrestrial locomotion, when the thumb may also be loaded in an abducted position. The macaque does present an ulnar collateral ligament (UCL), that in humans not only resists MC1 extension, but also abduction and pronation (Bettinger *et al.*, 1999). This is highly relevant for withstanding loads involved in positioning the thumb for digitigrade locomotion, but also for wide power grasps. Overall, the macaque TMC joint morphology shows little intraspecific variation in the sample. We expected the morphology to represent a shallow saddle-shaped morphology, however, I found that the centre of the joint is actually more curved than in the other primate taxa, yet the facet flattens out towards the periphery. This shape appears to reflect a more primitive morphology of the saddle-shaped joint that is geared towards restriction of angular movement and joint stability.

The gibbon ball-and-socket morphology shows a wide range of variation within the represented species in this study. In particular the shape, orientation, and robustness of the radial tubercle is highly variable. Expectedly, bone sizes vary as the gibbon sample included differently sized species (5kg – 12 kg body mass (Fleagle, 2013)), but even with respect to bone size the radii of articular curvatures are dissimilar. The joint flattens out particularly towards the radial periphery where the curvature is lower. The trapezium's ball is largely free of bony elements that would restrict the freedom that a ball-and-socket joint provides, with the exception of the variably shaped radial tubercle, which is likely to interfere during abducted-flexion, and the MC2 which limits MC1 adduction. The MC1

socket is relatively large and in the dorsopalmar plane the curvature is maintained towards the substantial dorsal and palmar 'beaks' (**Chapter 6**, **Fig. 4**), while the socket flattens out towards the periphery in the radioulnar plane. There are no indications of inherent restrictions preventing axial rotation or subluxation of the MC1. Despite this, the ligament structure in gibbons is markedly similar to that of humans, bonobos, and macaques. Yet, where humans have relatively well-developed dorsal ligaments, and both bonobos and macaques each have their own way of reinforcing the palmar structure, the gibbon has no particularly dominant ligament. Despite the dominant POL over the DRL, the overall ligament structure of gibbons appears relatively frail considering the low intrinsic stability of the ball-and-socket joint.

I conclude that the TMC joint morphologies correspond with the expectations related to locomotion and manipulation in each of these taxa. The macaque does indeed display a restricted and reinforced joint, the gibbon TMC joint is highly unrestricted, and the bonobo joint shows indications of both mobile and restrictive capabilities. I furthermore conclude that the ligament structure is highly similar not only between these non-human primates, but to modern humans as well. In bonobos, the dorsally located POL does appear to be more strongly developed than the DRL, which might be a structural requirement for the involvement of the hand in vertical climbing. However, such a strongly developed POL is not seen in macaques and gibbons.

Function of the TMC joint

The saddle-shaped TMC joint of bonobos and macaques is the physiological equivalent of a universal joint. This type of joint allows for two degrees of freedom, restricting axial rotation. In the thumb this would amount to extension-flexion and adduction-abduction being allowed, while axial rotation of the MC1 is restricted. This, however, is only the case if the joint is fully congruent. In the human TMC joint, this is not the case and axial rotation of the MC1 is possible, facilitating opposition of the thumb (Napier, 1955; Rafferty, 1990). When the joint is loaded, congruency increases and the joint is stabilized in the current position. The human TMC joint, therefore, offers great mobility during thumb extension-flexion and adduction-abduction and also allows for thumb opposition, while offering additional stability in particular when loaded.

The TMC joint mechanics of bonobos appear highly similar to that of humans. Bonobos are capable of comparable ranges of motion during thumb adduction-abduction, despite the difference in joint curvature when compared to humans. It appears that joint congruency in this plane is similar in both taxa. The resemblance between the bonobo and

human joint is further supported by the corresponding degree of axial rotation present in the joint during thumb flexion-extension and abduction-adduction. The main difference between humans and bonobos is found during thumb extension. The bonobo TMC joint allows for a similar level of MC1 flexion as in humans, a movement restricted by the palmar beak of the MC1 (Rafferty, 1990). MC1 extension is much more restricted in bonobos compared to modern humans. I was unable to find any mechanical explanation in the TMC joint bone morphology that explains this restriction, but the relative prominence of the volar ligament described above is likely to be involved. I conclude that the bonobo TMC joint capabilities correspond to our expectations, as the joint is capable of ranges of motion on par with that of humans, but the restriction during thumb extension does appear to be a compromise for reinforcement during wide power grasps.

Compared to the bonobo and human TMC joint, the macaque TMC joint is severely restricted, both in extension-flexion and adduction-abduction. The flattened out periphery of the articular facet counteracts the saddle-shape functionality that allows angular movement in the extension-flexion and adduction-abduction plane. However, the flattening of the reciprocal concavo-convex curvatures also removes the restriction to MC1 axial rotation that occurs in a fully congruent saddle-shaped joint. The progressively flattened reciprocal surface peripheries are allowed to slide with respect to each other, and as a result the macaque TMC joint does allow for large axial rotation. Furthermore, in order to achieve thumb opposition (Macfarlane and Graziano, 2009), MC1 axial rotation is combined with flexion at the more distal metacarpophalangeal and interphalangeal joints rather than at the TMC joint as is the case in humans. Due to this, the relatively long thumb (with respect to finger length) in macaques is likely key to achieve opposition (Almécija, Smaers and Jungers, 2015). I conclude that the macaque TMC joint is highly restricted as hypothesized. However, contrary to my hypotheses of a congruent and shallow saddle-shaped TMC joint, the macaque joint flattens out towards the periphery, reversing the functionality of a true saddle-shaped joint, and stabilising against MC1 flexion-extension and adduction-abduction.

The gibbon TMC joint, on the other hand, is an example of extreme mobility. During flexion-extension it presents a similar range of motion to that of the human TMC joint. This is perhaps unsurprising as both joints are similarly convex in this plane. The terminal positions of the MC1 are ultimately restricted before overloading the volar and dorsal beaks (**Chapter 6**, **Fig. 4b**), which are shown to interact with the trapezium during MC1 flexion and extension respectively. In the radioulnar plane, however, the gibbon ball-and-socket morphology is truly unique as it offers a convex articular surface similar to that of

the dorsopalmar plane. During thumb adduction-abduction, the gibbon joint can achieve MC1 mobility of close to 50 degrees. The terminal position of the MC1 is ulnarly dictated by the presence of the MC2, while the edge of the trapezial ball limits maximal abduction. This position is, however, pushed slightly farther by the flattened out periphery of the MC1 socket on the radial side (**Chapter 6**, **Fig. 4a**). In contrast to a saddle-shaped joint, the gibbon's ball-and-socket TMC joint has no intrinsic articular features that prevent MC1 axial rotation, leaving the restriction of MC1 rotation in all planes to the soft-tissue.

Our findings in this part support the hypotheses that the TMC joint mobility is correlated to thumb usage during locomotion. The mobility and restriction of the bonobo, gibbon, and macaque TMC joint correspond with the expectations set for them based on their locomotor mode.

Findings and conclusions of Part 3: Trapezial morphology and stress/strain distribution

An integrated FE/μFE approach was provided for the analysis of TMC joint articular surface stress distributions, but also the further internal distribution of stress and strain within the trapezium bone resulting from this articular stress. This approach is based on CT and μCT imaging data, and includes a workflow of Python scripts, also usable for further customisation and application to other joints. The method was used to investigate the effects of joint function and morphology on joint stress and strain distribution in relation to bone functional adaptation. Furthermore, the high resolution μCT image stacks of the trapezium were used to reconstruct and assess the internal trabecular morphology in eight bonobos, eight gibbons, and seven macaques..

The integrated FE/μFE workflow

The first objective of Part 3 was the design and development of an integrated FE/μFE analysis workflow, where parametric models could be efficiently generated for different grasping positions in different individuals of one primate group. This approach allows for a comparative analysis of joint force distributions, as well as the study of internal stress/strain distribution within the skeletal elements of the TMC joint. The workflow was successful, and in this project worked particularly well for the bonobo, the main species involved in the development of the method. Despite the workflow working well for gibbons and macaques as well, unforeseen difficulties were encountered with the CT scanning resolution.

The main issue that prevents proper application of the current workflow to the smaller taxa relates to mesh quality and scanning resolution. All specimens in this project were scanned at a slice thickness of 0.625mm, which provides a sufficient resolution even in

gibbon and macaque for kinematic analyses and visualisation of the bone morphology. It does, however, present issues for FE analysis which specifically uses the reconstructed morphology from these scans to generate individual elements that need to be of sufficient resolution. In the case of macaque and gibbon, whose TMC joint is significantly smaller than that of bonobos, the smaller element size with respect to the slice thickness results in relatively low resolution when compared to the bonobo. This allows for less detail per voxel and causes small structures of bone that are close to one another to merge into one. This presents problems with segmentation and 3D reconstruction of the bone, which in turn affects mesh quality. Compromised meshes cause the FE model to erroneously terminate. Even if the mesh quality is sufficient for the model to successfully initiate, compromised meshes increase potential stress peaks, causing individual elements to collapse. This decreases the opportunity for successfully model termination, especially at higher loads. Furthermore, the process of generating individual FE and µFE models manually is labour intensive. The integrated workflow was developed with the intention to both optimize and automatize certain steps in this process, while also introducing the parametric factor to the meshes to efficiently generate and analyse stress distribution. Some of these steps prove to be sensitive to low mesh quality. In particular, the RBF fitting that is used to reshape the template mesh of the master individual to the morphology of the remaining specimens within the taxon, enhances mesh quality issues in the new morphologies. This causes the non-master meshes to present similarly compromised if not worse mesh quality, further decreasing the chance that these models terminate successfully. Moreover, even if the model runs successfully, the chance of anatomical misrepresentation increases, making the outcome of the simulations questionable.

While the CT scanning resolution used was insufficient for the FE/µFE workflow of the gibbon and macaque TMC joint, there are some options to use the current dataset for future work. While in situ rescanning of the same positions in the same gibbon and macaque specimens is impossible as they have already been dissected, two solutions exist within the current framework of the method. The first, and best solution, is to use the digitized µCT image stacks and downscale the resulting volumetric point clouds to a serviceable resolution. From here, surface meshes can be generated using marching cubes (Lewiner *et al.*, 2003), similarly as has been done within the µFE workflow to align CT and µCT meshes. This method can be used to generate higher resolution surface meshes of the trapezium and MC1, which can be registered onto the position of the original, compromised, meshes to be used for modelling instead. Some testing will be required to determine which resolution is sufficient to accurately represent the gibbon and macaque

morphology. However, just slightly increasing the resolution from the current CT resolution (0.625 mm) will likely be beneficial as this approach inherently circumvents the segmentation process, which at insufficient resolutions introduces problems to the articular surface mesh quality. Most of the Python infrastructure required for this approach is already present in the current workflow, yet additional mesh quality testing, regenerating and running all FE models is labour intensive. The second solution focuses on the sensitivity of the RBF to mesh imperfections. The solution here is to manually generate template meshes for all non-master individuals, eliminating the RBF procedure. However, this would not only lose the parametric nature between individual specimen meshes, it would also be highly inefficient as the generation of template meshes with delineated articular surfaces is incredibly labour intensive due to the less than optimized toolset available for this procedure (Instant Meshes was not developed with this purpose in mind). Even so, some scans may still present similar issues due to imperfections in the original mesh. While solution (2) is a theoretical solution to the problem, practically, I highly recommend prioritizing solution (1).

TMC joint stress distribution

Intra-articular stress distributions for the TMC joint were calculated from simulated load case scenarios based on five functional grasps. Predictions were made on where the articular stress would be situated on the facet based on each grasp (**Chapter 4**). Hypotheses regarding joint mobility and the influence of morphology were set within the context of those predictions. For instance, during a power grasp with the thumb abducted, the thumb is loaded in wide abduction and so loads are expected on the radial aspect of the articular facet. The general expectations for the gibbon are that due to the higher TMC joint mobility, the stress will be situated further radially on the articular surface. For macaques, the opposite holds true, as their restricted joint allows for small MC1 excursions only, so only a slight radial shift is expected. The influence of individual morphology was further analysed when deviating patterns occurred.

Bonobo and gibbon stress patterns correspond well to the predicted patterns, and the influence of joint mobility is clearly distinguishable. The gibbon TMC joint stress patterns show wide excursions that correspond with expected patterns for each position. The main morphological influences found in gibbons are related to the increased joint congruency in the dorsopalmar plane with respect to the radioulnar plane, also reported in literature (Rafferty, 1990). This particularly interferes with the expected pattern during *pinch*. Furthermore, the dorsal periphery of the MC1 articular facet, which in bonobos, macaques,

and humans is shaped like a ridge, is shaped similarly to the palmar morphology of the MC1 articulation, which is usually described as the volar beak. This 'dorsal beak' combined with the relatively large size of the MC1 socket cause circular stress imprints on the dorsal aspect of the trapezial facet. However, with respect to the more ulnarly expected pattern, the relatively centrally situated stress pattern during *powerLA* does show how the MC2, and likely the first dorsal interosseus muscle, prevent further adduction of the thumb. The wide disparity between grasp-associated stress patterns confirm our hypothesis that the gibbon joint is highly mobile and relatively unconstrained.

The bonobo stress patterns are more restricted when compared to gibbons, and the patterns are more ambiguous as overlap is present between grasps. However, stress patterns corresponding to the expected patterns for each grasp are encountered in most simulations. Furthermore, divergent patterns that correspond with additional bony interactions with the individual morphology rather than only the simulated grasp were also frequently present. These diverging patterns were not associated with bony interactions resulting from any specific anatomical structure, but rather different morphological variations per individual present at the periphery of TMC articular surface. The bonobo TMC joint stress patterns meet our expectations in that considerable mobility is allowed, but its movements are contained within a bony morphology that provides stability.

The macaque stress distribution patterns are highly similar between grasps. Stress peaks are observed in the same areas for each grasp, with only slight variations per grasp. I expected the macaque TMC joint to be restricted and thus show low variation in loading patterns. However, the resulting stress patterns not only confirm that the macaque TMC joint is highly restricted in mobility, but further demonstrate that the joint is loaded similarly regardless of thumb position.

Trapezium internal morphology

Using μCT imaging, I was also able to investigate the bone micro-architecture of the trapezium in macaques, gibbons and bonobos. All three primate groups show a combination of isotropic trabecular clusters combined with uniformly oriented bone struts, particularly towards the proximal and ulnar articulations with the carpal complex. However, striking intraspecific differences can be observed in the internal trapezial architecture of both gibbons and macaques. Differences are clearly present between individuals in the lumen size, trabecular size, and BV/TV, although I did not perform a quantification of the bone microstructure. In gibbons, the internal architecture in the

middle of the trapezium is of relatively low concentration and the trabeculae near the cortex seem to be more conserved.

A visual distinction can be made between internal trapezial morphologies of the two types of TMC joints investigated. The saddle-shaped morphologies of the bonobo and macaque are highly similar to each other in terms of how the trabeculae are situated within the architecture. The distribution of trabecular bone is relatively uniform, the lumen present within the structure are of similar absolute size between both bonobo and macaque, despite the difference in scale. The architecture is spongious yet the orientation of the trabeculae have an overall direction toward the distal, ulnar and proximal articular facets. The direction of the trabeculae converge from the proximal articulations to the distal TMC joint facet. In bonobos this directionality is mostly found in the distal, ulnar and proximal clusters, while the radial aspect and in particular within the radial tubercle the architecture is more sporadic. In macaques, an additional connection for load transference with the prepollex appears to be present at the radioproximal aspect of the trapezium, and the radial trabeculae are oriented heavily towards this location. In correspondence with this, the cortical bone is particularly thick at the ulnar articulation in both bonobos and macaques. Inn macaques, the radial cortical bone is also thicker, while this is not the case for bonobos. As such, the large prepollex, with respect to other taxa, may facilitate habitual loading during palmigrade/digitigrade locomotion. While proximal load transmission appears to be sufficient for loading regimes experienced in the thumb of knuckle-walkers, as loads in great apes are transmitted through the proximal articulation with the scaphoid (Tocheri *et al.*, 2005).

The ball-and-socket joint in gibbons has more unevenly sized lumen. The complete centre of the structure often shows few to no trabeculae, as most of the trabeculae are directly below the cortical bone. There is some directionality to the individual trabeculae, but they are few in number and seldom parallel to each other. The overall structure supports the cortical dome that forms the ball of the joint from the proximal articulations in a diverging manner rather than the converging orientations I report in the saddle-shaped morphology. This is likely due to the ball-facet being fully convex, while the saddle-shape is concavo-convex and much flatter in comparison, increasing the amount of potential angles the structure can be loaded from. I conclude that this overall divergent trabecular reinforcement of the distal articular facet is a response to a wide range of loading orientations, but may be insufficiently strong to handle large single pointed loads due to the lack of parallel trabeculae.

Trapezium internal stress distribution

I investigated if the trapezium bone in bonobos, gibbons, and macaques is functionally adapted to withstand the joint stresses involved in different types of grasping, and how the resulting strain is distributed across internal architecture.

Detailed μFE models were generated with both subject- and grasp-specific loading regimes to analyse the resulting stress distributions throughout the internal bone morphology of the trapezium. Maximum and mean internal trapezial strain were calculated and compared to bone yield strain values to test the hypothesis that the trapezium is adapted to different loading regimes associated with grasping in bonobos, gibbons, and macaques. Mean strain values were used as an indicator for effective strain distribution, and compared between grasps to test if the trapezium was able to withstand the loading regimes corresponding to each grasp similarly. I furthermore used 3D image stack visualisation of strain to assess how strain is distributed along the internal bony architecture, and test if strain is transmitted differently throughout the trapezium depending on the applied loading regime.

I showed that the loading regimes involved during grasping are safely distributed throughout the trapezium in all three taxa. Maximum strain values associated with risk of bone failure were not encountered unless the most lenient and vulnerable bone material properties were assumed. This does emphasize that accurate determination of bone material properties, and by extension trabecular bone structural dimensions, are highly relevant in the assessment of bone failure and functional adaptation. Our calculations show that the strain levels involved in the five simulated grasps amount to bone stimuli associated with low physical activity (Lanyon and Smith, 1970; Burr *et al.*, 1996; Fritton, McLeod and Rubin, 2000; Frost, 2003; Yang, Brüggemann and Rittweger, 2011). This appears to be an accurate representation of the input 2D modelled applied force, which was modelled from passive PCSA only (i.e. without active components such as velocity or linear momentum of bodyweight).

Mean strain levels are similar between grasps in all three taxa, indicating that none of the grasps lead to higher overall strain levels. Gibbons not only showed the largest variation in intra-articular stress distribution, as a result of their highly mobile thumb, but they also display strong variation in the internal distribution of strain in the trapezium. Both the bonobo and macaque show a highly similar strain transmission across the internal trapezial architecture. In bonobos, strain dissipates mainly through the ulnar articulation with the trapezoid bone. This directs the pressure towards the distal row of the carpal

complex, before being oriented towards the proximal row and the radius. In macaques, I did note indications of this ulnarly-directed dissipation of strain, but strain transmission appears to mainly occur through radioproximally oriented trabecular struts. This implies not only a more direct path of strain transmission to the radius via the scaphoid, but also shows an additional option for radial reinforcement through the exceptionally large prepollex.

The low variability of both strain distribution and mean strain in bonobos suggest that the saddle-shaped joint causes the stress to be relatively unidirectional, regardless of MC1 position. This, potentially, allows for a single adaptive strategy where strain is always transmitted predominantly towards the a specific articulation and may explain why the bonobo (and macaque) internal trabecular architectures appear relatively isotropic, while the gibbon does not. The ball-and-socket morphology of gibbons allows for a large range of motion of the MC1, yet also entails multidirectional loading. This prohibits the anisotropic trabecular reinforcement of the distal facet.

Main conclusions

The overall goal of this thesis was to investigate the form and function of the thumb in three primate taxa in relation to adaptation. I have studied the morphology of the hand and thumb, and biomechanics of the TMC joint in bonobos, gibbons, and macaques on multiple levels. The broad hypothesis for the form and function of the thumb in these taxa was centred around the varying demands of manual manipulation and taxon specific locomotor repertoires.

For the gibbon, which is characterised by a highly arboreal lifestyle, I expected morphological adaptations related to high mobility and low thumb loading, given that the thumb is not used during brachiation. This means a highly mobile thumb with little-to-no soft or hard tissue restrictions on the thumb joint, and a high variation in loading patterns. Due to the low habitual loading of the thumb, I also expected the trapezial microarchitecture to be less adapted to high loading. I did expect the thumb musculature to be well-developed to be able to perform advanced manual tasks.

For the macaque that subjects its TMC joint to loading, particularly in palmigrade quadrupedal locomotion, I expected that the TMC joint would be severely restricted by both soft and hard tissue. The range of motion of the MC1 was expected to be minimal, but sufficient to allow for movements related to manipulation, leading to low variation in

loading patterns. Furthermore, the thumb musculature was expected to be well-developed for the purpose of both manipulation and active stabilisation.

For the bonobo, I expected to find a compromise between the arboreal and terrestrial morphologies. Due to the bone morphology and passive soft-tissue the TMC joint was expected to be less restricted in bonobos than in macaques, yet not as mobile as in gibbons, especially due to the difference in joint morphology. I expected a high range of motion of the MC1, but lower than that of the gibbon. Although the thumb is not loaded in knuckle-walking, I did expect the bonobo TMC joint morphology to approximate the macaque morphology due to the involvement of the thumb in climbing.

Based on these expectations, I came to the following conclusions:

Adaptations towards locomotion are clearly present

Despite the clear morphological similarities between bonobos, gibbons and macaques, we do find differences, particularly in structure dimensions, that influence the functionality of the hand and thumb.

The brachiating gibbon

The gibbon thumb is incredibly mobile due to the ball-and-socket morphology of the TMC joint. This morphology not only come with more degrees of freedom when compared to the saddle-shaped joint in bonobos and macaques, but it is furthermore relatively unconstrained by bone morphology and the ligaments do not compensate for this lack of joint stability. The thumb musculature and TMC joint ligaments, however, are not underdeveloped. A well-developed thumb musculature is likely maintained to perform manual tasks, such as grasps and pinches, as well as the capability for in hand manipulation. The muscles and ligaments of the gibbon TMC joint are likely sufficient to provide stability during thumb use with little to moderate loading, but may present difficulties when higher external forces are involved. During brachiation, the digits are loaded in tension while the thumb is tucked out of the way and remains unloaded. Also during vertical climbing, loading on the thumb is likely limited as the gibbon has been shown to use its feet in concert with its hands to push up and away from the substrate (van Horn, 1972). This possibly shifts the loading of the hand from a compressive power grasp to a tensile hook grip. In such a case, the thumb is only involved as a grip stabilizing factor that carries only a fraction of the load, as has recently been reported in bonobo vertical climbing (Samuel *et al.*, 2018). Presumably, the thumb and TMC joint can have low structural reinforcement because the thumb is never subjected to high loads. I showed that the gibbon trapezium is capable of withstanding loads associated with moderate

intensity grasps. The large range of motion of the thumb permitted by the relatively unconstrained TMC joint, results in a highly variable intra-articular stress. Due to this, internal trapezial loads are multidirectional and a more isotropic trabecular architecture needs to be maintained.

I conclude that the gibbon thumb shows adaptations towards moderate thumb loading, such as dextrous manual tasks. Loading of the thumb during any type of locomotion is likely limited, and the entire TMC morphology seems to be geared towards providing high mobility. This high TMC joint mobility is beneficial to move the thumb out of the way during brachiation and appears crucial for manipulation.

The palmigrade/digitigrade macaque

The macaque thumb is highly restricted due to the flattening out at the periphery of the articular surface, as such reversing the universal joint functionality that the saddle-shaped joint normally provides. Such a joint theoretically allows for rotation in two perpendicular planes, which in the TMC joint correspond with MC1 flexion-extension and adduction-abduction, while axial rotation of the MC1 is restricted. The macaque TMC joint configuration, however, largely provides the opposite functionality. Flexion-extension and abduction-adduction are reduced to a minimum, while internal rotation is permitted due the relatively flat surface and dulled bony protrusions. Both the active and passive surrounding soft-tissue is well developed, and the presence of the ulnar collateral ligament (UCL) further reinforces the MC1. This joint stability is likely important during palmigrade locomotion and powerful abducted grasps. The macaque TMC joint is so heavily restricted in its mobility that the intra-articular stress patterns and loading regimes on the trapezium are largely similar regardless of grasp type. Consequently, the internal microarchitecture is adapted to sufficiently withstand the resulting unidirectional loads on the articular facet. The internal strain is distributed radially towards the scaphoid bone and the enlarged prepollex. In macaques, the mobility of the thumb required for grasping and manipulation is achieved by relying on the more distal metacarpophalangeal and interphalangeal joints, which compensate for the limited mobility of the TMC joint. These joints, however, are primarily hinge joints with a single degree of freedom. However, advanced manipulation tasks require thumb opposition. The permitted axial rotation of the MC1 may provide the rotary motion required to achieve thumb opposition, and the consequential manual dexterity, as the macaque is capable of power grasps and pinches (Macfarlane and Graziano, 2009). The relatively large thumb-to-index digit ratio is also crucial for the manipulative skills of the macaque.

I conclude that the macaque TMC joint shows adaptations towards loading during locomotion. The structural reinforcement of the joint appears to be geared specifically for locomotion, as the mobility required for powerful grasps originates from the distal, less restricted joints. As such, locomotion and manipulation are integrated in the macaque thumb mostly by separating the two functionalities and dedicating the TMC joint to stability and the distal joints to mobility.

The knuckle-walking bonobo

The bonobo thumb is a compromise between the configuration of the arboreal and terrestrial TMC joints described above. The joint is saddle-shaped, like in humans, and both the active and passive soft-tissue morphology is well-developed. The dominant ligament in bonobos is the anterior oblique ligament (AOL), which is particularly relevant to limit thumb extension. The bonobo TMC joint allows for relatively large ranges of motion, on par with that of humans, with the exception of thumb extension. I suspect that allowing for a hyperextended thumb during any grasp involving the carrying of body weight-scale loads may present significant risks of dorsal subluxation, as a similar palmar ligament dominance is observed with the UCL in the macaque. However, where the macaque TMC joint is engaged in terrestrial locomotion, the bonobo thumb is not during knuckle-walking. Moreover, the bonobo thumb is also minimally loaded during vertical locomotion (Samuel *et al.*, 2018), likely due to the use of the hindlimbs to create suspensory-like loading of the fingers in a more arboreal fashion.

The bonobo TMC joint in not fully congruent. This appears to be common in the primate TMC joint, as it allows for axial rotation of the MC1 and the related opposition of the thumb (Napier, 1955; Rafferty, 1990). The stability of the bonobo thumb is, however, similar to that seen in humans in that it can be reinforced by muscle activation. The similarities between the bonobo and human TMC joint are further supported by the observation that intra-articular stress patterns in the bonobo TMC joint correspond well to those of the human TMC joint during similar grasps (Schneider *et al.*, 2017). With respect to gibbons and macaques, the mobility of the bonobo TMC joint falls in between the two, showing moderate MC1 excursions. The saddle-shaped morphology of the distal articular facet of the trapezium, however, appears to have a similar function as in macaques in ensuring that applied loading regimes are applied unidirectionally. The resulting strain dissipates through the ulnarly-oriented trabecular struts as well as the cortical bone and is transmitted mostly through the ulnar articulation towards the

trapezoid. The relatively isotropic internal architecture of the bonobo trapezium is well equipped to withstand the applied loads.

I conclude that the bonobo thumb is a hybrid between the arboreal and terrestrial thumb. It is likely derived from a more restricted thumb as seen in macaques, but showcases the alleviation from structural reinforcement as seen in gibbons. Both locomotion and manipulation are well integrated in the morphology of the bonobo TMC joint, as it offers mobility and stability in one structure, while muscle activation can further reinforce joint stability when required.

We encounter high amounts of intraspecific morphological variation

To quote my former labmate dr. Faes Kerkhof on the human hand morphology: "Anatomical variability is everywhere and substantial". His work, but also other studies in the human hand and forearm, stressed the importance of anatomical variation in the human hand and forearm, and this is clearly no different in other primate taxa. We find much of this variability in the musculature. My personal view is that the influence of an individual muscle tendon unit is far less relevant than the influence of a functional group. The entire musculoskeletal system is a large interplay of systems where multiple structures work together to achieve a specific function, and so the individual roles within that function are allowed to vary. To that end we see intraspecific differences that do not particularly impact the functional groups within taxa. However, in structures where the individual actor represents the function of the functional group, or at least its lion's share, less variability may be allowed. The thenar muscles are a good example of this, as the individual muscles (in most cases) represent the 'group' function. As a result, we see little intra- but also interspecific variation in this area. Therefore, it is relevant to consider not only the presence of variation but also the individual role of the varying structure within the whole.

High intraspecific variation is considered a sign of relaxed selection on that area, and we appear to further see this in the gibbon trapezial micro-architecture. Upon distal loading of the trapezium, the strain is invariably transmitted towards the ulnar side of the trapezium. As a result, we see that the ulnar side shows relatively little intraspecific variation, and usually displays anisotropic, ulnarly-oriented trabecular struts. While the radial aspect remains relatively free from loads during the different grasps, the corresponding micro-architecture in that area is far more variable. Similarly, the gibbon micro-architecture shows high intraspecific variability, likely due to the moderate loading regimes.

Medical imaging and imaging based modelling provide valuable tools for a broad range of biomechanical analyses, and can and should be designed with multiple purposes in mind.

In this project we have used and developed multiple tools, based on medical imaging, for the purpose of studying thumb biomechanics in not just one but multiple taxa of primates. Despite issues with the resolution of the input data, the medical imaging based analyses have proved to be incredibly powerful tools with nearly endless possibilities, in particular when combined with the modularity of open source scientific programming. The currently developed pipeline is shown to be a valuable tool for both FE and μFE analysis of the primate TMC joint. However, these methods can be employed for similar analyses in other joints and taxa. The development of these workflows was done with modularity and open source data sharing in mind, giving it a broad functionality for future work.

Holistic evolutionary research requires a broad and integrated approach, and collaborative research by a dedicated scientific community.

Throughout this thesis, I have shed light on important aspects of the primate thumb anatomy and biomechanics, however, I am convinced that the combined efforts of a broader community are required to obtain a full insight in this complex joint system. I emphasized the need for larger study samples covering more primate taxa; I showed the requirement of including all the morphological aspects of the TMC joint to be able to reconstruct its functionality; and I discussed the importance of having accurate material properties of ligaments and cartilage. This can be achieved more easily by actively optimizing the way researchers from different labs and fields interact with each other. Multidisciplinary projects should be facilitated by an infrastructure that promotes research collaboration not only for seeking out help when external help appears mandatory, but also through active and pre-emptive initiatives that make research more accessible through data sharing and open source alternatives to established instances.

Methodological considerations and solutions for future work

Understanding form, function, and the integration of the two is difficult in any type of joint. The anatomical and biomechanical factors involved are numerous. Add to that the vast scope of evolutionary interpretation and the implications that each added species brings, and you will end up with a multitude of variables that must be accounted for. Here I discuss some of the major considerations encountered in the approach, and how these challenges may be addressed in the future.

Joint modelling

Modelling always involves simplification, usually by design. However, some reconsiderations of the following points would likely benefit the predictive accuracy of the generated joint and bone models.

Computing joint angles

The currently employed kinematic analysis for assessing range of motion in the primate thumb is a relatively simplified method of calculating joint angles. This method assesses range of motion based on joint angles that are assumed to be unrelated to one another. However, it is likely that these movements do influence one another, as can be determined from the association levels depicted in the range of motion data of **Chapters 2** and **3**. Although I believe that the methods I have applied here provide a sufficient measure for the intended purposes, I must note that this methodology could benefit from an upgrade to more advanced, three dimensional analyses that do consider the orthogonal axes to be dependent on each other.

Mesh quality

The CT protocol used for bonobos included a scanning resolution (0.625 mm) that was too low to allow for clear joint separation in the smaller sized gibbon and macaque joints. As a result, most reconstructed meshes showed imperfections that presented issues for the generation of model meshes without negative Jacobians. Furthermore, in this project, the parametric mesh approach for the generation of FE models was sensitive to mesh imperfections resulting from the segmentation process. This further amplified the problem and made the parametric approach unusable in most cases. For future work, if collection of new data would be involved, I would suggest an additional step before medical imaging that focuses on testing the minimal scan resolution required to ensure mesh quality. If the current data will be used, I would suggest reconstructing the TMC joint bone morphologies

from high resolution μCT scans. The required tools for this are already present in the μFE workflow.

Cartilage

Future models could be improved using currently lacking cartilage information. Not only does cartilage geometry have a significant impact on joint congruency, and thus influences intra-articular stress distributions and joint mechanics, but the material properties of the cartilage layer will further influence the distribution of stress. The cartilage properties and geometry may be different between specimens and taxa, and thus lead to different joint mechanics. Our assumptions made around the cartilage layer were based on the human TMC joint. While the bonobo TMC joint shape is highly similar to that of humans, the macaque's joint shape is further removed from that of humans. The gibbon's joint shape represents an even more different joint type. Moreover, the ball-and-socket joint shape of gibbons presents additional issues as its relative incongruence complicated successful FE model termination due to limited articular contact. This causes high stress in the cartilage elements involved. Accurate cartilage representation should more accurately represent joint congruency and alleviate this issue. Furthermore, there is the difference in bone element size. We attempted to account for size by scaling to the articular surface area, but it is unknown if this relationship is linear as we assumed. I attempted to address the lack of cartilage information by developing an image processing script that was able to extract the articular cartilage layer from μCT images, however, the method was unsuccessful due to a lack in image contrast. For future work, we therefore suggest using contrast enhanced μCT through collagen staining and indentation testing to have an accurate representation of the cartilage layer (Nieminen *et al.*, 2015; Dourthe *et al.*, 2019). The modular nature of the current FE workflow does allow for easy implementation of such information if it would become available.

Force application

The integrated FE-μFE workflow was based on an estimated force vector which was derived from a 2D static analysis of the thumb based on anatomical parameters (i.e. bone dimensions, MTU dimensions and insertions, muscle PCSA), CT images (joint angles during grasping). The thumb tip force used was standardized between primate taxa based on average body weight. This is 1/6 the bodyweight of each taxon as this was a close approximation to the 2D analysis results of the applied force vector. This rough estimate appeared to be sufficient for the current purposes of simulating moderate thumb loading. However changing the thumb tip force vector on the 2D analysis has a close to linear

influence on the FE applied forces, as well as on the eventual μFE strain calculated. This emphasizes the importance of selecting an appropriate applied force vector. If more advanced thumb functionality would be tested, a different method of determining thumb forces should be considered. Musculoskeletal modelling would be able to provide a much better estimate of joint loading and although currently no accurate nonhuman primate thumb models exist, such models could be developed by building on existing musculoskeletal models of the human thumb (Barry, Murray and Kamper, 2018), or primate hand and digits (Mirakhorlo *et al.*, 2018; Synek *et al.*, 2019). A musculoskeletal model of the nonhuman primate thumb would not only enable more accurate predictions of the joint forces resulting from grasping, but would also allow simulations of a broader range of grasps and thumb functionalities.

Analysis

The quantitative analysis of stress distributions across the distal trapezial articulation, and the strain distributions throughout the trapezial internal microarchitecture were especially computationally intensive. The current analysis includes a qualitative analysis of the course of the strain distribution, and a quantitative method was part of the pipeline. Using 3D coordinates that accompany the stress and strain data in the model itself can be considered and expanded upon in the future. These coordinates would be tested against a 3D map of the total bone mesh to quantitatively assign quadrants, or other separation types, to assess correspondence to the expected pattern. While I conceptualized the idea, I was unable to include it in the current dissertation.

Material properties

Material properties were shown to play an important role in both comparative anatomy and the interpretation of biomechanics. We stressed the importance of such properties in almost all chapters. We showed that all factors of the joint should be taken into account when investigating its functionality. Some relevant parameters are discussed below, and methods for their acquisition in future work are suggested.

Soft-tissue

Our quantitative anatomical studies included a broad range of parameters required for the assessment of muscle dimensions and the calculation of force generating capacities. This work can be expanded by including sarcomere length, which is relevant for the calculation of optimal PCSA, a more accurate representation of force generating capacity (Brown and Gerling, 2012). These values can be determined using confocal microscopy. I

have performed these analyses in unpublished anatomical work I did during this project, the results showed that sarcomere length is remarkably similar between humans, bonobos, chimpanzees, gorillas, and gibbons, in all forearm muscles of a sample size of one specimen per taxon. Although this part of the study was not further pursued, the means and muscle tissue is still available for future work. Second, muscle fibre type composition is another muscle parameter relevant for muscle activation and force generating capacity. It has been shown to vary between humans and chimpanzees (O'Neill *et al.*, 2017). Such compositions can be determined histologically from biopsies, but non-invasive methods such as MRI, EMG, or dynamometry based studies are alternatives for living tissues (Winkler *et al.*, 2019). Similarly, ligament and tendon material properties may also play a role. We stressed the possibility for histological differences in ligament material properties in the assessment of the TMC joint passive soft tissue in **Part 2**. Both tendons and ligaments are comprised of specifically oriented collagen fibres, and particularly in ligaments the orientation of these fibres may be geared to their specific function. Material properties may thus vary between taxa or specimens. As knowledge on this is already lacking in humans, it should certainly be considered through histological and mechanical testing (Bettinger *et al.*, 2000; Martin *et al.*, 2015).

Bone

I emphasized the importance of accurate bone material properties in **Chapter 5** and **6**. Here it became evident that the variability in bone elastic properties (Young's modulus) reported in literature can make a difference in the resulting strain levels. This difference can be larger than the difference between the strain levels that are associated with different adaptive states of bone reported in the literature. Therefore, I stress that a near accurate assessment of both Young's modulus and bone yield and ultimate strain are crucial to assess potential bone failure. This is especially true since these highly variable parameters are currently based on human studies alone. Elastic properties were shown to be similar to humans in some non-human primates, like chimpanzee craniofacial external cortical bone (Gharpure *et al.*, 2016), and rhesus macaque mandible cortical bone (Dechow, Panagiotopoulou and Gharpure, 2017). But varying results were also found between different functional areas in the craniofacial cortical bone of those same rhesus macaques (Wang and Dechow, 2006). The same study also shows that the elastic properties in some of these areas differ from humans, warranting more caution when making assumptions on bone properties. In addition, trabecular bone shows the potential for even higher parameter variability and specimen dependency with respect to cortical bone. This is particularly relevant in the gibbon trapezium but also in bonobos and macaques. Ideally,

these types of parameters are again tested through mechanical testing and ultrasound (Grimal *et al.*, 2009). However our µCT data can also be used to assess bone parameters, such as BV/TV, degree of anisotropy, and trabecular thickness (Tsegai et al., 2017; Georgiou et al., 2019; Steiner, Synek and Pahr, 2020), which in turn are relevant as they affect bone elastic properties and yield strain

I highly recommend that when studying joint biomechanics, an evaluation of the material properties involved is made when conceiving the study. As such, the assessment of potential unknown or unreliable material properties can be incorporated in the study outline. I would furthermore suggest including material property assessment in the study design in general, as literature values can be highly variable. The extensive list of different tests and expertise required highlights the immense value of efficient interdisciplinary collaboration.

Specimens

This project uses data that were obtained from a unique collection of nonhuman primate specimens, which are typically difficult to obtain, and therefore under-represented in literature. However, I do want to point out some points for discussion with regards to our research sample.

Cadaveric specimens

All of our studies are performed on cadaveric samples. This of course is usually the case for detailed dissections, but it does require additional considerations. In living organisms, muscle tissue is dynamic and so is its function (Eng, Azizi and Roberts, 2018). Quantification of some muscle parameters, such as muscle fibre length, sarcomere length, pennation angle, and entire muscle tendon unit length to name a few, will be affected by the lack of muscle activation. And although modelling of muscle dynamics may yield insight in how parameters change through muscle activation (Dick and Wakeling, 2018), the assessment of muscle functionality and force generating capacity of cadaveric muscle will, for the foreseeable future, be a skewed approximation of the in vivo condition.

Captive specimens

Our analyses work under the assumption that form and function are derived from interaction with the environment. Most of study subjects, however, come from captivity and so their environment may no longer reflect the habitat that they are adapted towards. As a result, the animals may display different behaviour (Payne *et al.*, 2006), but also different morphology. This complicates the form-function debate, as we may be testing for functionality that is different from the wild situation. Furthermore, this effect may be

different across our studied taxa, as almost all macaques specimens came from the same facility, while the gibbons sample, in contrast, comprised multiple species. In addition, while macaque locomotion was shown to be similar in free ranging animals when compared to those in captivity (Dunbar and Badam, 1998), we do not know for certain if this is the case for our study sample, nor for the gibbons and bonobos.

Few specimens

Lastly, while the sample studied here is of respectable size with respect to what is available in literature, we have tried to avoid mentioning the objectively low sample size as much as possible. Sample size does present issues with some of the methods that could have been applied. In particular, the FE workflow that was originally used in humans (Schneider *et al.*, 2017), included a statistical shape modelling approach. This would have been a valuable addition to the analysis, it was however, purposely omitted due to sample size. Similarly, many of the comparative analyses between grasps, specimens and taxa could not be extensively tested due to lack of statistical power. As such there are countless reasons why larger sample sizes are always better, with perhaps the exception of data management for the undoubtably massive amount of gigabytes of μCT and μFE data. However, this could be addressed with workflow optimisation and perhaps automation.

Like with the issues presented around material properties, both the issues around captivity and low sample sizes can be addressed through international collaborations. In this case between zoos, natural and/or historical museums, breeding programmes, natural reserves, petting zoos, primatologists, biologists, psychologists… whichever source comes to mind can be the solution. Open source data sharing of raw data, medical imaging, behavioural study videos, images, analyses can facilitate an answer. I advocate for large scale integrated, optimized, multidisciplinary scientific research. Invite your colleagues and friends!

Interpretation

Lastly, I want to address the interpretation of these data. The emphasis of this work is on the functional interpretation of adaption, i.e. all adaptation occurs in response to the required function of the structure. There are however, alternative factors that may be at play. Hypotheses on functional adaptation should generally account for phylogenetic inertia (Blomberg and Garland, 2002), body size (Sibly and Brown, 2007), and even genetic drift (R. Nené, Mustonen and J. R. Illingworth, 2018). These factors may play even larger roles in smaller populations, such as captive populations, that display evolutionary stasis, as for instance has been claimed to be the case for bonobos (Diogo, Molnar and Wood,

2017). Methods that account for the influences of these factors (i.e. phylogenetic comparative methods (Martins, Diniz-Filho and Housworth, 2002), multiple regression (Lang *et al.*, 2004), and the Wide-Fisher drift model (Tataru, Bataillon and Hobolth, 2015)) typically require large sample sizes, and are beyond the scope of the current thesis. However, it is important to note that these factors do play a role and should be accounted for, especially in larger analyses. These methods become increasingly important when moving towards evolutionary interpretations of functional adaptation data.

Future perspectives

What has been achieved, and what is next?

For this project I have collected extensive and detailed morphological datasets, unique to three primate taxa. These datasets can be used as reference points in comparative studies on primate anatomy (be they clinical, anthropological, or otherwise). They may also serve as a basis for new anatomical and biomechanical analyses and can even be used as visualisation in demonstrational and educational settings. Furthermore, I have expanded on previous analysis tools and developed novel approaches to biomechanical analyses of the TMC joint. These approaches can be employed for broader analyses of datasets (hopefully) ever increasing in size, including both larger populations of the currently addressed taxa, but also additional primates. When data can be collected of sufficiently large populations, we can shift the focus from studying intraspecific variation and start to identify patterns and trends that indicate evolutionary adaptation within these taxa. Likewise, expanding towards other species, such as other hominids i.e. the chimpanzee, gorilla and orangutan, but also to Old World monkeys and beyond, will allow us to identify these patterns in even more species employing even broader functionalities. Of course, such an endeavour requires massive amounts of data, but doing so, we can slowly piece together the relationships between form and function that shape evolution. Moreover, these tools are not limited to the TMC joint, the thumb, or the hand. I have aimed to develop my approaches with an Open Source mentality, allowing for further iteration on the current workflows to refine the analytical power of these methods, or for the extraction of individual pieces of code for reimplementation in other pipelines. This should lead to broad biomechanical datasets, like those I presented in this thesis. Such data are important to gain insight into the form and function of extant species. They are also useful to produce a framework for the interpretation of the functional capabilities of fossil hominins in paleoanthropological research.

With this project I have provided morphological material to be studied, the biomechanical tools to study them, and the resulting analytics that provide insight in the adaptation of the thumb. I have done this in a sample of bonobos, gibbons, and macaques, a small piece of a much larger evolutionary puzzle. Overall, my work presents a valuable addition to the scarce information on non-human primate thumb morphology and biomechanics, which serve as a basis for the interpretation of primate hand evolution.

At the level of scientific communities

Foremost, academic research is humanly-centred, but much effort has gone towards expanding our knowledge to other species in order to find more and more pieces of the evolutionary puzzle. I am proud that my work in this thesis may contribute to this endeavour, but the truth is that even in humans much work is left to be done. My experiences during the last few of years as a doctoral student have made one thing clear to me above all: We need multidisciplinary involvement of a dedicated scientific community in, presumably, all types of research. Ideally, I would love to see an infrastructure that promotes research efficiency through the collaboration of an entire network of researchers, regardless of field or institution. For me, this road began by virtue of dr. Jeroen Stevens, who took the initiative to collect rare cadaveric specimens of the endangered bonobo and made them available for us to study. This could be further expanded by the good will of other European zoos with whom we came into contact through various means, such as the EAZA breeding programme or professional networking. I would love to see similar initiatives taken as Jeroen did, not just because one researcher had the insight to consider a broader scope, but as the standard for conducting scientific research. Open source data repositories, wide access to methodologies, and widespread multidisciplinary collaborations need to be the rule, not the exception. Developing an infrastructure of digital meeting points, conferences, fora, etcetera should be easier now more than ever since COVID-19 has skyrocketed us into the age of online meetings. The involvement of governments and the commercial sector would be ideal, but may present challenges. I do believe that a momentous difference can be made by individual dedicated and passionate researchers who can increase awareness and encourage new researchers to look towards making data, methodologies, code, analyses, and any tool that could be of help to others, widespread and available.

My part in this

Regardless of where my next challenge takes me, I will take this message with me. I will actively look towards not only collaboration but also enhancing the availability of my work.

This may take the form of publishing as much data as possible on open source repositories, such as we did with MorphoSource, or striving to publish manuscripts in specific journals, as I aimed to do here with **Chapter 4** in *PeerJ*. I also fervently believe that it is important to consider what one can improve close to home, and so I hope to contribute to work that will improve collaborative works within my next lab or work group, wherever I go next. Specifically, I aim to invest time into setting up an efficient lab repository framework for the sharing of data or methodologies through the likes of Git, or other platforms. These ideas that can also be scaled up to larger scopes such as broader collaborations. I am also passionate about optimizing more mundane tasks, such as in my case image segmentation. For this type of work I am eager to be apply machine learning algorithms, script optimization, and other types of automation.

During the course of my PhD, I have shifted towards primarily using Python and other open source software to conduct my research. I owe much to many anonymous authors of snippets of code and general tips on programming fora. I would like to return the favour for others in the future. To that end, I have started to take into account the fact that others might benefit from using my analyses, or bits of my approach. One of my goals for this project was to design the FE-μFE workflow, and develop it as an application to be used by the lab, or any others that are interested. While many things did not go as planned, I learned from the experience. It gave me the foresight of designing my workflows with sharable applications in mind, always. I hope to find the time to improve the workflow I designed here in the future. I feel that spreading awareness and starting close to home is key in building the foundation of a scientific community that looks beyond what is directly in front of them, and towards a broader scientific scope.

References

Almécija, S., Smaers, J. B. and Jungers, W. L. (2015) 'The evolution of human and ape hand proportions', *Nature Communications*, 6(1), p. 7717. doi: 10.1038/ncomms8717.

Ayhan, Ç. and Ayhan, E. (2020) 'Kinesiology of the wrist and the hand', in *Comparative Kinesiology of the Human Body*. Elsevier, pp. 211–282. doi: 10.1016/B978-0-12-812162-7.00013-8.

Barry, A. J., Murray, W. M. and Kamper, D. G. (2018) 'Development of a dynamic index finger and thumb model to study impairment', *Journal of Biomechanics*, 77, pp. 206–210. doi: 10.1016/j.jbiomech.2018.06.017.

Bettinger, P. C. *et al.* (1999) 'An Anatomic Study of the Stabilizing Ligaments of the Trapezium and Trapeziometacarpal Joint', *The Journal of Hand Surgery*, 24(4), pp. 786–798. doi: 10.1053/jhsu.1999.0786.

Bettinger, P. C. *et al.* (2000) 'Material properties of the trapezial and trapeziometacarpal ligaments', *The Journal of Hand Surgery*, 25(6), pp. 1085–1095. doi: 10.1053/jhsu.2000.18487.

Blomberg, S. P. and Garland, T. (2002) 'Tempo and mode in evolution: phylogenetic inertia, adaptation and comparative methods', *Journal of Evolutionary Biology*, 15(6), pp. 899–910. doi: 10.1046/j.1420-9101.2002.00472.x.

Brown, S. H. and Gerling, M. E. (2012) 'Importance of sarcomere length when determining muscle physiological cross-sectional area: A spine example', *Proceedings of the Institution of Mechanical Engineers, Part H: Journal of Engineering in Medicine*, 226(5), pp. 384–388. doi: 10.1177/0954411912441325.

Burr, D. B. *et al.* (1996) 'In vivo measurement of human tibial strains during vigorous activity', *Bone*, 18(5), pp. 405–410. doi: 10.1016/8756-3282(96)00028-2.

Cooney, W. P. and Chao, E. Y. (1977) 'Biomechanical analysis of static forces in the thumb during hand function.', *The Journal of bone and joint surgery. American volume*, 59(1), pp. 27–36.

D'Agostino, P. *et al.* (2014) 'Comparison of the Anatomical Dimensions and Mechanical Properties of the Dorsoradial and Anterior Oblique Ligaments of the Trapeziometacarpal Joint', *The Journal of Hand Surgery*, 39(6), pp. 1098–1107. doi: 10.1016/j.jhsa.2014.02.025.

Dechow, P. C., Panagiotopoulou, O. and Gharpure, P. (2017) 'Biomechanical implications of cortical elastic properties of the macaque mandible', *Zoology*, 124, pp. 3–12. doi: 10.1016/j.zool.2017.06.008.

Demes, B. *et al.* (1998) 'Patterns of strain in the macaque ulna during functional activity', *American Journal of Physical Anthropology*, 106(1), pp. 87–100. doi: 10.1002/(SICI)1096-8644(199805)106:1<87::AID-AJPA6>3.0.CO;2-A.

Dick, T. J. M. and Wakeling, J. M. (2018) 'Geometric models to explore mechanisms of dynamic shape change in skeletal muscle', *Royal Society Open Science*, 5(5), p. 172371. doi: 10.1098/rsos.172371.

Diogo, R., Molnar, J. L. and Wood, B. (2017) 'Bonobo anatomy reveals stasis and mosaicism in chimpanzee evolution, and supports bonobos as the most appropriate extant model for the common ancestor of chimpanzees and humans', *Scientific Reports*. Springer US, 7(1),

pp. 1–8. doi: 10.1038/s41598-017-00548-3.

Dourthe, B. *et al.* (2019) 'Assessment of healthy trapeziometacarpal cartilage properties using indentation testing and contrast-enhanced computed tomography', *Clinical Biomechanics*, 61, pp. 181–189. doi: 10.1016/j.clinbiomech.2018.12.015.

Drapeau, M. S. M. (2015) 'Metacarpal torsion in apes, humans, and early Australopithecus: implications for manipulatory abilities', *PeerJ*, 3, p. e1311. doi: 10.7717/peerj.1311.

Dunbar, D. C. and Badam, G. L. (1998) 'Development of Posture and Locomotion in Free-ranging Primates', *Neuroscience & Biobehavioral Reviews*, 22(4), pp. 541–546. doi: 10.1016/S0149-7634(97)00042-0.

Eng, C. M., Azizi, E. and Roberts, T. J. (2018) 'Structural Determinants of Muscle Gearing During Dynamic Contractions', *Integrative and Comparative Biology*, 58(2), pp. 207–218. doi: 10.1093/icb/icy054.

Fleagle, J. G. (2013) 'Apes and Humans', in *Primate Adaptation and Evolution*. Elsevier, pp. 151–168. doi: 10.1016/B978-0-12-378632-6.00007-0.

Fritton, S. P., McLeod, K. J. and Rubin, C. T. (2000) 'Quantifying the strain history of bone: spatial uniformity and self-similarity of low-magnitude strains', *Journal of Biomechanics*, 33(3), pp. 317–325. doi: 10.1016/S0021-9290(99)00210-9.

Frost, H. M. (2003) 'Bone's mechanostat: A 2003 update', *The Anatomical Record*, 275A(2), pp. 1081–1101. doi: 10.1002/ar.a.10119.

Georgiou, L. *et al.* (2019) 'Trabecular architecture of the great ape and human femoral head', *Journal of Anatomy*, 234(5), pp. 679–693. doi: 10.1111/joa.12957.

Gharpure, P. *et al.* (2016) 'Elastic Properties of Chimpanzee Craniofacial Cortical Bone', *The Anatomical Record*, 299(12), pp. 1718–1733. doi: 10.1002/ar.23466.

Grimal, Q. *et al.* (2009) 'Assessment of cortical bone elasticity and strength: Mechanical testing and ultrasound provide complementary data', *Medical Engineering & Physics*, 31(9), pp. 1140–1147. doi: 10.1016/j.medengphy.2009.07.011.

van Horn, R. N. (1972) 'Structural Adaptations to Climbing in the Gibbon Hand', *American Anthropologist*, 74(3), pp. 326–334. doi: 10.1525/aa.1972.74.3.02a00050.

Kerkhof, F. D. . *et al.* (2018) 'Trapeziometacarpal stabilization through dorsoradial ligament reconstruction: An early post-surgery in vivo biomechanical analyses', *Journal of Orthopaedic Research®*, Manuscript. doi: 10.1002/jor.24103.

Lang, D. H. *et al.* (2004) 'Adjusting Data to Body Size: A Comparison of Methods as Applied to Quantitative Trait Loci Analysis of Musculoskeletal Phenotypes', *Journal of Bone and Mineral Research*, 20(5), pp. 748–757. doi: 10.1359/JBMR.041224.

Lanyon, L. E. and Smith, R. N. (1970) 'Bone strain in the tibia during normal quadrupedal locomotion', *Acta Orthopaedica Scandinavica*. Taylor & Francis, 41(3), pp. 238–248.

Lewiner, T. *et al.* (2003) 'Efficient Implementation of Marching Cubes' Cases with Topological Guarantees', *Journal of Graphics Tools*, 8(2), pp. 1–15. doi: 10.1080/10867651.2003.10487582.

Lewis, O. J. (1977) 'Joint remodelling and the evolution of the human hand.', *Journal of Anatomy*, 123(Pt 1), pp. 157–201.

Macfarlane, N. B. W. and Graziano, M. S. A. (2009) 'Diversity of grip in Macaca mulatta', *Experimental Brain Research*, 197(3), pp. 255–268. doi: 10.1007/s00221-009-1909-z.

Manter, J. T. (1938) 'The Dynamics Of Quadrupedal Walking', *Journal of Experimental Biology*, 15(4), pp. 522 LP – 540.

Martin, R. B. *et al.* (2015) 'Mechanical Properties of Ligament and Tendon', in *Skeletal Tissue Mechanics*. New York, NY: Springer New York, pp. 175–225. doi: 10.1007/978-1-4939-3002-9_4.

Martins, E. P., Diniz-Filho, J. A. and Housworth, E. A. (2002) 'Adaptive constraints and the phylogenetic comparative method: A computer simulation test', *Evolution*, 56(1), pp. 1–13. doi: 10.1111/j.0014-3820.2002.tb00844.x.

Marzke, M. W. *et al.* (1998) 'EMG study of hand muscle recruitment during hard hammer percussion manufacture of Oldowan tools', *American Journal of Physical Anthropology*, 105(3), pp. 315–332. doi: 10.1002/(SICI)1096-8644(199803)105:3<315::AID-AJPA3>3.0.CO;2-Q.

Marzke, Mary W. *et al.* (1999) 'Chimpanzee thumb muscle cross sections, moment arms and potential torques, and comparisons with humans', *American Journal of Physical Anthropology*, 110(2), pp. 163–178. doi: 10.1002/(SICI)1096-8644(199910)110:2<163::AID-AJPA4>3.0.CO;2-A.

Marzke, Mary W *et al.* (1999) 'Chimpanzee Thumb Muscle Cross Sections , Moment Arms and Potential Torques , and Comparisons With Humans', 178(June), pp. 163–178.

Michilsens, F. *et al.* (2010) 'Muscle moment arms and function of the siamang forelimb during brachiation', *Journal of Anatomy*, 217(5), pp. 521–535. doi: 10.1111/j.1469-7580.2010.01272.x.

Mirakhorlo, M. *et al.* (2018) 'A musculoskeletal model of the hand and wrist: model definition and evaluation', *Computer Methods in Biomechanics and Biomedical Engineering*, 21(9), pp. 548–557. doi: 10.1080/10255842.2018.1490952.

Napier, J. R. (1955) 'The form and function of the carpo-metacarpal joint of the thumb.', *Journal of anatomy*, 89(3), pp. 362–9.

Nieminen, H. J. *et al.* (2015) 'Determining collagen distribution in articular cartilage using contrast-enhanced micro-computed tomography', *Osteoarthritis and Cartilage*, 23(9), pp. 1613–1621. doi: 10.1016/j.joca.2015.05.004.

O'Neill, M. C. *et al.* (2017) 'Chimpanzee super strength and human skeletal muscle evolution', *Proceedings of the National Academy of Sciences*, 114(28), pp. 7343–7348. doi: 10.1073/pnas.1619071114.

Parker, S. T. and Gibson, K. R. (1977) 'Object manipulation, tool use and sensorimotor intelligence as feeding adaptations in cebus monkeys and great apes', *Journal of Human Evolution*, 6(7), pp. 623–641. doi: 10.1016/S0047-2484(77)80135-8.

Payne, R. C. *et al.* (2006) 'Morphological analysis of the hindlimb in apes and humans. II. Moment arms', *Journal of Anatomy*, 208(6), pp. 725–742. doi: 10.1111/j.1469-7580.2006.00564.x.

R. Nené, N., Mustonen, V. and J. R. Illingworth, C. (2018) 'Evaluating genetic drift in time-series evolutionary analysis', *Journal of Theoretical Biology*, 437, pp. 51–57. doi: 10.1016/j.jtbi.2017.09.021.

Rafferty, K. L. (1990) *The Functional and Phylogenetic Significance of the Carpometacarpal Joint of the Thumb in Anthropoid Primates*. New York University.

Samuel, D. S. *et al.* (2018) 'Hand pressures during arboreal locomotion in captive bonobos (Pan paniscus)', *The Journal of Experimental Biology*, 221(8), p. jeb170910. doi: 10.1242/jeb.170910.

Sarmiento, E. E. (1994) 'Terrestrial traits in the hands and feet of gorillas. American Museum novitates; no. 3091'. New York, NY: American Museum of Natural History.

Schneider, M. T. Y. *et al.* (2017) 'Trapeziometacarpal joint contact varies between men and women during three isometric functional tasks', *Medical Engineering & Physics*, 50, pp. 43–49. doi: 10.1016/j.medengphy.2017.09.002.

Selby, M. S., Simpson, S. W. and Lovejoy, C. O. (2016) 'The Functional Anatomy of the Carpometacarpal Complex in Anthropoids and Its Implications for the Evolution of the Hominoid Hand', *The Anatomical Record*, 299(5), pp. 583–600. doi: 10.1002/ar.23333.

Sibly, R. M. and Brown, J. H. (2007) 'Effects of body size and lifestyle on evolution of mammal life histories', *Proceedings of the National Academy of Sciences*, 104(45), pp. 17707–17712. doi: 10.1073/pnas.0707725104.

Steiner, L., Synek, A. and Pahr, D. H. (2020) 'Comparison of different microCT-based morphology assessment tools using human trabecular bone', *Bone Reports*, 12, p. 100261. doi: 10.1016/j.bonr.2020.100261.

Synek, A. *et al.* (2019) 'Musculoskeletal models of a human and bonobo finger: parameter identification and comparison to in vitro experiments', *PeerJ*, 7, p. e7470. doi: 10.7717/peerj.7470.

Tataru, P., Bataillon, T. and Hobolth, A. (2015) 'Inference Under a Wright-Fisher Model Using an Accurate Beta Approximation', *Genetics*, 201(3), pp. 1133–1141. doi: 10.1534/genetics.115.179606.

Tocheri, M. W. *et al.* (2005) 'A 3D quantitative comparison of trapezium and trapezoid relative articular and nonarticular surface areas in modern humans and great apes', *Journal of Human Evolution*, 49(5), pp. 570–586. doi: 10.1016/j.jhevol.2005.06.005.

Tsegai, Z. J. *et al.* (2017) 'Trabecular and cortical bone structure of the talus and distal tibia in Pan and Homo', *American Journal of Physical Anthropology*, 163(4), pp. 784–805. doi: 10.1002/ajpa.23249.

Vanhoof, M. J. M. *et al.* (2020) 'The forearm and hand musculature of semi-terrestrial rhesus macaques (Macaca mulatta) and arboreal gibbons (fam . Hylobatidae). Part II. Quantitative analysis', *Journal of Anatomy*, p. joa.13314. doi: 10.1111/joa.13314.

Vanhoof, M. J. M., van Leeuwen, T. and Vereecke, E. E. (2020) 'The forearm and hand musculature of semi-terrestrial rhesus macaques (Macaca mulatta) and arboreal gibbons (Fam. Hylobatidae). Part I. Description and comparison of the muscle configuration', *Journal of Anatomy*. John Wiley & Sons, Ltd, n/a(n/a). doi: 10.1111/joa.13222.

Wang, Q. and Dechow, P. C. (2006) 'Elastic properties of external cortical bone in the

craniofacial skeleton of the rhesus monkey', *American Journal of Physical Anthropology*, 131(3), pp. 402–415. doi: 10.1002/ajpa.20438.

Williams, E. M., Gordon, A. D. and Richmond, B. G. (2010) 'Upper limb kinematics and the role of the wrist during stone tool production', *American Journal of Physical Anthropology*, 143(1), pp. 134–145. doi: 10.1002/ajpa.21302.

Winkler, T. *et al.* (2019) 'Development of a Non-invasive Methodology for the Assessment of Muscle Fibre Composition', *Frontiers in Physiology*, 10. doi: 10.3389/fphys.2019.00174.

Wunderlich, R. E. and Jungers, W. L. (2009) 'Manual digital pressures during knuckle-walking in chimpanzees (Pan troglodytes)', *American Journal of Physical Anthropology*, 139(3), pp. 394–403. doi: 10.1002/ajpa.20994.

Yang, P., Brüggemann, G.-P. and Rittweger, J. (2011) 'What do we currently know from in vivo bone strain measurements in humans?', *Journal of Musculoskeletal and Neuronal Interactions*. International Society of Musculoskeletal and Neuronal Interactions, 11(1), pp. 8–20.

Appendices

Appendix I: Curriculum vitae

Biography

Timo van Leeuwen obtained a Bachelor's degree in biology at the Wageningen University, The Netherlands in 2014, after which he broadened his interest towards physical anthropology, osteology, and archaeology at the university of Leiden and the Academic Medical Centre of Amsterdam. Simultaneously, he started his Master's degree in the biology specialisation of Animal Adaptation, which was dedicated towards research on the frontier with extended experimental projects, research master courses, and grant writing. He obtained his Master's in Biology at the start of 2017, at which point he had already moved to Ghent, Belgium, to start his PhD project on 'Anatomical adaptations to varying functional demands in the primate thumb' at the Muscles and Movement group, Department of Development and Regeneration of the KU Leuven, Campus Kulak, Kortrijk, Belgium.

Awards and funding

August 2017 August	The European Federation for Primatology Meeting, Art Contest, First Prize for Scientific Illustration (Strasbourg, France)
July 2018 July	Society for Experimental Biology (SEB) Grant for orally presenting at SEB2018 (Florence, Italy)
March – May 2019	FWO Long Research Stay Abroad Grant to a research collaboration at The Auckland Bioengineering Institute (Auckland, New Zealand)
April 2020	FWO Travel Grant for an invited oral/poster presentation at AAPA2020 (Los Angeles, USA)

Research Experience

2017 – 2021	**KU Leuven, Campus Kulak, Kortrijk, Belgium**
	PhD Student: Functional anatomy and biomechanics of the primate thumb
	Supervisor: Evie E. Vereecke
	Co-supervisor: G. Harry van Lenthe

March – May 2019 **The Auckland Bioengineering Institute, Auckland, New Zealand**

Research Stay Abroad: Finite Element modelling of the primate thumb

Supervisor: Marco T. Y. Schneider

March – August 2016 **Simon Fraser University, Vancouver, Canada**

Research Internship : EMG based analyses on muscle fibre-type composition in human calf muscle

Supervisor: James M. Wakeling

2013 - 2016 **Experimental Zoology Group, Wageningen, The Netherlands**

2016 Master thesis: Mechanics of bioadhesion and dynamics of locomotion in sea urchins (*Paracentrotus lividus*)

Supervisor: Johan L. van Leeuwen

Co-supervisor: Julian K. A. Langowski

2015 Research master: Artificial selection in Guppies

Supervisor: Martin J. M. Lankheet

2013 Bachelor thesis: Radula formation and adaptation in *Mollusca*

Supervisor: Sander W. S. Gussekloo

Peer reviewed publications

Lloyd, M., Claydon, V., Wakeling, J., Drapala, R., **van Leeuwen, T.**, and Koehle, M. (2017) 'The pathophysiology of carotid sinus hypersensitivity: Sensory block of the sternocleidomastoid muscles does not increase responses to carotid sinus massage.' *Canadian Journal of Cardiology*, 33, 10, pp. S152-S153. doi: 10.1016/j.cjca.2017.07.294.

van Leeuwen, T., Vanhoof, M. J. M., Kerkhof, F. D., Stevens, J. M. G., Vereecke, E. E. (2018) 'Insights into the musculature of the bonobo hand', *Journal of Anatomy*, 233(3), pp. 328–340. doi: 10.1111/joa.12841.

Kerkhof, F.D., **van Leeuwen, T.**, Vereecke, E.E., (2018) 'The digital human forearm and hand', *Journal of Anatomy,* 233, 5, p. 557-566, doi: 10.1111/joa.12877

van Leeuwen, T., Vanneste, M., Kerkhof, F. D., D'Agostino, P., Vanhoof, M. J. M., Stevens, J. M. G., van Lenthe, G. H., Vereecke, E. E. (2019) 'Mobility and structural constraints of the bonobo trapeziometacarpal joint', *Biological Journal of the Linnean Society*, 127(3), pp. 681–693. doi: 10.1093/biolinnean/bly162.

Vanhoof, M. J. M., **van Leeuwen, T.**, and Vereecke, E. E. (2020) 'The forearm and hand musculature of semi-terrestrial rhesus macaques (Macaca mulatta) and arboreal gibbons (Fam. Hylobatidae). Part I. Description and comparison of the muscle configuration', *Journal of Anatomy*. John Wiley & Sons, Ltd, n/a(n/a). doi: 10.1111/joa.13222.

Vanhoof, M. J. M., **van Leeuwen, T.**, Galetta, L., Vereecke, E.E. (2020) 'The forearm and hand musculature of semi-terrestrial rhesus macaques (Macaca mulatta) and arboreal gibbons (fam . Hylobatidae). Part II. Quantitative analysis', *Journal of Anatomy*, p. joa.13314. doi: 10.1111/joa.13314.

van Leeuwen, T., Vanneste, M., D'Agostino, P., and Vereecke, E.E. (2021) 'Trapeziometacarpal joint mobility in gibbons (fam. *Hylobatidae*) and rhesus macaques (*Macaca mulatta*).' *American Journal of Physical Anthropology*, In review.

van Leeuwen, T., van Lenthe, G. H., Vereecke, E. E., and Schneider, M. T. Y. (2021) 'Stress distribution and the influence of morphology during grasping in the bonobo (*Pan paniscus*) trapeziometacarpal joint.' *PeerJ,* In review.

van Leeuwen, T., Schneider, M. T. Y., van Lenthe, G. H., and Vereecke, E. E. (2021) 'The effect of different grasping types on internal trapezium strain distribution in bonobos (*Pan paniscus*).' *Journal of Biomechanics*, manuscript submitted.

Dunmore, C. J., **van Leeuwen, T.**, Karakostis, A., Lu, S-C, Proffitt, T. (2021) 'Tool use and the hand', Book chapter: 'Behaviour in our bones'. *Elsevier*, Book in revision.

International conferences

August 2017	European Federation for Primatology Meeting, Strasbourg, France
	Anatomical adaptations to conflicting functional demands in the primate thumb (poster)
September 2017	European Society for the study of Human Evolution, Leiden, The Netherlands
	Anatomical adaptation in the bonobo thumb (poster)
January 2018	Dutch/Flemish Anatomical Society, Lunteren, The Netherlands
	Primate anatomy; investigating variations in the bonobo thumb (poster)
April 2018	American Association of Physical Anthropologists, Austin, Texas, USA
	Investigating form-function relationships in the bonobo hand and thumb (poster)
November 2018	The Antwerp Zoo Bonobo Research Network, Antwerp, Belgium
	Form and function of the bonobo hand: Kinematics (invited oral)
July 2018	Society for Experimental Biology, Florence, Italy
	Kinematics of the bonobo thumb during functional movements (oral)
January 2019	Dutch/Flemish Anatomical Society, Lunteren, The Netherlands
	Relating trapeziometacarpal joint morphology to functional capabilities in the human and bonobo thumb (poster/oral)
July 2019	International Congress of Vertebrate Morphology, Prague, Czech Republic
	Relating thumb base joint morphology to functional capabilities in the primate thumb (oral)
April 2020	American Association of Physical Anthropologists, Los Angeles, California, USA
	An integrated (micro) Finite Element approach to analysing trapeziometacarpal force distributions in the primate thumb during various grasps (invited poster/oral)

Skills and qualifications

Functional Anatomy	Human/primate/mammal musculoskeletal system, Dissection, Osteology
Biomechanics	Kinematics, Finite Element, Micro Finite Element, EMG, Signal processing, Musculosketal modelling, Image analyses
Scientific programming	Python, Matlab, Mathematica, R
Medical imaging	CT, micro CT, Image processing, Meshing, Radioprotection

Teaching

2017 – 2019	Teaching: Introduction to medical scientific research Medical students 1st year bachelors
2018 – 2020	Teaching: Anatomy and function of the human musculoskeletal system Human osteology (Medical/Biomedical students 1st year bachelors) Human soft-tissue, dissection practicals (Medical students, 2nd year bachelors)
2017 – 2020	Supervision: Human and non-human primate anatomy and biomechanics. BSc thesis students, MSc thesis students, and extracurricular research students (BSc/pre-MSc)

Scientific illustration:

See **Appendix IV**

Published illustrations outside of own work

Aerts et al., 2018: 'The gibbon's Achilles tendon revisited: Consequences for the evolution of the great apes?' *Proceeding of the Royal Society B: Biological Sciences*

Kerkhof et al. 2018: 'Trapeziometacarpal stabilization through dorsoradial ligament reconstruction: An early post-surgery in vivo biomechanical analyses', *Journal of Orthopaedic Research*

Appendix II: Author contributions

An overview of the candidate's individual contributions to the published papers and submitted manuscripts included in this thesis.

van Leeuwen, et al. (2018) 'Insights into the musculature of the bonobo hand', *Journal of Anatomy,* 233(3), pp. 328–340. doi: 10.1111/joa.12841.

Study design, data collection, data analysis, data interpretation, manuscript writing, manuscript review.

Kerkhof, F.D., **van Leeuwen, T.**, Vereecke, E.E., (2018) 'The digital human forearm and hand', *Journal of Anatomy,* 233, 5, p. 557-566, doi: 10.1111/joa.12877

Experimental design, data collection, data analyses, data interpretation, manuscript review

van Leeuwen, T, et al. (2019) 'Mobility and structural constraints of the bonobo trapeziometacarpal joint', *Biological Journal of the Linnean Society*, 127(3), pp. 681–693. doi: 10.1093/biolinnean/bly162.

Study design, data collection, scientific programming, data analyses, data interpretation, manuscript writing, scientific illustration, manuscript review.

Vanhoof, M. J. M., **van Leeuwen, T.**, and Vereecke, E. E. (2020) 'The forearm and hand musculature of semi-terrestrial rhesus macaques (Macaca mulatta) and arboreal gibbons (Fam. Hylobatidae). Part I. Description and comparison of the muscle configuration', *Journal of Anatomy*. John Wiley & Sons, Ltd, n/a(n/a). doi: 10.1111/joa.13222.

Study design, data collection, manuscript review.

Vanhoof, M. J. M., **van Leeuwen, T.**, et al. (2020) 'The forearm and hand musculature of semi-terrestrial rhesus macaques (Macaca mulatta) and arboreal gibbons (fam . Hylobatidae). Part II. Quantitative analysis', *Journal of Anatomy*, p. joa.13314. doi: 10.1111/joa.13314.

Study design, data collection, manuscript review.

van Leeuwen, T., et al. (2021) 'Trapeziometacarpal joint mobility in gibbons (fam. *Hylobatidae*) and rhesus macaques (*Macaca mulatta*).' *American Journal of Physical Anthropology*, In review.

Study design, data collection, scientific programming, data analyses, data interpretation, manuscript writing, manuscript review.

van Leeuwen, T., et al. (2021) 'Stress distribution and the influence of morphology during grasping in the bonobo (*Pan paniscus*) trapeziometacarpal joint.' *PeerJ,* In review.

Study design, data collection, scientific programming, data analyses, data interpretation, manuscript writing, manuscript review.

van Leeuwen, T., et al. (2021) 'The effect of different grasping types on internal trapezium strain distribution in bonobos (*Pan paniscus*).' *Journal of Biomechanics*, manuscript submitted.

Study design, data collection, scientific programming, data analyses, data interpretation, manuscript writing, manuscript review.

Appendix III: Author affiliations

Priscilla D'Agostino

Louise Medical Center, Hand Clinic, Brussels, Belgium

Faes D. Kerkhof

Department of Orthopaedic Surgery - Orthopaedics, Stanford University, California, USA

Timo van Leeuwen

Department of Development and Regeneration, KU Leuven Campus Kulak, Belgium

G. Harry van Lenthe

Department of Mechanical Engineering, University of Leuven, Leuven, Belgium

Marco T. Y. Schneider

Auckland Bioengineering Institute, The University of Auckland, Auckland, New Zealand

Jeroen M. G. Stevens

Centre for Research and Conservation, Royal Zoological Society Antwerp, Belgium

Marie J. M. Vanhoof

Department of Development and Regeneration, KU Leuven Campus Kulak, Belgium

Maarten Vanneste

R&D Department, Denys NV, Ghent, Belgium

Evie E. Vereecke

Department of Development and Regeneration, KU Leuven Campus Kulak, Belgium

Appendix IV: Scientific illustration

A sample collection of my drawings and illustrations made over the course of my PhD for demonstrative purposes of either my colleagues' or my own research.

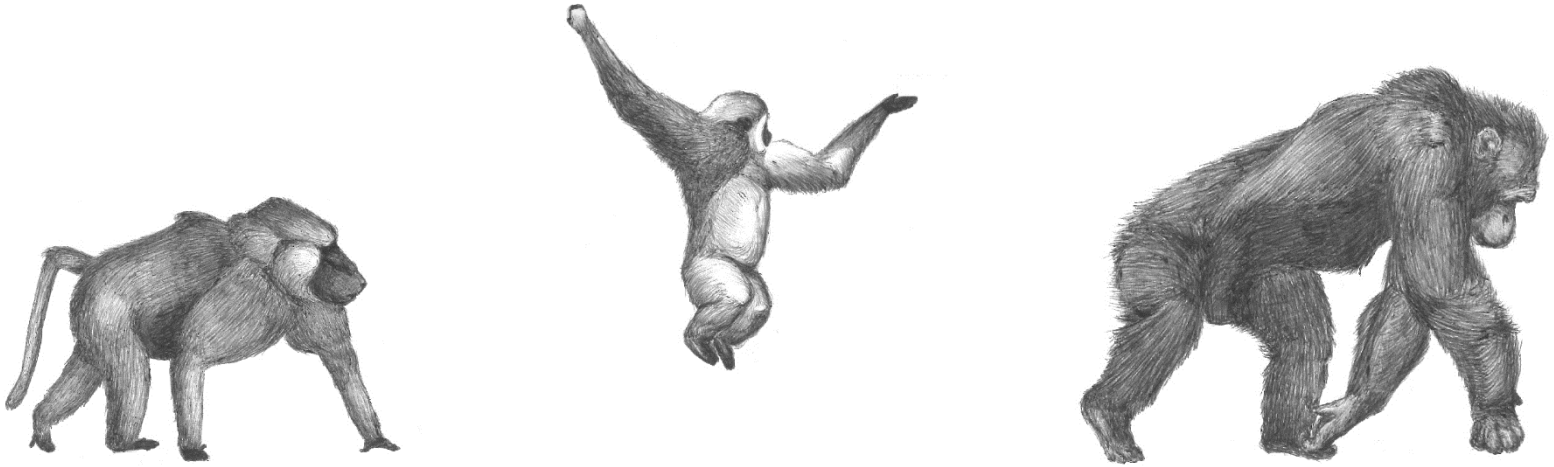

EFP2017: Winner of the first prize in the European Federation for Primatology Art Contest of 2017. Ballpoint pen on paper.

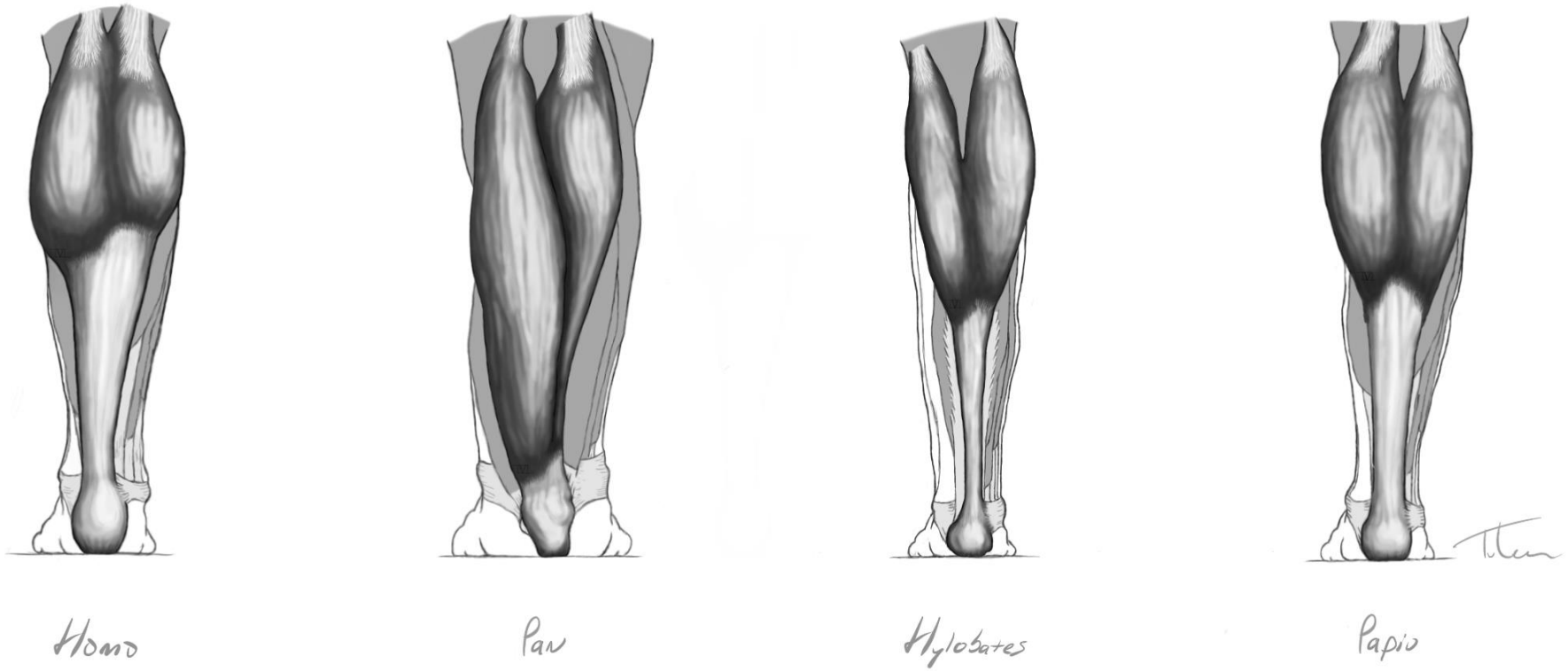

Aerts et al., 2018: Dorsal views of the baboon, gibbon, chimpanzee and human lower leg showing the Achilles tendon and the gastrocnemius muscle. Digital media.

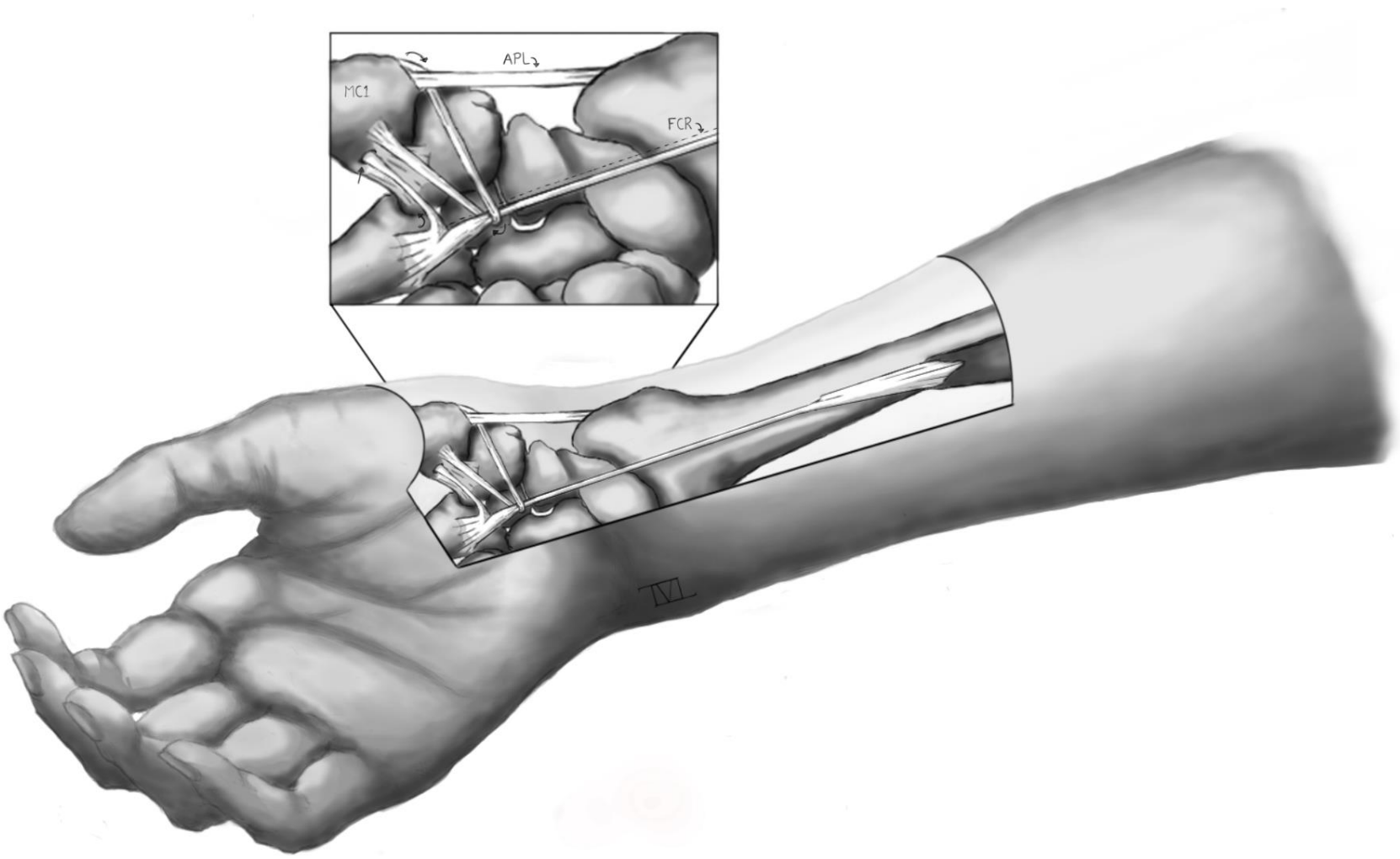

Kerkhof et al., 2018: A ligament reconstruction procedure in the human thumb. Digital media.



AAPA2018: A bonobo featured on the poster presented at the American Association of Physical Anthropology meeting in Austin, Texas, USA, 2018. Digital media.



Osteology 2018: The ventral femur, its morphological characteristics, and its orientation. An example of the 'Leergids' approach, to promote students actively engaging with the study material.



Thesis cover 2021: Primate selfie in the current year. Watercolour brush and Japanese ink on paper.

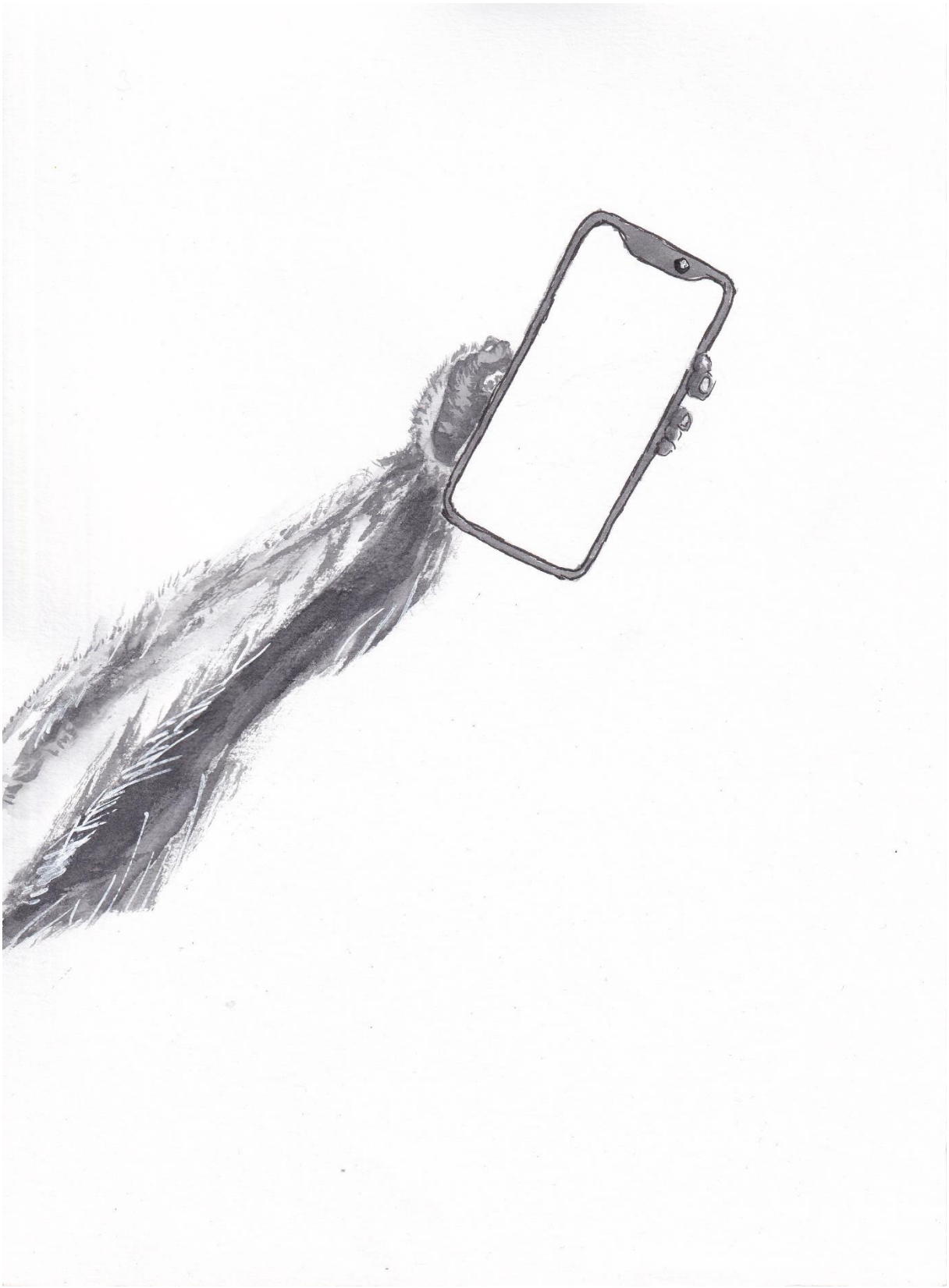

Thesis cover 2021: Primate selfie in the current year; primate point of view. A gibbon using the selfie function on the Banana Ookphone (Banana Inc.). Watercolour brush and Japanese ink on paper.